

**EVALUATION OF A NOVEL
ROTOR-STATOR DESIGN FOR
EMULSIFICATION AND THE
IMPACT ON CHEMICAL
REACTIONS**

Thesis submitted in
accordance with the
requirements of the University
of Liverpool for the degree of
Doctor in Philosophy

by

Daniel Henry Simon Harvey

May 2014

Contents

Table of Figures	vii
List of Tables.....	xv
Nomenclature.....	xix
Abstract	xxii
Acknowledgements	xxiv
Chapter 1 Introduction.....	1
1.1 Objectives of this Study	2
1.2 Commercial Significance	3
1.3 Overview of the thesis.....	5
1.4 References	9
Chapter 2 Fluid Processing and Emulsification	11
2.1 Introduction.....	11
2.2 Emulsification	11
2.2.1 Dispersive and Distributive Mixing.....	18
2.2.2 Laminar and Turbulent Flow.....	21
2.2.3 Droplet Creation Mechanisms	23
2.3 Overview of Droplet Break-up Mechanisms with Respect to Power Density	28
2.4 Overview of Droplet Break-up Mechanisms with Respect to Energy Density	30
2.5 Overview of Published Work on Rotor-Stators	31
2.5.1 Surfactants	46
2.5.2 Critical Micelle Concentration.....	50
2.5.3 Ostwald ripening.....	53
2.5.4 Dispersion Forces	54

2.5.5	Zeta Potential (ζ)	55
2.5.6	Pickering Emulsions and Steric Stabilization	58
2.6	Particle Sizing	59
2.7	Saponification and Biodiesel Formulation	66
2.7.1	Saponification	66
2.7.2	Biodiesel	70
2.8	References	77
Chapter 3	Mixing and Processing Equipment	89
3.1	Introduction	89
3.2	Small Scale Laboratory Mixing	90
3.2.1	Paddle Stirrer	91
3.2.2	Pitched-blade turbine	93
3.2.3	Homogenisers	94
3.3	Batch mixers	95
3.3.1	Fluid Division Mixer (FDM)	95
3.3.2	Microfluidizer	97
3.4	The Ultra Mixing and Processing Facility	98
3.4.1	Constraints	102
3.4.2	Equipment list	103
3.4.3	Operating Parameters	105
3.4.4	Capabilities	106
3.5	References	107
Chapter 4	High-Throughput Emulsification	108
4.1	Abstract	108
4.2	Introduction	109
4.3	Initial Experimental	112

4.3.1	Materials.....	112
4.3.2	Formax High-Throughput Formulation Platform	113
4.3.3	Initial Design.....	117
4.3.3.1	Factors.....	117
4.3.3.2	Variables.....	119
4.3.3.3	Design of Experiments	120
4.3.3.4	Particle Sizing	120
4.4	Initial Results and Discussion	121
4.4.1	Performance of the Formax.....	121
4.4.2	Effect of material and process parameters on drop size distribution	123
4.4.3	Statistical models for Sauter Mean Diameter and Volume Weighted Mean.....	125
4.5	Expanded Experimental	139
4.5.1	Materials.....	139
4.5.2	Expanded Design	139
4.6	Expanded Results and Discussion	140
4.6.1	Comparison of Mastersizer 2000 and Mastersizer X.....	140
4.6.2	Impact of Variables in Extended Method.....	142
4.6.3	Stability.....	144
4.7	Conclusion	144
4.8	Further Work	145
4.9	References	145
Chapter 5	Scaling-up High-Throughput Formulation.....	148
5.1	Abstract	148
5.2	Introduction.....	148
5.3	Experimental	150

5.3.1	Silverson 150/250 MS Mixer Experimental.....	152
5.3.2	UMPF Experimental	154
5.4	Results and Discussion	157
5.4.1	Silverson 150/250 MS 60L Batch reactor	157
5.4.2	UMPF	166
5.5	Conclusion	183
5.6	Further work.....	184
5.7	References	185
Chapter 6	Saponification using an Emulsion feasibility study.....	187
6.1	Abstract	187
6.2	Introduction.....	187
6.3	Benchmark Saponification Reactions.....	189
6.3.1	Benchmark experimental method.....	192
6.3.2	End point determination	194
6.4	Distributive mixing.....	196
6.4.1	Improvements to the Experimental Method.....	197
6.4.2	Distributive Mixing Trials Results and Discussion	198
6.5	Dispersive mixing Preliminary Bench-top Trials	199
6.5.1	Dispersive Mixing Trials Results and Discussion	201
6.6	High-Throughput Saponification	203
6.6.1	Experimental	204
6.6.2	Results and Discussion	210
6.7	Conclusion	214
6.8	References	215
Chapter 7	Batch Sunflower Oil Emulsion Production	216
7.1	Abstract	216

7.2	Introduction	217
7.3	Experimental	217
7.3.1	Surfactant.....	217
7.3.2	Droplet Sizing.....	218
7.3.3	Fluid Division Mixer (FDM)	219
7.3.4	Microfluidizer	221
7.3.5	Ultra Mixing and Processing Facility (UMPF)	222
7.4	Results and Discussion	223
7.4.1	Impact of the Phase Volume of Oil when using FDM Technology 223	
7.4.2	Processing emulsions using the Microfluidizer and Ultra Mixing and Processing Facility (UMPF)	230
7.5	Conclusion	236
7.6	References	238
Chapter 8	Formulation of Biodiesel	239
8.1	Abstract	239
8.2	Introduction	239
8.3	Experimental	240
8.3.1	Standard Method.....	240
8.3.2	Emulsification of Oil.....	241
8.3.3	Method Development	242
8.4	Results and Discussion	246
8.5	Conclusion	254
8.6	Future Work	255
8.7	References	256
Chapter 9	Conclusions and Further Work	257

Appendices.....	263
9.1 Dimensions of Equipment used	263
9.2 Wear and Damage to the UMPF	265
9.3 References for 9.1.....	268
9.4 Data from Chapter 4.....	269
9.5 Atlas Calorimeter Saponification Trials	277
9.6 List of symbols used throughout this document.	Error! Bookmark not defined.

Table of Figures

Figure 2-1 Illustration of emulsification.....	14
Figure 2-2 Illustration of distributive and dispersive mixing.....	20
Figure 2-3 Illustration of different types of flow.	22
Figure 2-4 Critical capillary number over viscosity ratio (Grace, 1982)	26
Figure 2-5 Graph showing the impact of shear and extensional flow on the capillary number of fluid at increasing velocity (Baker, 2011).	27
Figure 2-6 Summary of break-up mechanisms (based on work by Mike Baker and Adam J Kowalski).	28
Figure 2-7 Predicted and measured power consumption for soda ash slurry (Kowalski, 2009).	34
Figure 2-8 Theoretical power versus measured power, using constants from regression to torque data (Kowalski et al., 2011).	35
Figure 2-9 All power number data for Silverson 150/250 MS in-line rotor-stator mixer fitted with standard dual rotor-stator (Cooke et al., 2012).....	37
Figure 2-10 Droplet size as a function of rotor speed at 300 kg/h flow rate and a dispersed phase viscosity of 339 cSt (Hall et al., 2011).	38
Figure 2-11 Droplet size as function of flow rate for 1 wt% silicone oil emulsions at 6000 rpm and 11,000 rpm (Hall et al., 2011).	39
Figure 2-12 Droplet size as a function of energy density (Hall et al., 2011).	40
Figure 2-13 Droplet size as a function of the dispersed phase volume fraction at both 5000 rpm and 11,000 rpm, and a constant flow rate of 300 kg/h (Hall et al., 2011).	41
Figure 2-14 Droplet size as a function of viscosity of the dispersed phase (Hall et al., 2011).....	42
Figure 2-15 Droplet size as a function of tip speed (Hall et al., 2013).....	44

Figure 2-16 Stages of emulsion breakdown (IM-EMSAP, 2002). Oil is yellow, water blue and surfactant is present at the interface of the two phases.....	47
Figure 2-17 a) Simplistic drawing of a surfactant molecule. b) Chemical drawing of sodium dodecyl sulphate (SDS), an anionic surfactant.	48
Figure 2-18 Illustration of a micelle.	51
Figure 2-19 Phases adopted by surfactant molecules (Hamley, 2005).....	52
Figure 2-20 Illustration showing Ostwald Ripening.	54
Figure 2-21 A schematic representation of zeta potential for a negatively charged particle (Malvern, 2013a).	57
Figure 2-22 Simplified illustration showing how the Mastersizer 2000 or the Mastersizer X with a 45mm lens sizes particles.....	60
Figure 2-23 Simplified illustration showing how the Mastersizer X with either the 100mm, 300mm or 1000mm lens, sizes particles.	60
Figure 2-24 Simplified illustration showing how light is scattered by particles in the Mastersizers (Malvern, 2013b).....	64
Figure 2-25 Chemical reaction scheme depicting the hydrolysis of an ester and the formation of a carboxylate salt and alcohol.	67
Figure 2-26 Flow diagram of generic industrial saponification process.....	68
Figure 2-27 Chemical schematic depicting the formation of biodiesel from the largest possible triglyceride present within sunflower oil (three linoleic acid groups), where R is equal to one of the glyceride chains and R' is the rest of the triglyceride.....	71
Figure 2-28 Chemical schematic depicting the formation of Sodium Methoxide.	72
Figure 3-1 IKA hotplate stirrer (Savern, 2012)	90
Figure 3-2 a) Magnetic stirrer hot plate with digital dip temperature control b) Range of magnetic stirrer bars from small to large c) Magnetic stirrer bar creating a vortex within the reaction vessel at high rpm.....	91

Figure 3-3 Photograph of different mixing impeller types and the corresponding mixing they are designed for.	93
Figure 3-4 Four stages of how a homogeniser works (Silverson, 2012).	94
Figure 3-5 a) Direction of fluid when the mixer is turning. b) Fluid movement within the cavities of the mixer head. c) Direction of the fluid during mixing. d) The mixer head of the FDM. e) Inside of the mixer head showing the cavities.	96
Figure 3-6 Microfluidizer (Microfluidics, 2005).	97
Figure 3-7 Schematic drawing of the UMPF.	104
Figure 3-8 The Ultra Mixing and Processing Facility as it was in May 2008.	104
Figure 4-1 Chemspeed Formax high-throughput platform showing: a) Rotor-Stator head, b) Saw tooth impellor, c) 12 reaction vessels, d) robotic manipulator e) 4-needle liquid handling unit and f) GDU-HV: Gravimetric Dispensing Unit for High Viscosity reagents.	114
Figure 4-2 DSD of emulsions of varying size.	122
Figure 4-3 Droplet size of emulsion produced with respect to impeller speed, phase volume of oil and phase volume of surfactant respectively.	124
Figure 4-4 Comparison of observed droplet size values verses predicted droplet size values taken from MODDE software.	126
Figure 4-5; 4-D graph showing the impact of both formulation and process parameters on the product droplet size (D[3,2]) predicted by MODDE based on actual experimental results. Dissolver disk impeller used with scraper speed set to 100rpm.	128
Figure 4-6 Right hand column from Figure 4-5 rescaled using DoE software.	131
Figure 4-7; 4-D graph showing the impact of both formulation and process parameters on the product droplet size (D[3,2]) predicted by MODDE based on actual experimental results.	133

Figure 4-8; 4-D graph showing the impact of both formulation and process parameters on the product droplet size (D[4,3]) predicted by MODDE based on actual experimental results.	135
Figure 4-9; 4-D graph showing the impact of both formulation and process parameters on the product droplet size (D[4,3]) predicted by MODDE based on actual experimental results.	137
Figure 4-10 Graph produced using raw particle size data obtained after analysing the emulsions using a Malvern Mastersizer 2000.	141
Figure 4-11 Droplet size of emulsion as a function of scraper speed.....	143
Figure 5-1 Set-up of Silverson 150/250 MS mixer pilot plant rig.	153
Figure 5-2 Silverson 150/250 MS rotor (left) and stator (right) (Hall et al., 2011).....	153
Figure 5-3 Droplet size distribution graph produced using a Mastersizer X.	158
Figure 5-4 Droplet size distribution graph produced using a Mastersizer 2000 with both blue and red light sources.....	160
Figure 5-5 Droplet size values as calculated by a Mastersizer X versus the same measurements calculated by a Mastersizer 2000 (with both blue and red light sources).	161
Figure 5-6 Droplet size distribution graph produced using Mastersizer 2000 with red light source only.	162
Figure 5-7 Droplet size values as calculated by a Mastersizer 2000 with red light only versus the same measurements calculated by a Mastersizer 2000 with both blue and red light sources.....	163
Figure 5-8 Graphs from Figure 5-4 and Figure 5-6 combined.....	164
Figure 5-9 Droplet size as a function of the impeller speed [cubed].....	165
Figure 5-10 Droplet size as a function of tip speed.	166

Figure 5-11 Droplet size as a function of impeller speed at and varying oil to surfactant ratios. Analysis was performed using the Malvern Mastersizer X with a 45mm lens. 167

Figure 5-12 Droplet size of emulsion as a function of tip speed (U_T) with respect to flow rate and oil to surfactant ratios. Analysis of UMPF samples performed using the Malvern Mastersizer X with a 45mm lens, analysis of Silverson was performed with a Mastersizer 2000. 168

Figure 5-13 Droplet size of emulsion as a function of tip speed (U_T) with respect to flow rate and oil to surfactant ratios. Analysis of UMPF samples performed using the Malvern Mastersizer X with a 45mm lens, analysis of Silverson was performed with a Mastersizer 2000. 169

Figure 5-14 Graph showing the impact of the oil to surfactant ratio on the size of the droplets within the emulsion produced using the UMPF at 10,000rpm with a total flow rate of 20mL/s. 170

Figure 5-15 Graph showing the impact of the total flow rate on the size of the droplets within the emulsion produced using the UMPF with the impeller at static. Analysis was performed using the Malvern Mastersizer 2000 with both red and blue light sources. The phase volume of oil and surfactant for the formulations within each series was kept constant. 174

Figure 5-16 Droplet size distribution produced by Malvern Mastersizer X of samples displayed in Table 5-6 following analysis using a 45mm lens. 177

Figure 5-17 Droplet size distribution produced by Malvern Mastersizer 2000 of samples displayed in Table 5-6 following analysis using red light source only. 178

Figure 5-18 Droplet size distribution produced by Malvern Mastersizer 2000 of samples displayed in Table 5-7 following analysis of the samples using the Mastersizer 2000 with both red and blue light sources. 178

Figure 5-19 Droplet size distribution produced by Malvern Mastersizer X of samples displayed in Table 5-8. 179

Figure 5-20 Droplet size distribution produced by Malvern Mastersizer 2000 of samples displayed in Table 5-8 following analysis of the samples using the Mastersizer 2000 with a red light source only.	180
Figure 5-21 Droplet size distribution produced by Malvern Mastersizer 2000 of samples displayed in Table 5-9 following using both red and blue light sources.	180
Figure 5-22 Droplet size values as calculated by a Mastersizer X (red light only) versus the same measurements calculated by a Mastersizer 2000 with both blue and red light sources.	181
Figure 6-1 Chemical drawing of triglyceride;highlighted is one of the ester groups.	193
Figure 6-2 Chemical drawing of the predicted structure of the carboxylate salt produced following the saponification of sunflower seed oil.	193
Figure 6-3 Benchmark Saponification reactions were carried out using a 6 pitched blade turbine (PBT) connected to an overhead stirrer. A plate heater and oil bath was used to maintain reaction temperature at 80°C throughout the reaction.	197
Figure 6-4 POLYTRON® PT 2100 fitted with a 15mm rotor, 20mm stator impeller.	200
Figure 6-5 Photograph and labelled drawing of product HSH05.	203
Figure 6-6 Illustration of the layout and set-up of the ASW2000 used.	205
Figure 6-7 Illustration of two-phase system in ASW2000 reaction vessel.	207
Figure 6-8 Illustration of increasing interfacial area between two phases in ASW2000 reaction vessel.	208
Figure 6-9 Infrared spectroscopy data of experiment with an ester peak [peak 4] at 1741.41cm ⁻¹ indicating that the reaction has not yet reached completion.	210
Figure 6-10 Infrared spectroscopic data of an experiment that has reached completion. There is no peak in the region of 1735 – 1750cm ⁻¹ but there is a peak at 1550.49cm ⁻¹ [peak 3] indicating that the reaction has reached	

completion and the triglyceride has been broken down and formed a carboxylate salt.	213
Figure 7-1 a) Schematic drawing showing the clearance of the FDM mixer head from the mixing vessel walls. b) Photograph of the FDM head and shaft.	220
Figure 7-2 Graph showing the effect of varying the phase volume of oil within emulsification using a Fluid Division Mixer at 6000rpm. The level of surfactant in all processes was constant.	225
Figure 7-3 Graph showing the effect of phase volume whilst maintaining the surfactant to oil ratio within emulsification, using a Fluid Division Mixer at 6000RPM.	227
Figure 7-4 Graph showing the effect of varying the surfactant concentration within emulsification after an hour of processing using an FDM at 6000rpm. The phase volume of oil in all processes was constant (60%).	228
Figure 7-5 Droplet Size Distribution of emulsion after processing using UMPF.	232
Figure 7-6 DSD of emulsions with a $D[3,2]$ value of $\sim 1.5\mu\text{m}$ according to analysis using a Mastersizer X.	233
Figure 8-1 DSD of emulsion used to make biodiesel showing uniform distribution throughout the mixing vessel.	242
Figure 8-2 $^1\text{H-NMR}$ spectroscopy of an incomplete biodiesel reaction.	244
Figure 8-3 $^1\text{H-NMR}$ spectroscopy of biodiesel spiked with sunflower oil.	244
Figure 8-4 $^1\text{H-NMR}$ of the product formed using a sub-micron emulsion and two-step biodiesel formulation synthesis described in this paper.	248
Figure 8-5 Percentage of triglyceride converted with respect to reaction time.	250
Figure 9-1 Atlas Potassium Calorimetry Reactor equipment setup. A) Power controller for power compensation reactor heater, B) Jacket-In temperature probe (T_j), C) Vacuum triple jacketed 500mL reactor containing 400mL of $[1\text{M}] \text{NaOH}_{(\text{aq})}$ with pH, temperature (Tr) and turbidity probes, D)	

Controlled overhead mechanical stirrer, E), Reagent feed delivered by controlled Atlas syringe pump, F) Feed reservoir of 100mL sunflower oil [8].	278
Figure 9-2 Clear sodium hydroxide solution prior to the addition of any oil and thus at reaction time zero (left image); following oil addition the reaction began and a turbid emulsion was formed (right image) and continued to be formed during the reaction.	279
Figure 9-3 Graph calculated using the Atlas software showing real time monitoring of the addition of sunflower oil drop-wise (straight green line) and the corresponding increase in turbidity (wavy, red line) that occurs as soap is formed.....	280
Figure 9-4 Live time monitoring of the reaction occurring using the Atlas Calorimetric software.	281

List of Tables

Table 2-1 Examples of common household products that are emulsions	15
Table 2-2 Power constants obtained by Hall et al (2013).....	36
Table 2-3 Hydrophile-Lipophile Balance (HLB) values and common uses (ICI Americas, 1976).....	50
Table 2-4 Zeta potential ranges and corresponding degree of coagulation (American Water Works Association, 2003).....	56
Table 2-5 Size of lenses available for the Mastersizer X and the size range of particulates/droplets they are able to analyse.....	62
Table 2-6 Soap additives are commonly used to enhance the soap qualities.	70
Table 2-7 Conditions for standard biodiesel formulation.	73
Table 4-1 listing the properties of SLES.....	113
Table 5-1 Parameters and required values necessary to achieve droplets with smallest $D[3,2]$ value using the Formax.....	151
Table 5-2 Range of parameters observed when using the UMPF.	155
Table 5-3 Droplet size data produced from analysis using a Mastersizer X.	158
Table 5-4 Droplet size data produced from analysis using a Mastersizer 2000 with both blue and red light sources.....	159
Table 5-5 Droplet size data from analysis of samples using red light source only analysis from the Malvern Mastersizer 2000.	162
Table 5-6 Data taken from analysis of samples using red light source only [Malvern Mastersizer X] showing the impact of impeller speed on droplet size.	172
Table 5-7 Data taken from analysis of samples using red and blue light sources [Malvern Mastersizer 2000] showing the impact of impeller speed on droplet size.....	172

Table 5-8 Data taken from analysis of samples using red light source only [Malvern Mastersizer X] showing the impact of impeller speed on droplet size.	173
Table 5-9 Data taken from analysis of samples using red and blue light sources [Malvern Mastersizer 2000] showing the impact of impeller speed on droplet size.....	173
Table 5-10 Data taken from Table 5-6, Table 5-7, Table 5-8 and Table 5-9 for ease of analysis.	176
Table 5-11 Parameters and required values necessary to achieve droplets with the smallest D[3,2] value using the UMPF when analysed using a Malvern Mastersizer 2000 with both red and blue light sources during this work.	183
Table 6-1 Parameters of the distributive and dispersive mixers used.	191
Table 6-2 Benchmark Reaction Conditions.....	192
Table 6-3 Parameters and reaction time for four of the experiments performed using the 6 PBT.	199
Table 6-4 Table listing the parameters and reaction time for each of the experiments performed using the high-shear homogeniser.	202
Table 6-5 Table listing the high-throughput saponification trials parameters and time taken to reach completion.	211
Table 7-1 properties of polysorbate 20.	218
Table 7-2 Formulation parameters for data shown in Figure 7-2	224
Table 7-3 Formulation parameters for data shown in Figure 7-3	227
Table 7-4 Formulation parameters for data shown in Figure 7-4	228
Table 7-5 Size of droplets within emulsion after one pass through mixer. .	235
Table 8-1 Values used in the second step of the adapted method for biodiesel formulation using an emulsion.	247
Table 8-2 Values obtained from analysis of Figure 5.....	249

Table 8-3 Rate of reaction calculations values for sunflower oil when making biodiesel.....	251
Table 8-4 Rate of reaction calculations values for emulsified sunflower oil seconds step when making biodiesel.....	252
Table 9-1 Dimensions of Fluid Division Mixer	263
Table 9-2 Dimensions of Formax Vessels	264
Table 9-3 Results Table for the proposed wear rate method.	267
Table 9-4 Values of the variables used to produce three of the 22 emulsions and their corresponding $D[3,2]$ values.	269
Table 9-5 Predicted formulation and process parameters required to obtain the smallest possible droplet size and the value that would be obtained according to MODDE alongside the actual experiments that were subsequently carried out. The viscosity of the oil and the impeller type in all cases was 10cSt and dissolver disk respectively.....	270
Table 9-6 A summary of the proportionality constants used to obtain predicted $D[3,2]$ values for a dissolver disk impeller.	271
Table 9-7 A summary of the proportionality constants used to obtain predicted $D[3,2]$ values for a rotor-stator impeller.	272
Table 9-8 A summary of the proportionality constants used to obtain predicted $D[4,3]$ values for a dissolver disk impeller.	273
Table 9-9 A summary of the proportionality constants used to obtain predicted $D[4,3]$ values for a rotor-stator impeller.	274
Table 9-10 Comparison of products from two almost identical experiments obtained by analysis using Malvern Mastersizer X and Malvern Mastersizer 2000. Viscosity of oil used was 10cSt oil and impeller type was dissolver disk for both experiments.	275
Table 9-11 Parameters chosen for the latter 11 experiments. Reactor vessel 7 was undergoing routine maintenance. The reason the final three samples have no particle size measurement is because they formed either oil-in-water gel or oil-in-water-in-oil emulsions and couldn't be sized.	276

Nomenclature

Symbol	Description
τ_{BU}	Break-up stress required to break up the droplet
Ca	Capillary number
cSt	Centistokes
$^{\circ}\text{C}$	Degrees Celsius
ρ	Density of fluid
d	Diameter of pipe
τ_{DV}	Droplet viscosity resisting deformation
Γ	Interfacial tension
τ_{IT}	Interfacial tension stress holding the drop together
ΔP	Laplace Pressure
L	Litres
η	Matrix viscosity
m	Metres
μm	Micrometres
ml	Millilitres

mm	Millimetres
mV	Millivolts
R_n	Radii n (if more than one)
rpm	Revolutions per minute
$D[3,2]$	Sauter Mean Diameter
s	Seconds
$\dot{\gamma}$	Shear rate
Σ	Sum of
γ	Surface tension
u	Velocity of fluid
μ	Viscosity of fluid
τ	Viscous stress
$D[4,3]$	Volume Weighted Mean
wt%	Weight percent
Ej wt%	Weight percent of ethylene oxide
OH wt%	Weight percent of hydroxide groups
ζ	Zeta Potential

FOR DAN AND CATH HARVEY,
HARRY AND MARY DAY,
VINCENT, PATRICIA AND BETH HARVEY
TABITHA, ERIC, ESME AND CONSTANCE
FOR ALL MY FAMILY

Abstract

The work described in this thesis aims to present results regarding the exploration, validation and use of a novel rotor-stator type mixing equipment employing controlled deformation dynamic mixing (CDDM) technology in creating sub-micron emulsions for use in chemical reactions. Emulsification is the process by which one immiscible liquid (e.g. oil) is finely dispersed throughout another immiscible liquid (e.g. water) and stabilised, commonly through the addition of a surface active agent or emulsifier to the system.

Specific focus was given to the emulsification of plant oils (such as sunflower seed oil) as a way of improving their available reactive surface area. The addition of emulsifiers in this case was used to sufficiently reduce the interfacial tensions, allowing for greater droplet break-up, and provide adequate emulsion stability. Further testing of these emulsions was performed within biphasic saponification and transesterification reactions, such as those commonly employed in the production of soap and biodiesel. It was hypothesised that by reducing the dispersed oil phase droplet size in the presence of an emulsifier, and thus increasing the surface area to volume ratio, reaction rates could be manipulated. Testing of this hypothesis showed that despite the presence of surfactant and, in the case of the transesterification reaction, water, the use of sub-micron oil droplets caused a decrease in the overall reaction time (time spent at reaction temperature and under agitation).

In support of this work, high-throughput formulation (HT) and design of experiment (DoE) software was adopted to allow a quick and efficient way of screening which emulsification parameters had the greatest impact on the size of the droplets when

emulsifying oil. For this work a standard emulsion containing silicone oil and Sodium Lauryl Ether Sulfate (SLES) was used.

Following the identification of the optimum emulsification parameter set, work focused on the scaling up from small scale (50g) to pilot plant scale mixing devices (10kg – 300kg/hour) in order to formulate large quantities of emulsion. It was shown that the HT screening and DoE was sufficiently robust to predict emulsification parameters at scale. For an emulsion system of silicone oil and SLES, the formulation parameters that created an emulsion with the smallest droplet size using the high-throughput platform, also produced an emulsion with the smallest droplet size using the new pilot plant scale Ultra Mixing and Processing Facility (UMPF) fitted with CDDM technology.

In order to characterise the emulsions created, laser diffraction measurements were used throughout this work (Malvern Mastersizer X & 2000) and “side by side” emulsification experiments were carried out using commercially available fluid processing units. Utilising either a rotor-stator type inline mixer (high shear Silverson 150/250MS mixer) or a high pressure valve type homogeniser (M-110S Microfluidizer Processor, Small Volume) the emulsions produced and processed on the respective equipment were compared with those produced via the CDDM in order to assess its capabilities and performance against two of the leading mixers available.

Acknowledgements

The work presented in this thesis is dedicated to those who have maintained belief in my abilities as a research scientist when my own have been cast in self-doubt. Without you I am certain that this would not have been possible. To my family and friends, thank you for your continued support and for pushing me to complete what I felt at times was an impossible task.

I would like to thank my supervisors, Professor Adam J Kowalski and Professor Mathias Brust for giving me not only the opportunity to perform this work, but the support and guidance throughout the course of it.

Dr John Satherley and Professor Mark Simmons are both acknowledged and thanked for assessing this thesis and providing the necessary criticism to bring it up to the standard presented here.

The financial support of both the Engineering and Physical Sciences Research Council and Unilever R&D for funding the work that is reported within this thesis is also acknowledged.

My thanks and an acknowledgement to Dr Neil Campbell, who I describe as both a friend and a mentor. Without his guidance and tutelage I would not have become anywhere near as knowledgeable in the ways of high-throughput manipulation as I am to this day. I would also like to thank Rob Clowes, Neil Jones and Sean Higgins of the CMD at the University of Liverpool.

I would like to acknowledge and thank Mike Cooke of Manchester University for his assistance with work using the Silverion 150/250 MS in Chapter 5, Dr Elizabeth Hind for helping me format this entire thesis and Mr Brian Rea for proof reading this thesis.

Finally I would to thank the gaffer, Dr Mike J Egan. It is with certainty I can say that I would not be where I am today without his guidance, mentoring and friendship. Consistently demanding more of me throughout the course of my research he has been the devil's advocate I have needed on more than one occasion. My gratitude to him is as great as my love of beer.

Chapter 1 Introduction

The primary focus of this work is the evaluation of the novel, patented, Controllable Deformation Dynamic Mixing (CDDM) rotor-stator technology (Brown et al., 2010a; Brown et al., 2010b; Brown et al., 2010c) at the heart of the Ultra Mixing and Processing Facility [UMPF] at the University of Liverpool for processing emulsions for use in biphasic reactions. Interest was given to the impact of the equipment on the droplet size of the dispersed phase within a standard emulsion system, specifically how small the droplets were following processing. It was expected that smaller droplets would be produced using the UMPF. Smaller droplets of reagents would cause an increase in the rate of reaction and a decrease in the overall reaction time improving the reaction in terms of efficiency and reducing the amount of energy needed for it to reach completion.

Some hypotheses have been presented into the possible mechanisms of what occurs within the new mixer and a separate PhD research project has been commissioned to thoroughly investigate them and generate scale-up rules therefore they are not discussed within this thesis.

The work presented in this thesis involves a combination of research from the disciplines of chemistry and chemical engineering. The research areas included, but are not limited to;

- Droplet break-up
- Droplet size manipulation through process and formulation
- Benchmarking CDDM against other commercial mixers

- Technical assessment of the products the CDDM technology is capable of formulating and processing
- Technical assessment of the improved biphasic chemical reactions resulting from smaller droplet sizes obtained using the CDDM and the subsequent quantitative analysis of the products.

1.1 Objectives of this Study

Specific objectives for the research work reported in this thesis were chosen based on gaps in the existing related literature and on the scientific benefit they would provide. The objectives are listed below and an overview of the chapters relating to them is provided further on in this chapter.

- Devise a method to ascertain the formulation and process parameters required to create an emulsion quickly and efficiently using a high-throughput formulation suite.
- Evaluate Controllable Deformation Dynamic Mixing (CDDM) technology using a standard emulsion system.
- Benchmark the CDDM against a commercially available Silverson in-line rotor-stator mixer.
- Establish a proof of principle that smaller reagent droplet sizes, through emulsification, decrease the reaction time of a biphasic reaction.
- Ascertain whether the trade-off between reduction in droplet size and the increase in the rate of reaction improves a biphasic reaction system to the point that one usually hindered by the presence of water can be improved through the emulsification of one of the reagents.

1.2 Commercial Significance

Many common products are produced via the chemical reaction of at least two other materials. A number of biphasic reactions have significant commercial and societal importance, for example esterification and transesterification are used in the formation of soaps and in the production of biofuels, respectively. The degree of solubility, the available surface area of the reagents involved and the reduction of the concentration gradients are all factors that can have an impact upon the rate of reaction, and thus the overall time required for the reaction to reach completion.

The patented, CDDM rotor-stator processing technology designed by Unilever, in partnership with TecExec Ltd (Brown et al., 2010a; Brown et al., 2010b; Brown et al., 2010c), and developed through academic collaboration with the university of Liverpool (Almeida Rivera et al., 2012; Bongers et al., 2012a; Bongers et al., 2013a; Bongers et al., 2013b), is an advancement in high shear rotor-stator processing technology. This technology has been designed to enable energy efficient fluid mixing, and processing, of emulsions which exhibit high surface area to volume ratios.

Droplet break-up is an area of intense research that receives significant commercial interest globally. Industrial companies spend millions of pounds researching and protecting their developments in the field. Extrapolated calculations indicate that in 2013 Unilever spent over \$7million filing patents associated with emulsions alone. This value is based on the estimated cost of patents being approximately \$200,000 for global protection (increasing with inflation at 3% a year from 2004 when they cost approximately \$153,000, according to Kagan Binder PLLC, 2004) and Unilever

filing 36 patents containing the word “Emulsion” in 2013, according to the World Intellectual Property Organisation (WIPO, 2014).

Unilever and one of its competitors in the global home and personal care market, Procter & Gamble, have both funded academic research into the area of droplet break-up (Hall et al., 2013; Itachi Cohen Group, 2013). The subject is studied within academia and supported via governmental and private research bodies that actively fund research in the field [e.g. EPSRC, TSB, NASA] (Parliament, 2013; NASA, 2013) or provide bespoke training in the area of emulsification and droplet break-up/stability [e.g. Leatherhead Food Research] (Leatherhead, 2014).

The CDDM processing technology has been shown to be a very energy efficient route for producing finely dispersed emulsions encapsulating nutraceutical ingredients, compared to a high pressure homogeniser benchmark (Bongers et al., 2012a). As well as this, the CDDM has been found to have commercial applications within a number of other areas of the home and personal care sector (Almeida Rivera et al., 2012; Bongers et al., 2013a; Bongers et al., 2013b). Based on the published successes, there is great potential for the CDDM to improve biphasic reaction kinetics through reduction of reagent drop sizes, increasing the available reaction surface area and increasing the rate of reaction. The ability to optimise the CDDM equipment, processing parameters and process route, as well as the formulation itself, will thus allow the uptake of the CDDM technology by the commodity chemicals market. Using the CDDM to optimise droplet size, for example to achieve smaller droplets with larger surface area to droplet volume ratios for reactions, can be achieved in a potentially more energy efficient way.

Chapter 1 – Introduction

The CDDM technology presents a new design of mixer, one specifically designed to further reduce droplets in size through increase in speed and with multiple addition options, whilst maintaining high flow rates so that the products are commercially viable. An example of the commercially viable output of the CDDM is reported in Chapter 5 when flow rates of 100mL/s were used, which equates to an output of around 360 kilograms per hour.

1.3 Overview of the thesis

An overview of the chapters within this thesis is outlined below, the aim of this being to provide a brief summary of the chapters and how they relate to both the objectives discussed previously and the development of the thesis overall.

A review of the literature available involving rotor-stator devices in the formation of emulsions is presented in Chapter 2. Specifically, the review covers droplet break-up, emulsion stabilisation and the analysis of small droplets in an emulsion using a laser particle sizer. As well as an overview of these subject areas, Chapter 2 also discusses the impact of scaling up of rotor-stator mixers. From the published work analysed, a set of conclusions have been drawn. It is clear from these conclusions, that similar work must be undertaken for the new rotor-stator technology as there is disagreement on the scale-up principle; it has not yet been proved that the equations already available for predicting the impact of rotor-stator mixers apply to all available rotor-stators if they are of a different design. Further to this, the literature analysed showing work in similar areas with rotor-stator mixers involves formulation of emulsions with a low phase volume of oil (none greater than 50%); with the UMPF being designed to handle high pressures and high viscosity fluid one of the

aims of this research was to prove that the mixer was capable of processing viscous fluids and emulsions made with a high phase volume of oil (60–70% were observed).

Work was undertaken using standard, readily available processing equipment to establish the impact of formulation parameters in creating an emulsion with the smallest droplet size. Chapter 3 details the mixers used within each experiment of the research work undertaken and presented in this thesis, at ever increasing volumes. Bench-top mixers of varying dimensions and the impact they had on the subsequent reaction is discussed and reviewed in Chapter 6, a feasibility study.

The target aim of Chapter 4 was to produce an emulsion with the smallest droplet size and ascertain the parameters required to do so whilst ensuring that they are repeatable. A Formax high-throughput formulation platform and design of experiment (DoE) software was used to map both the process and formulation parameters and the impact altering them has on the size of the droplets within the emulsion produced. Prior to the work in Chapter 4 being published, there was no fast and efficient way of mapping out the impact that altering the formulation parameters has on the size of the droplets. The model system chosen consisted of silicone oil, water and SLES (Sodium Lauryl Ether Sulfate) surfactant. Chapter 4 discusses an investigation into the formulation parameters required to make an emulsion with the smallest droplet size. The research work in Chapter 4 was published in the *Journal of Dispersion Science and Technology* (Harvey et al., 2013).

Following the work in Chapter 4, the formulation parameters identified that created an emulsion with the smallest drop size were used to discover the size of the droplets in an emulsion produced using the UMPF. Chapter 5 presents the results of trials performed using the UMPF that include an investigation into which of the process

Chapter 1 – Introduction

parameters had the greatest impact on the size of the droplets in the final product. This work allowed an evaluation of the Controllable Deformation Dynamic Mixing (CDDM) technology using a standard emulsion system.

Using the formulation parameters that were discovered in Chapter 4 to produce an emulsion with the smallest droplet size, a series of trials were performed using both a Silverson in-line rotor-stator mixer and the UMPF allowing the CDDM technology to be benchmarked against a commercially available Silverson in-line rotor-stator mixer. Chapter 5 identifies key points about the novel design of the UMPF and presents the possibility of using high-throughput formulation mapping for future pilot-plant scale production.

Chapter 6 presents the outcome of a series of trials designed to establish a proof of principle that smaller reagent droplet sizes [through emulsification] decrease the reaction time of a simple biphasic reaction. The simplest reaction chosen to perform the feasibility study was saponification. The work displayed in Chapter 6 shows that using a high-throughput synthesis platform, the point at which the reaction reaches completion can be identified to a time with an error of a couple of minutes.

The final piece of work performed and reported within this thesis involves ascertaining whether a biphasic reaction system hindered by the presence of water can be improved upon by emulsifying one of the reagents. An investigation in Chapter 8 is reported which details the feasibility of forming biodiesel using a submicron emulsion of plant [sunflower] oil and methanol, despite methanol being miscible in water. Feasibility trials were performed prior to the creation of large batches of emulsion and large scale reactions. The impact of emulsifying the reagent prior to reaction was then investigated thoroughly with relation to the rate of

reaction, with samples taken at time points to monitor the reactions progress to completion.

1.4 References

ALMEIDA RIVERA, C. P., Bongers, P. M. M., Egan, M. J., Irving, N. G. and Kowalski, A. J. 2012. Mixing Apparatus and Method for Mixing Fluids.

WO/2012/065824

BINDER, Kagan. 2004. [http://www.kaganbinder.com/docs/7-o.ol,biknh\[-E\]-OustimatedPatentCosts.pdf](http://www.kaganbinder.com/docs/7-o.ol,biknh[-E]-OustimatedPatentCosts.pdf) Accessed 1st March 2014.

BONGERS, P. M. M., Santos Ribeiro, H., Irving, G. N. and Egan, M. J. 2012.

Method for Production of an Emulsion. WO/2012/089474

BONGERS, P. M. M., Egan, M. J., Flöter, E., Gupta, S., Irving, G. N., De Man, T.

and Santos Ribeiro, H. 2013a. Method for Production of Edible Water-In-Oil

Emulsion. WO/2013/056964

BONGERS, P. M. M., Egan, M. J. and Irving, G. N. 2013b. Method for Production of Structured Liquid and Structured Liquid. WO/2013/092118

BROWN, C. J., Irving, G. N. and Kowalski, A. J. 2010a. Mixing Apparatus of the CDDM- or CTM-Type, and its Use. WO/2010/091983

BROWN, C. J., Irving, G. N. and Kowalski, A. J. 2010b. Mixing Apparatus of the CDDM- or CTM-Type, and its Use. WO/2010/089322

BROWN, C. J., Irving, G. N. and Kowalski, A. J. 2010c. Distributive and Dispersive Mixing Apparatus of the CDDM Type, and its Use. WO/2010/089320

FRANCIS, M. J. and Pashley, R. M. 2009. Further studies into oil droplet size manipulation. *Colloids and Surfaces A: Physicochemical and Engineering Aspects*.

334 100-106

HALL, S., Pacek, A. W., Kowalski, A. J., Cooke, M. and Rothman, D. 2013. The effect of scale and interfacial tension on liquid–liquid dispersion in in-line Silverson rotor–stator mixers. *Chemical Engineering Research and Design*. **91** 2156-2168

HARVEY, D. H. S., Egan, M. J. and Kowalski, A. J. 2013. Use of Formax High-Throughput Platform to Create a Specific Emulsion. *Journal of Dispersion Science and Technology*. **34** 441-453

ITAI COHEN GROUP. 2013. Complex Matter Physics, Department of Physics, Cornell University. <http://cohengroup.ccmr.cornell.edu/> Accessed on 27th October 2013.

JANSSEN J. J. M., Boon, A. and Agterof, W. G. M. 1994. Influence of Dynamic Interfacial Properties on Droplet Break-up in Simple Shear Flow. *AIChE Journal*. **40** 1929-1939

LEATHERHEAD Food Research. 2014. <http://www.leatherheadfood.com/training-and-conferences>. Accessed 1st March 2014.

NASA. 2013.

http://www.nasa.gov/mission_pages/station/research/experiments/602.html
Accessed on 27th October 2013.

PARLIAMENT. 2013.

<http://www.publications.parliament.uk/pa/cm201011/cmselect/cmsctech/619/619vw70.htm> Accessed on 27th October 2013.

Chapter 2 Fluid Processing and Emulsification

2.1 Introduction

Fluid processing is of paramount importance to a diverse range of industries such as food, home and personal care, pharmaceuticals, petrochemical, agrochemicals, paints and coating industries, commodity and speciality chemicals sectors and many more. Many industrial processes require significant steps whereby liquids or fluid-like materials are transported, pre-treated, mixed and formulated in order to manufacture the final product or intermediates. Many of these processing steps, at some stage, require the mixing of two or more immiscible phases such as gas-liquid, liquid-liquid and solid-liquid etc. This chapter will introduce the importance of mixing and formulating in the process industries, discuss emulsions and their importance, look at the range of areas where fluid processing is utilised and observe some of the challenges currently faced by industry.

2.2 Emulsification

The degree to which two liquid phases can be blended or mixed together is highly dependent upon how miscible they are, e.g. two aqueous components can be readily blended to form a homogenous mixture. Materials with different chemistries (hydrophobic/hydrophilic) may well be either partially or wholly immiscible in each other leading to the creation of a 'multi-phase' system. An example of a stable multi-phase system is an emulsion; the method of mixing of two immiscible liquids to the point where one is finely dispersed throughout another is known as an emulsification (Forgiarini et al., 2001; Mason et al., 2006a; Mason et al., 2006b; Meleson et al.,

2004; Somasundaran et al., 2006). In order for emulsification to occur, two processes must happen; droplet creation and droplet stabilisation. Section 2.2.3 discusses droplet break-up and section 2.3 introduces droplet stabilisation through the addition of surface active agents [surfactants] which prevent coalescence of the droplets. Section 2.5.2 explains the critical micelle concentration and why this is important with relation to the addition of surfactant. Throughout this section (2.2) a number of other emulsion stabilisation techniques are described including; the use of solid particulates in Pickering emulsions, the use of polymers in steric stabilisation as well as the use of surfactants such as anionic Sodium Dodecyl Sulphate (SDS). The focus of the work within this thesis is on liquid-liquid only systems and as such techniques involving solids or gases are only discussed briefly.

The most common types of emulsion are made up of a mixture of oil and water phases (e.g. Sunflower oil and water). If the emulsion has oil dispersed and distributed throughout water, this is known as an oil-in-water emulsion (O/W) or a “direct emulsion” (Mason et al., 2006a; Mason et al., 2006b; Nakache et al., 2000). The milk produced during lactation of mammals is an example of a direct emulsion, and such ‘milks’ are an ideal vehicle to transport the vitamins, minerals, proteins, fats and carbohydrates necessary for the growing young as they are able to pass through the membranes within the infants stomach quickly and efficiently due to them consisting of both oil and water.

Milk is formed through a series of biological processes however emulsions can be made using oil, water and a stabilising agent, such as a surfactant. When these three reagents are placed into a mixing vessel they will separate out according to their density over time, occasionally [if there is enough surfactant present] with micelles being formed (micelle formation is discussed in 2.5.2). For micelles to be formed

enough surfactant must be present to surround an oil molecule with the hydrophobic tail pointing into the oil phase and the polarised head pointing towards the continuous water phase. When a mixer is placed within the vessel [surrounded by the reagents], and turned on, energy is added to the system.

The addition of mechanical energy to the system, through mechanical agitation, causes emulsion formulation due to either the shear forces in laminar flow or the inertial forces in turbulent flow (Sarkar et al., 2009). These forces provide the energy required to raise the system from the lowest thermodynamic state; in which the lower density fluid lies above the greater density fluid with as small an interfacial barrier as possible, to a higher energy state where the phases are mixed (Mason et al., 2006a; Meleson et al., 2004). The flows generated by the mixer are entirely dependent on its design, it must be designed in a way that when activated it provides the system with enough energy to overcome the forces operating to resist distortion and subsequent break-up of the droplets (Bowman et al., 2006). The range of mixing devices used, and the type of mixing they produce within emulsion systems, is discussed in Chapter 3.

The role of the surfactant in an emulsion is to stabilise the droplets of the dispersed phase to prevent flocculation and coalescence. If the right concentration of surfactant is used and an emulsion is formed (section 2.3) the surfactant creates a barrier around the droplets of the dispersed phase as depicted in Figure 2-1. In the illustration the oil (yellow) phase is dispersed and broken down into droplets, emulsified by the surfactant (red) and distributed throughout the water (blue).

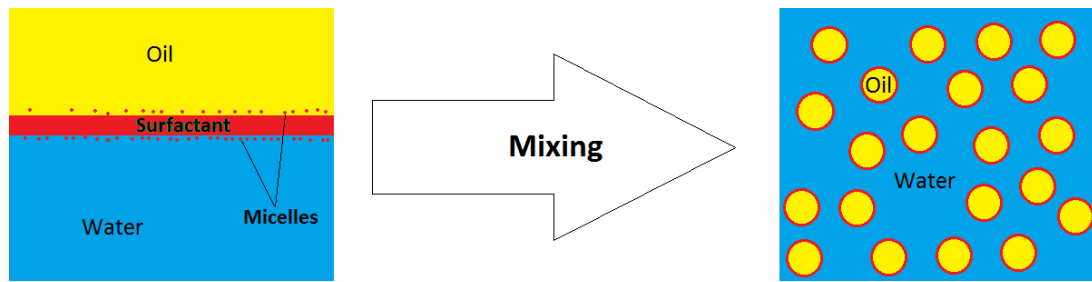




Figure 2-1 Illustration of emulsification.

While the most common form of emulsion is an oil-in-water emulsion, the inverse of this is also widely known. When the aqueous fraction is dispersed throughout an oil continuous phase then the emulsion formed is known as a water-in-oil emulsion (W/O) or an “inverse emulsion” (Forgiarini et al., 2001; Mason et al., 2006a). One of the most common examples of a water-in-oil emulsion is low fat margarine, whereby the water is dispersed through a continuous oil phase which is then stabilised by various monoglyceride derived emulsifiers including fat crystals. The fat crystals help stabilise the droplets in the emulsion as they act as a Pickering emulsion, discussed further in section 2.5.7.

Other less common but useful emulsions are oil-in-water-in-oil (o/w/o) emulsions and water-in-oil-in-water (w/o/w) emulsions. These emulsions are produced to overcome multiple barriers that would otherwise prevent the required reagents reaching the target destination; e.g. a pharmaceutical compound, only soluble in oil but to reach its target destination it must pass through a lipophilic barrier and then a hydrophilic barrier, would be possible using an oil-in-water-in-oil-emulsion. Using a water-in-oil-in-water emulsion it is possible to supplement products with sensitive micronutrients, mask flavours of bioactive compounds or even control the release of substances (Mun et al, 2011).

Many common consumer household products are an emulsion of sort, or they contain emulsions in their formulations, and a series of examples can be seen in Table 2-1.

Table 2-1 Examples of common household products that are emulsions

 <p style="text-align: center;">Milk (ARSN, 2012)</p>	<p>A complex oil-in-water emulsion that provides young mammals with necessary requirements to survive.</p> <p>Stabilised by phospholipids and protein, milk contains proteins in colloidal suspension as well as both fat and water soluble vitamins, minerals and enzymes in either or both of the phases, dependent on their properties (Redhead, 1990).</p>
 <p style="text-align: center;">Vinaigrette Dressings (Bauer, 2010)</p>	<p>Ranging from simple three ingredient recipes, to advanced unique recipes, vinaigrette dressings have been used to enhance green salads since ancient times (Sackett et al., 2009). The combination of vegetable oil, vinegar and salt forms a temporary emulsion that will eventually separate out which is why most pre-prepared bottles state “shake before use”.</p>



Mayonnaise

The order of addition of the ingredients involved, whilst mixing, makes mayonnaise an oil-in-water emulsion and not an inverse emulsion. Egg yolk, vinegar, salt and pepper are first homogenously dispersed throughout the mixing vessel before the oil is added slowly, sometimes as slow as drop by drop, forming a highly viscous oil-in-water emulsion [This, 2007].



Ice Cream
(Britton, 2007)




A complex colloidal product, ice cream is an oil-in-water emulsion, whilst also being a *sol* due to the presence of ice crystals and foam (a gas/water emulsion). Most common varieties of ice cream consist of 30% ice, 50% air, 5% fat and 15% sugar solution by volume [Clarke, 2012].

The formulation of ice cream in general terms is a combination of milk, corn syrup, emulsifiers and stabilizers (Hui, 2006).



Margarine

Margarine, unlike the other edible emulsions listed in this table, is a water-in-oil emulsion. By definition, a product can only be classed as margarine if there is a minimum of 80% by mass that is fat content (Hasenhuettl and Hartel, 2008).

 <p>Emulsion paints (Walfitpaints, 2012)</p>	<p>Paint pigments are bound to a synthetic resin such as urethane which is then dispersed within water forming an oil-in-water emulsion.</p> <p>When applied to a surface the water slowly evaporates away leaving the pigment carrier, in this example urethane, to coalesce which leads to polymerization reactions occurring of the particulates, and thus forms a single continuous layer containing the paint pigment (Monk, 2005).</p>
 <p>Insecticides/Pesticides</p>	<p>Formed (in basic terms) of a water insoluble active substrate dispersed within water and stabilised using one or more emulsifiers.</p> <p>The substrates in question are unique to the insecticide/pesticide and the organic matter it has been formulated to kill.</p>
 <p>Ointments and Creams</p>	<p>Can exist as either water-in-oil emulsions or oil-in-water emulsions. The greater the water content, the lower the viscosity and thus the easier to apply.</p> <p>It is known that of the two however only oil-in-water emulsions can be readily removed from both skin and clothing with water (Reilly, 2005).</p>

2.2.1 Dispersive and Distributive Mixing

Mixing is commonplace in households, businesses and commercial eateries throughout the world, from the simple distribution of solid particulates within a fluid medium (e.g. salt in water, sugar in tea, etc.) to more specialist dispersions such as home decorators formulating specific paint colours. There are three clear distinctive methods of mixing; dispersive mixing, distributive mixing and diffusive mixing (Werner et al., 2011). The breaking down of a large volume of liquid into droplets of the desired size is the definition of dispersive mixing, relevant when discussing work involving immiscible fluids (Todd, 2004). In order to reduce the size of the large droplets, energy is required and as such dispersive mixing can be thought of as the consequence of the fluid mechanic stresses imposed on the mixture (Todd, 2004). Unlike dispersive mixing, distributive mixing does not alter the size of the droplets but their location within the continuous phase (Vyakaranam et al., 2009). Distributive mixing seeks to alter the spatial uniformity of the droplets, upon reaching a perfectly uniform system there is nothing more distributive mixing can provide to that system (Todd, 2004; Wang, 2000). The number of droplets and their size range, per unit volume, in the continuous phase, becomes constant for perfect distributive mixing.

Diffusive mixing is characterised by an equilibrium concentration that results from the diffusion of molecules throughout a given volume. The diffusive process is a slow one when compared to the two mechanical mixing types however it is of importance for long term stability which is why, unlike the other types of mixing, it is less relevant in industrial processes (Werner et al., 2011). Diffusive processes can be described mathematically by Fick's first law (Equation 2-1) which accounts for

the transfer of material from an area of high concentration to an area of low concentration (Wang, 2008).

$$J = -D \frac{dc}{dx}$$

Equation 2-1 Fick's first law (Campbell, 2008)

Where:

J = flux (mol/m²·s)

D = diffusion coefficient (m²/s)

c = solute concentration (mol·m⁻³)

x = length (m)

The negative symbol is placed in front of the diffusion coefficient in Equation 2-1 because the concentration gradient is negative. According to Campbell this is because the diffusion is from a higher concentration to a lower concentration, however Bockris and Reddy, amongst others, claim the use of this is to make sure the value for the diffusion coefficient is positive (Campbell, 2008; Bockris and Reddy, 1998).

Improving diffusive mixing can be a positive secondary process of distributive mixing. Reducing the droplet size of a reagent that is the dispersed phase will increase the interfacial area between it and the continuous phase. Nguyen (2012) believes that by increasing the interfacial area, a larger concentration gradient is generated, and thus a higher diffusive flux (Nguyen, 2012).

Distributive and dispersive mixing of oil in water is displayed in an illustration in Figure 2-2 which also shows the impact of combining these two types of mixing techniques. The combination of these two types of mixing is highly sought after with respect to this work, as focus is on decreasing the droplet size and creating a

uniformly distributed system in order to maximise the available surface area of the dispersed phase.

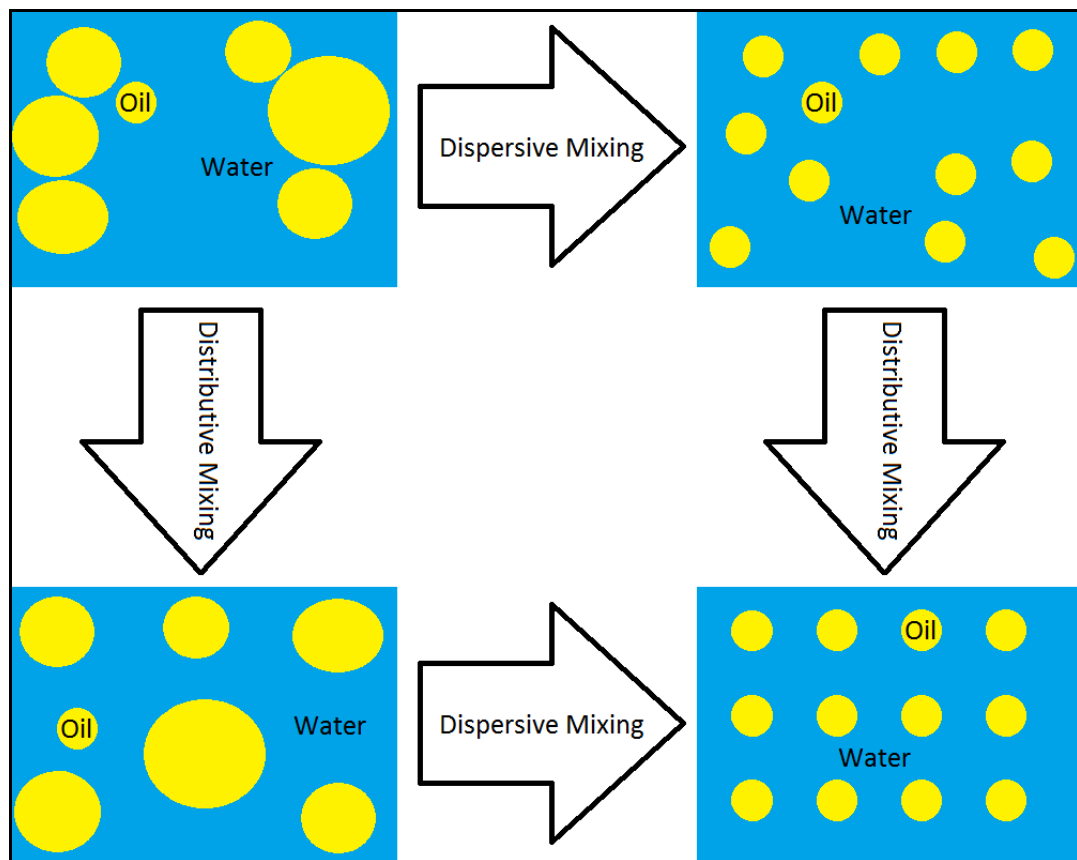


Figure 2-2 Illustration of distributive and dispersive mixing.

In order to uniformly distribute the *dispersed phase* within a *continuous phase* permanently the electrostatic forces need to be identified, quantified and balanced (i.e. the strength of the attractive and repulsive forces). The distribution of small, solid particulates within a fluid medium (e.g. Zeolite powder within water) requires the charge of the solid molecules and the polarity of the fluid medium to be taken into account; pouring solid particulates into a vessel of fluid immediately leads to sedimentation and agglomeration upon the bottom of the reaction vessel and a clear distinction between the two phases. The application of a mixer to this vessel, one capable of shear rates that provide greater energy than that required to break the attractive bonds between the particulates, leads to particulates being distributed

throughout the fluid medium within the vessel. With the right balance of charge, i.e. the formation of equilibrium, the particulates will remain uniformly distributed throughout the fluid medium.

Once the balance is tipped either way, the distribution will become minimal and focussed, and both the small droplets and particulates will begin to quickly coalesce. In the case of colloids or emulsions, flocculation will occur, the product of which is creaming.

2.2.2 Laminar and Turbulent Flow

There are three flow regimes that describe how fluid is behaving when it is flowing through a pipe. The two main types of flow are laminar and turbulent, the other type of flow is transitional and that is used to describe the flow of fluid that is between the laminar and turbulent flow regions.

$$Re = \frac{\rho u d}{\mu}$$

Equation 2-2 Reynolds equation

Where;

Re = Reynolds number

ρ = density of fluid (kg/m^3)

u = velocity of fluid (m/s)

d = diameter of pipe (m)

μ = viscosity of fluid ($\text{kg/m}\cdot\text{s}$)

The Reynolds number [Equation 2-2] was first published by Osbourne Reynolds in the late 19th century and is the ratio of inertial forces to viscous forces. The equation takes into account the density, velocity and viscosity of the fluid; as well as the

diameter of the pipe in which it is travelling, and could be regarded as the most important dimensionless number in fluid mechanics.

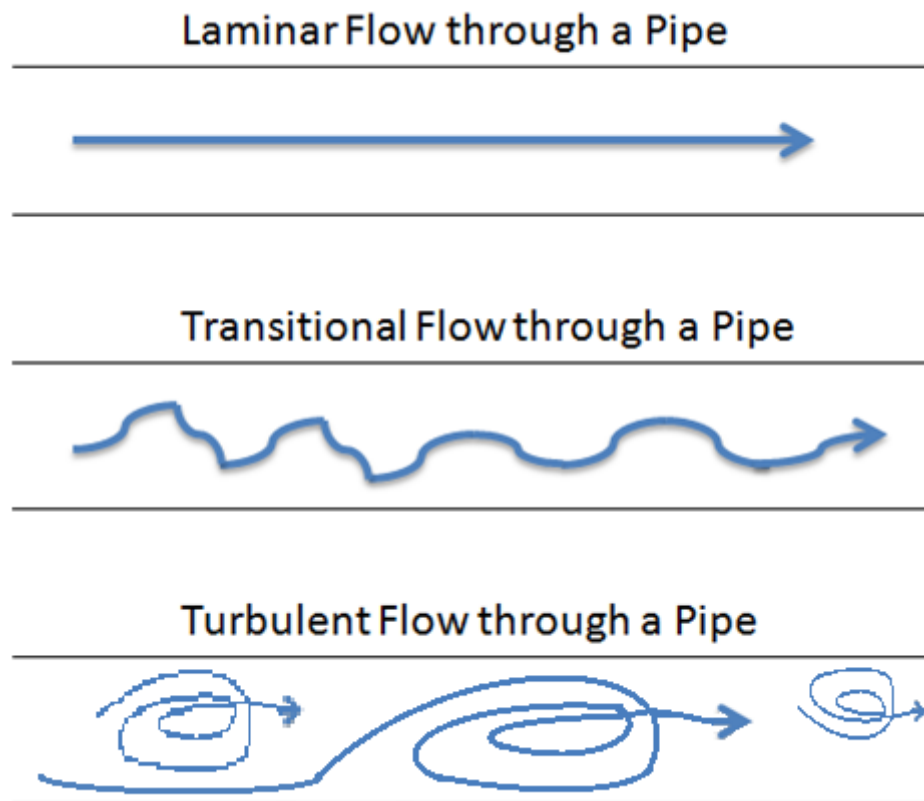


Figure 2-3 Illustration of different types of flow.

Laminar flow, in a pipe, occurs when the Reynolds number is less than 2000 and is dominated by fluid viscosity e.g. high viscosity fluid or narrow pipe-work. Within a flowing fluid system, the liquid will break-up into droplets should turbulent fluctuations and/or oscillations increase past the local shear rate (Liu, 1999).

Turbulent flow is commonly found when low viscosity fluid is travelling at high velocity through larger pipe-work and where the Reynolds number is in excess of 4000. Droplet break-up occurs within the turbulent flow if the interfacial tension and drop viscosity are exceeded by the instantaneous stresses generated during turbulent flow (Podogorska and Baldyga, 2000).

In between laminar and turbulent flow is another type of flow known as transitional flow. Transitional flow has a Reynolds number between 2000 and 4000 and has characteristics of both laminar and turbulent flow in that, although the flow is in one direction, it does not travel smoothly as in laminar flow but is not as turbulent as in turbulent flow.

2.2.3 Droplet Creation Mechanisms

When an emulsion is formed the dispersed phase consists of droplets within the continuous phase. To further break-up these droplets the viscosity of the droplet and the interfacial tension stress holding the droplet together must be taken into account. These factors must be overcome in order to further deform and eventually break-up the droplet. The Laplace pressure (Equation 2-3) is the name given to the resistance to deformation by the droplet and is the product of the surface tension and the inverse of the radius (Walstra, 2003) As the droplet size gets smaller, the Laplace pressure increases and thus a greater force is required to overcome it (Walstra, 2003).

$$\Delta P = \gamma \left(\frac{1}{R_1} + \frac{1}{R_2} \right)$$

Equation 2-3 The Young-Laplace Equation (Butt et al., 2003)

Where;

ΔP = Laplace Pressure

γ = surface tension

R_1 and R_2 = principle radii of curvature

$$\tau_{BU} = \tau_{IT} + \tau_{DV}$$

Equation 2-4 Stress balance equation (Leng and Calabrese, 2004)

Where:

τ_{BU} = Break-up stress required to break-up the droplet

τ_{IT} = Interfacial tension stress holding the drop together, namely the Laplace pressure

τ_{DV} = Droplet viscosity resisting deformation

The balance of stress equation [Equation 2-4] shows that the amount of force required to break-up a droplet is equal to the interfacial tension stress holding it together and the stress resisting deformation due to the viscosity of the droplet. Only when the interfacial tension stress and the viscosity of the droplet are overcome can the droplet be broken down.

Boonen et al (2010) describe four droplet break-up mechanisms for droplets within Newtonian fluids:

- Increasing flow strength, gradually, leads to the droplet “necking” in the middle and eventually forming two equal-sized daughter drops. This is referred to also as *Binary Break-up*.
- Increasing the flow strength quickly with a strong force results in a highly elongated thread. *Sinusoidal perturbations* (Rayleigh instabilities) are formed at the end of this thread which develop and subsequently lead to a break-up into a string of smaller droplets.
- When strong flow stops, or there are step changes in the flow, the *end-pinching mechanism* can occur.
- *Tip streaming* is a droplet break-up mechanism in which at the pointed ends of a parent drop, small drops are released. This is mainly attributed to the impurities or a non-uniform surfactant distribution along the droplet surface and as such is not a general break-up mechanism.

Capillary break-up is regarded as a laminar flow process and within emulsions the capillary number is what determines whether deformation will occur. This is because the capillary number is the ratio of interfacial stress resisting break-up to the imposed viscous stress promoting break-up (Nijenhuis et al., 2007).

$$Ca = \frac{\eta\dot{\gamma}a_0}{\sigma_1}$$

Equation 2-5 Capillary number equation (Nijenhuis et al., 2007)

Where:

Ca = Capillary number

η = viscosity of continuous phase

$\dot{\gamma}$ = shear rate

a_0 = droplet radius

σ_1 = interfacial tension

In Equation 2-5 it can be seen that the capillary number is subject to the force of the interfacial tension and the radius, otherwise known as the interfacial stress. When the interfacial stress is less than the viscous stress being applied, the capillary number is said to have exceeded the critical capillary number and it is when this occurs that the droplet undergoes break-up (Nijenhuis et al., 2007). At a lower capillary number, the droplet may be deformed or stretched but the shape is stable and no break-up occurs. Equation 2-5 was developed for Newtonian fluids, for non-Newtonian fluids it is not straight forward to use as the viscosity is dependent on the shear rate and can therefore be difficult to define.

The viscosity of the droplet is incorporated into this approach by plotting the critical capillary number (Ca_{cr}) for break-up to occur as a function of the viscosity ratio of the drop to continuous phase. Grace (1982) is generally acknowledged as the first to

summarise this graphically and to this day, when new data is generated and presented, it is referred to as a "Grace diagram" (Figure 2-4).

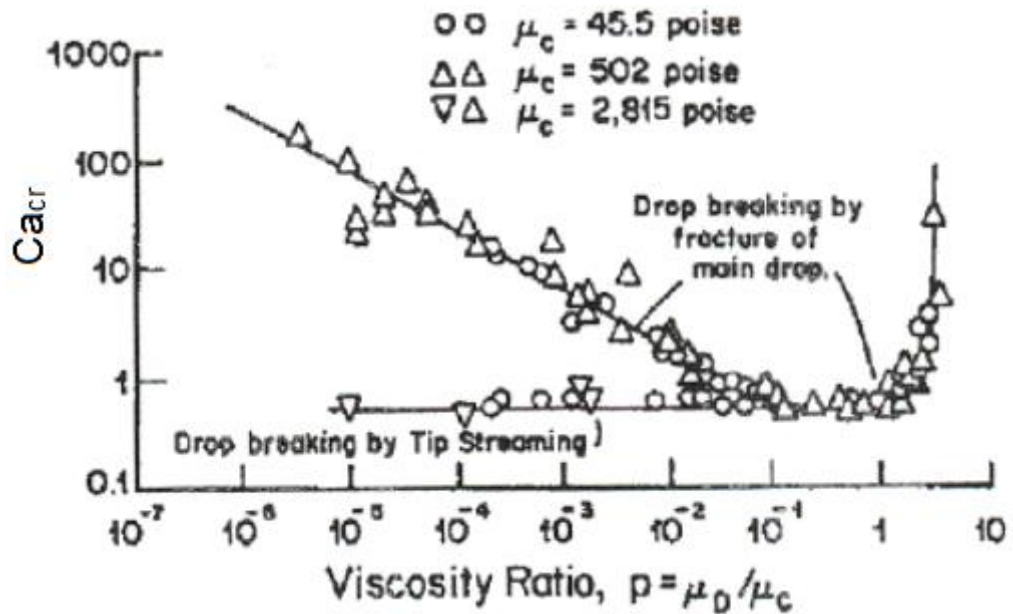


Figure 2-4 Critical capillary number over viscosity ratio (Grace, 1982)

The critical capillary number Ca_{cr} depends on the type of flow. In extensional flow it is possible to get break-up of a lower capillary number than in pure shear flow. Extensional flow also allows more viscous drops to be broken up. In turbulent flow the same principles apply, except that the flow component is produced by the turbulence. Droplets that are bigger than the turbulence length scale (referred to as the Kolmogorov length scale) are scaled using standard Weber number scaling (Adams, 2013).

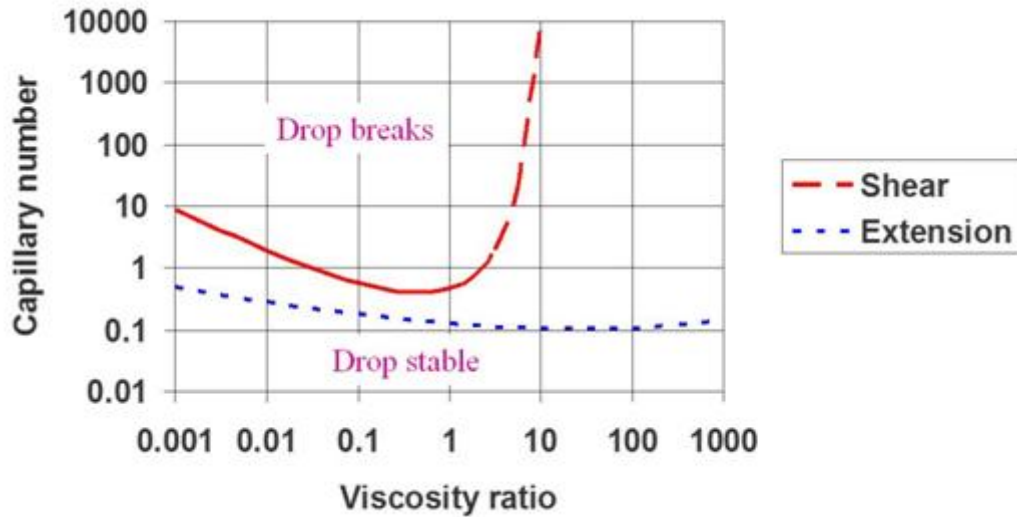


Figure 2-5 Graph showing the impact of shear and extensional flow on the capillary number of fluid at increasing velocity (Baker, 2011).

Figure 2-5 shows that in order to break a droplet of high viscosity, extensional flow is needed to deform the droplet. The design of the Controllable Deformation Dynamic Mixer (CDDM) within the UMPF is that it is able to break down droplets following deformation from extensional flow. The UMPF is discussed in greater detail in Chapter 3.

2.3 Overview of Droplet Break-up Mechanisms with Respect to Power Density

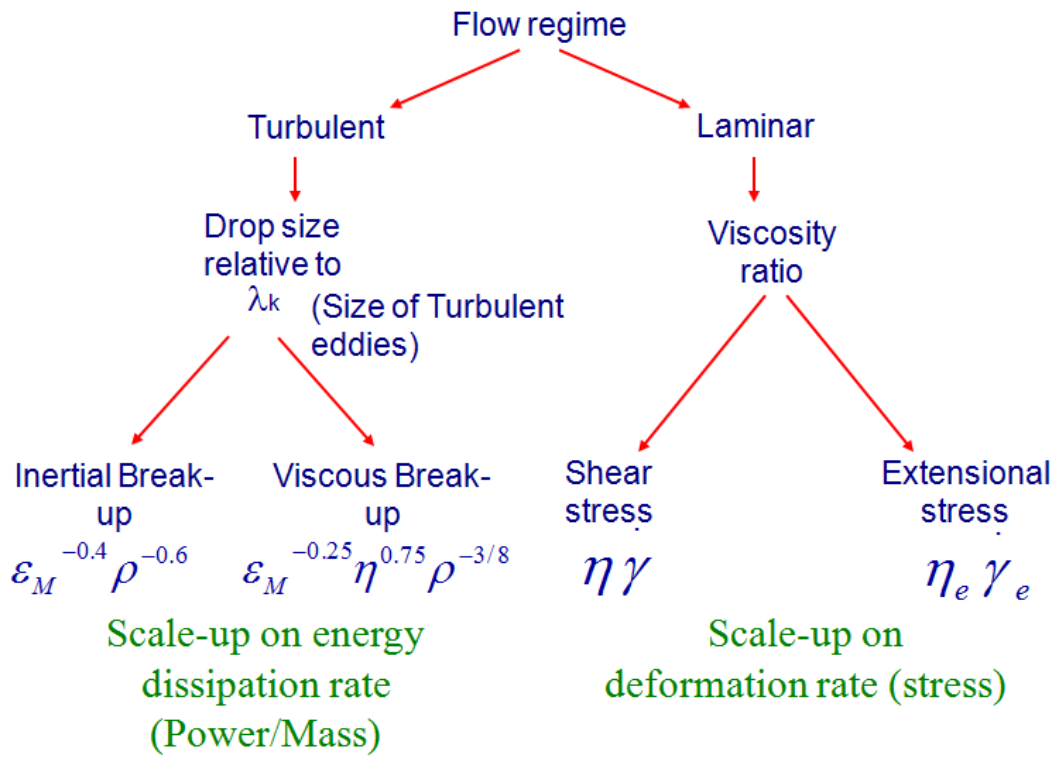


Figure 2-6 Summary of break-up mechanisms (based on work by Mike Baker and Adam J Kowalski).

Where:

λ_k = Kolmogorov length scale

ϵ_M = Energy dissipation rate per unit mass of mixer volume ($\text{W} \cdot \text{kg}^{-1}$)

ρ = Fluid density ($\text{kg} \cdot \text{m}^{-3}$)

η = Fluid viscosity ($\text{Pa} \cdot \text{s}$ or $\text{kg}/\text{m} \cdot \text{s}$)

$\dot{\gamma}$ = Shear stress (Pa or $\text{kg}/\text{m} \cdot \text{s}^2$)

The flow chart in Figure 2-6 presents a summary of break-up mechanisms. It can be seen that the two extreme types of flow regime, turbulent and laminar, are analysed separately with respect to droplet break-up. The Reynolds number allows determination as to which type of flow the fluid is undertaking, and thus which route of droplet break-up it will follow. From this information alone it can be seen why the

Reynolds number is regarded by many as the most important dimensionless number in fluid mechanics. If the fluid flow is turbulent, then the droplet break-up mechanism is likely to be either inertial break-up or viscous break-up. The size of the eddies within the fluid has an impact on which type of turbulent break-up the droplets will undergo. Eddy dimensions are the smallest scales of motion and are characterised by the Kolmogorov length scale (Kresta and Brodkey, 2004). When the inertial forces, due to turbulent velocity fluctuations, are approximately equal to the viscous forces in the eddy, then it is said to be residing within the Kolmogorov length scale (Kresta and Brodkey, 2004). In essence the Kolmogorov length scale defines the size of the largest eddy that can exist. Smaller eddies don't have enough energy to overcome the internal viscous forces and hence cannot exist. Should the droplets be larger in size than the eddies within the fluid, then inertial break-up occurs; if the droplets are smaller than the eddies, viscous break-up is responsible for further droplet break-up (Azzopardi et al., 2011).

Should the fluid be travelling as laminar flow then the droplet break-up mechanism will be shear stress or extensional stress, dependent on the viscosity ratio. The term *viscosity ratio* is used to describe the ratio of the viscosity of the dispersed phase, to that of the continuous phase. Both Figure 2-4 and Figure 2-5 show clearly the type of force required for droplet break-up to occur in fluid undergoing laminar flow with respect to the viscosity ratio. The droplet break-up mechanisms in laminar flow are expanded from the basic principle that when the cohesive effect of surface tension has been surpassed by the disruptive stress, caused by the viscous drag of the fluid, the droplet will break-up (Utracki and Favis, 1989).

When the viscosity ratios are very low the droplet will become deformed but not break, and when the viscosity ratios are too high then the viscous forces that disrupt

the drop cannot overcome those forces keeping it together. In either of these extreme instances, extensional stress (also referred to as extensional flow field) provides an effective droplet break-up mechanism (Utracki and Favis, 1989).

2.4 Overview of Droplet Break-up Mechanisms with Respect to Energy Density

An alternative method to using power density to assess droplet break-up mechanisms is to observe the energy density. In their work published in 1995 Karbstezh and Schuber declared that for continuous droplet disruption, that is droplet break-up where the residence time within the mixing chamber is less than a few tenths of a second and coalescence is avoided, the mean droplet diameter of emulsion droplets can be described as a function of the energy density.

Energy density values can be calculated through observation of both the power input and the flow rate of fluid into the mixer, and dividing the former by the latter (power input/flow rate).

$$x_{1,2} = C (E_v)^{-b}$$

Equation 2-6 Mean droplet diameter as a function of energy density
(Karbstezh and Schuber, 1995).

Where:

$x_{1,2}$ = mean droplet diameter (μm)

C = constant dependent on the dispersed phase viscosity

E_v = Energy density ($\text{J}\cdot\text{m}^{-3}$)

b = a second constant

Equation 2-6 was devised by Karbstezh and Schuber and is analogous to those developed by for power density (1995). They state that if the key factor of droplet disruption is turbulence, then b will be in the order of 0.4 (Karbstezh and Schuber,

1995). In 2004, Schubert and Engel published the results of further work expanding on this and show that if b is in the order of 0.4 then turbulent inertia forces are responsible for droplet break up, and if b is in the order of 0.5 then turbulent shear forces are the primary factor in droplet break-up (Schubert and Engel, 2004).

2.5 Overview of Published Work on Rotor-Stators

This sub-section looks to provide an overview of published work involving biphasic systems, in particular emulsions, formulated using rotor-stator mixing devices. According to Atiemo-Obeng and Calabrese [in 2004], “the fundamental basis for which the understanding of rotor-stators is based is nearly non-existent, in particular there is very little work reported on multiphase and high-viscosity fluids” (Atiemo-Obeng, 2004). They state quite clearly that with no clear knowledge base for performing work with rotor-stator devices, engineers perform scale-up trials “*through engineering judgement and trial and error instead of sound engineering principles*” (Atiemo-Obeng, 2004). It is through large-scale trials with no scientifically clear basis, that large amounts of resources and money are lost.

The measurement of power is required for the emulsification correlations based on both power density (section 2.3) and energy density (section 2.4). For pressure driven equipment (e.g. high pressure homogeniser) the power measurement is simply obtained from the pressure drop, which is easy to measure. The key challenge is the prediction of power draw and measurement of in-line rotor-stator mixers. In the review of emulsification, scale-up is done on the basis of energy dissipation rate (sometimes referred to power density), and is given by power draw divided by the mixer volume over which it is dissipated. In batch mixers the power characteristics

of a mixer is determined following the outcome of the power draw equation detailed in Equation 2-7.

$$P = P_o \rho N^3 D^5$$

Equation 2-7 Power equation for batch mixers.

Where:

P = power (W)

P_o = power number which remains constant for geometrically similar systems

ρ = density ($\text{kg}\cdot\text{m}^{-3}$)

N = impeller speed (s^{-1})

D = impeller diameter (m)

Whilst successfully used for batch mixers for decades, it does not adequately predict the power draw of an in-line mixer where the flow rate can be changed and controlled. In 2009, Kowalski developed an expression which would allow for the calculation of delivered power for an in-line rotor-stator device. This equation [Equation 2-8] is based on the traditional power number approach for batch vessels, with the addition of an extra term that takes into account the impact of flow rates.

$$P = P_T + P_F + P_L$$

Equation 2-8 Power equation for in-line rotor-stators (Kowalski, 2009).

$$P_T = P_{oz} \rho N^3 D^5$$

Equation 2-9 Power required to rotate the rotor against the liquid in the gap (Kowalski, 2009).

Nomenclature for Equation 2-9 is as per Equation 2-7 with the difference that P_{oz} is analogous to P_o in batch mixers when the flow through in-line mixers is zero. This is because as power draw increases with flow increase.

$$P_F = k_1 M N^2 D^2$$

Equation 2-10 Additional power requirements from the flow of liquid through the gap (Kowalski, 2009).

Nomenclature for Equation 2-10 is as per Equation 2-7 with the addition of:

k_1 = a proportionality constant determined as part of the fit.

M = mass flow rate ($\text{kg}\cdot\text{s}^{-1}$)

P_L in Equation 2-8 is the power lost which can be through vibration, noise, kinetic energy losses at the entrance and exit and/or the accuracy of the measurements taken.

When processing Equation 2-8, P_L is to be taken as a constant which is calculated by the fitting procedure (Kowalski, 2009).

The expression in Equation 2-8 was validated using a Siefer Trigonal mill to reduce the particle size of calcite and soda ash slurries, with the power being determined from the motor current. The expression collapsed the data from various conditions and is presented in Figure 2-7.

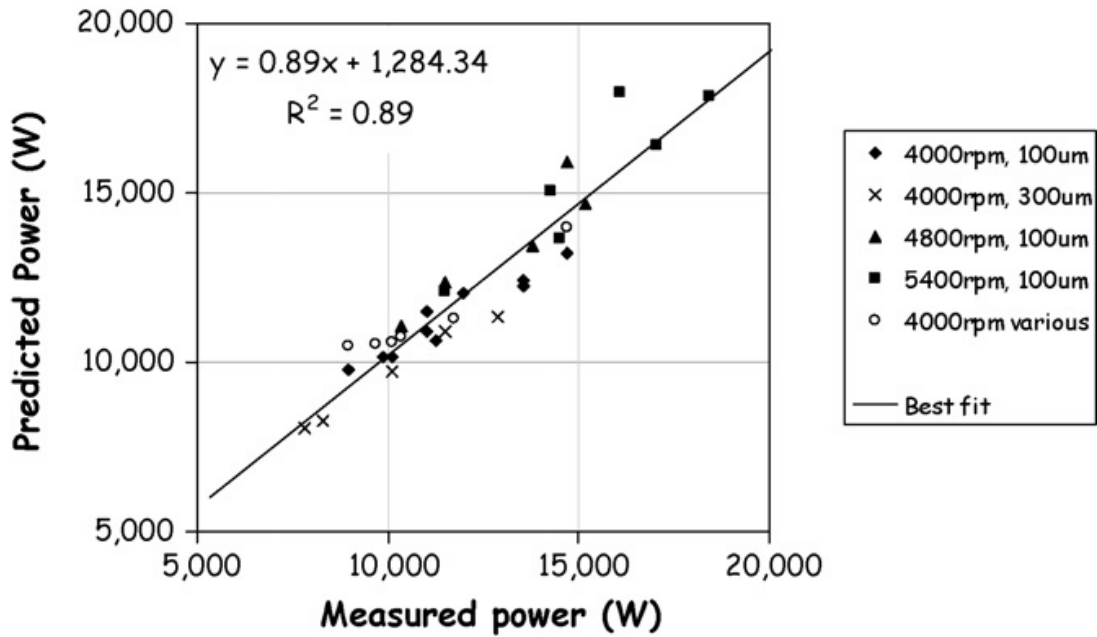


Figure 2-7 Predicted and measured power consumption for soda ash slurry (Kowalski, 2009).

Although the gradient of the line of best fit is significantly less than unity [R^2 being 0.89], and there is also an appreciable zero offset, these factors can be attributed to assumptions made about the characteristics of the motor under various loads, as well as the fact that the viscosity of the slurries changed as they were milled.

Building on the work published in 2009, Kowalski, Hall and Cooke we on to carry out much more careful experiments. They fitted a Silverson in-line with a torque meter, and also used a calorimetric technique [temperature assessment], to measure the power of the mixer. During these trials focus was given to turbulent flow where it is believed the power number should be constant. The predictions that resulted from this work were a great improvement on the previous work; the R^2 value was increased from 0.89 by 0.106 [12% increase] to 0.996. The alignment of data to the line of best fit is displayed in Figure 2-8.

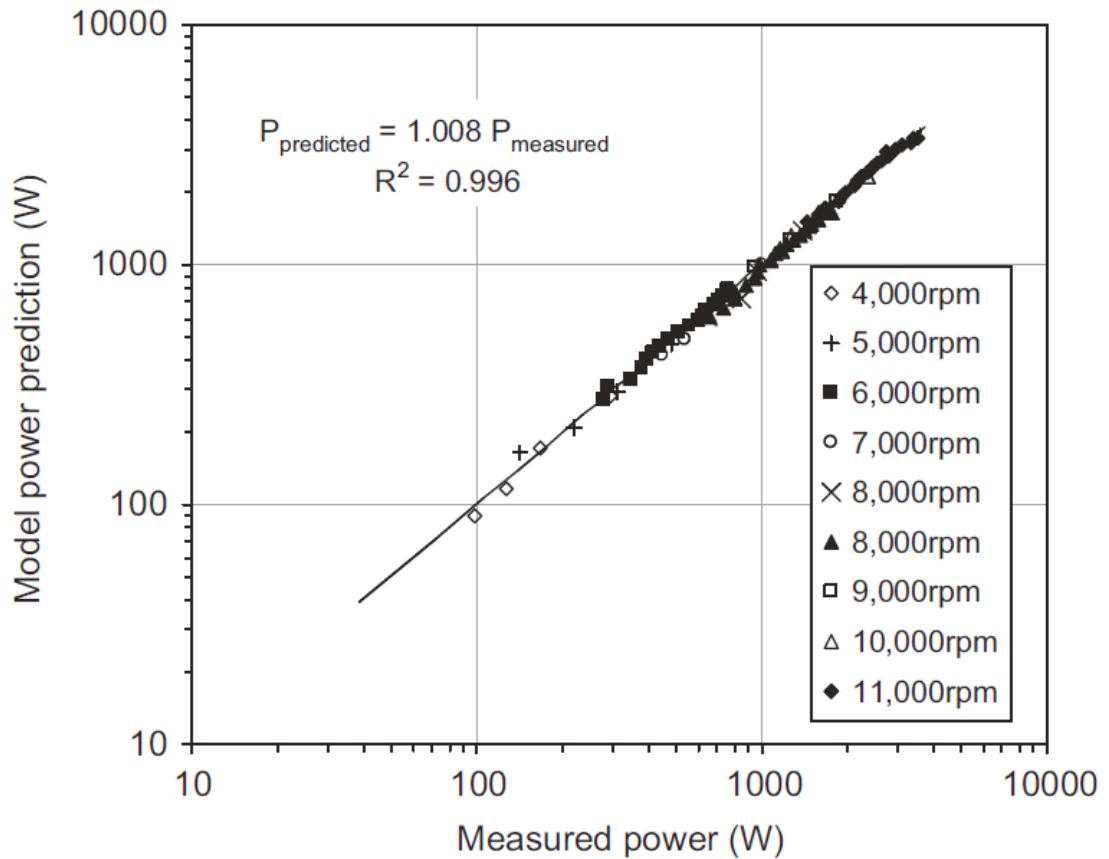


Figure 2-8 Theoretical power versus measured power, using constants from regression to torque data (Kowalski et al., 2011).

In 2013, Hall et al published work of scale-up trials that they had performed using the knowledge base they had been building on the impact of rotor-stator mixing devices on the size of droplets. They showed how they had measured the power draw characteristics of 3 different sizes of Silverson; ranging from a laboratory scale (1.5" rotor), to pilot plant (2.5" rotor) and finally, up to and including production scale size (6" rotor). Despite an increase in the size of the mixer (and therefore processing volume), all three machines maintained geometric similarity allowing for a scale-up laws to be determined using them. Unfortunately, only the pilot plant scale machine was fitted with a torque meter so the calorimetric technique was used to measure power and the constants obtained were similar at each scale and are displayed in Table 2-2.

Mixer Size	“Zero flow” Power Constant (P_{o_z})	Standard Error for P_{o_z}	Flow Power constant (k_1)
Laboratory	0.254	0.034	9.59
Pilot Plant	0.229	0.004	7.46
Factory Scale	0.231	Not published.	11.80

Table 2-2 Power constants obtained by Hall et al (2013).

This result is what they hoped to ascertain as it is consistent with batch mixers where, for mixers of similar geometry, the power number is constant and the effect of scale (i.e. rotor diameter) is accounted for by the inclusion of the D term (Equation 2-7, Equation 2-9 and Equation 2-10). This allowed the modification of the Kowalski power equation for rotor-stators, Equation 2-8, to be specific for Silverson in-line rotor-stator mixers, and is shown in Equation 2-11.

$$P = 0.252\rho N^3 D^5 + 6.90MN^2 D^2$$

Equation 2-11 Modified power draw equation for Silverson in-line rotor-stator mixers at varying sizes (Hall et al., 2013).

Using Equation 2-11 engineers can now predict, to within 20% accuracy (more than sufficient for engineering calculations), how much power will be used during Silverson in-line rotor-stator mixing experiments. The power used during the experiments is calculated as a function of both the process parameters and the scale, and as such it can be used for different sizes of mixer.

In their 2012 publication, Cooke, Rodgers and Kowalski discuss how they measured the full power curve for a Silverson 150/250 MS in-line rotor-stator pilot plant scale

mixer. They used silicone oils of varying viscosity, from 10 cSt, up to and including 10,000 cSt; as well as observing the torque during each run which allows for the determination of the power draw.

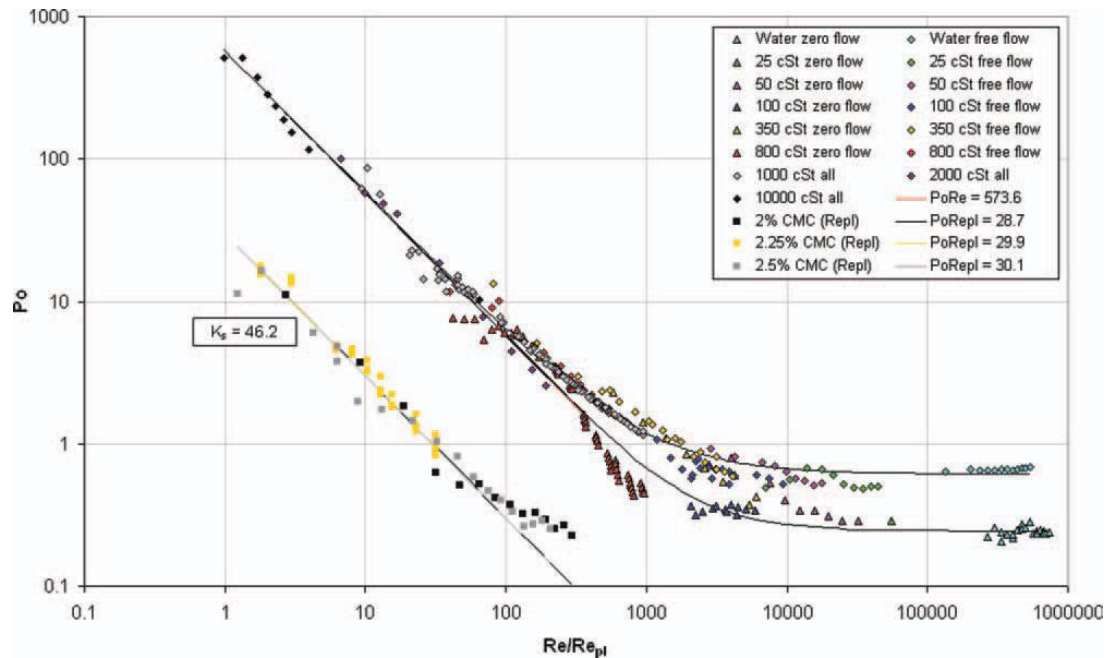


Figure 2-9 All power number data for Silverson 150/250 MS in-line rotor-stator mixer fitted with standard dual rotor-stator (Cooke et al., 2012).

The resulting power curve displayed in Figure 2-9 shows all the features expected with a constant power number in the turbulent regime ($Re > 10,000$); and in the laminar regime ($Re < 1000$), the power is proportional to $1/Re$. The effect of flow rate was only obvious in the turbulent regime where the higher the flow rate, the higher the effective power number.

The use of an in-line Silverson rotor-stator mixer and the impact it has on droplet break-up was published by Hall et al, in 2011. For all emulsions processed during the trials, a constant factor was the concentration of “SLES 2EO” surfactant that was used (Hall et al., 2011). For every experiment performed, the concentration of surfactant used was 0.5 wt%. The phase fraction of oil observed was at 1, 5, 25 and

50% of the emulsion formulation and the viscosity of the Dow Corning silicone oil used ranged from 9.4 to 969 cSt. The viscosity of the continuous phase was also increased, through addition of carboxyl methyl cellulose (this is shear thickening when a solution). The amount of carboxyl methyl cellulose used was increased with the phase fraction of oil and was added appropriately to create a range of viscosities when operating the mixer at 11,000rpm.

Their work concluded the primary influence on the size of the droplets within emulsions formulated using a Silverson in-line rotor-stator mixer is the rotor-speed (Figure 2-10).

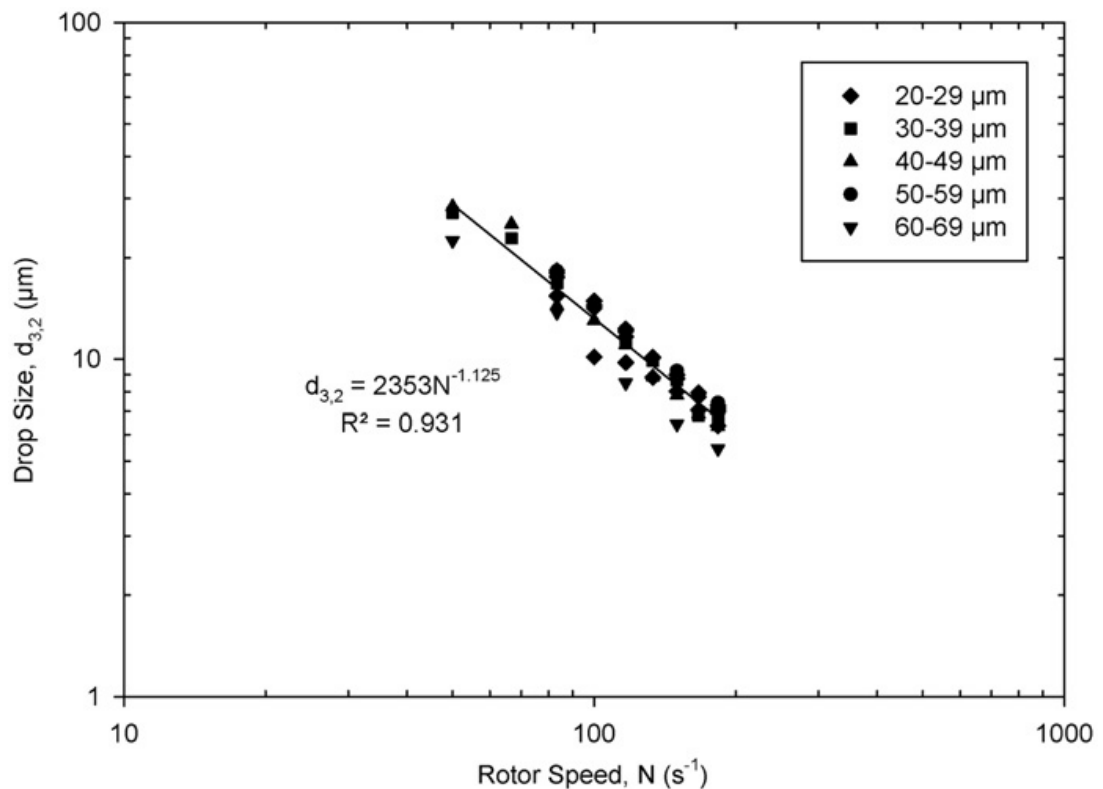


Figure 2-10 Droplet size as a function of rotor speed at 300 kg/h flow rate and a dispersed phase viscosity of 339 cSt (Hall et al., 2011).

Further to this, it was also discovered and concluded that reducing the droplet size of an emulsion through increasing the speed of the mixer head is almost independent of flow rate; as can be observed in Figure 2-11.

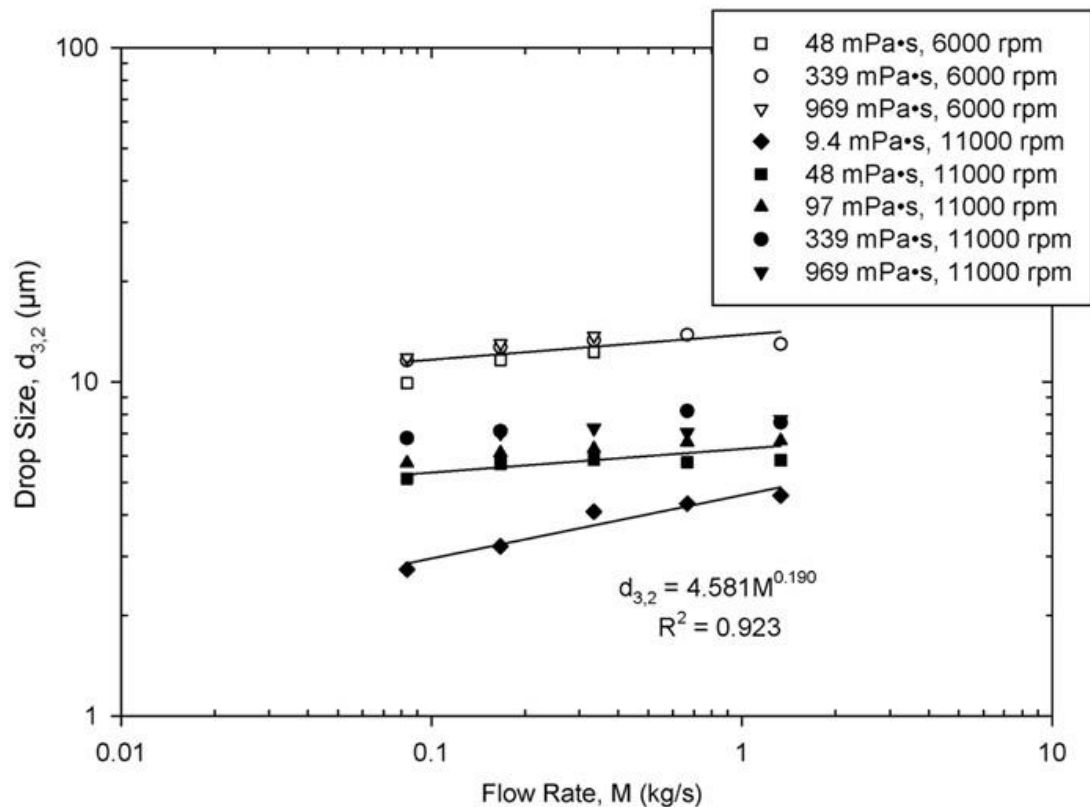


Figure 2-11 Droplet size as function of flow rate for 1 wt% silicone oil emulsions at 6000 rpm and 11,000 rpm (Hall et al., 2011).

The correlation between droplet size and rotor speed suggested turbulent inertial break-up as the size of the droplets within the emulsion were larger than the Kolmogorov scale.

The droplet size of the emulsion produced using the lowest viscosity oil was reduced slightly, as was the flow rate. For this low viscosity oil specifically, the results show that the residence time within the mixer head is a factor and the kinetic energy generated from increasing the flow is counterproductive when looking to reduce droplet size. For all the other oils, that is those with a viscosity greater than 10 cSt, the impact of the flow rate on the droplet size can be considered weak. Although a higher flow rate requires a larger power draw from the Silverson, the relative weak

dependence on flow rate means that it is much more energy efficient to process at a higher flow rate.

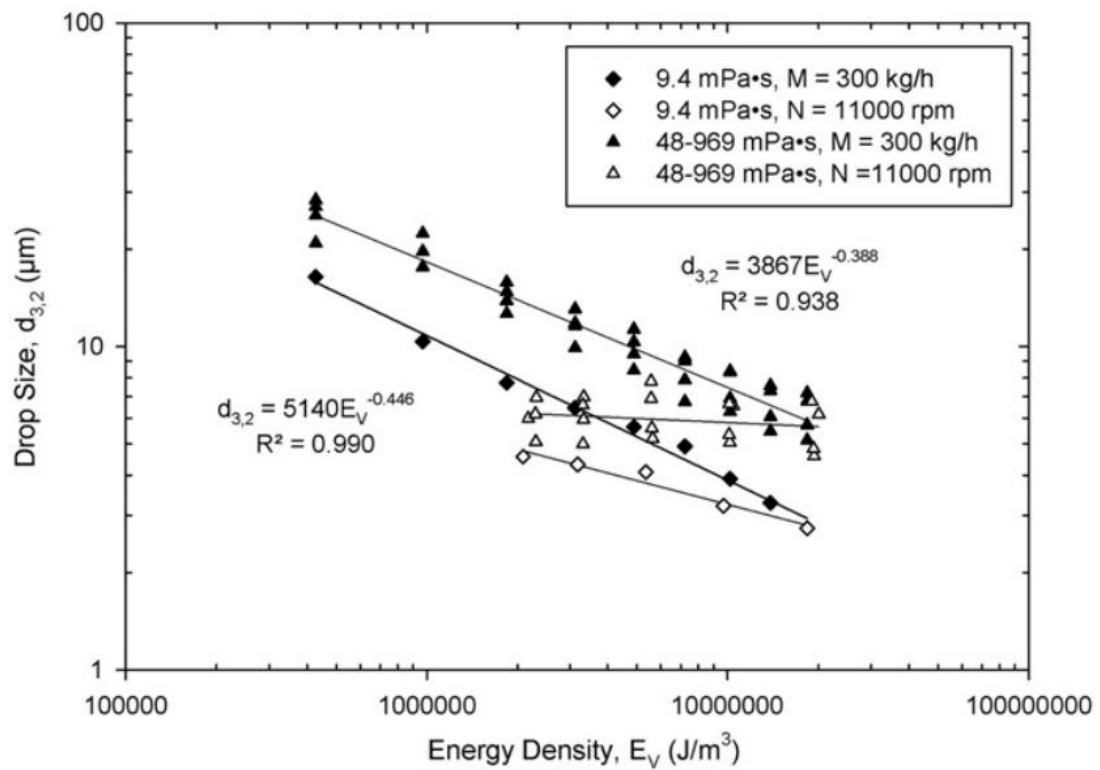


Figure 2-12 Droplet size as a function of energy density (Hall et al., 2011).

The data obtained by Hall et al (2011) displayed in Figure 2-12 shows the size of the droplets as a result of the energy density, that being a product of power divided by flow rate. It shows that for a given oil viscosity [48-969 cSt] it is possible to get a smaller droplet size for the same energy consumption per volume of liquid by operating at a high flow rate. It is therefore more economically efficient to run the Silverson at the highest rotor speed and at the highest flow rate, rather than a lower rotor speed and high residence time (i.e. low flow rate) as a greater volume of product will be processed, with a small increase on the size of the droplets. This is true even for the low viscosity oil (9.4 cSt) which showed the greatest dependency on flow rate, although the reduction in energy was not as great.

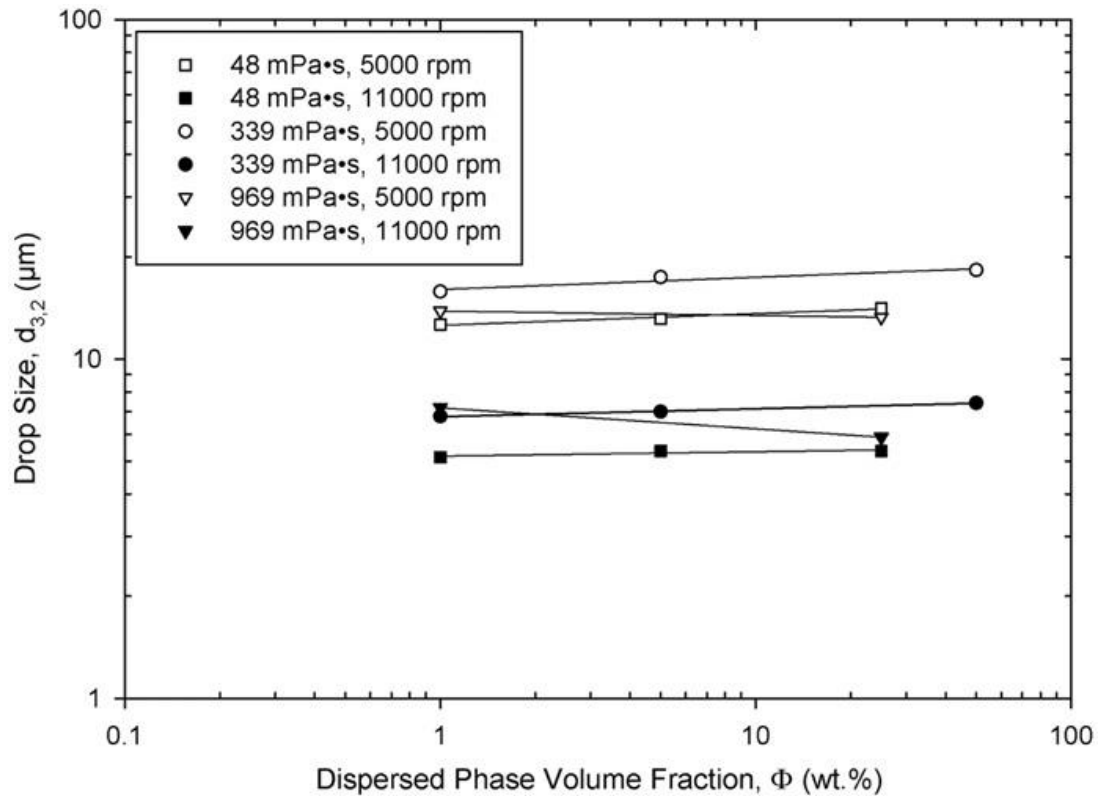


Figure 2-13 Droplet size as a function of the dispersed phase volume fraction at both 5000 rpm and 11,000 rpm, and a constant flow rate of 300 kg/h (Hall et al., 2011).

In addition, the dispersed phase volume fraction also made minimal impact on the resulting size of the droplets within the emulsion. Observation of the data displayed in Figure 2-13 leads to the conclusion that when increasing the dispersed phase volume fraction by a factor of 10 the droplet size increased by approximately 1%. As with the flow rate, the impact that the dispersed phase volume fraction had on the resulting droplet size of the emulsion was independent of the viscosity of the dispersed phase.

It can be stated from the data obtained and described, that processing the greatest phase volume of oil at the highest rotor speed and fastest flow rate is the most energy efficient way of running the equipment in order to obtain an emulsion with the smallest droplet size. Processing an emulsion with an oil phase volume of 50% is

fifty times more energy efficient, as the negative impact of larger droplets being produced is not an issue based on the working at 1% data displayed in Figure 2-13. Increasing the flow rate to allow for faster production has little negative impact also as the data displayed in Figure 2-11 shows. With the exception of the lowest viscosity oil (9.4 cSt), increasing the flow rate by a factor of 10 increases the droplet size by approximately 1%.

Further to this, Hall went on to report that the viscosity of the dispersed phase within the emulsion results impacts directly on the size of the droplets. As the viscosity increases, so does the droplet size until a plateau is reached between 97 mPa·s and 969 mPa·s (Figure 2-14). Extensional flow is believed to be the breakage mechanism at the highest viscosity fluid analysed based on the bimodal distribution of the volume drop size (Hall et al., 2011).

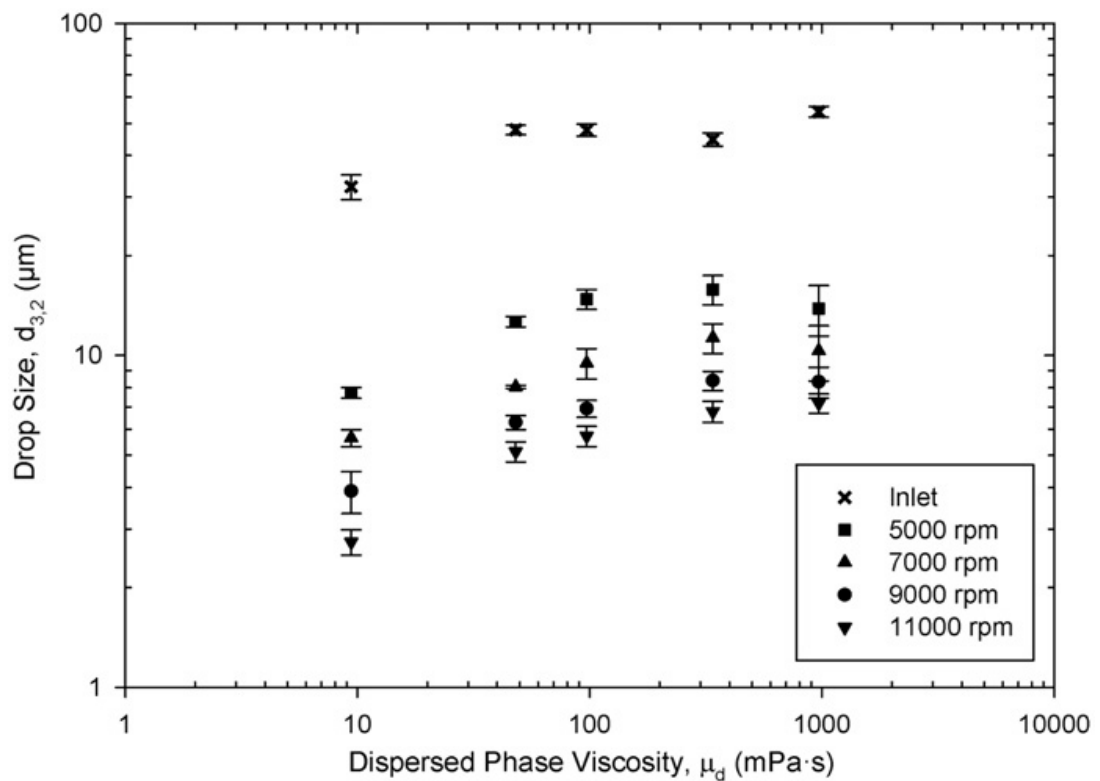


Figure 2-14 Droplet size as a function of viscosity of the dispersed phase (Hall et al., 2011)

As discussed previously, in 2013 Hall et al., published further research and development in investigating the impact of Silverson rotor-stator mixers in a paper entitled “The effect of scale and interfacial tension on liquid-liquid dispersion in in-line Silverson rotor-stator mixers” (Hall et al., 2013). The focus of this research was entirely on the impact of scaling up the rotor-stator mixer and so all emulsions were 1 wt% silicone oil with viscosities of either 9.4 cSt or 339 cSt in water, and all emulsions were stabilised with 0.5 wt% SLES.

Their work detailed that drop size distributions at laboratory, pilot-plant and factory scale are “practically identical” implying that the break-up mechanisms the droplets undergo must be similar. From the data in Figure 2-15 it can be seen that as the tip speed increases, the droplet size decreases. This is in line with previous findings that stated the most influential factor on the size of the droplets within an emulsion made using a Silverson in-line rotor-stator mixer was the mixer speed, as the calculation of the tip speed is reliant on the speed of the mixer. The rotor energy dissipation rate was also observed and recorded, however the correlation of droplet size as a function, for increasing viscosities, when the results were plotted was less accurate than the tip speed. When droplet size was plotted as function of rotor energy dissipation rate the R^2 value was 0.838 in comparison to the more accurate R^2 value of 0.971 obtained when droplet size is plotted as a function of tip speed, as shown in Figure 2-15.

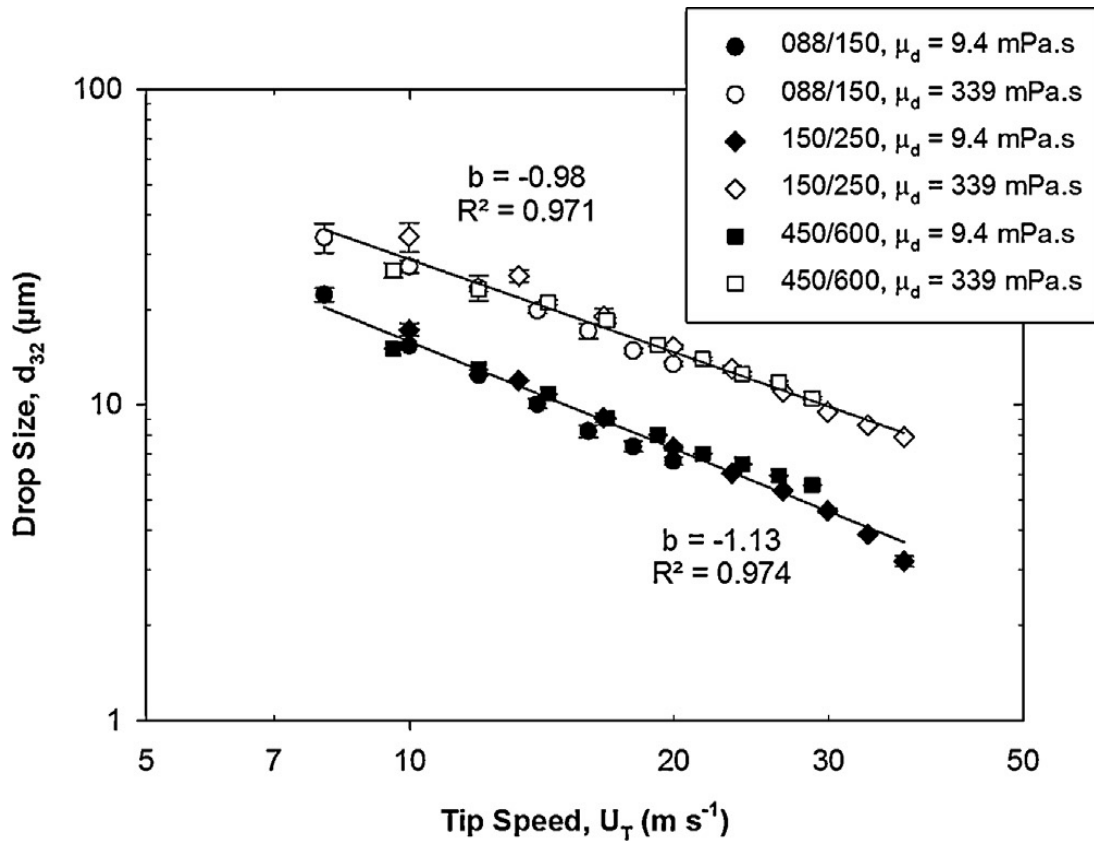


Figure 2-15 Droplet size as a function of tip speed (Hall et al., 2013).

This further insight provides a foundation for future work involving Silverson rotor-stator mixers and for mixers that operator on a similar design. While this foundation is of great scientific interest, similar work needs to be performed on other rotor-stator mixers as there is still little data available on them.

When mixing using a rotor-stator device it is known that the rotation of the rotor causes pressure changes in different areas which helps pull the fluid into the mixing chamber. To counteract this the operator will [usually] add the reagents to the mixing vessel using a separate pump; the Ultra Mixing and Processing Facility (UMPF) counteracts this through use of syringe pumps that surround the mixing chamber and force the fluid in, preventing the need for recirculation.

Computation Fluid Dynamics (CFD) modelling has recently produced results that are in line, qualitatively, with experimental data for Silverson type rotor-stators. It has

been published that earlier developed modelling methods which were used to predict reactive mixing in stirred tanks and tubular reactors can be used to predict mixing in high shear mixers (Jasińska et al., 2013).

In order to have a knowledge base for work, propositions for modelling such as using experimental data acquired from trial and error trials, is viewed as a sensible approach (Atiemo-Obeng and Calabrese, 2004). Work contained within this thesis involves high-throughput formulation robotics and design of experiment software used to create a model that will allow for logical predictions with regards to what process and formulations parameters will create an emulsion with the smallest droplet size using a new rotor-stator in the UMPF.

Smaller droplets within an emulsion are generally ascertained through powering the rotor-stator mixer with a greater amount of local energy during the mixing process. It is believed that due to the nature of the patented rotor-stator device at the heart of the UMPF there is now a way to make small droplets with less energy than conventional pilot plant mixers, however prior to this work, there was no data to currently support this.

2.5.1 Surfactants

Thermodynamically the lowest possible energy state of two immiscible liquids involves the greater density liquid occupying the lower half of the vessel they are present in, and the lower density liquid occupying the top half of the vessel, thus minimising the interfacial area between the fluids (Mason et al., 2006a). Forcing the fluids to mix requires energy, and when the mixing device in question stops applying that energy, the liquids are left with a much greater interfacial area which leads to thermodynamic instability. As a consequence, the two liquids will revert back to the lowest possible energy state they can occupy (Somasundaran et al., 2006).

The steps involved in emulsion breakdown are displayed in the illustration in Figure 2-16. Without stabilisation, droplets will coalesce and eventually reform two separate phases. If there is not enough stabilisation within the system, the droplets will slowly coalesce over time. If there is enough stabilisation in the system, but not enough distributive energy, then the dispersed phase will flocculate and cream. Both flocculation and creaming do not increase the size of the droplets within the dispersed phase. It is because of this that both processes can be reversed by applying energy to the system, through the medium of agitation, which then causes the droplets to revert back to the emulsion state (section 2.2.1). While flocculation is a colloidal process, creaming is a physical instability and is driven by both gravity and the density differences between the different phases.

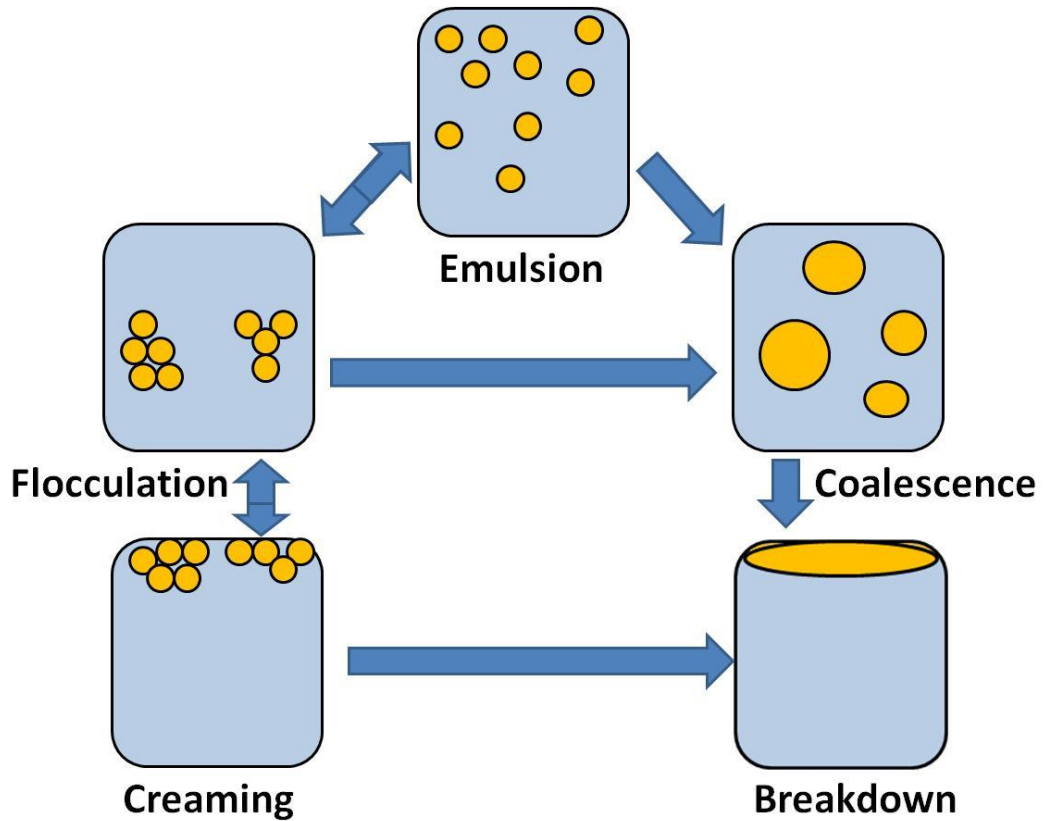


Figure 2-16 Stages of emulsion breakdown (IM-EMSAP, 2002). Oil is yellow, water blue and surfactant is present at the interface of the two phases.

There are a number of ways of colloidally stabilising an emulsion [thus preventing coalescence], from the use of polymers and solid particulates (discussed in section 2.5.7), to ensuring that the materials used will balance out due to the forces they possess both prior to, and following, emulsion formation (discussed in section 2.5.5). The most common method of emulsion stabilisation involves the addition of an emulsifier; otherwise known as a surface active agent [surfactant] (Mason et al., 2006a; Mason et al., 2006b; Meleson et al., 2004; Somasundaran et al., 2006).

Ionic surfactants prevent the coalescence of the droplets within the dispersed phase by providing a strong, repulsive force, creating in essence a barrier around the droplets that also reduces the interfacial tension, thus making them easier to break-up [as discussed in section 2.2.3] (Mason et al., 2006a; Mason et al., 2006b; Meleson et

al., 2004; Miller et al., 2001; Somasundaran et al., 2006). Surfactants also reduce the surface tension, which makes it easier to emulsify the oil. This occurs due to the fact that surfactants possess both hydrophilic and lipophilic properties which allows them to reside within both phases; thus enabling them to be able to stabilise the droplets against coalescence. The example shown in Figure 2-17 is of an anionic surfactant that is commonly used in household cleaning products, sodium dodecyl sulphate, and it has the molecular formula $\text{NaC}_{12}\text{H}_{25}\text{SO}_4$ (Witten and Pincus, 2004). The long hydrocarbon chain ($\text{C}_{12}\text{H}_{25}$) is very hydrophobic and thus lipophilic, whilst the polar group ($\text{SO}_4^- \text{Na}^+$) is hydrophilic. Anionic surfactants take their name from the anion present within the polar group of the molecule. Cationic surfactants, similarly, take their name from the cation present on the polar group and not the dissociated anion. Figure 2-17 shows both a simplistic sketch and a chemical drawing of an anionic surfactant, sodium dodecyl sulphate (SDS). The polar “head” group is hydrophilic and resides within the water phase whilst the lipophilic “tail” group resides within the oil phase at the interface of the two phases.

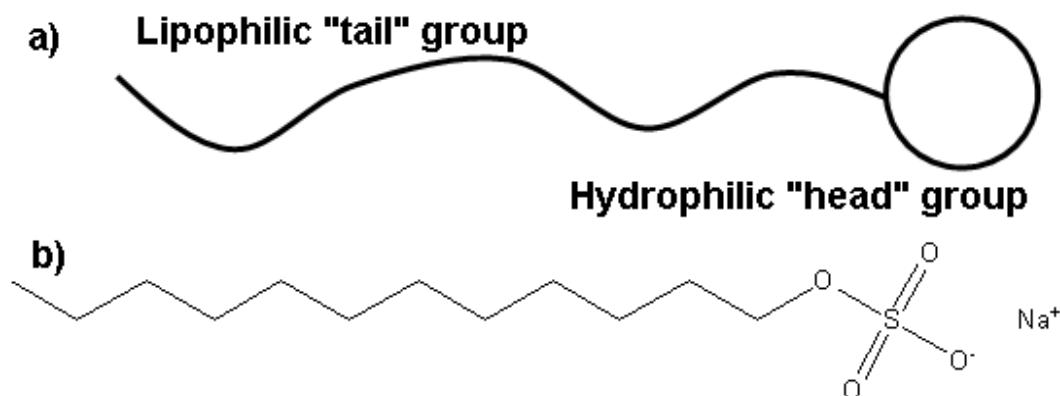


Figure 2-17 a) Simplistic drawing of a surfactant molecule. b) Chemical drawing of sodium dodecyl sulphate (SDS), an anionic surfactant.

The hydrophile-lipophile balance (HLB) is a system developed by William C Griffin for determining which surfactants to use with respect to non-ionic surfactants (Landfester and Hentze, 2001). The higher the HLB value, the greater the hydrophilic properties of the surfactant and the lower the HLB value, the greater the lipophilic properties (Equation 2-12 and Equation 2-13).

$$HLB = \frac{E_j \text{ wt}\% + OH \text{ wt}\%}{5}$$

Equation 2-12 HLB Equation by Griffin (Eastoe, 2010)

Where:

E_j wt% = weight percent of ethylene oxide

OH wt% = weight percent of hydroxide groups

A more general empirical formula was proposed by Griffin in 1954 that took into account hydrophilic and lipophilic groups, represented by S and A respectively, in Equation 2-13.

$$HLB = 20 \left(1 - \frac{S}{A}\right)$$

Equation 2-13 General HLB Equation by Griffin (1954)

Where:

S = saponification number of the ester

A = acid number of the acid

The HLB value allows one to determine which surfactant to use when creating a specific system; for example to create an oil-in-water emulsion a surfactant with a high HLB value would be chosen as these possess greater hydrophilic properties, however, when creating a water-in-oil emulsion a surfactant with a low HLB value would be preferred (Peters, 1992). Examples of HLB values and their common uses are displayed in Table 2-3.

Table 2-3 Hydrophile-Lipophile Balance (HLB) values and common uses (ICI Americas, 1976).

HLB Value	Range Use
4-6	W/O emulsifiers
7-9	Wetting agents
8-18	O/W emulsifiers
13-15	Detergents
10-18	Solubilizers

Non-ionic surfactants follow a structure similar to that of SDS shown in Figure 2-17, however they do not possess any dissociating ions; in the case of SDS the sodium ion and the corresponding negatively charged oxygen (Peters, 1992). Zwitterions are an excellent example of how non-ionic surfactants exist yet still maintain both hydrophilic and lipophilic properties as they contain both anionic and cationic groups.

2.5.2 Critical Micelle Concentration

The addition of surfactant to an emulsion system increases the concentration of said surfactant with, generally, no great alteration to the balance of the system until a critical concentration is reached. At this point the surfactant molecules begin to form micelles. In an oil-in-water system, micelles form as a combination of the oil and surfactant. The lipophilic “tail” on the surfactant molecule resides within the oil

droplet whilst the hydrophilic head faces outward. Many surfactant molecules will surround an oil droplet as can be seen in Figure 2-18.

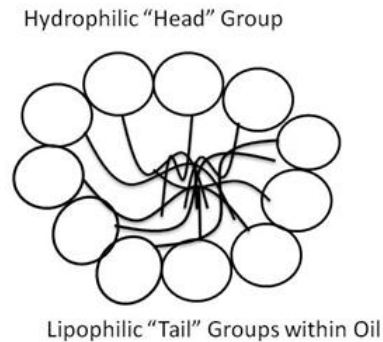


Figure 2-18 Illustration of a micelle.

The surfactant molecules encompass the oil droplets, reducing both the energy of the system and the surface tension. The further addition of surfactant to the system, past this point, does nothing to alter the surface tension, as all micelles that are possible to be formed will have been formed and so it is of no benefit to emulsification (Dutton, 2007). The critical concentration discussed is known as the critical micelle concentration (CMC) and it is important to know the magnitude for a given surfactant, especially when using large volumes of said surfactant, as adding anything above this value it merely becomes waste or a reservoir of surfactant which would increase the surface area.

The CMC is only important and effective as long as the temperature of the fluid is above the Krafft Point; below this micelles cannot form. The Krafft point is the temperature at which the solubility of the surfactant becomes equal to the critical micelle concentration. At temperatures greater than this, should the CMC be exceeded, the addition of further surfactant forms more micelles (McNaught and Wilkinson, 1997).

Micelles are commonly depicted as being spherical, with the surfactant molecules attached to the organic [oil] molecules by their lipophilic tail groups; however they can appear as other shapes and in varying sizes. Generally, the hydrophilic head groups cluster together to protect the lipophilic tail groups and form a ball, the surface of which is made entirely of the head groups with all the tail groups pointing inside for an oil-in-water emulsion system as shown in the illustration in Figure 2-18.

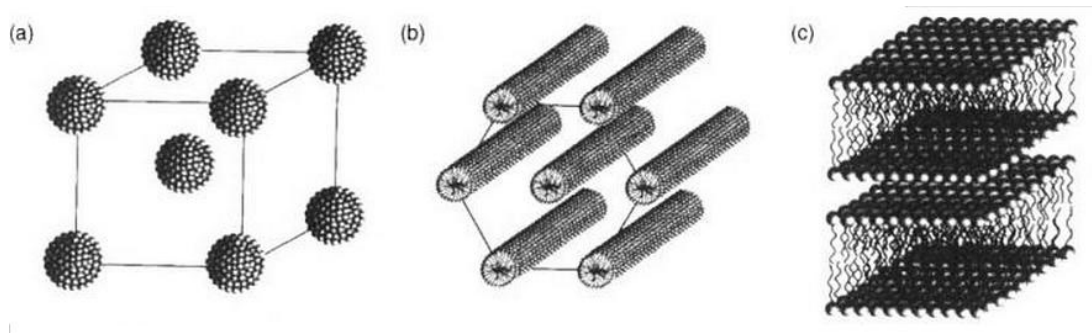


Figure 2-19 Phases adopted by surfactant molecules (Hamley, 2005).

There are generally considered to be three main types of structure that surfactant molecules adopt, dependent on the concentration of surfactant within a given system; micellar, hexagonal and lamellar (Hamley, 2005). Micellar phase forms when there is the minimum amount of surfactant to form micelles, and is generally found in systems containing less than 30% surfactant. The micelles then stack in different formations, such as cubic formation shown in Figure 2-19a. When there is 30–69% surfactant within a system then generally hexagonal phase surfactants form, however it should be noted that these values change for each surfactant system. Figure 2-19b shows that when surfactant is in hexagonal phase it is tightly packed, with little room for movement and as a result this phase is avoided by those working in the liquid surfactant industry as the surfactant is almost solid. Lamellar phase is usually adopted by surfactants when they are in 70%+ concentration (Figure 2-19c), the surfactant molecules form lamellar “sheets”. These sheets, provide flexibility and

flow, much more so than hexagonal phase surfactant, and as they are found at high concentrations only, are ideal for industry as they have similar effects to micellar phase but are in greater concentration so require less money to transport.

2.5.3 Brownian Motion

During the 19th century microscopic observations of colloidal particles showed a tendency to form aggregates through collisions. Through observing, using a microscope, pollen particles floating in water, Robert Brown is recorded as being the first to report that solid particles small enough to be suspended in water can continue to portray ceaseless random motion (Brown, 1828). Such findings were of great interest to the scientific community and this phenomenon was named Brownian motion. The observation of small solid particles moving is still the most common example of Brownian motion, however the particles need not necessarily move in relation to the vessel, rotating is deemed a characteristic of Brownian motion (Mazo, 2002).

2.5.4 Ostwald ripening

It is regarded that Ostwald ripening involves the growth of larger particles at the expense of smaller ones. Although initially this sounds like the definition of coalescence, it should be noted that coalescence is caused when two or more droplets collide (Nijenhuis et al, 2007). An illustration of Ostwald ripening is shown in Figure 2-20. When discussing Ostwald ripening it can be said that smaller particles, having a larger surface area to volume ratio, have a greater amount of free energy on the long curvature of the droplets. As a result of this, the free energy is significantly greater, to the point that it causes the smaller droplets to decrease in size and the larger droplets to increase in size (Wang and Glicksman, 2010). Smaller droplets

have a greater Laplace pressure and the material, as a result of the large amount of free energy, dissolves and deposits on the larger droplets.

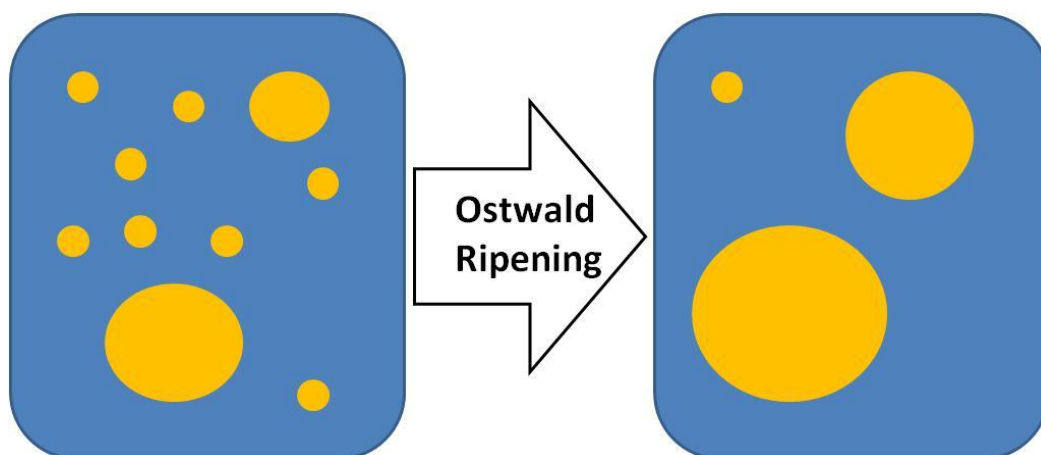


Figure 2-20 Illustration showing Ostwald Ripening.

When discussing Ostwald ripening within emulsions, the focus is on the droplet size distribution (DSD) as this is what allows the analyst to know how many small, medium and large droplets there are within the sample. McClements (2005) believes that the smaller the mean droplet size within an emulsion, (and the greater the rate at which the droplets decrease in size), the faster Ostwald ripening will occur, as the solubility of the dispersed phase is higher (McClements, 2005).

As well as droplet size, the polydispersity and solubility in the continuous phase are two more factors that increase the rate of Ostwald ripening (Landfester, 2004). In fact, according to Nijenhuis et al, Ostwald ripening occurs only in polydisperse emulsions (Nijenhuis et al., 2007).

2.5.5 Dispersion Forces

Within a colloidal suspension/system the primary attractive force is van der Waals force and the primary repulsive force is the electrostatic forces (Chattopadhyay and Puls, 2000). It is known that between similar particles suspended in a chemically

different liquid, forces can be found causing attraction of the particles to each other and thus providing a driving force toward macroscopic phase separation. As a result of this electrostatic forces in aqueous dispersions are required to prevent coalescence. The ability of electrolyte to flocculate a variety of aqueous dispersions was discovered experimentally by Schulze (1882), Hardy (1900) and Freundlich (1910) who proposed stability is dependent primarily on electrostatic repulsion (Russel et al., 1989a).

The thermodynamically stable state, in the absence of other short-range forces and with respect to colloidal systems, comprises mainly of the deep primary minimum during which the particles can be described as being in contact (Zhong et al., 1994). Theoretically, pairs residing within this state would be bound together irreversibly with the only option of escape relying entirely on thermal fluctuations (Russel et al., 1989b). At low-to-moderate ionic strengths the repulsive barrier is large, thus making diffusion of initially dispersed particles into the primary minima very slow (Russel et al., 1989b). When the ionic strength of the medium is high, past a certain point, the repulsive barrier becomes negligible and as a result rapid, irreversible flocculation occurs (Russel et al., 1989b).

2.5.6 Zeta Potential (ζ)

Particles, when suspended in solution, have a surface charge. The adsorption of a charged species from the surrounding ionised solution is one of the most common methods for the production of these charges (Clark, 1992; Sjöblom et al., 2006). In order to cancel out the charge present on the particle surface, counter-ions will surround the particulate and thus the charged surface. This helps to balance out the charges present, whilst at the same time it creates an electric double layer around the

particulate (Sjöblom et al., 2006). When these particulates then move, by gravitational or induced field or even by diffusion, a shear plane exists outside which the ions in the double layer will no longer be influenced by the movements of the particulates (Sjöblom et al., 2006).

The potential at this boundary has been defined as the zeta potential (ζ) and it can be measured using a number of analytical techniques (Sjöblom et al., 2006). The simplest way of measuring the zeta potential is to use a zeta meter or zeta sizer, both of which are able to produce a reading measured in millivolts (mV). The value depends on how likely the particulates are to coagulate and a number of examples are displayed in Table 2-4.

Table 2-4 Zeta potential ranges and corresponding degree of coagulation
(American Water Works Association, 2003).

Zeta Potential Range (mV)	Degree of Coagulation
3 – 0	Maximum
-1 – -4	Excellent
-5 – -10	Fair
-11 – -20	Poor
-21 – -30	Remote

Zeta (ζ) potential best describes the electrostatic state of a surface, created via the movement of liquid through a capillary, under the action of an electric field. An example of a negatively charged particle can be seen in Figure 2-21. In

emulsification, when surfactant molecules attach to the droplet all the head groups align on the outside and because they are all of the same charge, the droplet has said charge and an electric double layer is formed. Adjacent droplets repel each other due to their charge being the same which helps stabilise the emulsion and prevent coalescence.

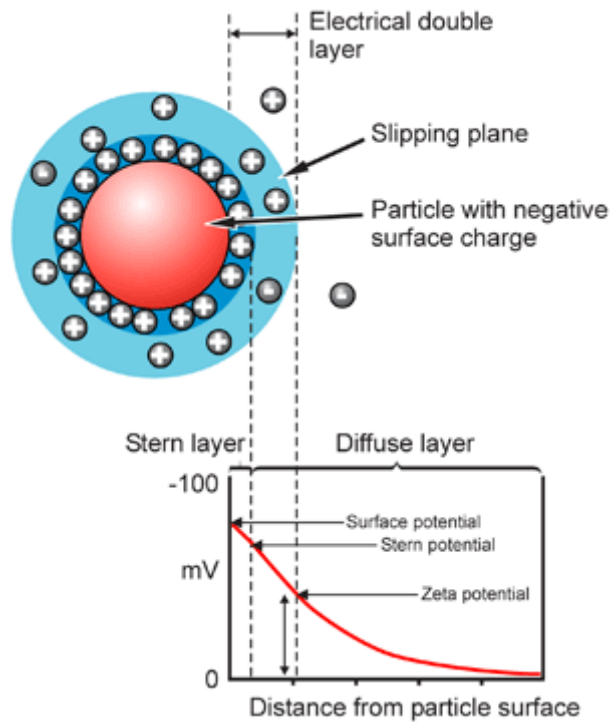


Figure 2-21 A schematic representation of zeta potential for a negatively charged particle (Malvern, 2013a).

The structure of the attractive inter-particle potential was unknown until de Boer (1936) and Hamaker (1937) developed a theory based on pair-wise summation of the intramolecular forces (Russel, 1989). Representing total interparticle potential as the sum of the “attractive + repulsive” components led to a detailed theory on colloidal stability (Russel, 1989). Hamaker and de Boer assumed intramolecular forces to be strictly ‘pairwise additive’; local fluctuations occurring within the polarization of one particle induce [via the propagation of electromagnetic waves] a correlated response in the other (Durand-Vidal et al., 2000).

2.5.7 Pickering Emulsions and Steric Stabilization

Surfactants are not the only method of stabilising emulsions. There exists the use of polymers and particles which can also be used either separately or together. Pickering emulsions are emulsions that have been stabilised by the presence of solid particles at the oil/water interface (Binks and Horozov, 2006; Salari et al., 2010; Salari et al., 2011). The high energy desorption of the particles at the interface prevents dispersed droplets from coalescing as the free energy within the system is used in providing stabilisation, thus the tension (of the attractive/repulsive forces) that would exist without them present is reduced greatly (Binks, 2006; Salari, 2010). It was discovered by Pickering and Ramsden that the emulsions were formed by the self-assembly of colloidal particles at the interface between the two immiscible fluids (Popp, 2010). Pickering is credited with noticing and reporting that emulsifying agents for oil-in-water emulsions can be particles of colloidal dimension that are “wetter more by water than by oil” (Tambe, 1994).

Steric stabilisation involves the use of polymers, macromolecules, which are grafted or adsorbed onto the droplets of the dispersed phase (Berg, 2009). This prevents them aggregating but without the foaming properties of surfactants (Salari, 2010; Salari, 2011). Steric stabilisation relies on the repulsion caused during limited interpenetration of the polymer chains and stabilises the colloidal dispersion against flocculation (Hamley, 2007). The three factors which make steric stabilization unique to other methods of colloidal stabilization are; it works independent of ionic strength of the solution, it is effective in both organic and aqueous solutions and it can operate within a wide range of colloid concentrations. Other stabilisation methods, such as surfactants, can only operate within a specified range (i.e. low

concentration is the only suitable condition for charge stabilization to be effective) (Hamley, 2007).

2.6 Particle Sizing

The focus of this research was on the size of the droplets of the reagent(s), following processing, and the subsequent impact that they had on the rate of reaction. To observe the size of the droplets required use of a particle sizer. The Mastersizer range of particle sizers, manufactured by Malvern, is able to analyse both dry and wet samples, and specifically it is able to analyse emulsions and suspensions (Malvern, 2012).

During the majority of this work the Mastersizer X was used, however, access was obtained for some of the activities to a Mastersizer 2000. It is for this reason that both the Mastersizer X and the Mastersizer 2000 are referenced throughout this thesis.

To analyse wet samples with either Mastersizer requires the sample to be added to a small volume dispersion unit. The unit contains an impeller which is set to an rpm value that forces fluid in a circular loop out the unit, through the sample cell where the measurements are performed and back into the unit.

To allow analysis using small sample volumes (a few millilitres at most), the small volume dispersion unit is filled with distilled water. Prior to the sample being analysed, a measurement of any particulates present within the water is taken. Measurements taken using the Mastersizer 2000 involves a combination of red and blue light being shone through a lens, through the sample cell and landing on a detector, this is classed as the background scan.

Sizing particulates and/or droplets using the Mastersizer X with a 45mm lens works in a way almost identical to the Mastersizer 2000, with the main difference that there is no blue light source, only a red light source. Figure 2-22 shows a simple illustration of how a background scan is performed using the Mastersizer 2000 or the Mastersizer X with a 45mm lens, while Figure 2-23 shows in a similar style how the Mastersizer X with either the 100mm, 300mm or 1000mm lens, analyses samples.

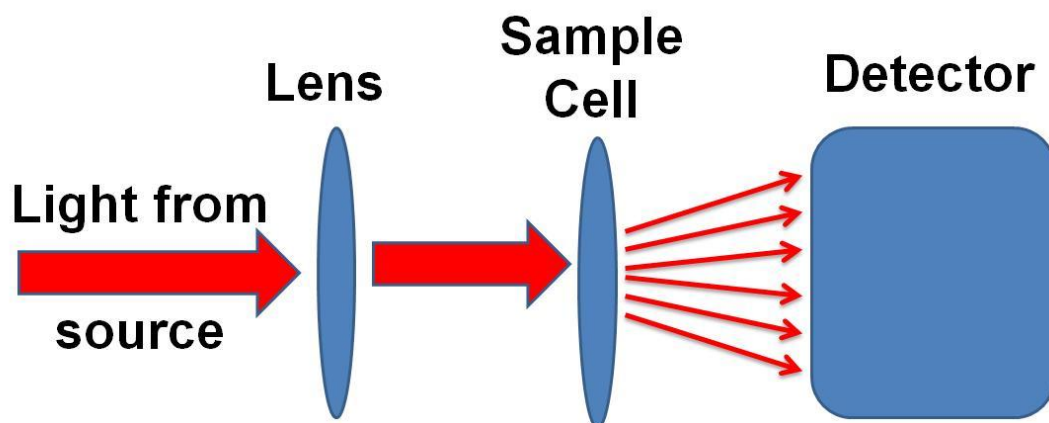


Figure 2-22 Simplified illustration showing how the Mastersizer 2000 or the Mastersizer X with a 45mm lens sizes particles.

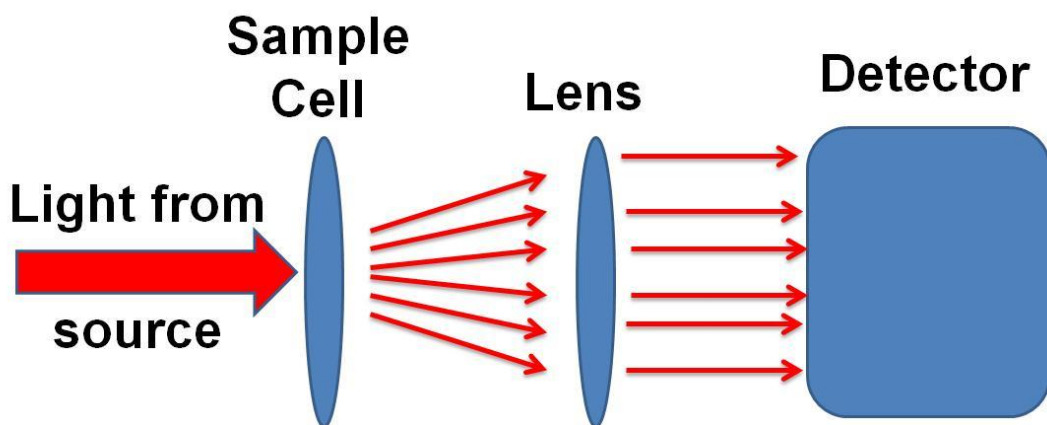


Figure 2-23 Simplified illustration showing how the Mastersizer X with either the 100mm, 300mm or 1000mm lens, sizes particles.

The main differences between the Mastersizer X and the Mastersizer 2000 are:

- The Mastersizer 2000 has only one lens whereas the Mastersizer X has different lenses, dependent on the size range that the operator wishes to observe.
- There are more detectors present in the Mastersizer 2000. Figure 2-22 is a simplified illustration of how the equipment works, in actuality there are a large number of detector cells in the area and more located around it to allow the observation of very small droplets [small droplets scatter light at a greater angle than larger droplets].
- The Mastersizer 2000 has two light sources, blue (466nm wavelength) and red (633nm wavelength) whereas the Mastersizer X has only a red light source. The red light source allows the observation of particulates between $\sim 0.1\mu\text{m}$ and $1000\mu\text{m}$ and the blue light source allows the observation of particulates down to $0.020\mu\text{m}$ in size. When combining the blue and red light sources the particle size range increases to $0.020\text{-}2000\mu\text{m}$.

As well as having different lenses dependent on the size range the operator of the Mastersizer X wishes to look at, the location of the larger lenses (100mm – 1000mm inclusive) is behind the sample cell, not in front of it, as shown in Figure 2-23. The reason for this is the location of the detectors in the Mastersizer X are behind the sample chamber. This is because the Mastersizer X, for the larger lenses, works on the principle of the “classic forward Fourier optical set-up” (Malvern, 2014). With the “data collection lens” located behind the sample chamber, a large working range with respect to the wide path length can be analysed (Malvern, 2014). This means that samples can be distributed throughout the sample chamber and do not have to be placed on the sample chamber wall next to the lens. The 45mm lens on the

Mastersizer X, and the Mastersizer 2000, work on “Reverse Fourier set-up”, which is when the lens is placed in front of the sample chamber (Malvern, 2014). Having the lens in front of the sample chamber allows for detectors to be placed in front and behind the sample chamber, which means that the Mastersizer is able to analyse a much larger range of particle sizes.

The different lenses that can be used with the Mastersizer X to refract the laser light onto the detectors, and the corresponding size range they are able to observe, is listed in Table 2-5.

Table 2-5 Size of lenses available for the Mastersizer X and the size range of particulates/droplets they are able to analyse.

Lens size (mm)	Size range able to analyse (µm)
45	0.1 – 80
100	0.5 – 180
300	1.2 – 600
1000	4 – 2000

Following a background scan, the sample to be analysed is added to the small volume dispersion unit and left to fully disperse throughout the water. As the sample disperses, the obscuration the sample causes to the detector fluctuates and is displayed in live-time by the software. There is an optimal obscuration level for both Mastersizers which will allow the operator to obtain the most accurate droplet size reading.

Small quantities of the sample are added to the dispersion cell until the optimal obscuration value is reached; if this value is exceeded upon addition of a droplet of sample, usually due to the sample containing very small droplets scattering the light greatly in comparison to large droplets (Figure 2-24), then the sample is dispersed in distilled water prior to being added to the small volume dispersion unit. The reasoning behind this is that if the obscuration exceeds a certain limit then multiple scattering will occur. If there is too little sample and not a high enough obscuration then the light will not reach the detectors. In either case, if the obscuration created by the sample is not at the optimal level then the reading will be inaccurate. Upon addition of the sample to the dispersion unit the obscuration value begins to fluctuate as the sample causes diffraction of the laser light while it disperses throughout the distilled water. Eventually the obscuration value becomes stable and it is when this happens that the recording of the light diffraction pattern on the detector cells can commence.

The particle size produced by the Mastersizer is done so inversely. The Mastersizer predicts the size of the droplet by measuring the angular variation in intensity of light scattered; for small droplets, large scattering and large droplets, small scattering (Figure 2-24).

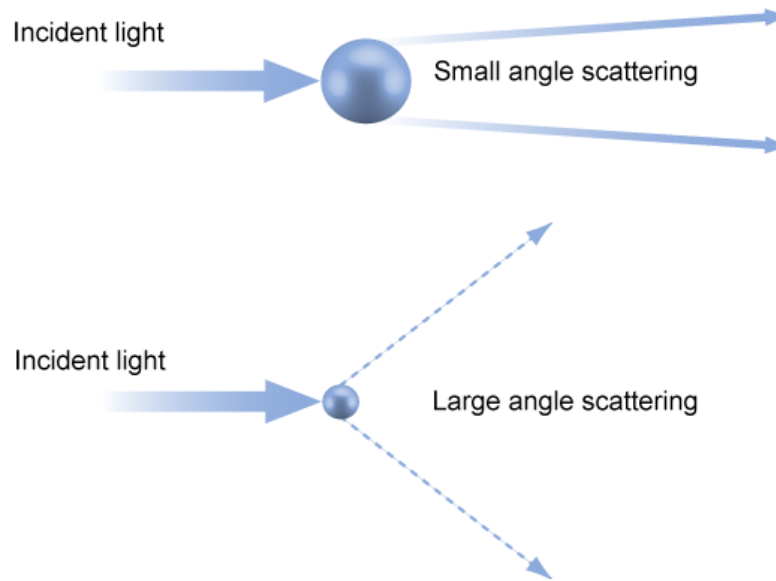


Figure 2-24 Simplified illustration showing how light is scattered by particles in the Mastersizers (Malvern, 2013b).

Following this it then works out the scattering pattern (through the angular scattering intensity of the light on the detectors) and analyses the size of the particles responsible for creating the pattern using the Mie theory of light scattering, incorporated into an specifically designed algorithm (Equation 2-14).

$$\text{Droplet Size} = \text{Angular Scattering Intensity} * \text{Malvern Algorithm}$$

Equation 2-14 How the Malvern Mastersizer predicts droplet size.

The combination of the refractive index of the sample, the refractive index of the continuous phase and which of the many detectors the light has hit (and thus the scattering angle of the sample) are all taken into account when processed by the Mastersizer software algorithm. Taking these factors into account the algorithm is able to produce a droplet size value for the sample.

The Mastersizer technology works on Mie theory; that is to say it assumes that all particulates are homogenous spheres within the system that scatter the light on the way to the detector (Jonasz and Fournier, 2011). In order to interpret the data that is

recorded by the detectors the refractive index of the particulates and the dispersed phase they are in must be known. These values are inputted by the operator and the software then interprets the detector readings and produces the size of the particulates analysed in various formats. Mie theory is preferred over the use of the Fraunhofer Approximation within the technology used, as the latter is based on more assumptions; that is to say it does not require information on the optical properties of the material being analysed, nor the optical properties of the medium that the sample is placed within for analysis. When analysing droplets less than a micron in size, the blue light source, with a wavelength of 466nm, is necessary. This is because the red light wavelength is 633nm in size and assumptions that the optical properties of the droplets have no impact on the determination of the size of the droplets being analysed can no longer be taken (Ryżak and Bieganowski, 2011). For analysis of particles significantly larger than 633nm, Fraunhofer Approximation is an acceptable and used form of analysis. Samples with particles approaching the wavelength of the light in size (and smaller) need to use Mie theory because it takes into account the interaction of the particle with the light. The Mie theory needs the optical properties of the material, specifically the RI of the particles and the RI for the dispersant.

The two particle size values discussed throughout this work, that are produced by the Mastersizers following analysis of a sample, are the $D[4,3]$ and the $D[3,2]$ values. The $D[4,3]$ value is the volume weighted mean and the $D[3,2]$ is the surface area moment mean. Both these equations take into account the number of particles, and the mean diameter of said particles, when calculating the value (Equation 2-15).

$$D[3,2] = \frac{(\sum n_i D_i^3)}{(\sum n_i D_i^2)}$$

$$D[4,3] = \frac{(\sum n_i D_i^4)}{(\sum n_i D_i^3)}$$

Equation 2-15 D[3,2] and D[4,3] equations.

Where:

n_i = frequency of occurrence of particles of in size class i

D_i = Diameter of particles in size class i

With the focus of the emulsification being on improving the ratio of the total volume of the particles, to the total surface area, reducing the D[3,2] value was of primary focus; reducing the D[4,3] was a secondary factor.

2.7 Saponification and Biodiesel Formulation

Two phase systems consist of a combination of solid, liquid and/or gas. The focus of the work presented here was on the improvement of systems involving two immiscible liquids through manipulation of the droplet size of one of the phases.

Plant oil is used in the production of soap and biodiesel; the chemical reactions of both follow similar mechanisms, with the distinct difference that to create biodiesel requires the use of an alcohol and to create soap requires the use of a hydroxide (sodium or potassium). Both saponification and transesterification contain two immiscible liquids that undergo chemical reactions when placed under certain conditions.

2.7.1 Saponification

The term *saponification* is commonly used to describe the chemical process that results in the formation of soap. Saponification involves the hydrolysis of an ester,

under basic conditions (i.e. pH 12 – 14.0), to form an alcohol and a carboxylate salt.

When aqueous sodium hydroxide is added to pure oil/fats (e.g. coconut oil, tallow)

hydrolysis occurs and the reagents react to form soap and glycerol.

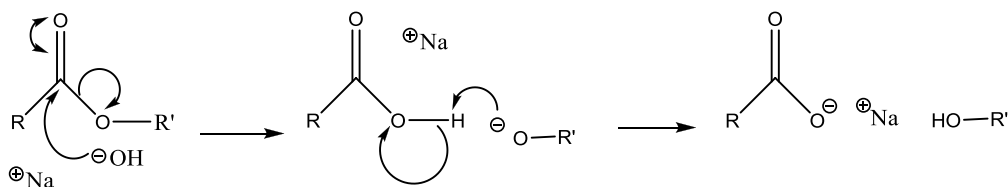


Figure 2-25 Chemical reaction scheme depicting the hydrolysis of an ester and the formation of a carboxylate salt and alcohol.

Soap has been one of the most important man made products which has had long reaching impact of society. From the first evidence of soap manufacture in ancient Babylonia where animal fats and vegetable oils were mixed with ashes to make crude soap like substances, until the widespread commercial soap manufacture of the industrial revolution, soapmaking was conducted on a small scale and the product was generally rough (Toedt, 2005). This changed in the 18th and 19th centuries with industrialists making a high-quality soap which was cheap and widely available to the general public (Lawrence, 1985). This availability of a cheap surfactant for use as both a clothes detergent and for general personal hygiene had huge societal impact as well as the birth of the modern chemical processing sector.

There are several industrial saponification processes used within industry today, discussion of them all is outside the scope of this research, however, an overview is given in Figure 2-26 (Wansbrough, 1998).



Figure 2-26 Flow diagram of generic industrial saponification process.

Industrial Saponification can be described as requiring four basic steps.

1. **Saponification:** Typically a combination of animal fat (tallow) and vegetable oil (palm oil, coconut oil, etc.) are mixed in the presence of a metal hydroxide (sodium or potassium hydroxide) while steam is bubbled through the reaction vessel. Bubbling steam through the process provides both water and heat to the reaction (typically 60°C – 160°C are used depending on the process used). The soap produced is the salt of a long chain carboxylic acid and the reaction generally completes within 6 – 12 hours. Phenolphthalein is used to assess the endpoint because when at a pH value greater than 12 it is colourless however between pH values of [approximately] 8 and 12 it appears pink in colour.

2. **Glycerol removal:** Glycerol is a valuable by product of soap manufacture, therefore most of it is removed prior to purification and used in other processes, in some cases it is left in the soap to help make it soft and smooth. Separation of the soap from the glycerol is done via a brine wash; soap is not very soluble in salt water, whereas glycerol is, and so salt is added to the wet soap to cause it to separate out into soap and glycerol in salt water.
3. **Soap purification:** Any remaining sodium hydroxide at the end of the reaction is neutralised with a weak acid [such as citric acid] and two thirds of the remaining water removed using either spray or vacuum drying.
4. **Finishing:** Additives such as preservatives, colour and perfume are added and mixed in with the soap and it is shaped into bars for sale. Detergents are similar in structure and function to soap, and for most uses they are more efficient than soap and so are more commonly used. In addition to the actual 'detergent' molecule, detergents usually incorporate a variety of other ingredients that act as water softeners, free-flowing agents etc.

Alterations/additions to the saponification process can be made in order to alter the final properties of the product; Table 2-6 outlines typical soap additives and the properties they give the soap.

Table 2-6 Soap additives are commonly used to enhance the soap qualities.

Property	Additive
Fragrance	<p>Aromatic oils such as lavender, tea tree, peppermint are widely added to soaps to enhance fragrance and castor oil and Bentonite or Kaolin Clay help hold fragrances.</p> <p>Herbs and spices such as chamomile and cinnamon can be added also to give the product a soothing or spicy fragrance [respectively].</p>
Soap hardness	<p>Stearic acid and salt can cause the product to be harder in texture whereas cocoa butter and milks give soap soothing, creamy properties.</p>
Medicinal properties	<p>Tea tree oil, aloe vera, coal tar, shea butter, silver salts etc. are all common additives used to add beneficial properties to the soap such as microbial/antibacterial</p>
Lather properties	<p>Sugar, canola oil, castor oil, coconut oil and corn oil are added to soap to improve the lather and, in the case of the oils mentioned, make the lather creamy.</p>

2.7.2 Biodiesel

Transesterification is the process that occurs when an ester group reacts with an alcohol (Brown, 2010). During the reaction the terminal oxygen-carbon group of the ester is replaced with the oxygen-carbon group of the alcohol. When

transesterification occurs under basic conditions the ester forms an anionic intermediate and as such the process is a reversible reaction (Demirbas, 2008).

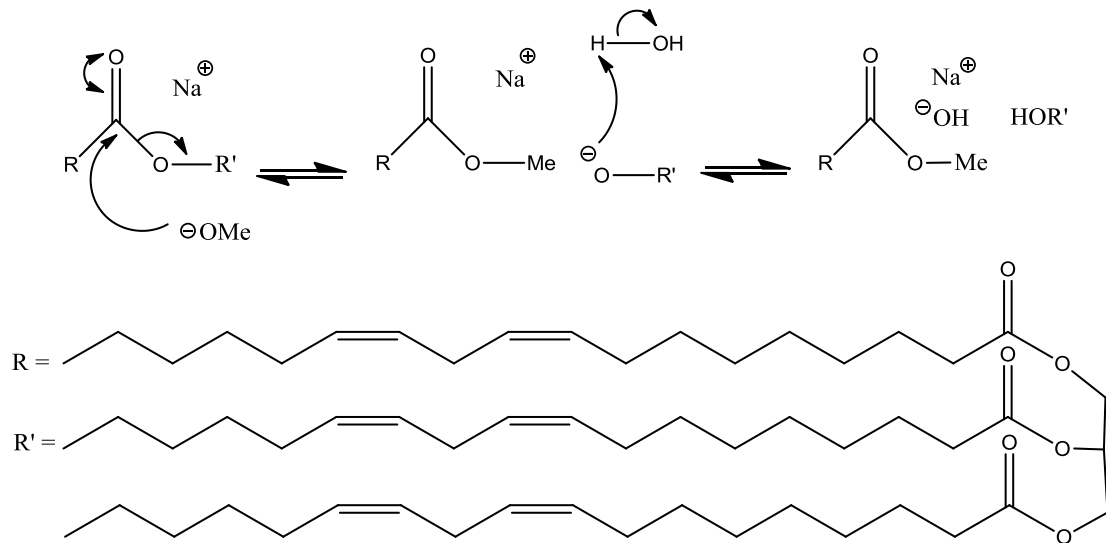


Figure 2-27 Chemical schematic depicting the formation of biodiesel from the largest possible triglyceride present within sunflower oil (three linoleic acid groups), where R is equal to one of the glyceride chains and R' is the rest of the triglyceride.

Figure 2-27 shows the mechanism by which sodium methoxide reacts with the ester group of one of the glyceride chains that make up the larger triglyceride. This results in the formation of a fatty acid methyl ester (FAME) and diglyceride. In the presence of excess sodium methoxide the reaction continues with the diglyceride being converted into FAME and glyceride, which then undergoes the same process until all the triglyceride is converted into FAME and glycerol.

There are several documented methods for making biodiesel at scales suitable for individual usage (Biodiesel, 2008; Home-Made Biodiesel, 2009). The recipes for making biodiesel at home contain very basic instructions with no exact time for the reaction to reach completion. Previous research into improvements of biodiesel formulation however quote varied reaction times for the formulation of biodiesel

from pure oil, the quickest being 45 minutes and the average reaction time length being an hour (Chai, 2007; Leung and Guo, 2006).

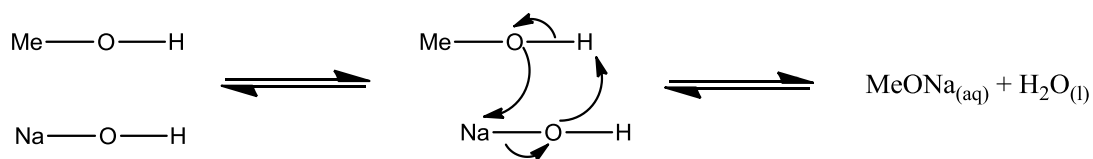


Figure 2-28 Chemical schematic depicting the formation of Sodium Methoxide.

The standard experimental method for the formulation of biodiesel is to heat the oil up to temperature before adding sodium methoxide (formation of which is depicted in Figure 2-28) and allowing the reaction to occur at temperature under agitation (Chai, 2007; Ting, 2008).

Table 2-7 Conditions for standard biodiesel formulation.

Parameter	Range	Value Used
Oil	Vegetable, Sunflower seed, Rapeseed, Soybean,, Jatropha, Waste cooking oil, excess frying, etc.	80% Phase Volume
Sodium hydroxide	Dispersed within methanol before addition to reaction vessel.	1% w.t.
Methanol to oil molar ratio	3:1 and above	6:1
Temperatures	20-65°C	60°C

Table 2-7 lists the conditions for standard biodiesel formulation as well as some of the variables that can be applied. The main variables are the oil used and the temperature however the hydroxide base can be changed as can the ratio of methanol to oil. The standard method is listed in Chapter 8.

As populations expand and modern industry becomes ever more energy intensive, the global demands on the planet's meagre resources becomes greater. It is globally recognised fact that fossil fuel reserves are a finite resource, the cost of them will increase as demand increases and this fact is widely quoted by today's scientists, journalists and politicians as a cause for great concern and a reason to bring about urgent change to the global energy consumption habits (Kaygusuz, 2008). It has been predicted that in the year 2014 conventional crude oil production will peak and be

maintained until all supplies have been exhausted (Nashawi, 2010). As a result, scientists around the globe have been researching into alternative energy sources that are renewable and sustainable. Renewable sources at present are solar, hydro, wind, tidal and geothermal (Harmsen, 2011; Liu, 2011; Solangi, 2011). Current nuclear energy production has advanced in the 60 or more years since its initial inauguration; fast breeder reactors, fuel enrichment facilities and better waste management means nuclear power is a relatively clean energy source and has been classified as a sustainable and partially renewable energy source (although this is still under debate). Along with the need for long term solutions to radioactive and toxic waste, the downside of the modern nuclear powered future has been demonstrated by the Chernobyl disaster in 1986 and the more recent Fukushima Daiichi nuclear disaster. The risks associated with accidental leaks and exposure to nuclear fallout is not fully known. Both of these disasters have shown that should a problem occur at a nuclear power plant, injury and death is not restricted to that one location but travels and can become a global issue.

Whilst nuclear power is used in electricity generation for powering submarines, warships and more recently to power the Mars rover 'Curiosity', the use of nuclear power sources for both personal and public transport devices will likely always be limited by cost. One of the largest sources of green-house gases outside heavy industry is the rise of the modern motor car, utilising the internal combustion engine. Whilst hybrid technologies are now on the market there is still pressure to supply greener fuels to these engines and to reduce the pressure on crude oil sources.

It is known that the replacement of diesel extracted from fossil fuel with biodiesel involves a significant reduction in the number of greenhouse gasses emitted by the engine using the fuel. Biodiesel's chemical structure is free of both sulphur and

aromatic ring groups, thus when burned there is no release of $\text{SO}_{x(g)}$ and a minimal release of $\text{CO}_{(g)}$ (with respect to that released when diesel is burned) (Chai, 2007). As biodiesel is broken down by combustion engines, the stored energy within is released as the large carbon chains are broken down into $\text{CO}_{2(g)}$, $\text{H}_2\text{O}_{(l)}$ and short alkane chains. Despite the combustion of the fuel, biodiesel still falls into the category of renewable fuel as the source from which it is produced can be re-grown.

The problem faced with the use of certain natural oils is the impact it has upon the food economy as many of them are also used either directly or indirectly for food production which has led to claims that biofuel production has a direct impact on the price of feedstock, and thus food (Ajanovic, 2011; Mueller, 2008). As a result of this, numerous scientific research groups have taken it upon themselves into finding an inedible oil source of biodiesel aside from fossil fuel (Ndong, 2009). It has been discovered that the inedible jatropha oil produces a biodiesel that has a higher cetane number than most other biodiesels produced and is in fact so similar to diesel produced from fossil fuels that current diesel engines require no modification when switching to it as a fuel (Koh, 2011).

Jatropha curcas, the plant that produces the seeds which produce jatropha oil, is a member of the Euphorbiaceae family and is known for being drought resistant (Koh, 2011). It is this property that allows the plant to flourish in Central America, South America, East Africa, India and Thailand (Koh, 2011; Leduc, 2009; Ndong, 2009). Biomass is used as a fuel source for energy in many of the world's poorer countries and accounts for as much 90% of the total quantity in the poorest countries of the world (Cadenas, 1998). The problem they face is the cost of producing the fuel is dependent on the cost of the biomass; investment, transportation and glycerol price have little importance or influence (Leduc, 2009).

The use of biodiesel as a replacement fuel is merely one application. Another is that it can convert fuel with poor lubricating properties, such as modern ultra-low-sulphur diesel fuel into an acceptable fuel when added to regular diesel in an amount equal to 1–2% (Gerpen, 2005).

It is for all the reasons listed previously that research was undertaken to ascertain whether emulsifying oil would increase the available surface area of the oil, subsequently increasing the rate of reaction, decreasing the overall reaction time and making the process greener and cheaper. The results of this experiment are detailed in Chapter 8.

2.8 References

ACIDREFLUXSYMPTOMSNOW. <http://www.acidrefluxsymptomsnow.com/can-milk-cause-heartburn.html?>. 19th August 2012

ADAMS, E. E., Socolofsky, S. A. and Boufadel, M. 2013. Comment on “Evolution of the Macondo Well Blowout: Simulating the Effects of the Circulation and Synthetic Dispersants on the Subsea Oil Transport”. *Environ. Sci. Technol.* **47** 11905–11905

AJANOVIC, A. 2011. Biofuels versus food production: Does biofuels production increase food prices?. *Energy.* **36** 2070–2076

AMERICAN WATER WORKS ASSOCIATION. 2003. *Water Treatment Third Edition*. Denver, CO: American Water Works Association. p. 76

ATIEMO-OBENG, V. A. and Calabrese, R.V. 2004. *Handbook of Industrial Mixing: Science and Practise*. Chichester: John Wiley & Sons. Chapter 8

AZZOPARDI, B. J., Mudde, R. F., Lo, S., Morvan, H., Yan, Y. Y. and Zhao, D. 2011. *Hydrodynamics of Gas-Liquid Reactors: Normal Operation and Upset Conditions*. West Sussex: John Wiley and Sons Ltd. p. 140

BAKER, M. 2011. *Mixing Course Part 2: Blending and Droplet Break-up*. Internal Unilever presentation.

BAUER, E. 2010. http://www.simplyrecipes.com/recipes/basil_vinaigrette/. 19th August 2012

BERG, J. C. 2009. *An Introduction to Interfaces & Colloids: The Bridge to Nanoscience*. Singapore: World Scientific Publishing Co. Plc. Ltd

- BINKS, B. P. and Horozov, T. S. 2006. *Colloidal particles at liquid interfaces*. Cambridge: Cambridge University Press. 298–300
- BOCKRIS, J. O'M. and Reddy, A. K. N. 1998. *Modern Electrochemistry 1*. New York, NY: Kluwer Academic/Plenum Publishers. p. 370
- BOWMAN, B. J., Ofner III, C. M. and Schott, H. 2006. *Remington: The Science and Practice of Pharmacy 21st Edition*. Philadelphia, PA: Lippincott Williams & Wilkins. p. 319
- BRITTON, I. 2007. http://www.freefoto.com/images/09/36/09_36_1---Ice-Cream_web.jpg credit to FreeFoto.com web site for allowing use in non commercial printed use. 19th August 2012
- BROWN, W. H., Foote, C., Iverson, B. and Anslyn, E. 2010. *Organic Chemistry, Enhanced Edition*. Belmont, CA: Brooks/Cengage Learning. p. 684
- BROWN, R. 1828. A Brief Account of Microscopical Observations made in the Months of June, July and August 1827, on the Particles contained in the Pollen of Plants; and on the General Existence of active Molecules in Organic and Inorganic Bodies. *Edinburgh New Philosophical Journal*. **5** 358-371
- BUTT, H-J., Graf, K. and Kappl, M. 2003. *Physics and Chemistry of Interfaces*. Weinheim: Wiley-VCH. p 8.
- CADENAS, A. and Cabezudo, S. 1998. Biofuels as sustainable technologies: perspectives for less developed countries. *Technol Forecast Social Change*. **58** 83–103
- CHATTOPADHYAY, S. and Puls, R. W. 2000. Forces dictating colloidal interactions between viruses and soil. *Chemosphere*. **41** 1279-1286

- CHAI, F., Cao, F., Zhai, F., Chen, Y., Wang, X. and Su, Z.. 2007. Transesterification of Vegetable Oil to Biodiesel using a Heteropolyacid Solid Catalyst. *Advanced Synthesis and Catalysis*. **349** 1057–1065
- CLARKE, C. 2012. *The Science of Ice Cream 2nd Edition*. Cambridge: The Royal Society of Chemistry. p. 15
- COOKE, M., Rodgers, T. L. and Kowalski, A. J. 2012. Power Consumption Characteristics of an In-Line Silverson High Shear Mixer. *American Institute of Chemical Engineers*. **58** 1683-1692
- DEMIRBAS, A. 2008. *Biodiesel: A Realistic Fuel Alternative for Diesel Engines*. London: Springer-Verlag London Limited. p.136
- DURAND-VIDAL, S. Simonin, J.-P. and Turq, P. 2000. Electrolytes at Interfaces. The Netherlands: Kluwer Academic Publishers. p. 47
- DUTTON, H. M. 2007. *The Behaviour of Surfactant Lamellar and Gel Phases Under Flow*. PhD Thesis. Manchester: University of Manchester
- EASTOE, J. 2010. *Colloid Science Principles, Methods and Applications*. West Sussex: John Wiley & Sons Ltd. p. 99
- FORGIARINI, A., Esquena, J., González, C. and Solans, C.. 2001. Formation of Nano-emulsions by Low-Energy Emulsification Methods at Constant Temperature. *Langmuir* **17** 2076–2083
- GERPEN, V. 2005. Biodiesel processing and production. *Fuel Process Technol.* **86** 1097–1107

- GRACE, H. P. 1982. Dispersion phenomena in high viscosity immiscible fluid systems and application of static mixers as dispersion devices in such systems. *Chem. Eng. Comm.* **14**. 225–277
- GRIFFIN, W. C. 1954. Calculation of HLB Values of Non-Ionic Surfactants. *Journal of the Society of Cosmetic Chemists.* **5** 249–256
- HALL, S., Cooke, M., Pacek, A. W., Kowalski, A. J. and Rothman, D. 2011. Scaling Up Of Silverson Rotor–Stator Mixers. *The Canadian Journal of Chemical Engineering.* **89** 1040 – 1050
- HALL, S., Pacek, A. W., Kowalski, A. J., Cooke, M. and Rothman, D. 2103. The effect of scale and interfacial tension on liquid–liquid dispersion in in-line Silverson rotor–stator mixers. *Chemical Engineering Research and Design.* **91** 2156–2168
- HAMLEY, I. W. 2005. *Block Copolymers in Solution: Fundamentals and Applications*. Chichester: John Wiley & Sons. p. 106
- HAMLEY, I. W. 2007. *Introduction to soft matter: synthetic and biological self-assembling materials*. Chichester: John Wiley and Sons. Section 3.6
- HARMSEN, R., Wesselink, B., Eichhammer, W. and Worrell, E. 2011. The unrecognized contribution of renewable energy to Europe’s energy savings target. *Energy Policy.* **39** 3425–3433
- HASENHUETTL , G. L. and Hartel, R. W. 2008. *Food Emulsifiers and Their Applications Second Edition*. New York: Springer Science. p. 309
- HUI, Y. H. 2006. *Handbook of Food Science, Technology, and Engineering Volume 4*. Boca Raton, FL: CRC Press. p. 154

- ICI AMERICAS. 1980. *The HLB SYSTEM a time-saving guide to emulsifier*. Wilmington, Delaware: ICI Americas Inc. p. 4
- IM-EMSAP, W., Siepmann, J. and Paeratakul, O. 2002. *Modern Pharmaceutics, Fourth Edition*. New York: Marcel Dekker, Inc. p. 409
- JASIŃSKA, M., Bałdyga, J., Cooke, M. and Kowalski, A. 2013. Application of test reactions to study micromixing in the rotor-stator mixer (test reactions for rotor-stator mixer). *Applied Thermal Engineering*. **57** 172–179
- JONASZ, M and Fournier, G. R. 2011. *Light Scattering by Particles in Water: Theoretical and Experimental Foundations*. London, UK: Elsevier. p. 359
- KARBSTEIN, H. and Schubert, H. 1995. Developments in the Continuous Mechanical Production of Oil-in-Water Macro-emulsions. *Chemical Engineering and Processing*. **34** 205–211
- KAYGUSUZ, K. 2008. The Future of Nuclear Power and Renewable Energy Sources in the European Union. *Energy Sources Part B*. **3** 348–361
- KOH, M. Y. and Mohd. Ghazi, T. I. 2011. A review of biodiesel production from *Jatropha curcas* L. oil. *Renewable and Sustainable Energy Reviews*. **15** 2240–2251
- KOWALSKI, A. J. 2009. An expression for the power consumption of in-line rotor-stator devices. *Chemical Engineering and Processing*. **48** 581–585
- KOWALSKI, A. J., Cooke, M. and Hall, S. 2011. Expression for turbulent power draw of an in-line Silverson high shear mixer. *Chemical Engineering Science*. **66** 241–249
- KRESTA, S. M. and Brodkey, R. S. 2004. *Handbook of Industrial Mixing: Science and Practice*. Chichester: John Wiley & Sons. p. 48

- LANDFESTER, K and Hentze, H.-P. 2001. *Reactions and Synthesis in Surfactant Systems*. New York, NY: Marcel Dekker. p. 473
- LANDFESTER, K. and Antonietti, M. 2004. *Colloids and Colloid Assemblies: Synthesis, Modification, Organization and Utilization of Colloid Particles*. New Jersey: John Wiley & Sons. 177–178
- LAWRENCE, J. and Warne, C. 1985. *A Pictorial History of Balmain to Glebe*. Sydney: Kingclear books. p. 56
- LEDUC, S. Natarajan, K., Dotzauer, E., McCallum, I. and Obersteiner, M. 2009. Optimizing biodiesel production in India. *Applied Energy*. **86** S125–S131
- LEUNG, D. and Guo, Y. 2006. Transesterification of neat and used frying oil: Optimization for biodiesel production. *Fuel Processing Technology*. **87** 883–890
- Leng, D. E. and Calabrese, R. V. 2004. *Handbook of Industrial Mixing: Science and Practice*. New Jersey: John Wiley & Sons. p. 658
- LIU, H. 1999. *Science and Engineering of Droplets: Fundamentals and Applications*. Norwich, NY: Noyes Publications / William Andrew Publishing. p127.
- LIU, L., Liu, C., Sun, Z. and Han, R. 2011. The development and application practice of neglected tidal energy in China. *Renewable and Sustainable Energy Reviews*. **15** 1089–1097
- MALVERN. 2012.
<http://www.malvern.com/labeng/products/mastersizer/ms2000/mastersizer2000.htm>.
[23rd August 2012](#)

MALVERN, 2013a.

http://www.malvern.com/labeng/technology/images/zeta_potential_schematic.png

7th October 2013.

MALVERN, 2013b.

http://www.malvern.com/labeng/technology/laser_diffraction/laser_diffraction.htm

[2nd September 2013.](#)

MALVERN. 2014. The enduring appeal of laser diffraction particle size analysis . Malvern White Paper.

<http://www.malvern.com/en/pdf/secure/WP110325EnduringAppealLaserDiff.pdf>

MASON, T. G., Graves, S. M., Wilking, J. N. and Lin, M. Y. 2006a. Extreme emulsification: formation and structure of nanoemulsions. *Condensed Matter Physics*. **9** 193-199

MASON, T. G., Wilking, J. N., Meleson, K., Chang, C. B. and Graves, S. M.. 2006b. Nanoemulsions: formation, structure, and physical properties. *J. Phys.: Condens. Matter*. **18** 635-666

MAZO, R. M. 2002. *Brownian Motion: Fluctuations, Dynamics, and Applications*. Oxford, Oxford University Press. p. 46

MCCLEMENTS, D. J. 2005. *Food Emulsions: Principles, Practices, and Techniques Second Edition*. Boca Ranton, FL: CRC Press Inc Press. p. 333

MCNAUGHT, A.D. and Wilkinson, A. 1997 IUPAC. *Compendium of Chemical Terminology, 2nd ed. (the "Gold Book")*. Oxford: Blackwell Scientific Publications

MELESON, K., Graves, S. and Mason, T. G. 2004. Formation of Concentrated Nanoemulsions by Extreme Shear. *Soft Materials*. **2** 109-123

- MERKUS, H. G. 2009. *Particle Size Measurements: Fundamentals, Practice, Quality*. Heidelberg: Springer-Verlag Berlin Heidelberg. p. 24
- MILLER, R., Kragel, J., Fainerman, V. B., Makievski, A. V., Grigoriev, D. O., Ravera, F., Liggieri, L., Kwok, D. Y. and Neumann, A. W. 2001. *Encyclopaedic handbook of emulsion technology*. New York: Marcel Dekker Inc. pp. 35-38
- MONK, P. M. S. 2005. *Physical chemistry: understanding our chemical world*. New Jersey: John Wiley and Sons
- MUELLER, S. A. 2008. Impact of biofuel production and other supply and demand factors on food price increases in 2008. *Biomass & Bioenergy*. **35** 1623
- MUN, S., Choi, Y., Shim, J.-Y., Park, K.-H. and Kima, Y.-R. 2011. Effects of enzymatically modified starch on the encapsulation efficiency and stability of water-in-oil-in-water emulsions. *Food Chemistry*. **128** 266-275
- MYERS, D. 2006. *Surfactant science and technology*. New Jersey: John Wiley & Sons. p. 130
- NAKACHE, E., Poulain, N., Candau, F., Orecchioni, A.-M. and Irache, J. M. 2000. *Handbook of Nanostructured Materials and Nanotechnology. Volume 5: Organics, Polymers and Biological Materials*. San Diego, CA: Academic Press. p. 582
- NASHAWI, I. S., Malallah, A. and Al-Bisharah, M. 2010. Forecasting World Crude Oil Production Using Multicyclic Hubbert Model. *Energy Fuels*. **24** 1788–1800
- NDONG, R., Montrejaud-Vignoles, M., Saint Girons, O., Gabrielle, B., Pirot, R., Domergue, M. and Sablayrolles, C. 2009. Life cycle assessment of biofuels from *Jatropha curcas* in West Africa: a field study. *GCB Bioenergy*. **1** 197–210

NGUYEN, N-M. 2012. *Micromixers: Fundamentals, Design and Fabrication Second edition*. Oxford: William Andrew. p. 163

NIJENHUIS, K., McKinley, G. H., Spiegelberg, S., Barnes, H. A., Aksel, N., Heymann, L. and Odell, J. A. 2007. *Springer Handbook of Experimental Fluid Mechanics*. Heidelberg: Springer-Verlag Berlin Heidelberg. Chapter 9

OBAYYA, S. 2011. *Computational Photonics*. Chichester: John Wiley & Sons. Chapter 2.3

PETERS, D. C. 1992 *Mixing in the Process Industries Second Edition*. Oxford: Butterworth Heinemann; pp. 294-301

PODOGORSKA, W and Baldyga, J. 2000. *10th European Conference on Mixing*. Amsterdam, The Netherlands: Elsevier.

POPP, N., Kutuzov, S. and Böker, A. 2010. *Complex Macromolecular Systems II*. Heidelberg: Springer-Verlag Berlin Heidelberg. p. 41

REDHEAD, J. F. and Boelen, M. 1990. *Utilization of Tropical Foods: Animal products. . Food Policy and Nutrition Division: Food and Agriculture Organization of the United Nations*. p. 42

REILLY, W. J. 2005. *Remington; The Science and Practice of Pharmacy 21st Edition*. Philadelphia, PA: Lippincott Williams & Wilkins. p. 1078

RUSSEL, W. B., Saville, D. A. and Schowalter, W. R. 1989a. *Colloidal Dispersions*. Cambridge: Cambridge University Press. p. 8

RUSSEL, W. B., Saville, D. A. and Schowalter, W. R. 1989b. *Colloidal Dispersions*. Cambridge: Cambridge University Press. p. 261

- RYŻAK, M. and Bieganowski, A. 2011. Methodological aspects of determining soil particle-size distribution using the laser diffraction method. *Journal of Plant Nutrition and Soil Science*. **174** 624–633
- SACKETT, L., Pestka, J. and Gisslen, W.. 2009. *Professional Garde Manger: A Comprehensive Guide to Cold Food Preparation*. New Jersey: John Wiley and Sons. p. 22
- SALARI, J. W. O., van Heck, J. and Klumperman, B. 2010. Steric Stabilization of Pickering Emulsions for the Efficient Synthesis of Polymeric Microcapsules. *Langmuir*. **26** 14929-14936
- SALARI, J. W. O., Leermakers, F. A. M. and Klumperman, B. 2011. Pickering Emulsions: Wetting and Colloidal Stability of Hairy Particles—A Self-Consistent Field Theory. *Langmuir*. **27** 6574-6583
- SARKAR, A. 2009. *Molecular Farming*. New Delhi: Discovery Publishing House Pvt. Ltd. p. 231
- SCHMITT, V., Arditty, S. and Leal-Calderon, F. 2004. *Emulsions: Structure, Stability and Interactions*. London: Elsevier Ltd. p. 608
- SCHUBERT, H. and Engel, R. 2004. Product and Formulation Engineering of Emulsions. *Chemical Engineering Research and Design*. **82** 1137–1143
- SJÖBLOM, J., Øye, G., Glomm, W. R., Hannisdal, A., Knag, M., Brandal, Ø., Ese, M.-H., Hemmingsen, P. V., Havre, T. E., Oschmann, H.-J., Kallevik, H. 2006. *Emulsions and emulsion stability*. Boca Raton, FL: CRC Press 456–457

- SOLANGI, K. H., Islam, M. R., Saidur, R., Rahim, N. A. and Fayaz, H.. 2011. A review on global solar energy policy. *Renewable and Sustainable Energy Reviews*. **15** 2149–2163
- SOMASUNDARAN, P., Mehta, S. C. and Purohit, P. 2006. Silicone emulsions. *Adv. Colloid Interface Sci.* **128-130** 103-109
- TAMBE, D. E. and SHARMA, M. M. 1994. The effect of colloidal particles on fluid-fluid interfacial properties and emulsion stability. *Advances in Colloid and Interface Science.* **52** 1–63
- THIS, H. 2007. *Building a meal: from molecular gastronomy to culinary constructivism*. New York: Columbia University Press. p. 33
- TING, W.-J., Huang, C.-M., Giridhar, N. and Wu, W.-T.. 2008. An enzymatic/acid-catalyzed hybrid process for biodiesel production from soybean oil. *Journal of the Chinese Institute of Chemical Engineers.* **39** 203– 210
- TODD, D. B. 2004. *Handbook of Industrial Mixing: Science and Practice*. New Jersey: John Wiley & Sons. p. 998
- TOEDT, J., Koza, D. and Van Cleef-Toedt, K. 2005. *Chemical Composition Of Everyday Products*. Westport CT; Greenwood Press. p. 4
- UTRACKI, L. A. and Favis, B. D. 1989. *Handbook of Polymer Science and Technology*, Volume 4. New York: Marcel Dekker, Inc. p.174
- VYAKARANAM, K., Evans, M., Ashokan, B. and Kokini, J. L. 2009. *Food Mixing: Principles and Applications*. Chichester: Wiley-Blackwell. p. 253
- WALFITPAINTS. 2012. <http://www.walfitpaints.com/full-images/acrylic-emulsion-paint-730233.jpg>. 19th August 2012

- WALSTRA, P. 2003. *Physical Chemistry of Foods*. New York, NY: Marcel Dekker, Inc. p. 434
- WANG, K. G. and Glicksman, M. E. 2010. *Materials Processing Handbook*. Boca Raton, FL: CRC Press. p. 5-2
- WANG, L., Zhou, X. and Wei, X. 2008. *Heat Conduction: Mathematical Models and Analytical Solutions*. Heidelberg: Springer-Verlag Berlin Heidelberg. p. 138
- WANG, Y. 2000. *Compounding in Co-Rotating Twin-Screw Extruders*. Shrewsbury: Rapra Technology Ltd. p. 10
- WANSBROUGH, H. 1998. *Chemical Processes in New Zealand (second edition)*. New Zealand Institute of Chemistry. Chapter 11A
- WEISS, J. and McClements, D. J. 2006. *Encyclopedia of Surface and Colloid Science: Second Edition*. Boca Raton, FL: CRC Press. p. 3528
- WERNER, S., Kraume, M. and Eibl, D.. 2011. *Single-Use Technology in Biopharmaceutical Manufacture*. New Jersey: John Wiley & Sons. Chapter 3.2
- WITTEN, T. A. and PINCUS, P. A. 2004. *Structured fluids*. Oxford: Oxford University Press. p. 178-180
- ZHONG, J. P., Fathi, Z., LaTorre, G. P., Folz, D. C. and Clark, D. E. 1994. *Proceedings of the 18th Annual Conference on Composites and Advanced Ceramic Materials: January 9-14, 1993*. Westerville, OH: The American Ceramic Society. p. 1020

Chapter 3 Mixing and Processing Equipment

3.1 Introduction

This chapter presents an introduction to some of the diverse types of mixing technologies typically employed when formulating emulsions. Also discussed is the next generation of mixing/ and processing research tools now available.

Fluid processing equipment has been used since man first started to process foods for both cooking and preservation. The simple spoon is a device which allows the distributive mixing of materials into one homogenous mass, the simple stirring mechanism employed when stirring a spoon within a cup of coffee for example utilises distributive mixing of the hot water and coffee granules which in turn leads to dispersion of the coffee into smaller parts to increase the rate of diffusion of the coffee concentrate into solution.

Throughout the course of the research undertaken and presented within this thesis, numerous mixing devices were used in order to formulate the emulsions analysed and/or subsequently reacted. The mixers used include both distributive and dispersive mixers. The distributive mixers used included a simple magnetic flea and a magnetic stirrer plate, pitched-blade turbines (both 4 and 6 bladed) and simple impellers (3 blade). Used more often throughout this work were dispersive mixers as the focus was on reduction of droplet size. Dispersive mixers used included a saw-tooth impeller, high-shear homogenisers, including a fluid division mixer (FDM), and a microfluidizer. The Ultra Mixing and Processing Facility (UMPF) can operate as a distributive mixer, a dispersive mixer or using the CDDM technology it can

operate as both. Although care has been taken to describe the specific equipment used, this section is not expected to present a full review of all mixing devices.

3.2 Small Scale Laboratory Mixing

The simplest device used within this work consisted of magnetic stirrer bars and a magnetic stirrer plate. These small bars sit at the base of the chosen mixing vessel, which in turn is placed on a magnetic stirrer plate, an example of which can be seen in Figure 3-1.



Figure 3-1 IKA hotplate stirrer (Savern, 2012)

The bars are then made to rotate at a designated speed using a series of magnets within the stirrer plate which causes the stirrer bar to stir at the predetermined speed. This stirring subsequently creates a vortex within the mixing vessel which pulls the reagents within the vessel down, if great enough, forcing them to interact with each other. An example of the equipment, magnetic stirrer bars and vortexing is shown in Figure 3-2.

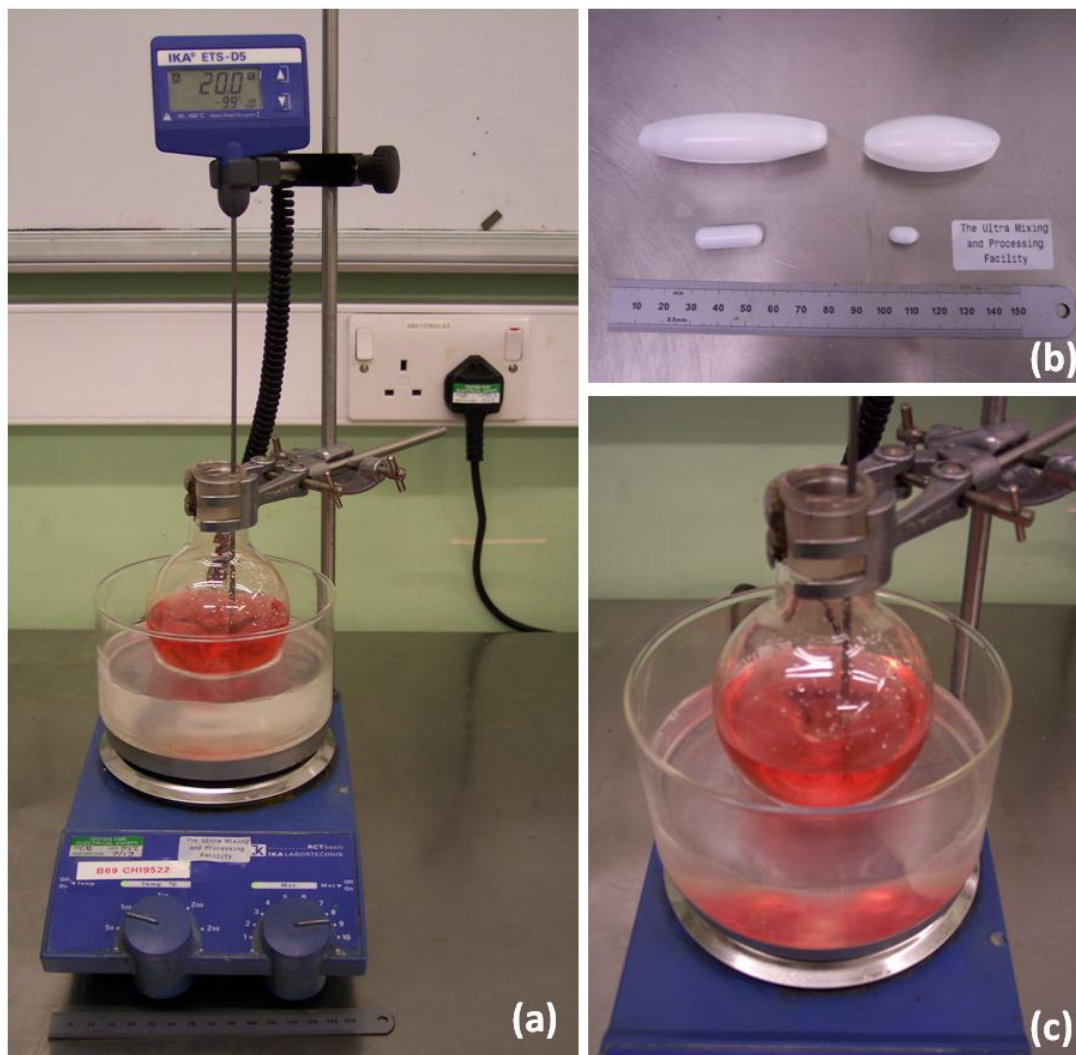


Figure 3-2 a) Magnetic stirrer hot plate with digital dip temperature control
b) Range of magnetic stirrer bars from small to large
c) Magnetic stirrer bar creating a vortex within the reaction vessel at high rpm.

For more viscous materials stirrer bars have little to no impact as there is not enough force driving them to cause the viscous fluid to begin moving.

3.2.1 Paddle Stirrer

Paddle stirrers are the simplest electrically powered mixer available commercially.

They consist generally of three paddles attached to a central shaft which rotates at

speeds determined by the operator. A selection of impellers is displayed in Figure 3-3 with the paddle stirrer shown second in from the right side of the image.

As the shaft of the impeller rotates, the paddles are forced to rotate also. With the paddles being slightly angled, they have a significantly large surface area and are able to force the fluid within the vessel they are placed in to travel in the same direction as them, at a speed similar to them. The flow generally produced by this type of mixing devices is laminar flow (although it is entirely dependent on the Reynolds number) as the flow is all in the same direction, and with the absence of baffles there is little in the way of turbulence, especially after the initial input of energy into the system and when the system has reached an equilibrium state.

Initially the paddles are unable to move at the full speed set by the operator as the fluid is static and the most of the energy initially is used to get the fluid moving. The rate at which the fluid moves increases until eventually the fluid is moving round the vessel at almost the same rate as the paddles.

When placed in a cylindrical reaction vessel a paddle stirrer (when operated) causes fluid to circulate the vessel repeatedly until it is travelling around the vessel at almost an equal speed to the paddles, this creates a vortex above the paddles, similar to that seen when using a magnetic stirrer bar. Due to the design of the mixer, it is best used with low viscous fluids as the force generated to cause the vessel contents to mix is almost entirely reliant on the motor.

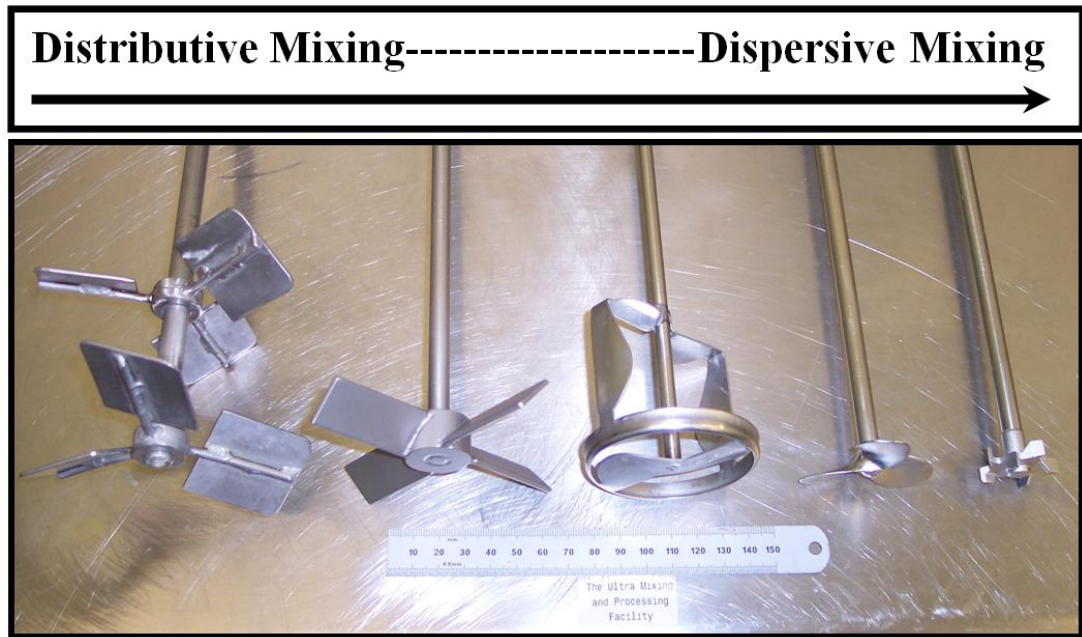


Figure 3-3 Photograph of different mixing impeller types and the corresponding mixing they are designed for.

Figure 3-3 displays a photograph of different mixing impeller types that were used. In the image, from left to right are; 6-pitched-blade turbine, 4-pitched-blade turbine, a turbine stirrer, a 3-blade-propeller and a saw-tooth impeller.

3.2.2 Pitched-blade turbine

Pitched-blade turbines are based on the design of a paddle-stirrer, however they contain more blades, and as the name implies the blades are pitched at an angle (commonly 45°). Two pitched blade impellers are displayed in Figure 3-3, a six pitched blade impeller [far left] and a four pitched blade impeller [second from left].

In order to improve the mixing efficiency of the devices that create a vortex when used within a cylindrical vessel, the implementation of baffles on the sides of the mixing vessels was followed. Baffles are flat, rectangular strips that are attached to the vessel, usually, at a 90° angle along the wall of the mixing vessel from the base

to the top. They are used to improve mixing and do so by diverting the flow of fluid from merely going round and round the mixing vessel, to also up and down the baffles upon impact with them, thus greatly increasing agitation and mixing capability.

3.2.3 Homogenisers

Unlike those mixing devices listed so far, homogenisers do not require baffles for good mixing. They function well in a standard cylindrical mixing vessel and were used during this research primarily for formulating emulsions with small droplets uniformly dispersed throughout the mixing vessel. Homogenisers come in a range of sizes and capabilities, from ones designed to grind/mince-up biological tissue samples to the industrial ones used to produce emulsions. The difference between those two namely being the “teeth” used to grind up samples. During this research focus was given to the use of high-shear homogenisers for emulsion production.

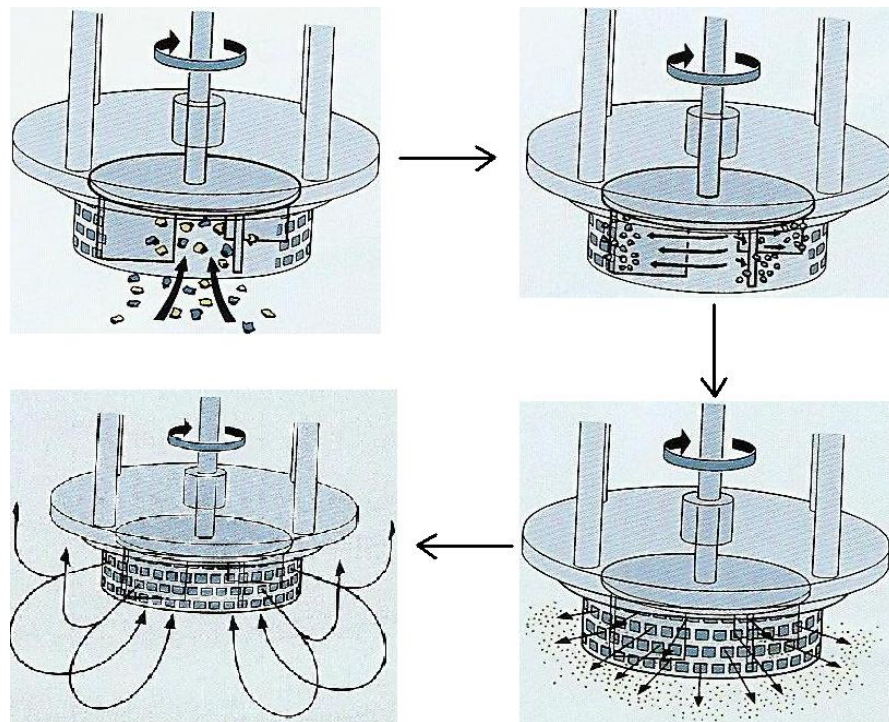


Figure 3-4 Four stages of how a homogeniser works (Silverson, 2012).

Figure 3-4 explains graphically how a homogeniser works as it operates on a rotor-stator principle, shown in the figure is how the Silverson L4R works. The impeller rotates at high speed creating a low pressure region at the centre that pulls the reagents up and into the stator where they are forced to interact with each other whilst being subjected to shear forces. The reagents are then forced out of the small holes in the stator reducing their size. The final stage shows that upon exiting through the small holes in the stator, due to the turbulent forces generated by the high rotation of the impeller, the reagents are forced down to the base of the vessel and then up to the top, creating turbulent flow of fluid within the vessel.

When mixing fluids with a low viscosity, the homogeniser was able to both reduce the droplet size of the fluids and cause good dispersion to the point of uniformity, however the mixer was unable to mix high-viscosity fluids. This is because the pressure differential is not large enough to pull thick viscous fluid through the mixer. Another negative issue that can occur when using the homogeniser at high speed is foaming. As the system works on pressure differentials, occasionally during mixing air can be pulled into the system. When using high concentrations of a known-to-foam surfactant, then once air has entered the system, it starts a chain reaction of bubble formation, which eventually leads to the whole process being put on hold until the fluid is deaerated.

3.3 Batch mixers

3.3.1 Fluid Division Mixer (FDM)

The Fluid Division Mixer (FDM) can be used for creating large batches of emulsions. The way in which the FDM works is similar to a high-shear homogeniser in that it generates its own force that pulls the fluid through the channels in order to

force the reagents present to mix, as shown in Figure 3-5a-c. Unlike other high-shear homogenisers, such as the Silverson L4R, the FDM is able to process higher viscosity fluids (up to 50,000 cSt) and use self-generated centrifugal action to ensure the fluid is consistently processed (Maelstrom APT, 2001).

The diameter of the FDM is 86.0 mm; however it should be noted that it has a shaft running through the centre of it. The inflow hole, Figure 3-5e, in the centre of the stator is 20.05mm wide. The distance from the top of the first cavity to the centre of the inflow hole is 24.07 mm, and the height of each cavity is 4.95mm (exact values in appendix 9.1). Each cavity was measured and the details for these are in the appendices (appendix 9.1).

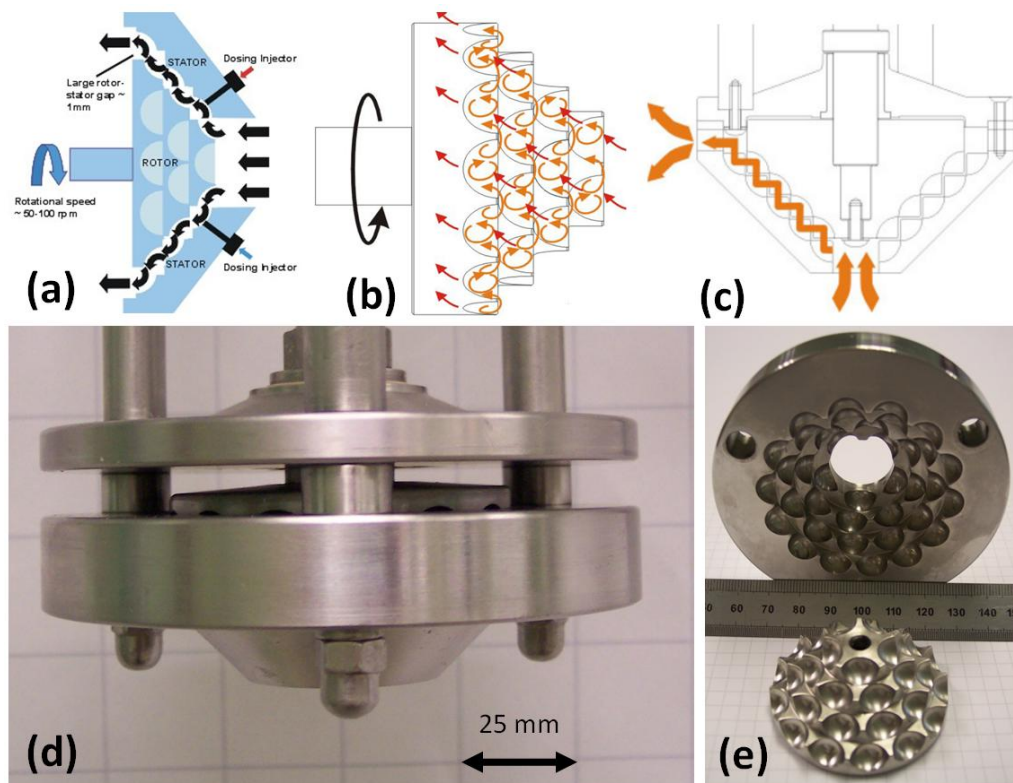


Figure 3-5 a) Direction of fluid when the mixer is turning.
 b) Fluid movement within the cavities of the mixer head.
 c) Direction of the fluid during mixing.
 d) The mixer head of the FDM.
 e) Inside of the mixer head showing the cavities.

Inter-cavity fluid transfer between the rotor and stator elements are the existing principles upon which the FDM has been designed. The theory behind how the process works is shown visually in Figure 3-5b. Fluid passes between moving cavities before it is then forced apart and dispersed. The combination of turbulent shear and inter-cavity transfer in combination with the centrifugal forces generated during the mixing process, ensure that all fluid within the mixing vessel is processed and after a short amount of time is uniformly dispersed throughout the vessel. Further mixing leads to a decrease in particle size until the droplets become so small the mixer has no more impact upon them.

3.3.2 Microfluidizer

The microfluidizer is a high-pressure mixing device and is displayed in Figure 3-6. The air-powered intensifier pump provides high pressure throughout each pumping cycle. As the pump forces the air out, the pressure generated forces the reagents within the microfluidizer through a series of microchannels causing them to interact and reduce in size greatly, usually to submicron.



Figure 3-6 Microfluidizer (Microfluidics, 2005).

It is this design that allows the microfluidizer to be used at the beginning, the middle or the end of the development chain when it comes to working with emulsions and their subsequent products; shampoos, conditioners, etc. At the beginning of the development chain it works well, as it forces the reagents to mix at high pressure in an enclosed environment by pushing them all through microchannel pipe-work at once. At the middle/end of the development chain the premixed fluid can be placed in the machine, where it is reduced in droplet size as it is forced through the small pipe-work under high pressure until it is of a droplet size smaller than the diameter of the pipe. Reprocessing premade fluid subsequently will further reduce the droplet size of the fluid until the droplets become so small that the Laplace pressure cannot be exceeded.

The microfluidizer attempts to force the fluid through the microchannels at a flow rate of $4\text{mL}\cdot\text{s}^{-1}$ to $10\text{mL}\cdot\text{s}^{-1}$. If the size of the droplets is too large then the fluid cannot pass through the microchannels at this flow rate and an energy build-up from the force being applied occurs. One way in which some of the energy is transferred out of the system is in the form of heat. This causes a temperature rise within the system, however to ensure this does not alter the chemistry of the fluid the bottleneck prior to the microchannels [and the microchannels themselves] can be kept in cool water/ice to ensure no extreme temperature fluctuations occur.

3.4 The Ultra Mixing and Processing Facility

The “Ultra Mixing and Processing Facility” or “UMPF” is a pilot plant scale prototype fluid mixing and processing laboratory based in the Department of Chemistry in the University of Liverpool, U.K. The UMPF Laboratory houses unique fluid dispensing and processing equipment; up to five streams of different

process fluids can be metered and mixed under precisely specified conditions of relevance to the manufacture and dispersion of fluid like materials into products. With the ability to measure, characterise and alter a number of process variables, including fluid flow rates (combined and individual) and temperatures, mixer speed and pressure regime (section 3.4.3 details the specification and modes of operation of the UMPF).

A key aspect of the UMPF system is its ability to extend certain performance parameters beyond those achievable through commercially available equipment, in particular combining both dispersive and distributive mixing while maintaining a high flow rate. With the dual role of a precise experimental tool for fundamental research, and an open access facility primed to facilitate innovation across the process sector of UK industry; the UMPF was built with multi scale, flexible operation for rapid product roll out in mind.

The UMPF prototype is a high-pressure mixing device capable of mixing five fast moving, separate, streams at once. Each of these streams is forced into the central mixing chamber by a dosing injector, referred to as syringe or intensifier pump, and these are each fed by their own eleven litre feed vessel. The feed vessels, which provide the reagents for the intensifier pumps, are kept under “top pressure” when in use. The top pressure forces the reagent within the feed vessel into the pump as it opens (draws back) before it is subsequently driven into the mixing chamber as the pump closes.

Unlike most mixing devices the UMPF is able to operate in either batch mode or continuous mode; it is not restricted to one or the other except when it is in use. Batch mode allows for up to all five pumps to be used at once, in a one shot mixing

run. When running the UMPF in continuous mode, there is a trade off that occurs; only three different reagents can be used. In order to run in continuous process the four medium intensifier pumps (MIPs) have to work in pairs. When running in continuous mode the MIPs operate alternately so whilst two are closing and dispensing fluid, the other two are opening and filling. The MIPs are numbered anti-clockwise starting from one, through to four, with the LIP located between MIP 1 and MIP 4 as can be seen in Figure 3-7. MIPs 1 and 2 operate as a pair in continuous mode, as do MIPs 3 and 4.

The mixing device at the centre of the UMPF is a rotor-stator of unique, patented design that can operate at speeds of up to 18,000rpm. It is able to operate under pressure and deal with high viscosity fluids in excess of 100,000cSt. The design of the mixer head itself is such that when assembled the machine can be used to process fluid as per one of any different mixing regime; for example it can be set to process fluid in a manner similar to that of a High Stress Mixer (HSM) with great dispersive properties, or it can be realigned to have greater distributive properties such as the way the FDM works. The combination of extensive dispersive properties and extensive distributive properties is the heart of the UMPF technology and is labelled as Controllable Deformation Dynamic Mixing (CDDM) due to it being able to operate in a fashion to almost any current mixing device.

The high-torque motor connected to the rotor-stator is, as the name implies, designed to cope with viscous materials, which generate large amounts of torque when mixed. Prior to the high-torque motor being installed a low-torque; high-speed motor was used to turn the impeller. Significantly smaller than the high-torque motor, the high-speed motor was capable of operating at speeds up to, and including, 50,000rpm. This motor, due to the low tolerance of viscosity had to be replaced in order to allow

greater and further exploration of formulation space as high phase volumes of oil formulated a product too viscous for the motor to process as well as limiting the viscosity of the oils that could be observed prior to emulsion formulation.

The UMPF was designed to explore the range of distributive and dispersive mixing techniques on a range of viscous materials from natural oils, such as sunflower seed oil, to highly viscous oils, such as 100,000cSt silicone oil. It is through both high shear and the ability to use extensional flow to deform droplets, and through the design of the CDDM to subsequently break these droplets, that makes the UMPF a unique mixer.

Capable of achieving and coping with pressures up to and including 5000 bar initially, there was discussion of using the UMPF as an industrial scale reactor vessel. Being a prototype machine, a methodology had to be designed, tested and implemented to vet potential reagents before they were used in the UMPF to ensure they would not cause significant damage to the equipment. Following numerous discussions the idea for using the UMPF as a reactor vessel was placed on hold, and put under the “further work” bracket of research and development for the facility.

The only reagents to be given clearance to be used as reactants in the UMPF before a formal vetting system was devised and implemented were silicone oil, Sodium Laureth Ether Sulfate (SLES) solution and filtered/distilled/purified water. The main components of the UMPF are built out of 17/4PH (Precipitation Hardened) Stainless Steel and Zirconia-Ceramic steel. Both of these materials were chosen for their highly resistive properties and the great strength they possess. Precipitation hardening is a technique used to increase the strength of a metal via heat treatment (AK Steel, 2007; Coriell, 2001). The strength of the metal is not the only property

that is altered following precipitation hardening; it improves the corrosion resistance, the formability, whilst maintaining its weldability (AK Steel, 2007). As a result the steel is capable of withstanding high pressures and temperatures and was chosen as it will not only last for an extensive period of time but more importantly for the purpose of safety.

As the mixer has been designed for liquid only systems a method for testing proposed reagents to be used was devised and can be found in section 9.1 of the appendix.

3.4.1 Constraints

The UMPF is accessible by hire to all academic and industrial institutions [without prejudice]. Whilst it is important the UMPF is flexible enough to cope with the demands of a wide range of users and remains respectful of the grant funding provided by the Department of Trade and Industry (DTI), an essential consideration of the performance specification detailed below is the personnel safety of the facility users. This cannot be compromised by either technical (in terms of experimental flexibility) or budgetary constraints.

It is to this end that any access to the equipment will not be direct but rather through a suitably qualified and trained member of University staff (Dr Mike Egan, UMPF Operations Manager), and will always be subject to a risk assessment to determine what, if any, limits will need to be applied to the system and its mode of operation for the experiments to proceed.

The work performed using the UMPF within this thesis, was subject to this process.

3.4.2 Equipment list

With reference to Figure 3-7 and Figure 3-8, the UMPF Equipment asset includes:

- Five dosing injectors (intensifier) pumps: each with feed vessels for loading raw materials into the system four with a maximum internal volume of 200mL and one with a maximum internal volume of 750mL
- Mixer body: containing mixing head, plain bearing annular seals, body constrains fluid flow over mixer and supports pipework and instrumentation from pumps.
- Pipework and fittings
- Post mixer cooling system incorporating a heat exchanger
- Sampling and dump vessels for output materials
- Electrical drive and control system for the mixer
- Hydraulic drive and control system for the pumps
- Instrumentation
- SCADA type data entry, display and storage system

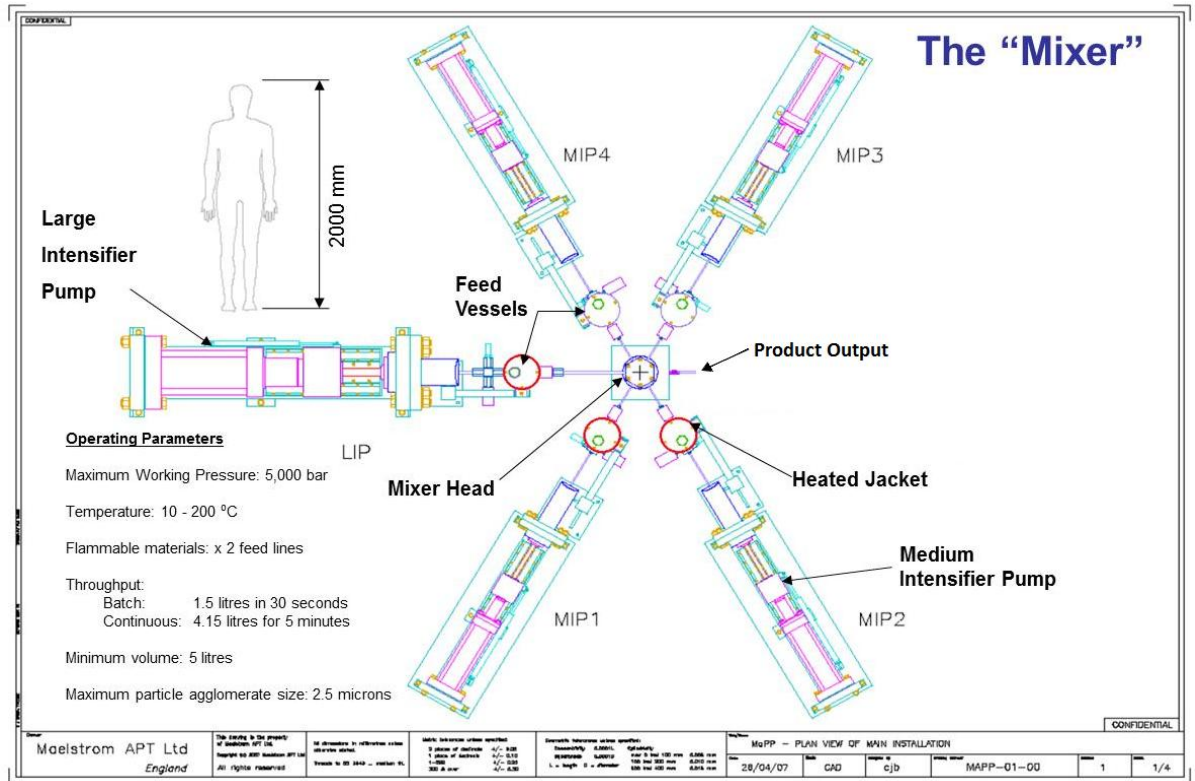


Figure 3-7 Schematic drawing of the UMPF.

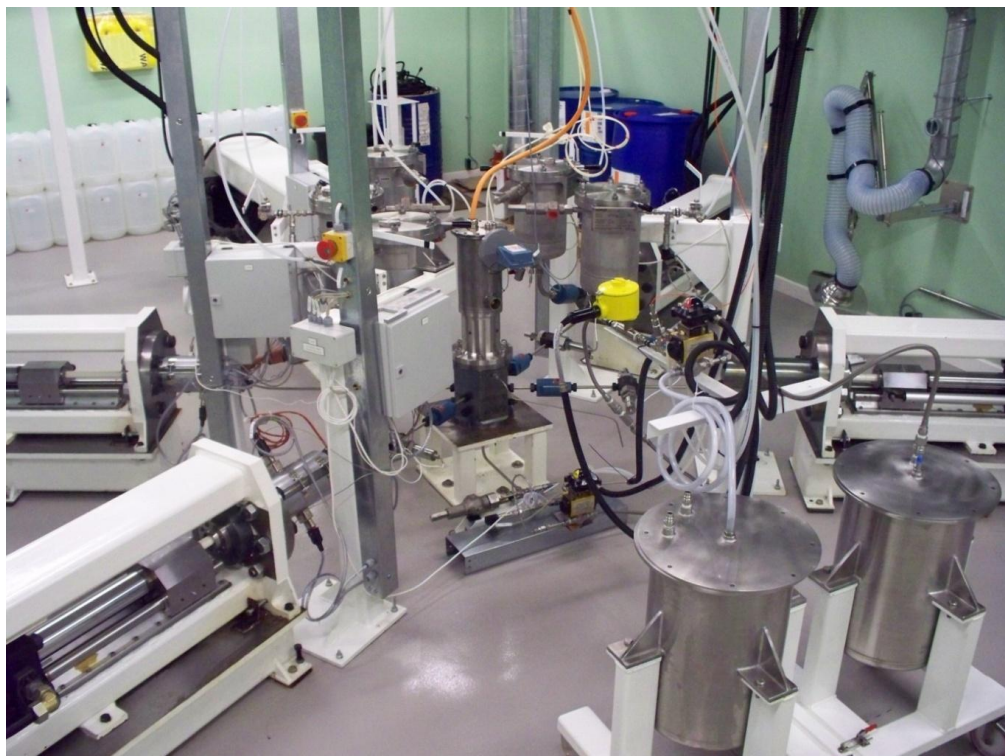


Figure 3-8 The Ultra Mixing and Processing Facility as it was in May 2008.

3.4.3 Operating Parameters

- **Maximum Working Pressure:** (Viscosity and flow rate dependent) – 5000 bar +/-500 bar maximum with mixer stationary
- **Temperature:** Large Intensifier Pump (LIP), Medium Intensifier Pump (MIP) 1 & MIP 2 only: 15 – 200 °C
- **Fluid types:** Liquid/liquid and soft solid/liquid mixtures [including slurries], provided that no solids fall out of suspension in a static fluid within 30 minutes. No hard inorganic solid particles are allowed, at any point, into the system.
- **Permitted materials:** The system is designed to handle as wide a range of materials as possible, subject to the following acceptable user constraints:
 - not highly flammable (this excludes IEC IIC type materials from being used)
 - not containing pathogens
 - non-radioactive, non-ionising
 - non-energetic
 - non-carcinogenic or mutagenic
 - materials must be compatible with the materials of construction of the system
- **Flammable materials within MIP 3 & MIP4 only.**
- **Throughput:**
 - **Batch mode:** 3.1 L/min +/- 0.3 L/min up to 5000 bar and 15.5 L/min +/-1.5 L/min up to 1000 bar
 - **Pseudo continuous mode:** 4.15 L/min +/-0.4 L/min up to 1000 bar

- **Minimum volume required for each pump:** 5 litres.

3.4.4 Capabilities

The UMPF was still undergoing validation during the entirety of the work presented within this thesis. From the design of the equipment it is believed that laminar flow occurs when fluid is forced through the pipe-work from the feed vessels due to the pumps acting as syringes and due to the pressure the liquid is under preventing turbulent flow. When fluid is forced out into the mixing chamber, it is believed that it is here that turbulent flow can occur, as well as mixing, allowing for the UMPF to be capable of manipulating fluid through all flow types.

A full assessment of the mixing regimes and confirmation of flow types the UMPF is capable of putting fluid through is being undertaken by a fellow researcher and is a research project within itself. The focus of the work presented within this document was to assess the impact that the UMPF has on reducing the droplet size of emulsions, both during emulsification, and post emulsification.

3.5 References

AK STEEL. 2007. 17-4 PH Stainless Steel Product Data Sheet.

[http://www.aksteel.com/pdf/markets_products/stainless/precipitation/17-4 PH Data Sheet.pdf](http://www.aksteel.com/pdf/markets_products/stainless/precipitation/17-4_PH_Data_Sheet.pdf). 19th August 2012

CORIELL, S. 2001. *A Century of Excellence in Measurements, Standards, and Technology*. Boca Ranton, FL: CRC Press Inc. p. 14 – 15

MAELSTROM APT. 2001. FDM Technology brochure. Maelstrom Advanced Processing Technologies

MICROFLUIDICS, 2005. Image obtained from M-110S Microfluidizer® Materials Processor brochure. Copyright of this image belongs to Microfluidics and has been used with permission.

SERVERN 2012. Images owned by Serven Sales, used with permission.

SILVERSON M. 2012. Images owned by Silverson Machines, Inc. obtained from catalogue.

Chapter 4 High-Throughput Emulsification

4.1 Abstract

As discussed in section 2.2 forming emulsions requires mechanical agitation to provide energy to overcome the thermodynamic lowest energy state of the two immiscible liquids. The work that was performed and is presented in this chapter looked to not only emulsify liquids but to produce emulsions with a droplet size as small as possible. Using a high-throughput platform and design of experiments (DoE) software, both process and formulation parameters were mapped out and the emulsions made at the most extreme conditions of the variables possible. These emulsions were then analysed to assess the size of the droplets that made them up. A series of algorithms were then used to predict the conditions required to make an emulsion with the smallest possible droplet size within the limits set. These parameters were followed, and an emulsion made, to ascertain whether within the time-frame provided it is possible to create an emulsion with the smallest droplet size possible. The data presented shows that, to our knowledge, an emulsion with the smallest droplet size possible was obtained (within the parameters set for the variables) within a number of days.

The work in this chapter has been published in:

- NanoFormulation; Riding, V., Harvey, D., Martin, P. J. and Kowalski, A. J. 2012. *The Effect Of Formulation And Process Variables On Droplet Size Reduction Using A High-Throughput Platform*. Cambridge: The Royal Society of Chemistry. p. 160
- Journal of Dispersion Science and Technology; Harvey, D. H. S., Egan, M. J. and Kowalski, A. J. 2013. Use Of Formax High-Throughput Platform To Create A Specific Emulsion. *Journal of Dispersion Science and Technology*. **34** 441–543 DOI:10.1080/01932691.2012.657131

4.2 Introduction

For direct and inverse emulsions, once the immiscible liquid has been dispersed throughout the continuous phase, it is necessary to stabilize the droplets using a surface active agent, more commonly known as a surfactant or an emulsifier, in order to prevent the newly formed droplets coalescing. The surfactant provides a stabilizing repulsion between the droplet interfaces and is usually soluble within the continuous phase (Mason et al., 2006a). When choosing which surfactant to use, the hydrophilic-lipophilic balance (HLB) concept is commonly used (discussed in section 2.3).

In order for droplet deformation to occur the surface and internal viscous forces must firstly be overcome. The most common practise for this is to apply mechanical forces to the surrounding fluid. For droplet break-up to occur the combined resistance forces must be exceeded by the fluid forces. Elongated droplets do not always break-up, in fact in some cases the unconventional shape can be a precursor for the

establishment of internal rotation or circulation which then helps in the stabilising of the droplet.

Interfacial tension opposes drop deformation and in the absence of a driving force causes the elongated droplet to regain its spherical shape. Unless critical deformation is reached during stretching of the droplet, breakage does not occur. Should it not occur, the droplet reverts to a condition of lower deformation as it passes to a region of lower shear rate and the drop becomes more spherical. Collisions with solid surfaces cause droplets to disperse through the vessel. As a result of this the geometry of the impeller, blades, baffles, tank and vessel walls are all important for dispersion. In stirred tanks fluid shear forces are the main cause of drop dispersion whereas in static mixers and rotor-stator machines impingement can be of importance (Leng and Calabrese, 2004).

For emulsions made up of significantly smaller droplets, other factors arise and become a requirement. This is particularly important for nanoscale colloids. Repulsive interactions between the colloids, due to excluded volume, charge on the particles' surfaces, or 'steric' interactions arising from brush-like coating of polymers on their surfaces, can effectively prevent particles from aggregating together, and the suspension will remain homogeneous (Mason et al., 2006b). Conversely, attractive interactions arising between structures within the dispersed phase can arise, leading to aggregation and rapid sedimentation (Mason et al., 2006b).

Often, it is desirable to reduce the size of the droplets within the emulsion to increase the available surface area of a given volume of oil/water (dependent on which constitutes the continuous phase). Consequently the $D[3,2]$ value which is a surface

area weighted mean, often referred to as the Sauter mean diameter, is the preferred measurement although the $D[4,3]$ which is the volume weighted mean, and is conceptually similar to a sieve measurement, is also worth taking into account. The $D[3,2]$ value is calculated to be the ratio of the total volume of the particles to the total surface area; thus the smaller the number, the greater the available surface area (Phadke and Eichorst, 1991). Most commercial particle sizers will automatically calculate these various types of mean particle size.

The definition of the adjective “nanoemulsion” has been the subject of debate amongst the academic community, with different authors quoting different ranges of size; Mason and Meleson define a nanoemulsion as droplets that are smaller than a 100nm in size, Wang defines a nanoemulsion as being made up of droplets within the size range of 20 to 200nm whereas Forgiarini describe an emulsion made up of droplets within the region of 20 to 500nm in size being a nanoemulsion (Mason et al., 2006a; Mason et al., 2006b; Meleson et al., 2004; Forgiarini et al., 2001; Wang et al., 2007). On 31st October 2010 ISO/TS 80004-1:2010 was published and defined the nanoscale as size range from approximately 1nm to 100nm.

Microemulsions is a term reserved for thermodynamically stable emulsions consisting of nanodroplets, droplets with a particle size less than 100nm which spontaneously form with very little mechanical agitation as a consequence of a specific combination of surfactants (Nir et al., 2010; Spernath and Aserin, 2006). Despite the differences in opinion on these points, all those involved in the area of nanoemulsions agree that the function and impact nanoemulsions potentially have for improving commercial products such as pesticides, improved drug delivery and sterilising aids are huge (Gottenbos et al., 2002; Spernath and Aserin, 2006; Wang et al., 2007).

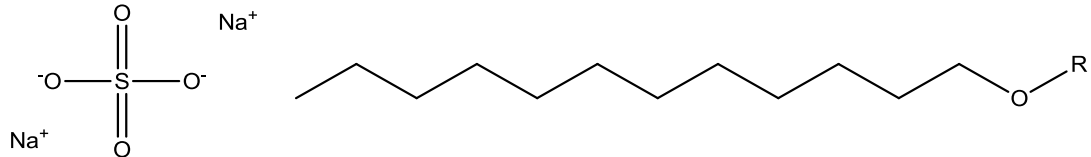
The aim of this work was to use a combination of a high-throughput platform and design-of-experiment (DoE) software to obtain the process and formulation parameters required to make an emulsion with the smallest possible drop size [within the limitations of the equipment].

4.3 Initial Experimental

4.3.1 Materials

The reagents used for these trials involved DOW CORNING® 200 FLUID, a polydimethylsiloxane polymer, more commonly known as silicone oil. TEXAPON® N 70, a highly concentrated [70%] sodium lauryl ether sulphate (SLES) that is derived from natural fatty alcohols and displayed in Table 4-1. Any reference to water within this chapter is to distilled water.

Table 4-1 listing the properties of SLES.

Surfactant Name: Sodium Lauryl Ether Sulfate	CAS Numbers: 9004-82-4
Common Names: Sodium laureth sulphate, Sodium Lauryl Ether Sulfate	Surfactant type: Anionic
Chemical Formula: C ₂₄ H ₅₀ Na ₂ O ₅ S Molecular Weight: 496.70  R = C ₁₂ H ₂₅	
CMC:	HLB: 5.72
Appearance: Yellow Paste	Relative Density: 1.040

4.3.2 Formax High-Throughput Formulation Platform

The high-throughput platform used to complete this work is marketed by Chemspeed Technologies AG and access to the kit was provided by the Centre for Materials Discovery (CMD) at the University of Liverpool. The Formax platform, shown in Figure 4-1, is highly versatile and employs a range of tried and tested tools from other platforms developed by Chemspeed and newer tools.

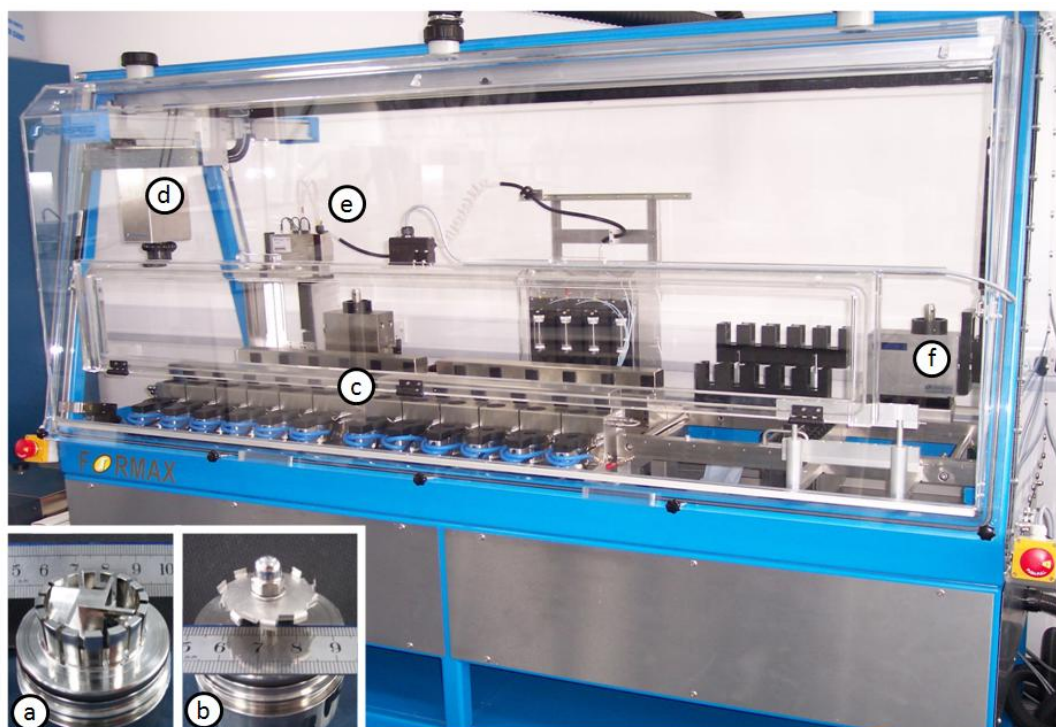


Figure 4-1 Chemspeed Formax high-throughput platform showing:
 a) Rotor-Stator head, b) Saw tooth impellor, c) 12 reaction vessels,
 d) robotic manipulator e) 4-needle liquid handling unit and
 f) GDU-HV: Gravimetric Dispensing Unit for High Viscosity reagents.

For dispensing reagents there is the option of liquid transfer, viscous liquid transfer, solid dispensing and powder dispensing.

- Liquid transfer is performed by the 4-needle liquid handling unit. Each needle within this tool is connected to its own syringe, allowing different syringe sizes to be placed on the platform for more accurate dispensing of varying volumes of liquid. Within the CMD there is the option of three different needles that can be placed on the tool; standard diameter needle for water/solvent transfer, wide-bore diameter needle for slightly viscous materials and a spray needle for dispensing liquid uniformly into a reaction vessel. The fluid is drawn up into the syringe by the negative pressure as the plunger is drawn back and as a consequence is not suitable for high viscosity

fluids. Dispensing accuracy is based on volumetric depression by the syringe and knowledge of the density of the fluids.

- Viscous liquid transfer is performed by the Gravimetric Dispensing Unit-High Viscosity (GDU-HV). The GDU-HV works by picking up pre-filled 60mL cartridges from known locations on the deck of the platform, transferring them to the required location and then a plunger slowly forces the viscous liquid out through a pipette tip of chosen diameter. The diameter of the pipette tip is based on the viscosity of the fluid being dispensed, for low viscosity fluids a small diameter pipette tip is required whereas the higher the viscosity of the fluid the greater the diameter of the opening of the pipette tip required. The speed at which the plunger operates is determined via a series of preliminary calibration trials. The speed at which the reagent can be dispensed is inversely proportional to the viscosity of the reagent being dispensed.
- There is also the potential to have heated cartridges on the deck which can be programmed to remain at temperature until needed and are kept at temperature whilst being dispensed. The maximum number of standard 60mL cartridges able to fit on the deck of the Formax is fifteen as well as four 60mL heated cartridges.
- Solid [granular] dispensing and powder dispensing are both carried out by a GDU similar to the GDU-HV, however these were not used during this project and consequently are not described further here.

The Formax platform used to obtain the data within this paper had a deck containing 12 reactor vessels, however for the model used there is the potential to double this and have a further 12 installed. Each reactor vessel has a maximum internal volume

of 100mL and can have a different impeller type to those vessels around it (the impeller types are shown in Figure 4-1). The two impeller types available at present are the dissolver disk and the rotor-stator. The dissolver disk is effectively a saw-tooth impeller or a Cowles disk; a thin disk with “teeth” around the edge. The rotor-stator impeller meanwhile is a four bladed rotor moving within a close fitting stator. The dimensions for both mixers can be found in appendix 9.1, Table 9-2.

Each reactor vessel can be individually controlled with regards to the internal temperature, the rpm of the impeller and the rpm of the scrapers and these can be varied throughout the trials.

- The reactors each have two circumferentially mounted ‘scrapers’ that can act as static baffles to minimise vortexing of low viscosity fluids or can be driven counter to the direction of the impellor to act as scraper blades to remove viscous materials from the sides of the reactor. The scrapers are powered by a circumferentially mounted spur gear and this arrangement is advantageous as the centre is open which allows the dosing of ingredients directly into the reaction vessel without stopping the impeller or scrapers.
- The impeller is powered by a geared motor built into the base of the deck of the Formax.

- The chamber that each reaction vessel sits in is connected to warm oil and coolant pipes that circulate fluid throughout the course of run. When heating or cooling is required, the fluid needed is allowed to flow through the chamber around the vessel, when it is not needed then the fluid is prevented from doing so by simple valve-lock devices. The temperature of the content of the vessel can be controlled from a dip in PT100 temperature probe with a sensitivity of 0.385 ohm/°C. The temperature of the vessels can thus be used by the program to provide closed loop control of the whole reactor rack.

The logging software enables the live-time recording of;

- Every transfer made, accurate to 0.01mL and/or 1mg.
- The electrical current to the impellers and scrapers can be used to determine the power draw.
- The pressure in each individual reaction vessel is recorded.
- The internal temperature of the product as well as the external temperature of the reaction vessel.

4.3.3 Initial Design

4.3.3.1 Factors

When formulating an emulsion, there are a wide range of formulation and process variables available and the Formax is designed to allow a systematic exploration of them. As a result initial trials were designed in which a number of the potentially variable factors were kept constant. The factors chosen to remain constant consisted of:

- Scraper speed; the purpose of the scraper design and implementation is two-

fold as discussed previously. The scrapers prevent viscous fluid from sticking to the sides of the reaction vessel and improve the heat transfer so that temperature can be controlled more accurately (when rotating they do so in an opposite direction to the impeller) as well as preventing the entrainment of air. The separate motor can drive them within the range of 20rpm to 200rpm.

- The total volume of reagents within each reaction vessel was kept constant at 60mL. This value was chosen, partly because is it recommended by Chemspeed not to exceed this value when operating at the greatest impeller speeds, and partly because preliminary trials indicated that some foaming can be expected and some free space was required to prevent the reaction vessel from overflowing.
- The temperature of each reaction vessel and its contents was kept at a constant 25°C using a combination of a heater/chiller unit and a livetime feedback system. If the temperature dropped below the required value, warm oil was circulated around the vessel to raise the temperature appropriately, should the temperature exceed the required value coolant was circulated around the vessel to lower the temperature until the target value was reached.
- At the start of addition of the reagents the impeller was set initially at 200rpm. The slowest impeller rotation speed is 100rpm but the current required to turn at this speed continuously is so small that the rotor speed fluctuates around the target value. As a result an impeller speed of 200rpm was chosen as this could be maintained consistently.
- The surfactant is added first to the reaction vessel and then the water is added. The reagents are mixed for a minimum of 10 minutes to ensure the

surfactant is evenly distributed throughout the water phase. In its concentrated form SLES is very thick and exists as a lamella phase surfactant. Upon dilution the lamella phase forms a hexagonal phase which is considerably more difficult to disperse. At concentrations below about 25% (by volume) the hexagonal phase reverts to a lamella phase again which is relatively easy to disperse. As a consequence it is essential to allow sufficient mixing time to fully disperse the SLES. Once the SLES was fully dispersed to form a dilute surfactant solution the oil was added to the vessel.

- Once all reagents were in the reactor vessel, then the impeller would begin rotating at the required speed.
- The vessel contents were mixed for 80 minutes. Droplet size reduction during emulsification is typically very rapid initially, but the rate tends to drop with time eventually approaching a steady state. In practice droplet size continues to reduce but the rate is so slow that it has effectively reached steady state.
- Once mixing was completed the contents of the vessel was decanted into a sample bottle
- Particle sizing was done using a Malvern Mastersizer X as described in section 2.6.

4.3.3.2 Variables

The impact of altering the following factors was investigated:

- Oil viscosity – three different viscosities of silicone oil were used in order to observe whether the Formax was capable of dealing with all of them. The viscosities chosen were; 10cSt, 350cSt and 1000cSt.

- The phase volume of oil within the emulsion ranging from 5 – 60%.
- The phase volume of surfactant ranged from 0.25 – 8%. The highest surfactant percentage of 8% ensures that at the lowest volume of water, the concentration would not exceed 25% in the water and thus would avoid the hexagonal phase.
- A range of impeller speeds; 1000rpm, 2000rpm, 4000rpm & 6000rpm. It would have been ideal to continue increasing the impeller speed logarithmically, however, the impellers within the formulation vessels are limited to a speed of 6000rpm.
- Impeller type; rotor-stator & dissolver disk impeller.

4.3.3.3 Design of Experiments

After deciding upon which factors were to be varied and which were to be kept constant, the information was placed in the appropriate fields within MODDE – Design of Experiments software. Trials were selected using a minimised D-efficiency value to ensure that residuals were even across the experimental space. The software suggested a list of 22 experiments for each impeller. This method is known as screening as it allows the researcher to ascertain which factors generate the greatest response by taking every combination of highest and lowest variable and generating a matrix of experiments, along with three centre points consisting of experiments with the middle value for each variable used.

4.3.3.4 Particle Sizing

Once formulated the emulsions were analysed using a Malvern Mastersizer X with a 45mm lens with the focus of the results produced being primarily the D[3,2] value with the D[4,3] value being a secondary concern.

To analyse samples using the Mastersizer, the sample is added to a small volume dispersion unit and the red light is scattered by the particles and droplets within the sample onto the detectors and this then calculates the size of them, as discussed in section 2.6.

The presentation code interprets the readings that are received by the detector dependent on the fluid being analysed. It interprets the data appropriately and produces a result of what the size of the sample is based on the refractive index (RI) of the sample and the location on which the detector was hit with the laser light.

When analysing the samples using the Mastersizer X the presentation code used consisted of a refractive index of 1.403 (RI of silicone oil), absorption of 0.001 (translucent) and as the samples being made were polydispersed oil droplets in water the refractive index of water made up the last part of the presentation code; 1.330.

4.4 Initial Results and Discussion

4.4.1 Performance of the Formax

The emulsions produced during the trials were made up of droplets with a range of size values. Figure 4-2 presents three droplet size distribution (DSD) traces of; a sample with a small particle size (see Figure 4-2, trace labelled C), a large particle size but which can still be measured entirely with the 45mm lens (see Figure 4-2, trace labelled B) and finally one where much of the material is in a size range above the range that the 45mm lens can measure (see Figure 4-2, trace labelled A). The aim of this investigation was to obtain small particle sizes and thus it was decided unnecessary to re-measure samples with a large droplet size on the Mastersizer X with a longer focal length lens.

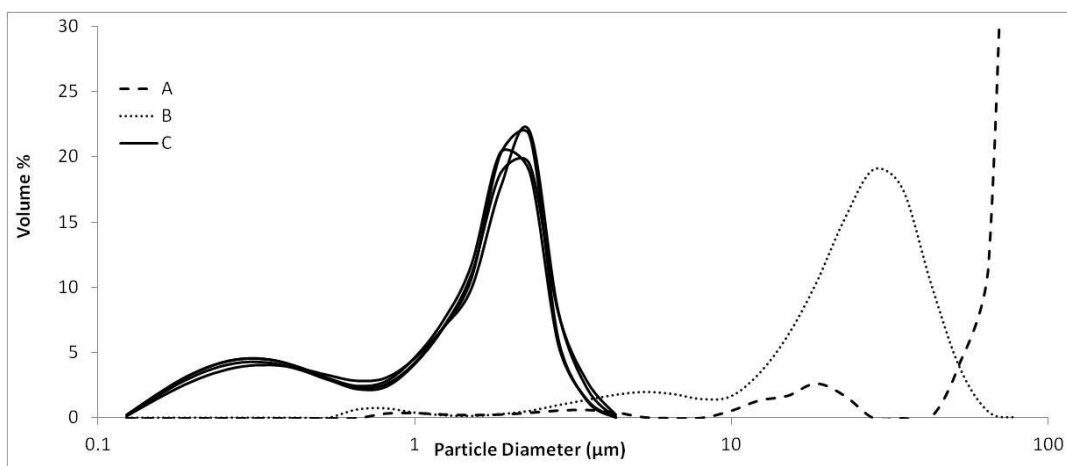


Figure 4-2 DSD of emulsions of varying size.

On occasions where there was an excess of oil or surfactant added to a reaction vessel (due either to operator or technical error) the logging system on the Formax recorded the exact quantity and thus allowed back-calculations to be performed to determine the exact phase volumes of the emulsions after the run had been completed. As well as the reagent transfers being logged, the temperature was monitored and logged, as was the current to the impeller and the scrapers for every reaction vessel. This allowed the performance of the Formax to be monitored throughout the run.

To test reproducibility a number of repeats were done using the parameters that were used to create sample C in Table 9-4 (see appendix) and Figure 4-2. The results for the reproducibility trials can be seen in Table 9-5 (see appendix) and the multiple traces are also included in Figure 4-2.

These repeats were done in a single run by choosing four vessels where the conditions were reproduced. The data logs indicated that the runs were essentially identical with oil phase volume of 60% \pm 1% and surfactant level of 8% \pm 0.2%. With these parameters the Formax is able to manufacture the emulsion with a high degree of reproducibility. The reproducibility at such small droplet sizes is very good

with the mean $D[3,2] = 0.68 \pm 0.03 \mu\text{m}$ and $D[4,3] = 1.36 \pm 0.04 \mu\text{m}$. The individual traces lie almost perfectly on top of each other showing that not only are the values reproducible but the shape of the distribution is also.

4.4.2 Effect of material and process parameters on drop size distribution

Completing the 22 experiments for both impellers allowed for a direct comparison of the impact that the impeller type had on the droplet size distribution. The data presented in Figure 4-3 shows that the dissolver disk impeller creates an emulsion consisting of smaller droplets than that produced by the rotor-stator and that for both impellers the greater the rpm value, the smaller the droplets produced.

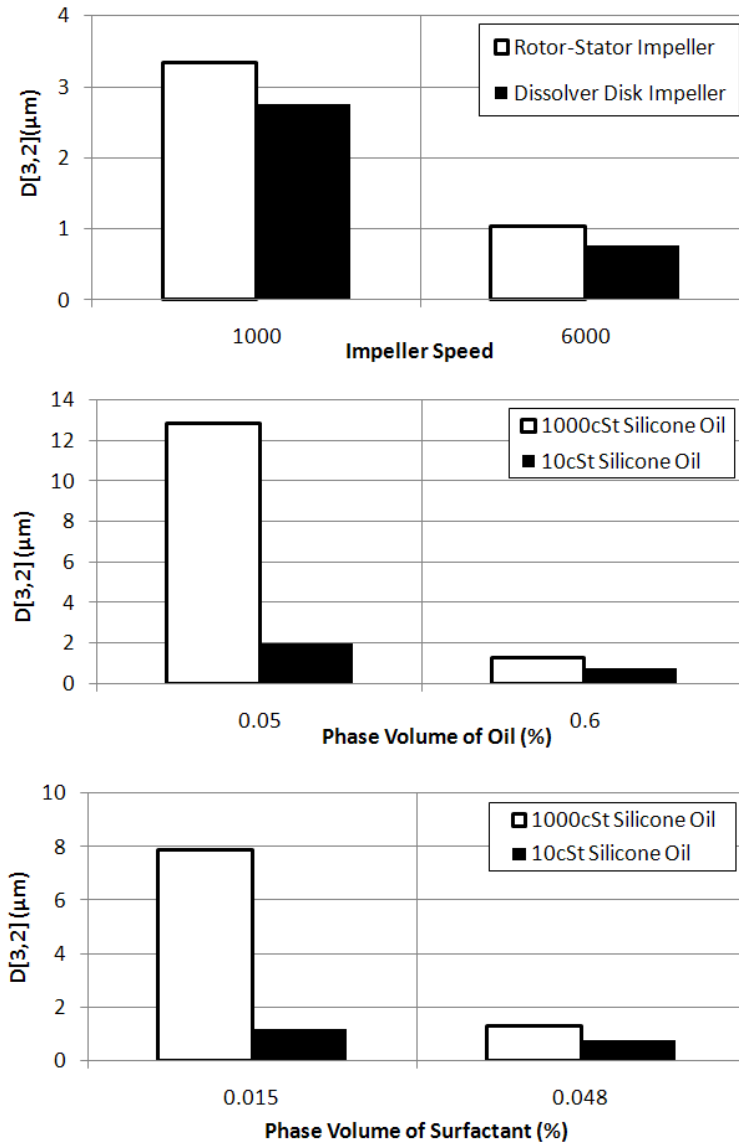


Figure 4-3 Droplet size of emulsion produced with respect to impeller speed, phase volume of oil and phase volume of surfactant respectively.

The experimental design tends to suggest the extremes of parameters, both formulation and process, be investigated. Figure 4-3 shows the effect of the phase volume of oil and the phase volume of surfactant on producing the smallest droplet size and that to do so requires the highest value of both. The impact of the viscosity on the droplet size of the emulsions analysed to produce Figure 4-3 agree with previous research in that the greater the viscosity, the greater the size of the droplets within the emulsion (Seekkuarachchi et al., 2006).

4.4.3 Statistical models for Sauter Mean Diameter and Volume Weighted Mean

The previous section reassuringly shows that the droplet size responds to process and formulation parameters as much as expected. Here we consider the whole data set to build a statistical model using the MODDE software [18]. For both impeller types the software package suggested a transformation of the particle size using Equation 4-1;

$$\textit{Transformed } D[3,2] = 10 \log \left(\frac{D[3,2]}{100 - D[3,2]} \right)$$

Equation 4-1 used to transform $D[3,2]$ values by MODDE software.

Using this transformed particle size a statistical model was built based on the parameters listed in section 4.3.3.

Figure 4-4 displays two pairs of graphs that show the size of the droplets observed following analysis of an emulsion produced against the predicted size of the droplets by MODDE software. Figure 4-4a and Figure 4-4b present a comparison between the measured and predicted $D[3,2]$ values after they have been transformed using Equation 4-1 for the two impeller types. The dissolver disk shows a good fit (Figure 4-4a) with an $R^2 > 97\%$ whereas the rotor-stator shows a poorer fit (Figure 4-4b) in comparison with an R^2 value of 89%. For both impellers the gradient of the line of best fit is $=1$ and the intercept is close to 0. The statistical model is a simple summation of the variables as main effects and as interaction terms with appropriate proportionality constants. A summary of these constants is available within the appendix Table 9-6 and Table 9-7.

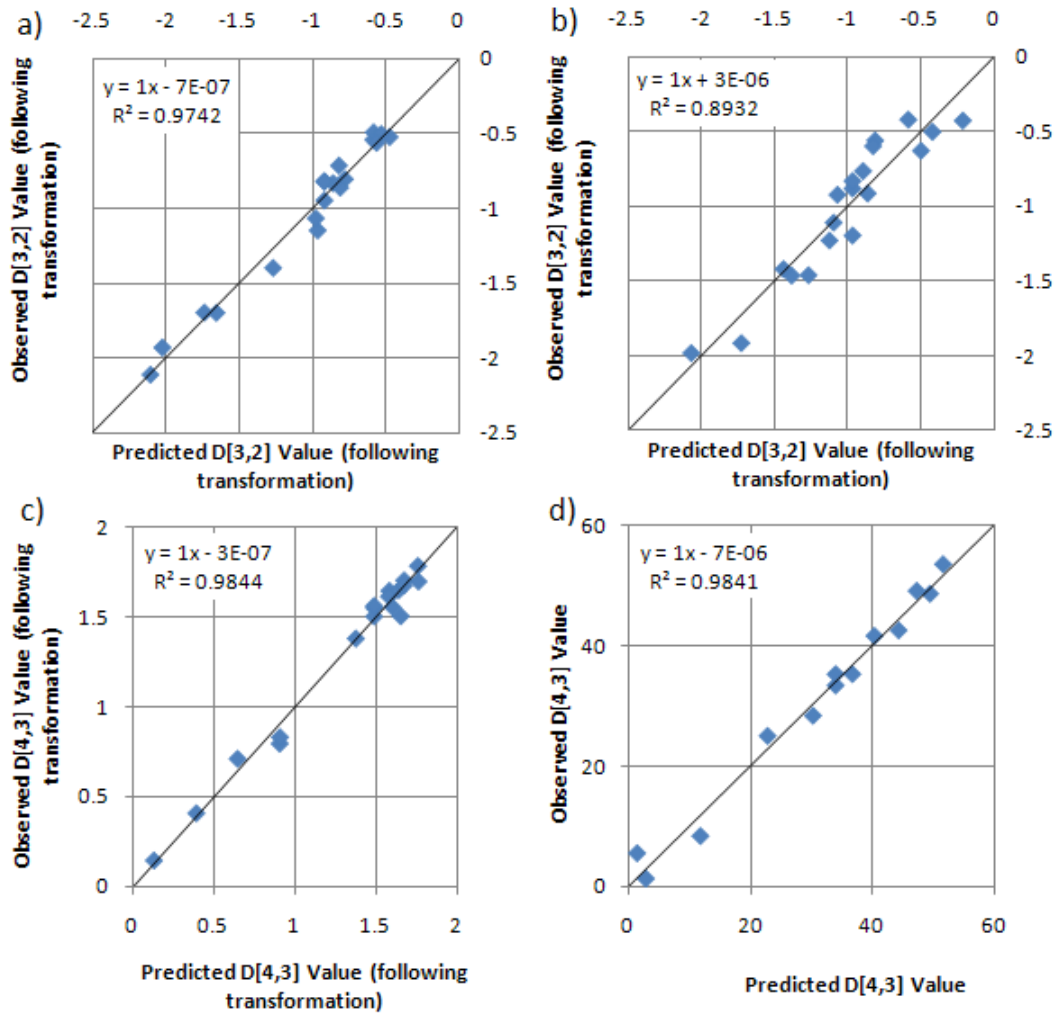


Figure 4-4 Comparison of observed droplet size values verses predicted droplet size values taken from MODDE software.

Similar analysis was performed for the D[4,3] values. For the dissolver disk impeller data set shown in Figure 4-4 the transformation required the formula in Equation 4-2, yet the data set produced by the rotor-stator impeller required no transformation whatsoever (Figure 4-4d);

$$\text{Transformed } D[4,3] = 10 \log(D[4,3])$$

Equation 4-2 used to transform the D[4,3] value of the emulsion produced by the dissolver disk impeller.

With the focus of the investigation being on minimising the $D[3,2]$, achieving a small $D[4,3]$ value would be an added benefit as it would confirm the small droplet size being reported. The fit however is even better (for the $D[4,3]$ value than that for the $D[3,2]$ value) with the $R^2 > 98\%$ for both impellers, as can be seen when comparing the data shown in Figure 4-4. The proportionality constants for how the statistical model predicted the values are presented in the appendix (Table 9-8 and Table 9-9).

Using the known data points the software generates a statistical model that could be described as a map. One representation is shown in Figure 4-5, a four dimensional colour coded graph. The key to the graph is colour coded and ranges from red, signifying large drop sizes, to blue, signifying small drop sizes. The graph is made up of nine triangles set out in a three by three matrix. The triangles are divided into columns and rows, with each column representing a different rotor speed (increasing from left to right) and each row a different oil viscosity (increasing from the base to the top). Each triangle is a ternary phase diagram of the three components; oil, surfactant and water. We also examined 4000rpm however there were only two data points and so those triangles are not shown in Figure 4-5.

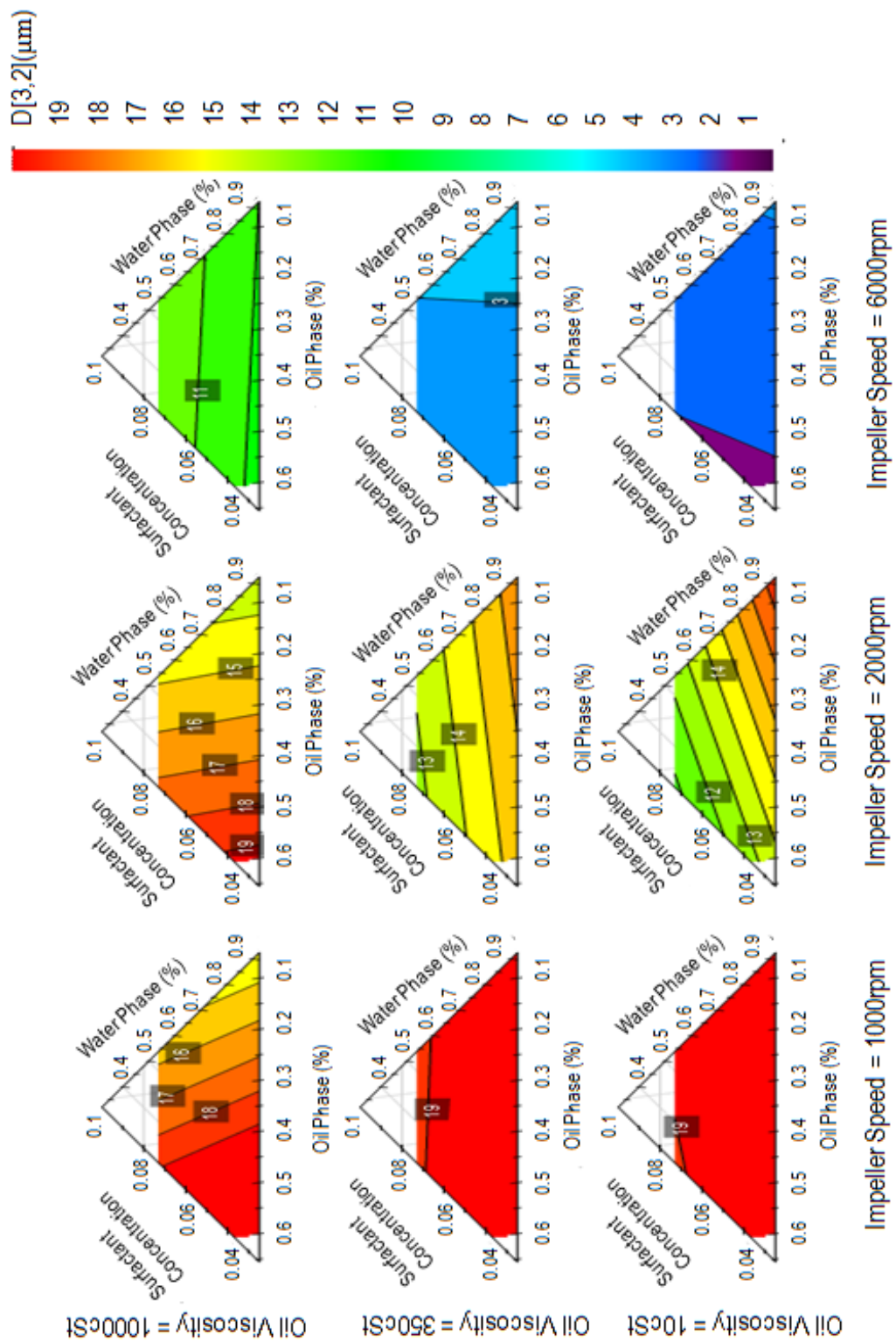


Figure 4-5; 4-D graph showing the impact of both formulation and process parameters on the product droplet size ($D[3,2]$) predicted by MODDE based on actual experimental results. Dissolver disk impeller used with scraper speed set to 100rpm.

It can be seen that as the rotor speed increases, the droplet size decreases (contours become green and blue). As the viscosity increases, the smallest droplet size at 2000 and 6000rpm is obtained for lower viscosity oils. This is consistent with both the literature and expectation. However, at 1000rpm the smallest droplet sizes are obtained with higher viscosity silicone oils. Note in the left hand column that the higher viscosity oil has yellow colouring, with previous work involving silicone oils yielding similar results (Mason et al., 2006a; Meleson et al., 2004).

As the viscosity of the oil is increased, the direction/angle of the contours lines alters. For the lower viscosity oils (10cSt and 350cSt) the contours point from the bottom left of the triangle, to the middle of the right side of the triangle and as the rotor-speed increases these lines move in an anti-clockwise direction so instead of being at an angle they become almost vertical. The higher viscosity oil [1000cSt] contour lines point from the top left of the triangle to the bottom right and as the rotor-speed increases they move clockwise until they are flat at the highest rotor speed. This suggests that surfactant level becomes more important as rotor speed becomes higher and this may be because excess surfactant is required to stabilise the newly created surface. At the intermediate oil viscosity of 350cSt the contour lines show similar behaviour to the lowest viscosity oil (10 cSt), which suggests that as rotor speed becomes more important, the oil phase also becomes progressively more important in reducing the droplet size.

To understand these figures it is easiest if they are divided into four quadrants. The four triangles in the bottom left hand corner indicate smaller droplet sizes are obtained with increasing surfactant level (10 cSt and 350 cSt, 1000rpm and 2000rpm). The two triangles in the bottom right hand corner (10 cSt and 350 cSt, 6000rpm) indicate smaller droplets are obtained at a high phase volume of oil. In fact

the data at 2000rpm also suggests a higher phase volume of oil is beneficial in achieving small droplet sizes. This indicates that the higher phase volume of the oil promotes the transition of shear stress for droplet break-up due to the higher viscosity of the emulsion. The two triangles in the top left hand corner (1000cSt, 1000 and 2000rpm) indicate the smallest droplet sizes are obtained at a low phase volume of oil and is aided by higher surfactant levels. Finally, the figure in the top right hand corner (1000cSt, 6000rpm) suggests smaller droplets for lower surfactant levels. This is counterintuitive but it should be noted that the range of droplet sizes is only 1-2 μ m and consequently it is likely that this is an artefact of the model fitting.

Altering the scale of the graph to observe the sub-micron range at an impeller speed of 6000rpm produces Figure 4-6. The decrease in viscosity causes the angle of the contours lines to alter from approximately a vertical line for the 350cSt oil triangle to a thirty degree angle for the 10cSt oil triangle with the smallest droplets produced in the region of highest phase volume of oil and highest phase volume of surfactant.

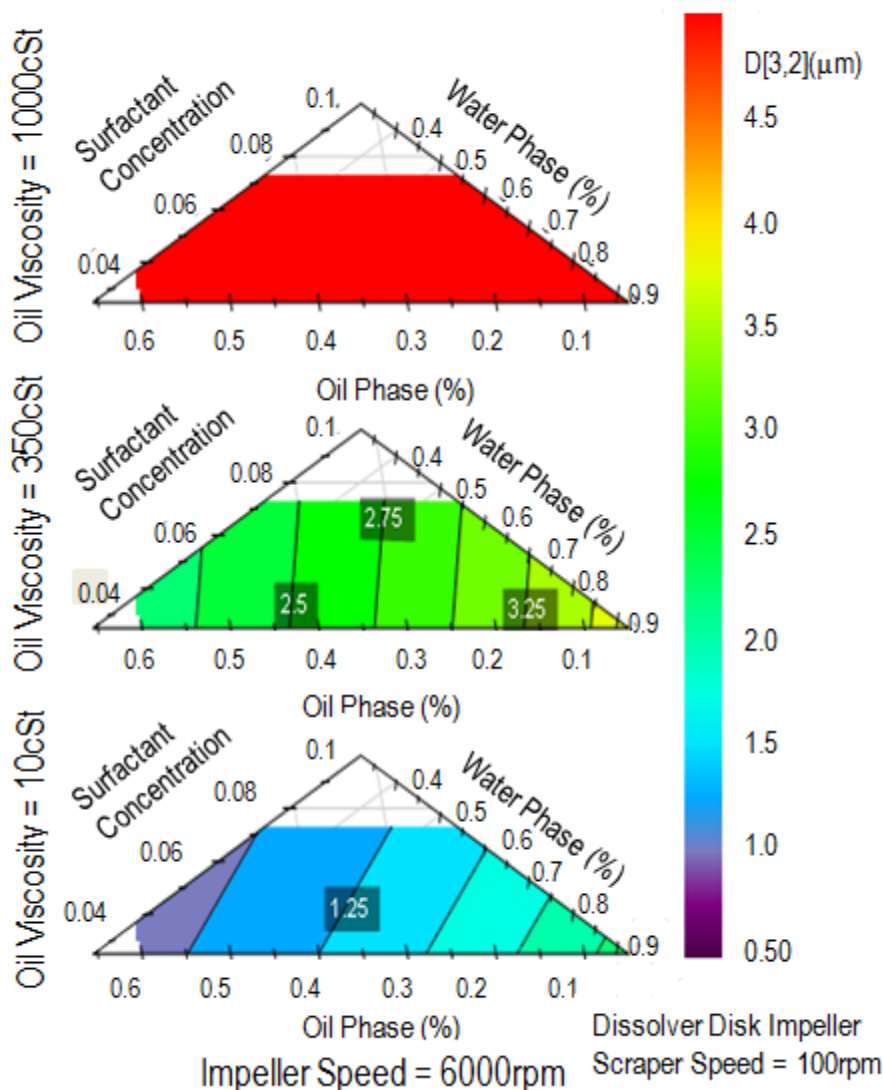


Figure 4-6 Right hand column from Figure 4-5 rescaled using DoE software.

The response of droplet size with the rotor-stator is qualitatively similar to the dissolver disk impeller (Figure 4-7). In comparison to the graph produced by the dissolver disk impeller (Figure 4-5), there are significantly more contour lines on each of the triangles, note that both Figure 4-5 and Figure 4-7 have the same range of contours, from 0 μm to 20 μm . The trends are similar, but when the detail within each of the quadrants is examined, there are some important differences. For example in the bottom right hand corner, droplet size is largely determined by surfactant

concentration. Here a much stronger response of droplet size to surfactant quantity and rotor speed, such that the rotor-stator produces smaller droplet sizes. In the second quadrant (10 cSt and 350 cSt, 6000rpm) a much stronger response to the oil phase volume although the smallest droplet size appears to be similar. The third quadrant (1000 cSt, 1000rpm and 2000rpm) suggests a similar size range although this occurs only at lower phase volumes of oil. In the fourth quadrant (1000 cSt, 6000rpm) it can be observed again that the droplet size increases as the surfactant level increases but as discussed earlier it is believed to be an artefact of the statistical model.

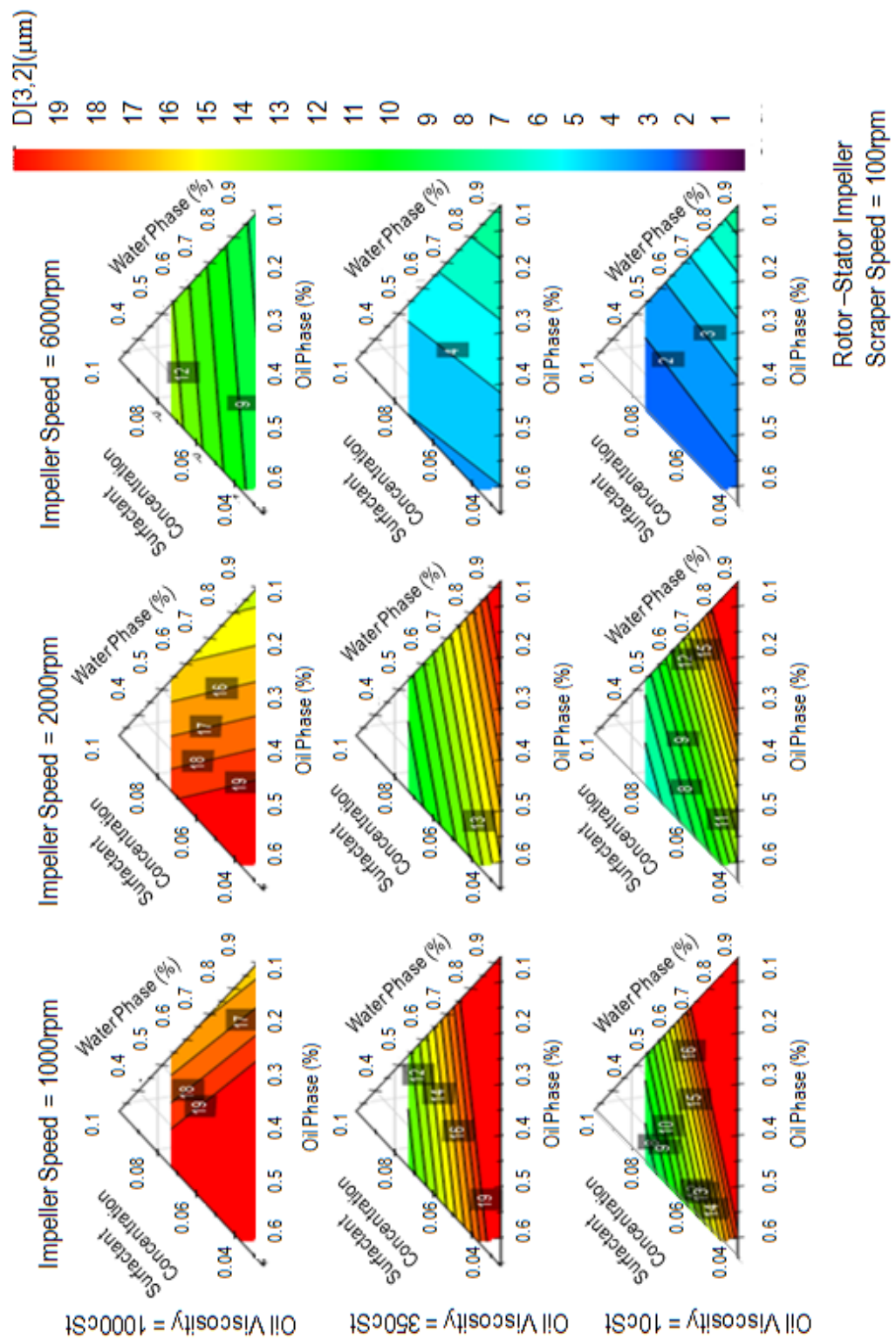


Figure 4-7; 4-D graph showing the impact of both formulation and process parameters on the product droplet size (D[3,2]) predicted by MODDE based on actual experimental results.

It can be seen that the rotor-stator is more suited to reducing the droplet size of emulsions for 10cSt and 350cSt at lower impeller speeds 1000 and 2000rpm. For highest viscosity oil or for the highest impeller speed (6000rpm) the dissolver disk produces emulsions with the smallest droplet size.

The data for the $D[4,3]$ values obtained using a dissolver disk impeller were placed in the design of experiment software and subject to similar treatment as the $D[3,2]$ values. The software produced a statistical model of the impact that the chosen parameters would have on the $D[4,3]$ value of the droplets within the emulsions (Figure 4-8).

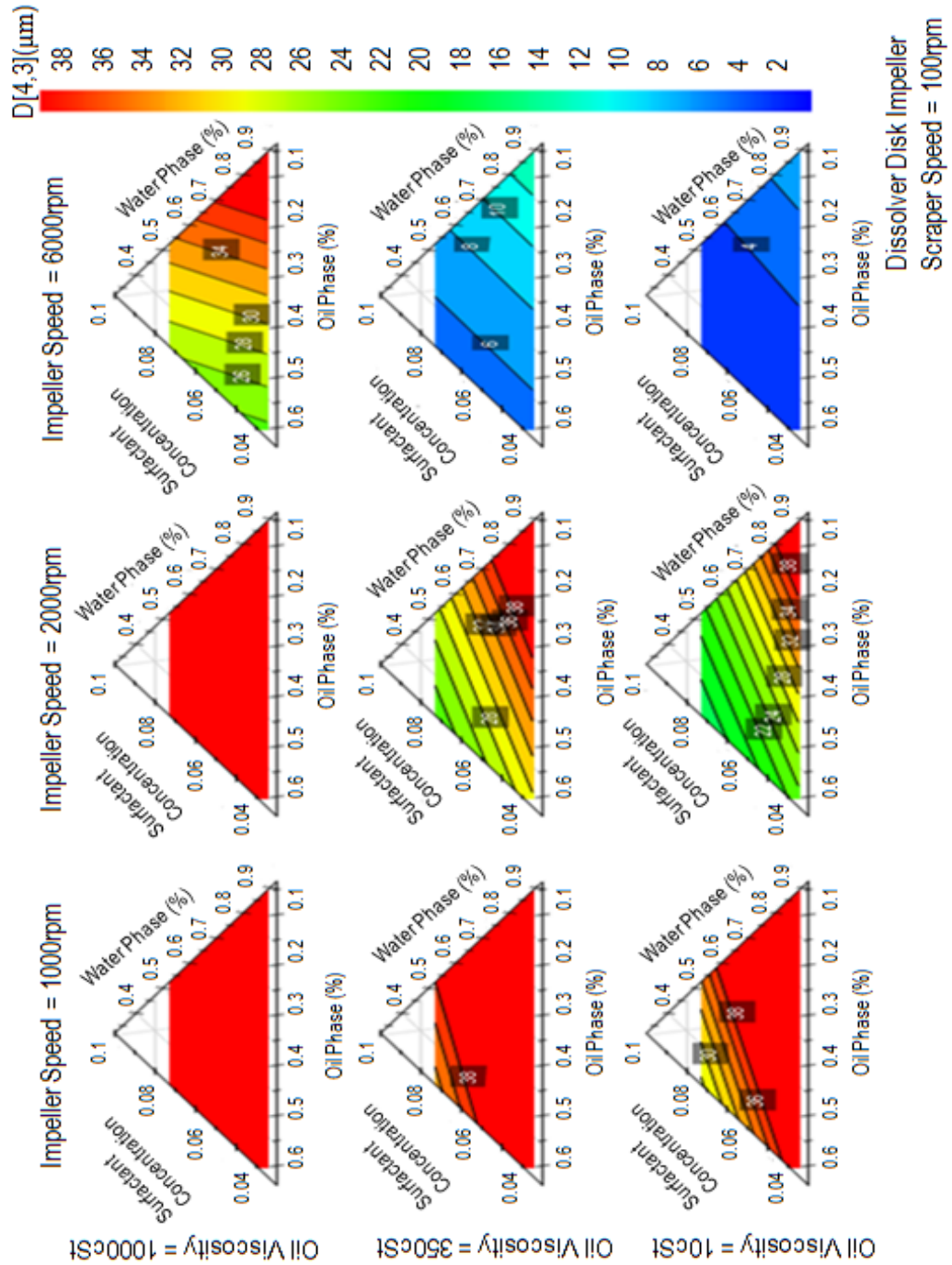


Figure 4-8; 4-D graph showing the impact of both formulation and process parameters on the product droplet size ($D[4,3]$) predicted by MODDE based on actual experimental results.

For those triangles showing contour lines an increase in the phase volume of oil leads to a decrease in the size of the droplets, an increase in the surfactant concentration leads to a decrease in the droplet size. This is even seen for the 1000cSt at 6000rpm triangle although the dependence on surfactant concentration is weak. In all cases an increase in rpm leads to a decrease in the droplet size. Figure 4-8 provides the same conclusion as Figure 4-5, that the smallest possible droplet size requires the lowest viscosity oil at the greatest phase volume, the greatest phase volume of surfactant and the impeller operating at maximum speed.

The statistical model generated by the software for $D[4,3]$ value of droplets using the rotor-stator device (Figure 4-9) is significantly different to the other results (Figures 4-5 to 4-8).

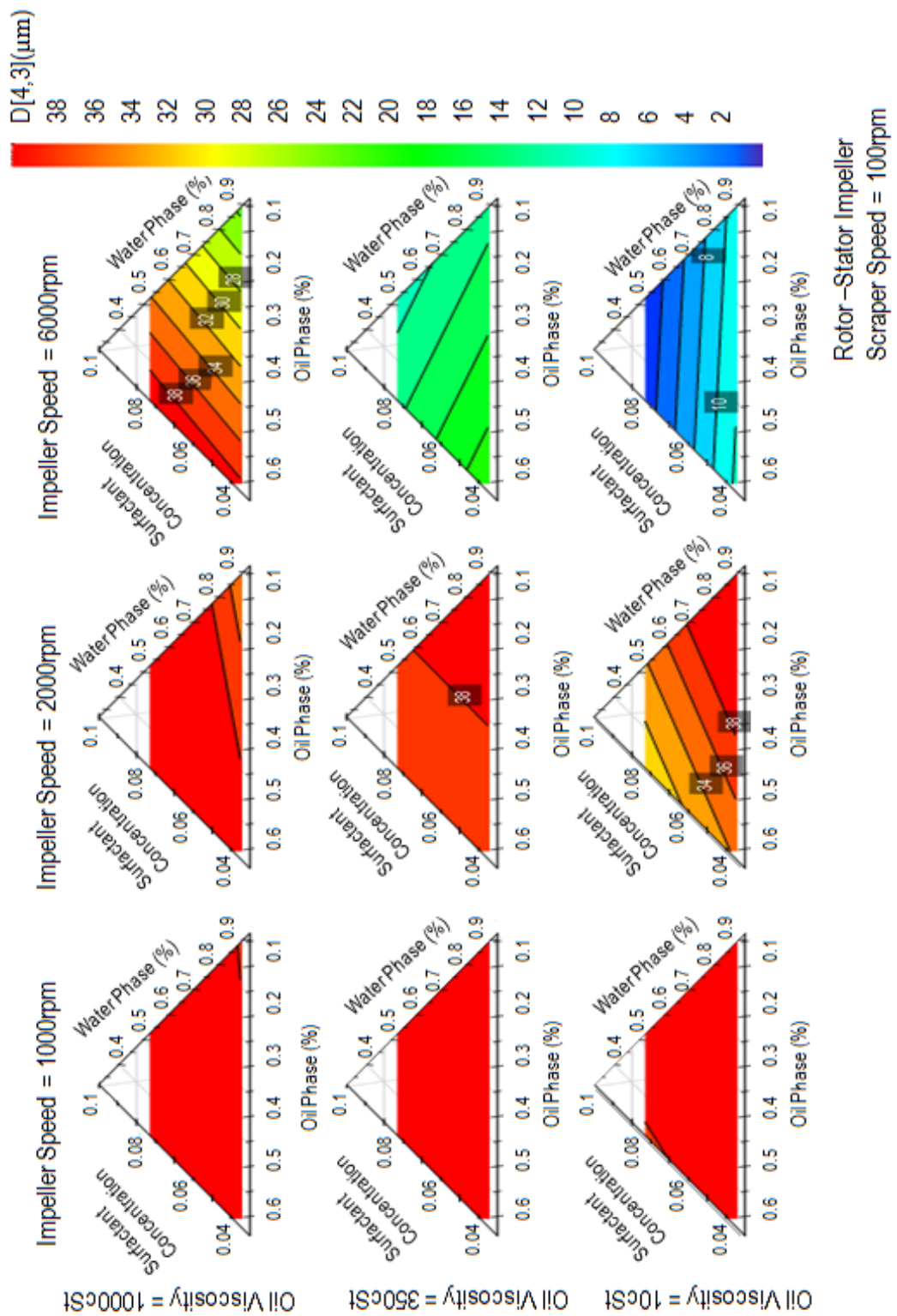


Figure 4-9; 4-D graph showing the impact of both formulation and process parameters on the product droplet size ($D[4,3]$) predicted by MODDE based on actual experimental results.

Figure 4-9 is best observed as being divided into three separate sections; the first consists of the three triangles for the 1000cSt oil, the second consists of the triangles made up from 10cSt and 350cSt oil with an impeller speed of 6000rpm and the final one is made up of the other four triangles. Starting with the largest grouping of four triangles (10cSt and 350cSt, 1000rpm and 2000rpm) the two at the 1000rpm show almost no difference and are both in excess of 40 μ m. However closer examination reveals that at the highest oil and surfactant phases there is a slight change in colour showing slightly smaller droplet sizes. It is much clearer for the 2000rpm data that a higher phase volume of oil reduces the size of the droplets formed. Overall then in this region higher phase volume of oil and higher surfactant phase volume reduces particle size. Qualitatively these results are similar to the dissolver disk.

The next grouping to be discussed is the one that contains the two triangles at 6000rpm (10cSt and 350cSt). These two triangles are qualitatively different from the first set (previous paragraph) and also from the corresponding triangles for the dissolver disk (Figure 4-8). More specifically the angle of the contour lines are reversed so that small droplet sizes are obtained with a reduction in the phase volume of oil. This is more noticeable for the 350cSt oil whereas the 10cSt has a stronger dependence on surfactant level. There is far less impact from the oil phase volume as indicated by the almost horizontal contour lines.

The final grouping in Figure 4-9 to be discussed involves the 1000cSt oil for all rotor speeds. It can be seen that as the impeller speed increases, the minimum droplet size possible to formulate is reduced greatly as at 6000 rpm there is the presence of multiple contours. From the direction of the contour lines it can be determined that the smaller the phase volume of oil and the greater the volume of water, the smaller the droplet size possible to obtain.

From the data displayed in Figure 4-5 and Figure 4-9 it was concluded that emulsions formulated with the dissolver disk impeller operating at the highest possible rpm with the lowest viscosity of oil at the highest possible phase volume and a high surfactant phase volume should be looked at to obtain an emulsion with the smallest possible droplet size. The data presented in Table 9-5 in the appendix shows that the conditions not only produce an emulsion with a small droplet size (smaller than predicted) they confirm the reproducibility that is possible when using the Formax.

To extend the study further in attempt to obtain even smaller droplet sizes it was decided to investigate greater phase volumes of oil and to increase the surfactant phase to 20%/25% of the water phase.

4.5 Expanded Experimental

4.5.1 Materials

The reagents used for these trials were identical to those involved in the initial experimental trials.

4.5.2 Expanded Design

Following the initial trials we concluded that in order to obtain the smallest possible droplet size; 60% phase volume of oil of 10cSt oil and 8% phase volume of surfactant were required within the emulsion formulation and a dissolver disk impeller operating at 6000rpm with scrapers operating at 100rpm were required from the process parameters. In the initial trials the oil phase was capped at 60% of the emulsion formulation and the surfactant phase at 8% whereas 6000rpm was the limit of the Formax operating speed. The impact of phase volumes greater than these

values needed investigating to see whether the effect of increasing the phase volume of oil and of surfactant to decrease the size of the droplets in the final product would occur or whether the limit of this variable had been discovered. The effects of 70% and 90% oil phase volume (at 10cSt viscosity), and 20% and 25% surfactant within the water phase were chosen values to expand the initial formulation space. At 90% oil phase volume this limits the surfactant level to 2.5% surfactant although the concentration on the water phase is high.

Since the rotor speed of the impeller had such an impact on the droplet size of the emulsion formed we chose to keep to a high speed (6,000rpm) to ensure the smallest drop sizes were obtained. During these trials the impact of the scraper speed, which was kept constant in the initial trials, was chosen to be varied with the aim of identifying its effect on the size of the droplets within the product formed. The scraper speed was low compared to the high shear dissolver disk impeller and it was assumed that the speed of the scraper would have a minimal impact on the drop size. The order of addition of reagents to the reaction vessel was the final factor chosen to vary and observe the impact that doing so had on the droplet size within the product formed. These factors were initially chosen to be kept constant however it was concluded that the impact they have when using the Formax to formulate an emulsion should be identified and discussed.

4.6 Expanded Results and Discussion

4.6.1 Comparison of Mastersizer 2000 and Mastersizer X

When analysing the initial emulsions it was observed that the droplets being analysed were so small they were pushing the limitations of the Malvern Mastersizer X. This is because the Mastersizer X is unable to observe particulates or droplets

smaller than 100nm in size and is fairly insensitive below about 1 μm (section 2.6). Taking this into consideration the analysis method was adapted to include a Malvern Mastersizer 2000 as this advanced model allows observation of particulates down to 20nm in size.

For the smallest drop sizes (Figure 4-2) re-measuring them on the Malvern Mastersizer 2000 (Figure 4-10) shows the peak at the $\sim 0.3\mu\text{m}$ moves to a smaller size $\sim 0.1\text{--}0.2\mu\text{m}$ with a small percentage below 0.1 μm ($\sim 3\%$ by volume). The larger peak at about 2 μm remains where it is.

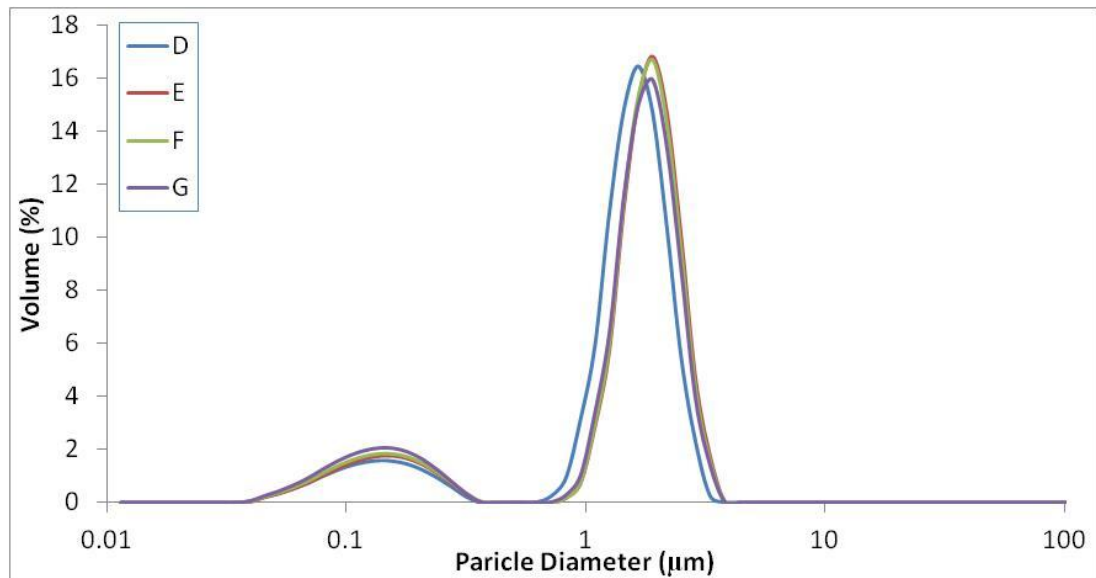


Figure 4-10 Graph produced using raw particle size data obtained after analysing the emulsions using a Malvern Mastersizer 2000.

All emulsions that had a droplet size ($D[3,2]$ value) of less than a micron that were measured on the Masterizer 2000 were re-measured on the Mastersizer X. This procedure ensured that the data for the initial results was accurate as following analysis on the Mastersizer 2000 the samples were again analysed on the Mastersizer X to ensure no coalescence had occurred within the time between sizing of the droplets within the emulsion. Once it had been confirmed that the emulsions had not

coalesced, the D[3,2] values from the Mastersizer X and the Mastersizer 2000 were compared. It was found that the D[3,2] as measured by the Mastersizer 2000 were about 150nm smaller in size (Table 9-10 in the appendix) and as a consequence it was decided to switch to the Mastersizer 2000 to ensure the effect of reducing particle size was captured.

4.6.2 Impact of Variables in Extended Method

The data in Table 9-11 (in the appendix) shows that the order of addition of reagents has a large impact on the size of the droplets formed within the product produced, and allowed for a further reduction in the droplet size. The order of addition that produced the smallest drop size was found to be; add the oil first and start the rotor at 200rpm, then add the surfactant, then the water and finally start the impeller at 6000rpm. The size of the droplets produced by this method are less than a third of what they are if the water and surfactant are added first to the reaction vessel and the oil added last.

The graph shown in Figure 4-11 compares two identical formulations under identical process parameters with the exception of the rpm of the scraper speed. As mentioned earlier, the scrapers are powered by a separate motor located on the outside of the reaction vessel. This motor is capable of speeds between 50 and 200rpm. From the graph shown in Figure 4-11 it can be seen that increasing the rpm of the scraper speed leads to a reduction in droplet size of approximately 30% for that given formulation.

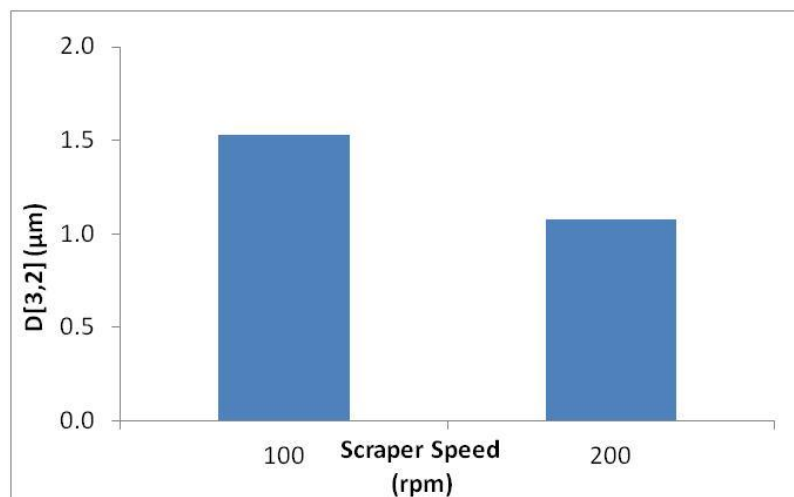


Figure 4-11 Droplet size of emulsion as a function of scraper speed.

Finally we consider the impact of increasing the oil phase above the 60% limitation that was in place during the initial trials. Trials with focus on 70% and 90% phase volumes of oil were performed. These experiments yielded unexpected results. Although the phase volume of oil was increased, the droplet size remained very similar as to that when the 60% cap was placed on it as can be seen by comparing the values in Table 9-5 and samples 2,3 6 in Table 9-11.

It was noted that an emulsion made up with an oil phase of 90% forms an oil-in-water-in-oil emulsion; however it was interesting to find that by increasing the speed of the scrapers from 100rpm to 200rpm formed a substantially different product. Instead of an oil-in-water-in-oil emulsion being the product, a gel was created merely by the alteration of this one process parameter. The hypothesis behind this is that the increased speed of the scrapers provided enough force to push the oil into the middle of the reaction vessel where it was then coated with the small quantity of liquid and surfactant and formed an oil-in-water gel.

4.6.3 Stability

The emulsions produced with a high phase volume of oil, in excess of 50% of the total volume, have remained stable for over a year. At the time of this article submission they are still showing the same characteristics with regards to droplet size as they did when they were produced and visibly the appearance is identical to that of when first produced.

4.7 Conclusion

The aim of this investigation was to use a high-throughput formulation platform and design of experiment software to map out both formulation and process space to obtain a range of drop sizes with a specific focus on small drop sizes.

The combination of the Formax high-throughput platform and MODDE design of experiment software was employed and we were able to produce emulsions made up of sub-micron droplets quickly and efficiently. The Formax proved to be an easy and versatile tool for the manufacture of emulsions, with good control over the addition of ingredients and the ability to handle viscous oils

A total of six trials comprising of twelve samples each identified the factors which have the greatest impact on the droplet size. To achieve the smallest possible droplet size the following combination of parameters were required; the lowest viscosity of oil, high phase volume of oil (60%), a 25% concentration of surfactant in the water phase, a dissolver disk impeller operating at the highest rpm and the speed of the scrapers set to 100rpm. The smallest particle size obtained had a $D[3,2] = 459\text{nm}$ but we believe that smaller sizes could be achieved by focussing within the phase volume of oil range from 60 and 70%.

4.8 Further Work

The methodologies used throughout this chapter to identify the parameters that had the greatest impact on the droplet size of the emulsion produced, using design of experiment software and the Formax, have been applied successfully on two other emulsion systems. Due to confidentiality restrictions the two systems have been excluded from this thesis, however the two work packages did further validate the methods used.

The first system involved high-throughput formulation of a long chain hydrocarbon emulsion stabilised with polysorbate 20 as the surfactant (discussed further in section 7.3.1) for use in a home and personal care application.

The second system also for use in a home and personal care application, involved high-throughput formulation of another long chain hydrocarbon emulsion stabilised with SLES as the surfactant (discussed previously in this chapter). The hydrocarbon used in this system resembled a low melting point wax which meant it was necessary to monitor temperature as an additional process parameter in order to observe the effect of viscosity of the dispersed phase.

4.9 References

COGNIS. 2007. Product Data Sheet; TEXAPON® N 70

FORGIARINI, A., Esquena, J., González, C. and Solans, C. 2001. Formation of Nano-emulsions by Low-Energy Emulsification Methods at Constant Temperature. *Langmuir* **17** 2076-2083

GOTTENBOS, B., van der Mei, H. C., Klatter, F., Nieuwenhuis, P. and Busscher, H. J. 2002. In vitro and in vivo antimicrobial activity of covalently coupled quaternary ammonium silane coatings on silicone rubber. *Biomaterials*. **23** 1417-1423

LENG, D. E. and Calabrese, R. V. 2004. *Handbook of Industrial Mixing: Science and Practise*. New Jersey: Wiley-Interscience; pp. 641-643.

MASON, T. G., Graves, S. M., Wilking, J. N. and Lin, M. Y. 2006a. Extreme emulsification: formation and structure of nanoemulsions. *Condensed Matter Physics*. **9** 193-199

MASON, T. G., Wilking, J. N., Meleson, K., Chang, C. B. and Graves, S. M.. 2006b. Nanoemulsions: formation, structure, and physical properties. *J. Phys.: Condens. Matter*. **18** 635-666

MELESON, K., Graves, S. and Mason, T. G. 2004. Formation of Concentrated Nanoemulsions by Extreme Shear. *Soft Materials*. **2** 109-123

MODDE Version 9.0.0.0, Sept 30 2009 Copyright © Umetrics AB

MUN, S., Choi, Y., Shim, J.-Y., Park, K.-H. and Kima, Y.-R. 2011. Effects of enzymatically modified starch on the encapsulation efficiency and stability of water-in-oil-in-water emulsions. *Food Chemistry*. **128** 266-275

NIR, I., Aserin, A., Libster, D. and Garti, N. 2010. Solubilization of a Dendrimer into a Microemulsion. *J. Phys. Chem. B*. **114** 16723-16730

PETERS, D. C. 1992 *Mixing in the Process Industries Second Edition*. Oxford: Butterworth Heinemann; pp. 294-301

PHADKE, D. S. and Eichorst, J. L. 1991. Evaluation of Particle Size Distribution and Specific Surface Area of Magnesium Stearate. *Drug Dev. Ind. Pharm.* **17** 901-906

SEEKKUARACHCHI, I. N., Tanaka, K. and Kumazawa, H. 2006. Formation and Characterization of Submicrometer Oil-in-Water (O/W) Emulsions, Using High-Energy Emulsification. *Ind. Eng. Chem. Res.* **45** 372-390

SOMASUNDARAN, P., Mehta, S. C. and Purohit, P. 2006. Silicone emulsions. *Adv. Colloid Interface Sci.* **128-130** 103-109

SPERNATH, A. and Aserin, A. 2006. Microemulsions as carriers for drugs and nutraceuticals. *Adv. Colloid Interface Sci.* **128** 47-64

WANG, L., Li, X., Zhang, G., Dong, J. and Eastoe, J.. 2007. Oil-in-water nanoemulsions for pesticide formulations. *J. Colloid Interface Sci.* **314** 230-235

Chapter 5 Scaling-up High-Throughput

Formulation

5.1 Abstract

To map out the formulation space, and the impact that the varying formulation parameters can have on the product, takes time and the expenditure of reagents; more so when using a pilot plant scale mixer. Using formulation parameters obtained from the work using the high-throughput formulation platform, this work focuses on the size of the droplets within an emulsion formulated when processed using industrial scale mixers.

The results obtained from the trials show that the prototype UMPF (Ultra Mixing and Processing Facility) is capable of producing smaller droplets than a Silverson 150/250 MS mixer. The UMPF was able to produce an emulsion with droplets 0.20 μm in size with respect to the D[3,2] value in comparison to those 2.17 μm in size produced by the Silverson 150/250 MS mixer. It was also discovered that the formulation parameters required to obtain these small droplets were similar to those from the previous high-throughput trials, paving the way for reduced research time and less waste.

5.2 Introduction

As discussed in 2.2, the use of emulsions as a building block for industrial products covers many areas; from personal care such as shampoos to food such as mayonnaise, even through to road surfaces which are made from bitumen emulsions prior to setting (Hall et al., 2011; Read and Whiteoak, 2003; Robbins, 2012; Sackett

et al., 2010). Creating the initial emulsion for each different product requires a significant amount of time and money.

To reduce the time, cost and waste generated during research, previous work was carried out using high-throughput equipment and design of experiment software to map out which formulation and process parameters produced an emulsion to a predetermined specification (Chapter 4). The focus of previous work was on the droplet size, as the smaller the size of the droplets that make up the emulsion, the larger the available surface area of the dispersed phase, thus the maximisation of the quantity of reagent used. In the case of shampoo, the hydrophobic molecules within the emulsion attach to the oil and grease molecules coating the hair and when slight friction and water is applied they are washed off together.

When scaling-up formulations from bench top to pilot-plant to factory scale, there is a continuing debate on whether the energy dissipation rate (mean or maximum) or the tip speed should be used for scale up (El-Hamouz et al., 2009). The energy dissipation rate, when being calculated for in-line rotor-stator mixers can be obtained from either the total power draw or the from the power draw of the rotor only (Hall, 2011). The tip speed on the other hand is simply calculated using the tip speed equation shown in Equation 5-1.

$$U_T = \pi ND$$

Equation 5-1 Tip speed equation.

Where:

N = impeller speed (ms^{-1})

D = diameter of the impeller (m)

The focus of this work involves scaling up a predetermined formulation and to see the impact that pilot plant scale mixers have upon it with regards to the product

made. Observation of whether the product created on the small volume Formax can be scaled up to large quantities, whilst maintaining or even further decreasing the size of the droplets within the emulsion was of great interest and the results produced led to some interesting conclusions.

5.3 Experimental

The experimental work performed using the Formax is reported in Chapter 4, the method being reported within this chapter involves an investigation into whether scaling-up those parameters to a quantity suitable for use by industry is feasible and if not what the difference in formulation and process parameters is required. The results discovered using the Formax concluded that in order to achieve a stable emulsion made up of the smallest possible droplets, the formulation and process parameters listed in Table 5-1 needed to be adopted.

Table 5-1 Parameters and required values necessary to achieve droplets with smallest $D[3,2]$ value using the Formax.

Formulation Parameters	Oil Type	Oil Phase Volume (%)	Oil Viscosity	Surfactant Type	Surfactant Phase Volume (%)	Water Phase Volume (%)
Values:	Silicone	60	10cSt	SLES	8	32
Process Parameters	Impeller Type	Impeller Speed (rpm)	Scraper Speed (rpm)	Order of Addition		
Values:	Dissolver Disk	6000	100	Oil, impeller speed increased to chosen value before water and then surfactant added to vessel.		

Two devices were chosen to perform the trials at an industrial scale and observe whether the parameters listed in Table 5-1 produced an emulsion made of droplets of a similar size to that produced when using the Formax. The two devices chosen to be tested during this work were an inline Silverson 150/250 MS mixer, which was fed from a sixty litre batch tank and the Ultra Mixing and Processing Facility (UMPF) fitted with CDDM technology.

As performed during the work in Chapter 4, the size of the droplets in the products was obtained using Malvern Mastersizers X and 2000 with focus given to the $D[3,2]$ value.

The oil used for these experiments was 10 cSt Xiameter PMX 200 Silicone Fluid which is chemically equivalent to Dow Corning® 200 Fluid 10CS (10cSt). The reason behind using this oil type is that it is the standard used when performing research into new mixing devices and assessing their impact in both academia and industry.

The Sodium Lauryl Ether Sulfate (SLES) used was Texapon© N70 SLES with three ethoxyl groups.

Any reference to water within this article is in fact reference to distilled water.

5.3.1 Silverson 150/250 MS Mixer Experimental

Work has been performed on the Silverson 150/250 MS mixer used previously by Hall during their investigation into scaling parameters of Silverson rotor-stator mixers (Hall et al., 2011). A similar procedure was followed in this work. The reagents were placed, in appropriate volumes according to the formulation parameters in Table 5-1 with a total volume of sixty litres, into a stirrer tank with a working volume of fifty-four litres. The extra six litres were required to fill the recycle line, prior to the trials beginning, an illustration of the set-up can be seen in Figure 5-1. The feed tank is 0.42m in diameter and is fitted with an anchor stirrer and side scraper configuration. The stirrer is left to run at 55rpm to prevent the reagents sticking to the vessel walls, as well as gently aid the flow of the fluid from the tank through the Silverson 150/250 MS mixer.

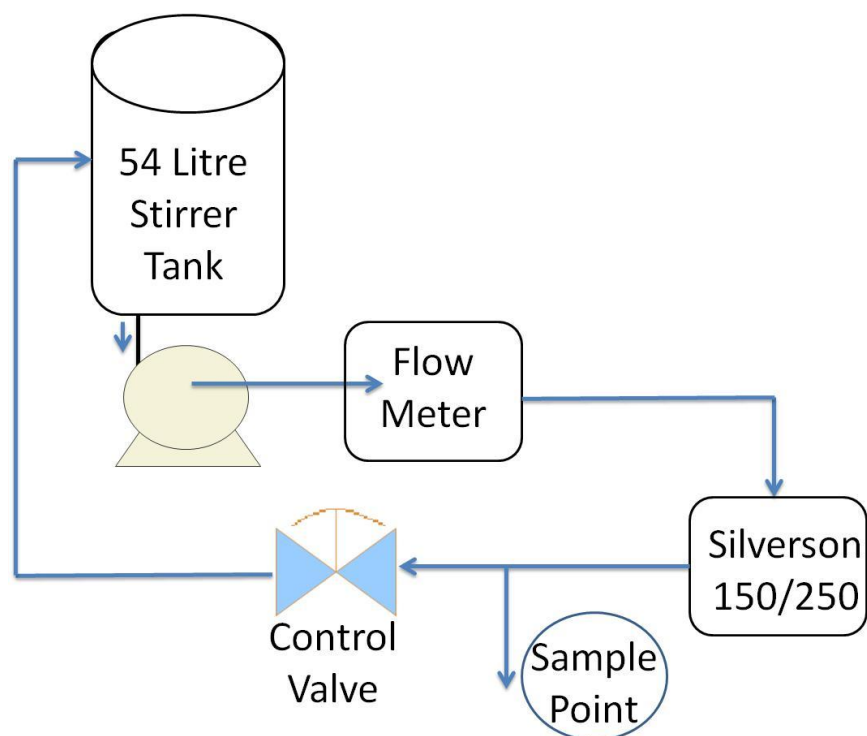


Figure 5-1 Set-up of Silverson 150/250 MS mixer pilot plant rig.

The Silverson 150/250 MS mixer has an inner rotor swept diameter of 1.5” (38.1mm) and an outer eight blade rotor swept diameter of 2.5” (63.5mm) and can be seen in Figure 5-2.



Figure 5-2 Silverson 150/250 MS rotor (left) and stator (right) (Hall et al., 2011)

The clearances between the rotors and screens are quoted as 9 thousandths of an inch (0.22mm), and the tolerances are given as 5 thousandths of an inch. The outer screen

of the stator has 7 rows of 80 x 1/16" holes (1.6 mm) on a 0.1" triangular pitch and the inner screen is slightly smaller, consisting of 6 rows of 50 x 1/16" holes on a 0.1" triangular pitch.

Reagents are passed from the batch tank, through the mixer head at a flow rate of $86.7\text{mL}\cdot\text{s}^{-1}$ and collected. Once all the fluid had been processed and collected it was all poured back into the feed tank, the rotor speed of the mixer was increased and the fluid was processed again to see if the droplets could be further reduced in size. During each pass through the mixer head a 10mL sample was taken following processing to be analysed.

5.3.2 UMPF Experimental

The UMPF is a prototype high-shear mixing device capable of processing five separate fluids at pressures of up to 5000bar and impeller speeds of up to 18,000rpm. The UMPF is described in detail in section 3.4 of this document.

The two main process parameters that were chosen to be investigated during this research work were the rotor speed and the flow rate. The rotor-speed is the speed at which the mixer head is rotated and the flow rate is the speed [recorded in millilitres per second ($\text{mL}\cdot\text{s}^{-1}$)] at which the reagents are forced from the feed vessel to the mixing chamber.

The total flow rate is the sum of all the flow rates, for example an emulsion with a phase volume of 60% oil and a flow rate of $60\text{mL}\cdot\text{s}^{-1}$ would be formulated using a total flow rate of $100\text{mL}\cdot\text{s}^{-1}$. Table 5-2 displays the range of values investigated. The schematic of the UMPF displayed in Figure 3-7 shows that there are five intensifier pumps [four medium, one large] which can be used to inject reagents into the mixing chamber. For these trials four pumps were used with Medium Intensifier Pump

[MIP] 1 and MIP 4 containing SLES solution, the large intensifier pump [LIP] containing oil and the MIP 3 containing water. The order in which these pumps can inject the reagent into the mixing chamber can be altered however for this work the order of addition was kept constant. The order of addition chosen was to flood the mixing chamber with water, then add the surfactant solution, and add the oil last. This allowed the mixer to reach the desired speed without wasting any of the surfactant solution or oil. The fastest total flow rate that was used during these trials was $110\text{mL}\cdot\text{s}^{-1}$. This value is not the fastest the UMPF is capable of, however with the restrictions in place it was decided for safety reasons not to exceed this value.

Table 5-2 Range of parameters observed when using the UMPF.

Process Parameter	Total Flow Rate ($\text{mL}\cdot\text{s}^{-1}$)	Impeller Speed (rpm)	Temperature ($^{\circ}\text{C}$)	Order of Addition
Range	10 – 110	0 – 10,000	Constant	Constant

During preliminary trials on the UMPF it was discovered that slower flow rates, $10\text{mL}\cdot\text{s}^{-1}$ total flow rate or less, are temperamental with respect to formulating an emulsion. The product produced by the UMPF following processing was commonly an unstable, biphasic system with large globules of one reagent dispersed in the other, too large to analyse using either particle sizer available. Further work is being undertaken to discover the reason behind this however it was decided the slowest total flow rate used would be $20\text{mL}\cdot\text{s}^{-1}$ as numerous trials at this total flow rate had proved successful in previous research trials.

The pipework connecting the feed vessels to the mixing chamber can be altered, depending on the viscosity of the materials being used and the desired flow rate. From the previous work on the high-throughput platform it was concluded that the viscosity of the reagents and the final product produced would be within the limitations of the UMPFs low pressure pipework. This was concluded as the emulsion produced had a viscosity of a lesser value than that of other products produced in earlier research trials. As a result the low pressure pipework configuration was used.

Upon the completion of the investigation into the impact of the process parameters on the formulation predetermined by earlier work, it was concluded to expand the investigation into the impact of the formulation parameters on the product. This was decided to ascertain whether the formulation values that had been chosen were producing emulsions made up of the smallest possible droplet size. This expanded the investigation and allowed the mapping out of both the formulation and process space for emulsions produced using silicone oil and SLES surfactant solution, with the aim of formulating an emulsion with the smallest possible droplet size.

The SLES surfactant, prior to being diluted into a solution, was initially at 70% concentration. This value is far greater than required and also is a lot more viscous than desired. The 70% SLES surfactant was diluted down to 25% by adding it dropwise to the appropriate volume of water, whilst gentle mixing was provided by a large anchor stirrer. The anchor stirrer not only caused improved dispersion of the surfactant throughout the water phase but also prevented any sticking to the base of the mixing vessel. Once the solution was uniform with regards to the SLES distribution, it was left to deaerate before being placed in the feed vessel.

5.4 Results and Discussion

As the scale-up trials were performed on two pieces of kit the results from each experiment are discussed separately.

5.4.1 Silverson 150/250 MS 60L Batch reactor

The trials performed on the Silverson 150/250 MS 60L Batch reactor produced emulsions which, when analysed with the Malvern Mastersizer X, displayed the trend that increasing the rotor speed leads to a decrease in the droplet size. Figure 5-3 shows the droplet size distribution [DSD] of the droplets within the emulsions that the values displayed in Table 5-3 have been calculated from. It is clear from looking at the data displayed in Figure 5-3 that as the size of the $D[4,3]$ and $D[3,2]$ values decrease with increasing rotor speed, the percentage volume of smaller droplets that make up the emulsion increases. It should be noted that the DSD graph in Figure 5-3 shows that the first sample analysed did not have a complete curve, it stops at $80\mu\text{m}$, and this is because the emulsion analysed contained droplets too large to be detected as explained in section 2.6 under the title particle sizing.

Table 5-3 Droplet size data produced from analysis using a Mastersizer X.

Pass Number	SLES PV %	Oil PV %	Oil : SLES	Total Flow Rate (mL·s ⁻¹)	Rotor Speed (rpm)	D[4,3] (µm)	D[3,2] (µm)
1	8	60	7.5	86.7	0	34.95	19.25
2	8	60	7.5	86.7	3000	8.25	2.37
3	8	60	7.5	86.7	5000	4.44	1.47
4	8	60	7.5	86.7	7000	2.81	1.15
5	8	60	7.5	86.7	9000	2.02	0.89

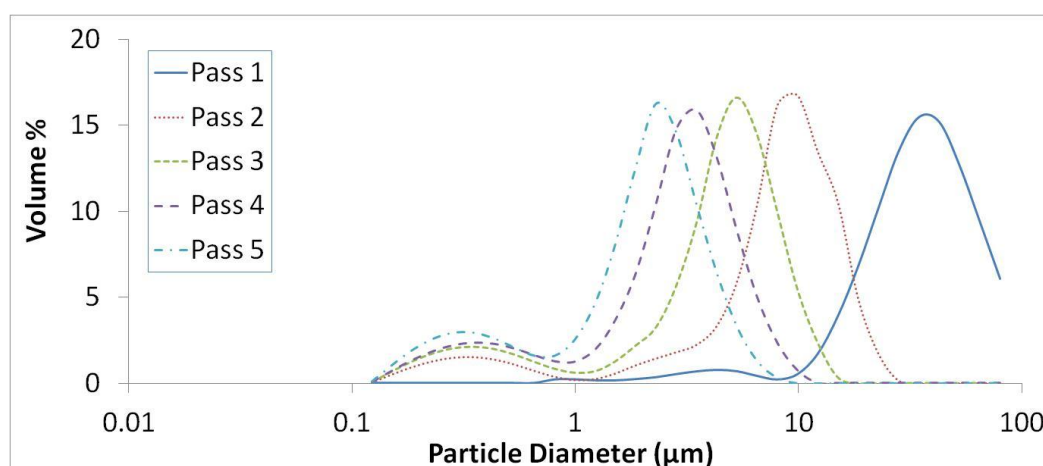


Figure 5-3 Droplet size distribution graph produced using a Mastersizer X.

The fact that both the D[4,3] and the D[3,2] values decrease as the rotor speed is increased implies that these values are not merely artefacts of the Mastersizer as the trend applies for both particle size values. With the majority of the smaller droplet peaks starting at approximately 1µm and all ending at approximately 0.2µm, it was believed that the limit of the Mastersizer X detector was being reached (0.1µm). If droplets are too small to be analysed by the Mastersizer X then the values it

generates will be greater than they actually are and thus provide a false reading. To remove any uncertainty as to the actual sizes of the droplets within the emulsions created we chose to analyse the emulsions again using a Malvern Mastersizer 2000. This is because as well as the red laser light source that the Mastersizer X uses, the Mastersizer 2000 also uses a blue light source that allows the analyser to observe particulates down to 20nm in size.

The results produced following analysis with the Malvern Mastersizer 2000, with respect to the Sauter Mean Diameter, are significantly different to those obtained using the Malvern Mastersizer X. Analysis using both the red and blue light sources of the Malvern Mastersizer 2000 yielded D[4,3] values similar to those determined during analysis using only red laser light [from the Mastersizer X]. The comparison of the data displayed in Table 5-3 and Table 5-4 displays both the trend of the results and the mean D[4,3] values obtained from analysis.

Table 5-4 Droplet size data produced from analysis using a Mastersizer 2000 with both blue and red light sources.

Pass Number	SLES PV %	Oil PV %	Oil : SLES	Total Flow Rate (mL·s⁻¹)	Rotor Speed (rpm)	D[4,3] (µm)	D[3,2] (µm)
1	8	60	7.5	86.7	0	29.243	23.954
2	8	60	7.5	86.7	3000	8.861	7.446
3	8	60	7.5	86.7	5000	5.251	4.857
4	8	60	7.5	86.7	7000	3.565	3.117
5	8	60	7.5	86.7	9000	2.569	2.18

The D[3,2] values displayed in Table 5-4 obtained from analysis with both red and blue light sources, are significantly larger than those displayed in Table 5-3 which were obtained using the Mastersizer X red light source. This graph displayed in Figure 5-3 shows the droplet size distribution for the emulsions analysed using both red and blue light sources. It can be seen from Figure 5-3 that the emulsions produced appear as being unimodal, with only the larger of the two peaks that made the emulsion appear bimodal in Figure 5-3 present. It is the lack of the smaller peak that causes the significant increase in the D[3,2] value. This is because the D[3,2] value is calculated as being the diameter of a sphere with the same surface area as the particulates being analysed. With the removal of so many smaller particulates, the overall available surface area decreases, as the larger particulates cause the area per particulate to increase at the expense to the number of particulates present.

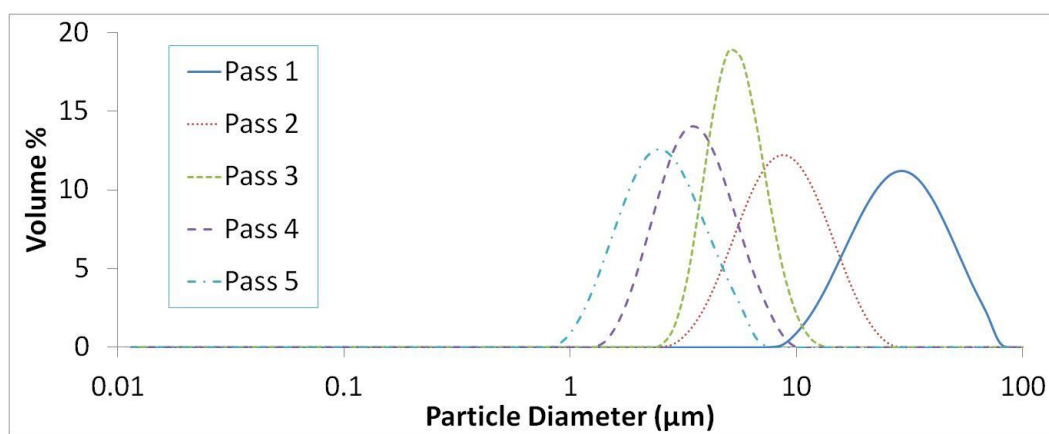


Figure 5-4 Droplet size distribution graph produced using a Mastersizer 2000 with both blue and red light sources.

It was initially believed that the sudden stop by all the samples [bar the largest] at approximately 200nm in Figure 5-3 was due to the particle sizer using only a red light source, which is unable to analyse anything below 100nm in size. The use of a blue light allowed us to see down to 20nm in size, however according to the

apparatus and the data interpretation there was nothing smaller than 900nm present in any of the samples analysed.

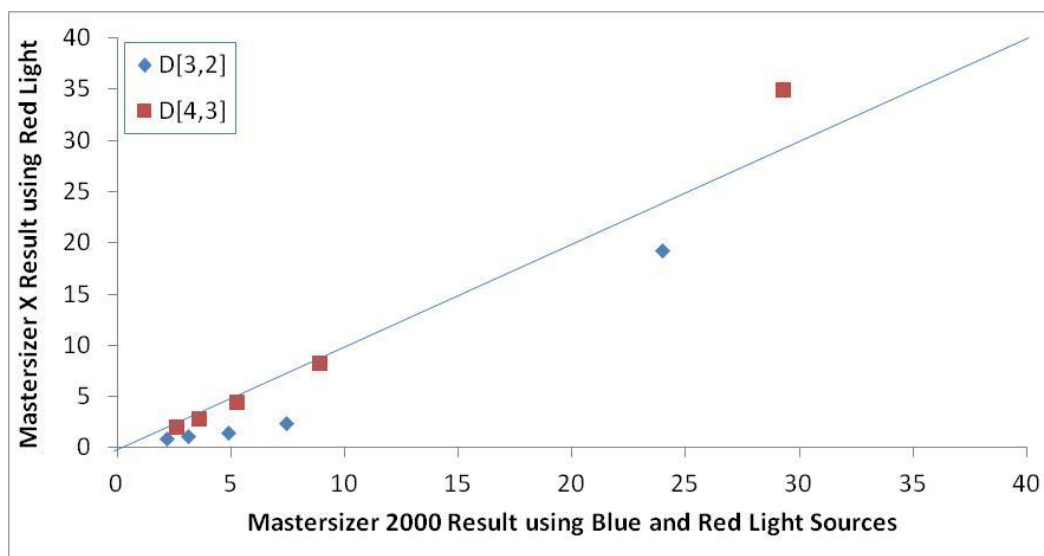


Figure 5-5 Droplet size values as calculated by a Mastersizer X versus the same measurements calculated by a Mastersizer 2000 (with both blue and red light sources).

The graph presented in Figure 5-5 shows that the Mastersizer X calculated smaller D[3,2] values than the Mastersizer 2000 for all the emulsions analysed. The D[4,3] values calculated by both Mastersizers was almost identical. From this data it can be proposed that when analysing emulsions using the Mastersizer X, the D[4,3] is the more reliable value.

In order to ensure that this was not a fault with the blue light source the samples were analysed using the Mastersizer 2000 but with the red light source only [the blue light was turned off]. The droplet size distribution of each of the emulsions analysed using only red light is displayed in Figure 5-6 and the values calculated by the software from the data shown are presented in Table 5-5. It can be seen in Figure 5-6 that the first sample analysed [pass 1] is bimodal. This is a misinterpretation by the software, from the detectors the light has hit. This smaller peak is merely an artefact of the

software. This can be said with certainty as when manipulating the software using the results generated to produce the graph in Figure 5-4, to interpret the results if only red light was used, the peak appears on the droplet size distribution graph.

Table 5-5 Droplet size data from analysis of samples using red light source only analysis from the Malvern Mastersizer 2000.

Pass Number	SLES PV %	Oil PV %	Oil : SLES	Total Flow Rate (mL·s ⁻¹)	Rotor Speed (rpm)	D[4,3] (µm)	D[3,2] (µm)
1	8	60	7.5	86.7	0	28.685	20.532
2	8	60	7.5	86.7	3000	8.602	7.208
3	8	60	7.5	86.7	5000	5.245	4.838
4	8	60	7.5	86.7	7000	3.623	3.159
5	8	60	7.5	86.7	9000	2.512	2.174

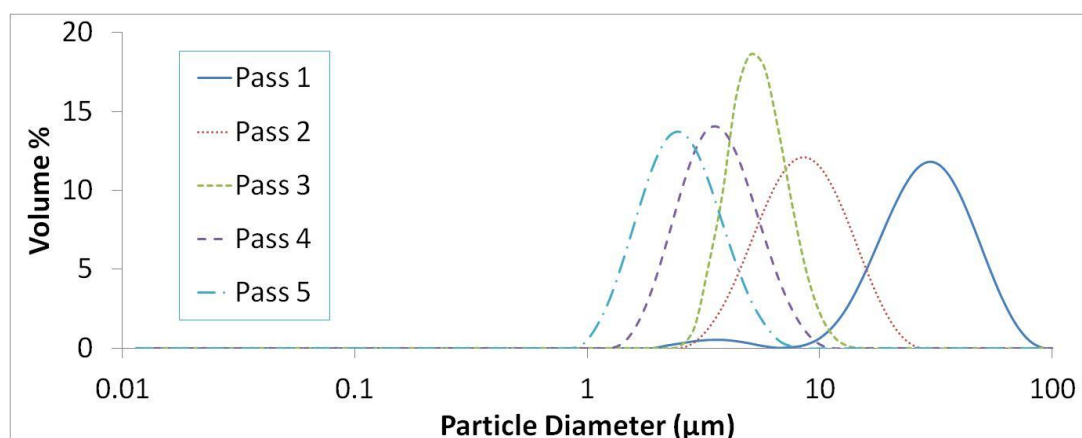


Figure 5-6 Droplet size distribution graph produced using Mastersizer 2000 with red light source only.

Comparing the data for the samples analysed using both red and blue light sources with analysis done using a red light source only [Table 5-4 and Table 5-5] yields

negligible differences implying that there is nothing within the emulsion below 900nm in size. Figure 5-7 displays the results from the same samples analysed using the Mastersizer 2000 with red light only against the results obtained using the same apparatus with both red and blue light sources. With the exception of the data points discussed previously that are artefacts from analysis using only red light to analyse samples it can be seen that the data points all correlate with each other.

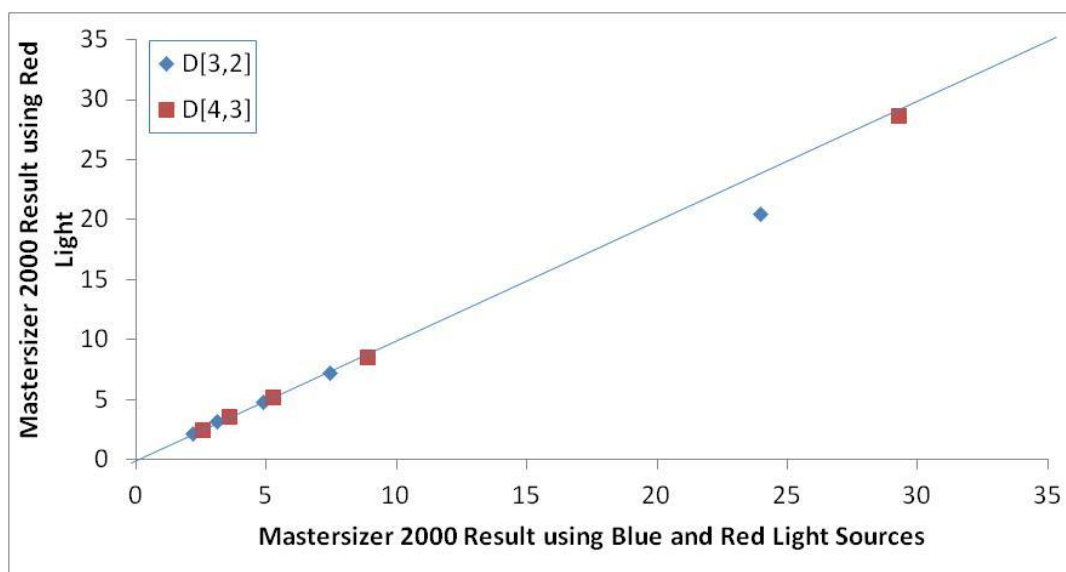


Figure 5-7 Droplet size values as calculated by a Mastersizer 2000 with red light only versus the same measurements calculated by a Mastersizer 2000 with both blue and red light sources.

The droplet size distributions displayed in Figure 5-4 and Figure 5-6 are almost identical with focus on peak location, height and overall trace. Figure 5-8 confirms how alike the two traces are as they have been plotted on the same axis.

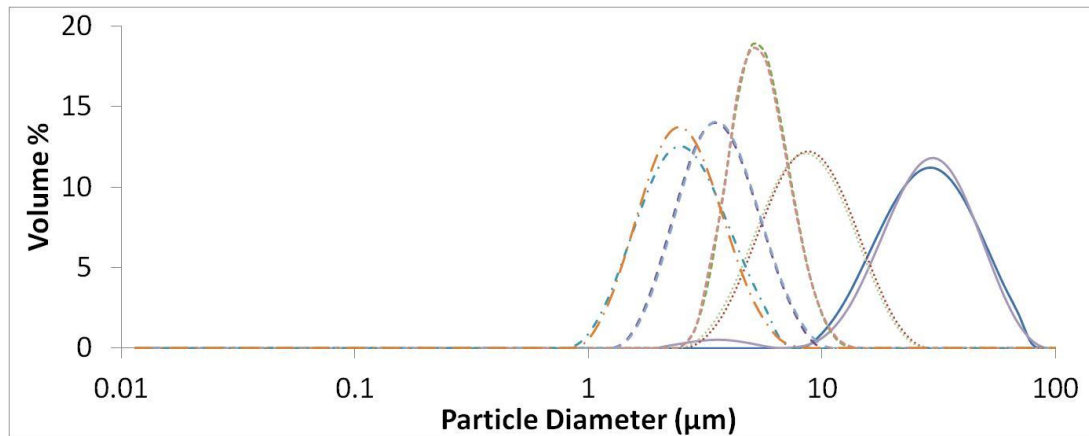


Figure 5-8 Graphs from Figure 5-4 and Figure 5-6 combined.

A proposed reasoning for the presence of the smaller peaks, when analysed using the Mastersizer X, is that they are artefacts and misinterpretations of diffraction patterns by the software. The reasoning behind this is due to the fact that the blue light and the red light on the Mastersizer 2000, when working together and when just the red light is used, do not detect any second smaller peak [with the exception of the small peak for the first sample when analysed using only red light]. The main physical differences between the two pieces of analytical apparatus are:

- The Mastersizer X requires different lenses dependent on the size of the particulates to be analysed, each lens has a range that it can be used to analyse. For the smallest particulates the Mastersizer X is capable of detecting the 45mm lens is used to diffract the red laser light onto the sample and then onto the detector.
- The Mastersizer 2000 uses a blue light source also to analyse samples which enables confirmation of results interpreted by the red light source.

- The Mastersizer 2000 has more detector cells than the X model, both side scatter detectors and back scatter detectors, as well as focal plane detectors behind the sample cell. This allows for accurate observation of small particulates.

From the data in Table 5-4 and Table 5-5 we can say that processing the formulation parameters displayed in Table 5-1 using a Silverson 150/250 MS mixer, after one pass at low speed, creates a unimodal emulsion.

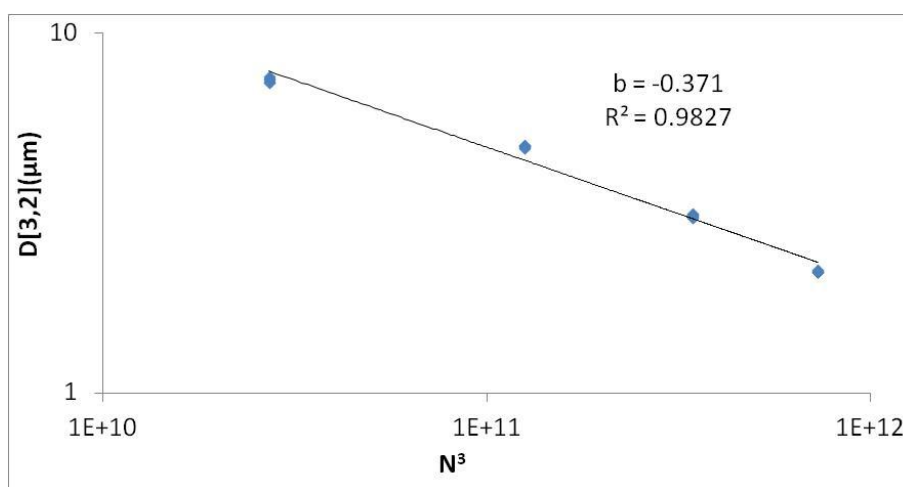


Figure 5-9 Droplet size as a function of the impeller speed [cubed].

Increasing the impeller speed of the mixer leads to the droplet size of the emulsion decreasing. The data displayed within Figure 5-9 and Figure 5-10 confirms that increasing the rotor speed, and thus increasing the tip speed, of the mixer leads to a decrease in the size of the droplets within the emulsion produced. Figure 5-9 is consistent with the work performed by Hall that when using a Silverson 150/250 MS the rotor speed is the strongest influence on droplet break-up (Hall, 2011). This suggests that, theoretically, should other flow rates have been investigated, the impact they would have had upon the $D[3,2]$ value of the droplets within the emulsion would have been minimal. It is believed this is due to the flow within the

mixing vessel being turbulent inertial. This is confirmed by the b value calculated and displayed in Figure 5-9 being almost 0.4 (section 2.4). A further look at the tip speed data shows that, as per the work performed by Hall (2011), the droplet size measurements fall in a single line in logarithmic co-ordinates. As well as the

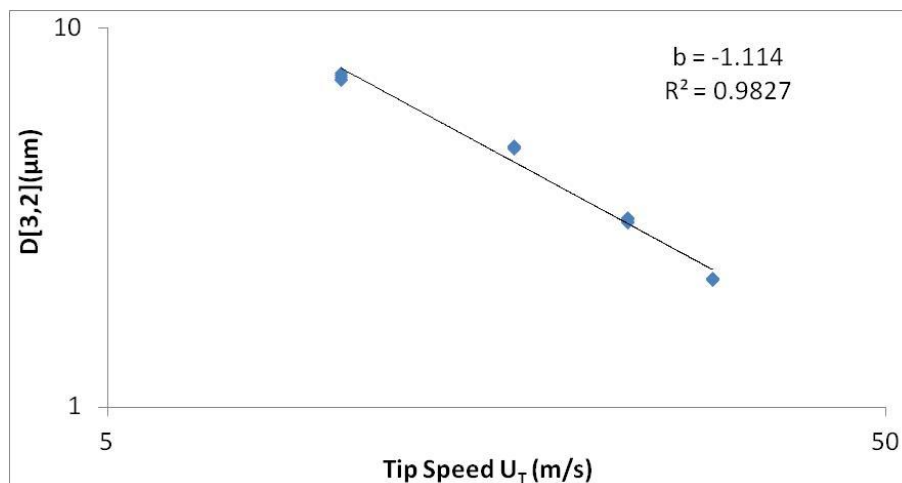


Figure 5-10 Droplet size as a function of tip speed.

5.4.2 UMPF

Trials on the UMPF produced results that show the tip speed is not the determining factor with regards to the size of the droplets in the final emulsion. As can be seen in Figure 5-11 by the spread of the results, the total flow rate of the reagents and the oil-to-surfactant ratio had a great impact on the final droplet size.

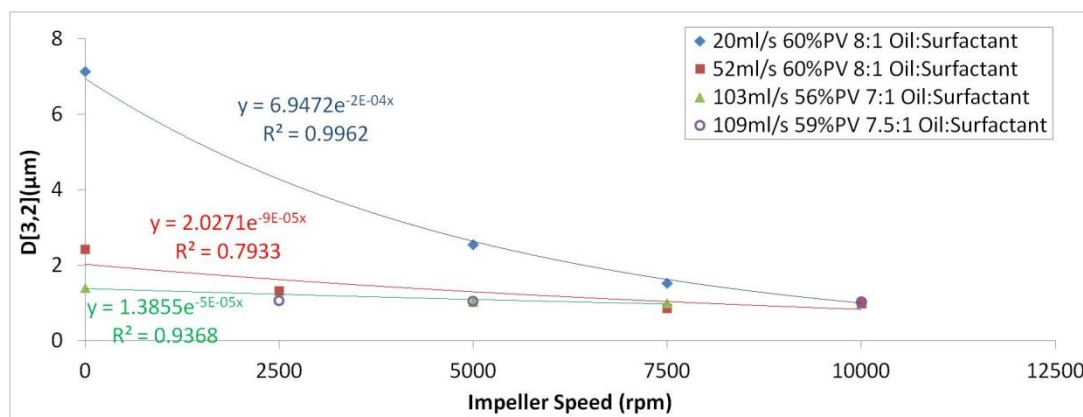


Figure 5-11 Droplet size as a function of impeller speed at and varying oil to surfactant ratios. Analysis was performed using the Malvern Mastersizer X with a 45mm lens.

It can be observed from the lines of best fit that have been applied to the data shown in Figure 5-11, that as the total flow rate increases, the gradient of the line decreases until it becomes an almost horizontal line. One of the most interesting results is the decrease in droplet size when the rotor is not turning. It can be seen that with no energy input from the rotor and at a total flow rate of only $20\text{mL}\cdot\text{s}^{-1}$, the emulsion formulated has a droplet size of $7\mu\text{m}$. Further to this by increasing the total flow rate by a factor of 2.5, the droplet size is reduced by approximately 3 times and when the flow rate is increased by a factor of 5 the droplet size is decreased by the same factor. From this it can be hypothesised that further increases to the total flow rate will lead to greater decreases in droplet size. Due to limitations on the mixer at the time of use total flow rates of over $110\text{mL}\cdot\text{s}^{-1}$ were not possible however this hypothesis has been noted for future work.

Figure 5-12 confirms the theory that the tip speed is not the defining factor of the size of the droplets within the emulsion formulated when using the UMPF. Even though the tip speed is increased greatly, as was observed from the data in Figure

5-11, the flow rate plays a large part in the final droplet size of the emulsion produced.

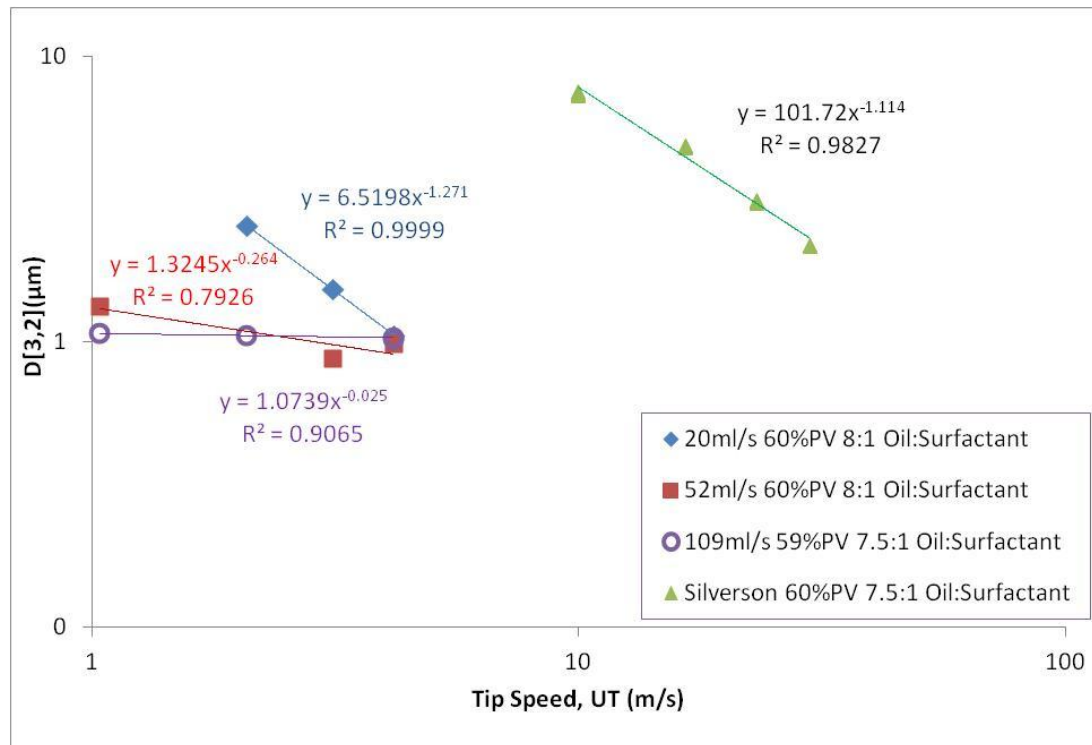


Figure 5-12 Droplet size of emulsion as a function of tip speed (U_T) with respect to flow rate and oil to surfactant ratios. Analysis of UMPF samples performed using the Malvern Mastersizer X with a 45mm lens, analysis of Silverson was performed with a Mastersizer 2000.

It is fair to say that the data in Figure 5-12 shows that the impact of the tip speed of the UMPF at flow rates in excess of $100\text{mL}\cdot\text{s}^{-1}$ was negligible. From the three data points and the equation generated from the trend line there is little to no change despite the large increase in tip speed.

The opposite can be said of the data obtained from flow rates of $20\text{mL}\cdot\text{s}^{-1}$. As the tip speed increases, the droplet size decreases almost in perfect correlation. The comparison between the tip speed of the Silverson and that of the UMPF operating at $20\text{mL}\cdot\text{s}^{-1}$ shows that at a fraction of the speed, the UMPF is able to produce emulsions made up of smaller droplets.

When operating at total flow rates of $52\text{mL}\cdot\text{s}^{-1}$ and $109\text{mL}\cdot\text{s}^{-1}$ the UMPF is able to produce emulsions with a smaller droplet size than the Silverson is able to at the slowest impeller speed that was operated at. Going back to Figure 5-11 we can observe that at zero impeller speed but these flow rates, the UMPF was capable of producing emulsions with a smaller droplet size than those of the Silverson after five passes with increasing rotor speeds up to, and including, 9000rpm. To ensure that this was not merely an artefact of the Mastersizer X using only red light the $D[4,3]$ values were plotted against tip speed as it was discovered earlier that there is good correlation between the results from both Mastersizers with regards to this equipment.

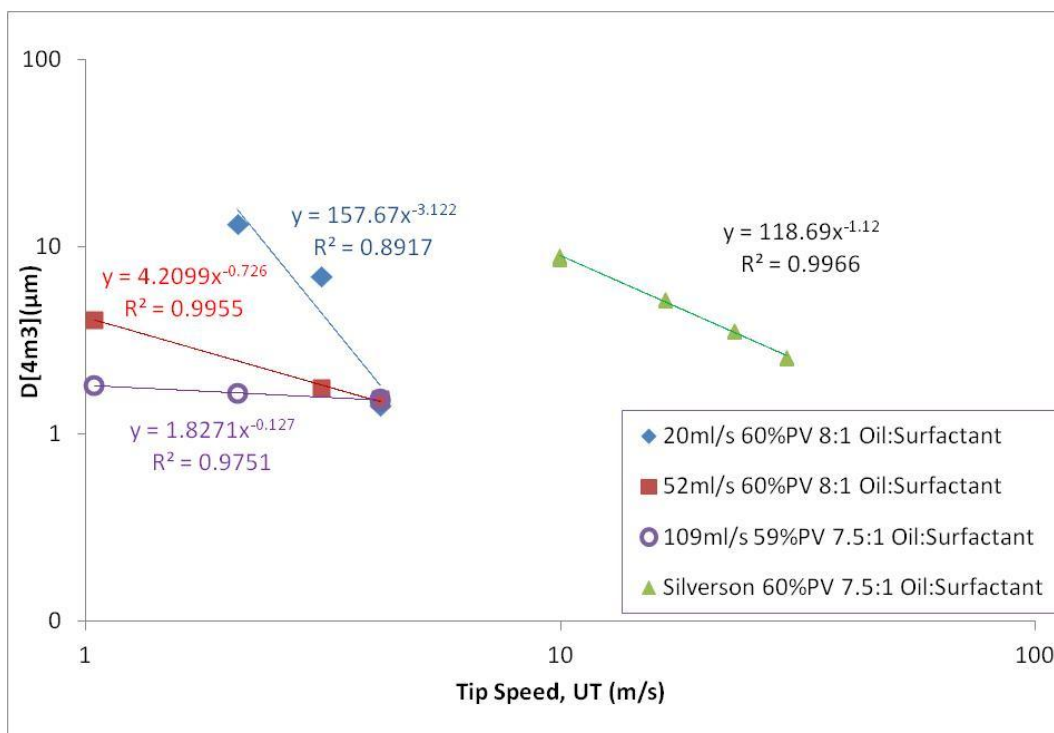


Figure 5-13 Droplet size of emulsion as a function of tip speed (U_T) with respect to flow rate and oil to surfactant ratios. Analysis of UMPF samples performed using the Malvern Mastersizer X with a 45mm lens, analysis of Silverson was performed with a Mastersizer 2000.

The data in Figure 5-13 shows similar results to the data in Figure 5-12; that at significantly lower tip speeds the UMPF is able to generate emulsions with a smaller droplet size.

Initially the phase volume of oil chosen to formulate the emulsions was that determined from the high-throughput trials, however after samples had been processed using this formulation emulsions with different phase volumes of oil were created using the UMPF. The graph shown in Figure 5-14 displays the D[3,2] values of some of these emulsions of varying oil to surfactant ratio processed at the same total flow rate and rotor speed.

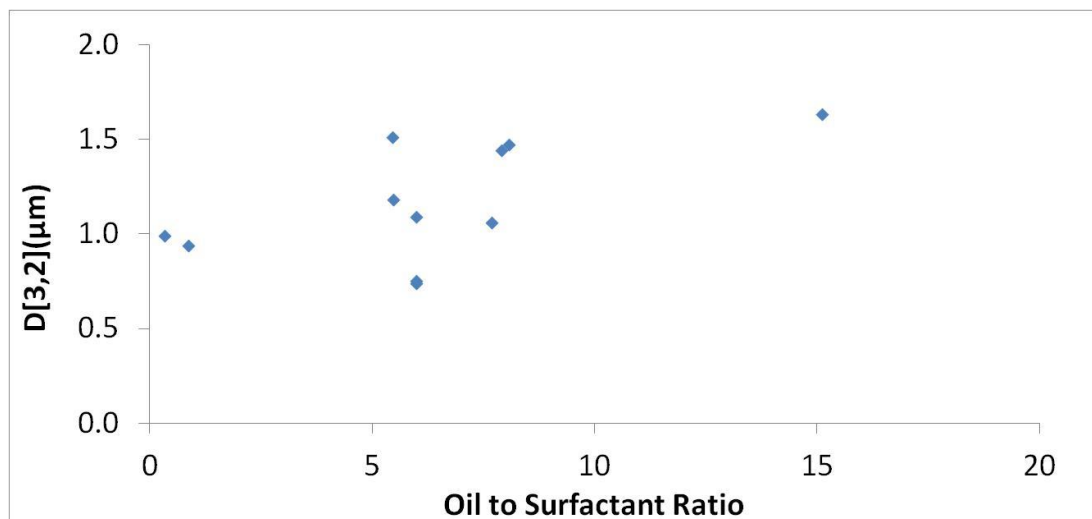


Figure 5-14 Graph showing the impact of the oil to surfactant ratio on the size of the droplets within the emulsion produced using the UMPF at 10,000rpm with a total flow rate of 20mL/s.

It can be seen from the data presented in Figure 5-14 that the UMPF is capable of processing emulsions and reducing the D[3,2] value of the droplets in the product to a micron for varying oil to surfactant ratios. This data also shows that the UMPF is capable of processing large phase volumes of oil and reducing the droplet size of the emulsions produced to the same extent that it is able to process emulsions made from a much smaller oil to surfactant ratio. This is of great benefit, as emulsions with a

170

large phase volume of oil are preferred for subsequent reactions where oil is the reagent required for the reaction and the other components of the emulsion are not necessary for the reaction, in some cases they even hinder the reaction.

When formulating emulsions using the UMPF it was confirmed that there is a trade-off between the two main process parameters, total flow rate and impeller speed. The greater the flow rate, the less time the reagents have within the mixing chamber and as a result the rotor-speed becomes almost redundant as can be seen by the data presented in Table 5-6. Aside from the first trial done with the impeller kept at static, increasing the impeller speed had a very small impact on the droplet size. Despite a significant decrease in the $D[4,3]$ value between emulsions produced when the impeller remains static and when it is turning, there is little to no impact on the $D[3,2]$ value of the droplets produced. When taking into account the fact that the rotor speed is being doubled each time the resulting impact on the droplet size being produced within the emulsion is minimal to negligible.

Table 5-6 Data taken from analysis of samples using red light source only [Malvern Mastersizer X] showing the impact of impeller speed on droplet size.

No.	SLES%	Oil %	Oil : SLES	Total Flow Rate (mL·s ⁻¹)	Rotor Speed (rpm)	D[4,3] (µm)	D[3,2] (µm)
5.1	8.17	57.00	6.977	105.6	0	5.06	1.41
5.2	7.79	59.00	7.57	108.20	2500	1.82	1.07
5.3	7.89	58.50	7.42	113.40	5000	1.66	1.06
5.4	7.75	59.20	7.64	107.02	10000	1.50	1.03

Table 5-7 Data taken from analysis of samples using red and blue light sources [Malvern Mastersizer 2000] showing the impact of impeller speed on droplet size.

No.	SLES%	Oil %	Oil : SLES	Total Flow Rate (mL·s ⁻¹)	Rotor Speed (rpm)	D[4,3] (µm)	D[3,2] (µm)
5.1	8.17	57.00	6.98	105.6	0	5.87	4.61
5.2	7.79	59.00	7.57	108.20	2500	2.15	1.76
5.3	7.89	58.50	7.42	113.40	5000	1.64	0.59
5.4	7.75	59.20	7.64	107.02	10000	1.47	0.67

Table 5-8 Data taken from analysis of samples using red light source only [Malvern Mastersizer X] showing the impact of impeller speed on droplet size.

No.	SLES%	PV Oil %	Oil : SLES	Total Flow Rate (mL·s ⁻¹)	Rotor Speed (rpm)	D[4,3] (µm)	D[3,2] (µm)
6.1	6.96	56.50	8.12	50.00	0	12.31	2.44
6.2	6.90	56.60	8.20	53.80	2500	4.12	1.34
6.3	6.63	56.40	8.51	54.70	7500	2.52	1.10

Table 5-9 Data taken from analysis of samples using red and blue light sources [Malvern Mastersizer 2000] showing the impact of impeller speed on droplet size.

No.	SLES%	PV Oil %	Oil : SLES	Total Flow Rate (mL·s ⁻¹)	Rotor Speed (rpm)	D[4,3] (µm)	D[3,2] (µm)
6.1	6.96	56.50	8.12	50.00	0	7.11	5.80
6.2	6.90	56.60	8.20	53.80	2500	2.55	0.20
6.3	6.63	56.40	8.51	54.70	7500	3.02	2.24

Table 5-6 through to, and including, Table 5-9 contain data points of great interest; experiments performed with the impeller static. The data involving the static rotor from these tables has been collated into one table, Table 5-10, for easier analysis.

The trials reported in these tables were performed without the impeller turning and thus the emulsion formulation is reliant entirely on the formulation parameters, the total flow rate and the design of the rotor-stator mixer chamber to produce an emulsion from the separate reagents. If an emulsion was not produced then the reagents would come out the mixer chamber and separate over time due to density differences. Stable emulsions were in fact made, and consisted of droplets a few microns. These emulsions consisting of relatively small droplets were produced with no additional energy input from the impeller and is a find that proves the geometry and total flow rates of the UMPF are significant in the formulating of emulsions with small droplet sizes. Figure 5-15 shows clearly that increasing the total flow rate, with the mixer static, causes the size of the droplets in the product to be smaller. It is theorised that this is due to the increase in kinetic energy within the system provided by the increase in force of injecting the fluid into the central mixing chamber.

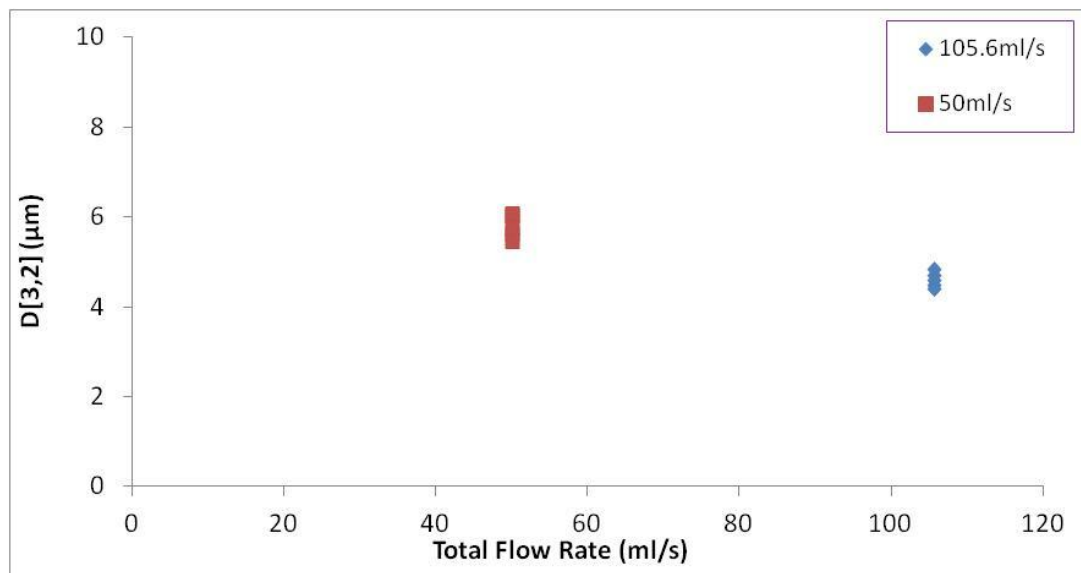


Figure 5-15 Graph showing the impact of the total flow rate on the size of the droplets within the emulsion produced using the UMPF with the impeller at static. Analysis was performed using the Malvern Mastersizer 2000 with both red and blue light sources. The phase volume of oil and surfactant for the formulations within each series was kept constant.

The emulsion formulated without the impeller turning was made up of droplets only a few microns in size; $D[3,2]$ of $5.8\mu\text{m}$ when processed at $50\text{mL}\cdot\text{s}^{-1}$ and a $D[3,2]$ of $4.61\mu\text{m}$ when processed at a total flow rate of 100ml/s . In order to produce emulsions made up of droplets with a $D[3,2]$ of $5\mu\text{m}$ using the Silverson 150/250 MS mixer required three passes and increasing impeller speeds of 0rpm , 3000rpm and 5000rpm . Even after this the emulsion produced contained droplets $5.25\mu\text{m}$ in size with respect to the $D[3,2]$.

These results show the potential that the UMPF has to formulate large quantities of emulsion with small droplet sizes. The total flow rate was found to be the driving factor in obtaining this result as when it was increased, the droplet size decreased. It should be noted that the flow rates used during these trials are not the greatest that the UMPF is capable of operating at, nor near it, as discussed in the method section.

Table 5-10 Data taken from Table 5-6, Table 5-7, Table 5-8 and Table 5-9
for ease of analysis.

No.	SLES%	PV Oil %	Oil : SLES	Total Flow Rate (mL·s ⁻¹)	Rotor Speed (rpm)	D[4,3] (µm)	D[3,2] (µm)	Analysed using?
6.1	6.96	56.50	8.12	50.00	0	12.31	2.44	Mastersizer X
6.1	6.96	56.50	8.12	50.00	0	7.11	5.80	Mastersizer 2000
5.1	8.17	57.00	6.98	105.6	0	5.06	1.41	Mastersizer X
5.1	8.17	57.00	6.98	105.6	0	5.87	4.61	Mastersizer 2000

As happened when analysing samples produced using the Silverson 150/250 MS mixer, analysis of the samples using a Mastersizer X with focus on the droplet size distribution, leads to the observation that all the samples tail off and finish at ~0.2µm (Figure 5-16). To ensure that this was in fact the case and not an artefact of the Mastersizer X the samples were analysed using the Mastersizer 2000, first with red light only to ensure that the previous analysis matched up and then with blue and red light sources to observe whether there were droplets smaller than 100nm present.

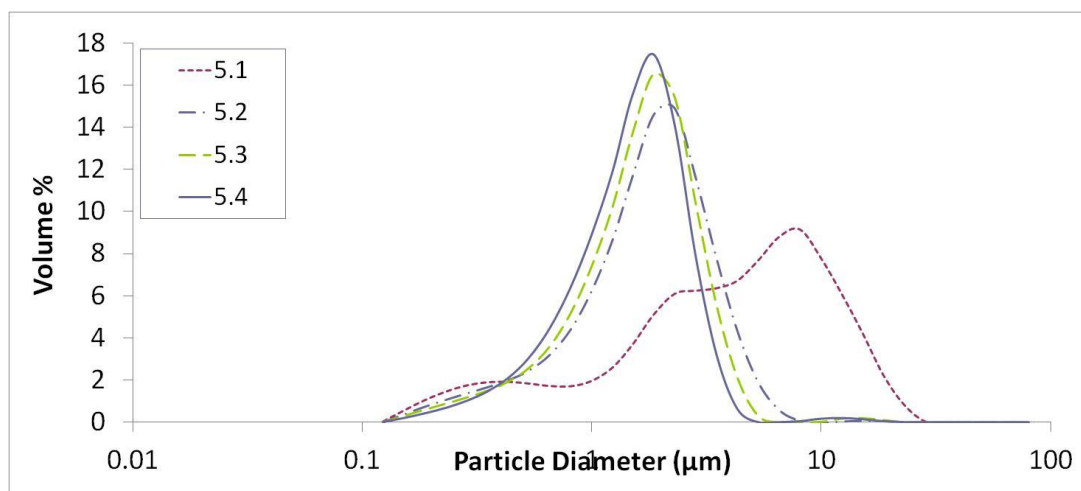


Figure 5-16 Droplet size distribution produced by Malvern Mastersizer X of samples displayed in Table 5-6 following analysis using a 45mm lens.

Figure 5-16 shows the droplet size distribution of the samples listed in Table 5-6 produced by the Mastersizer X. It can be seen that not only do all traces end at $0.2\mu\text{m}$ but that but samples 5.2-5.4 [inclusive] are unimodal with the exception of sample 5.1 which appears trimodal.

In contrast to this Figure 5-17 shows the droplet size distribution of the exact same samples from analysis using the Mastersizer 2000 with red light only. When analysing using only red light, if the sample contained the droplet size distribution shown in Figure 5-16, then the Mastersizer 2000 would confirm this as the red light source operates on the same wavelength (633nm).

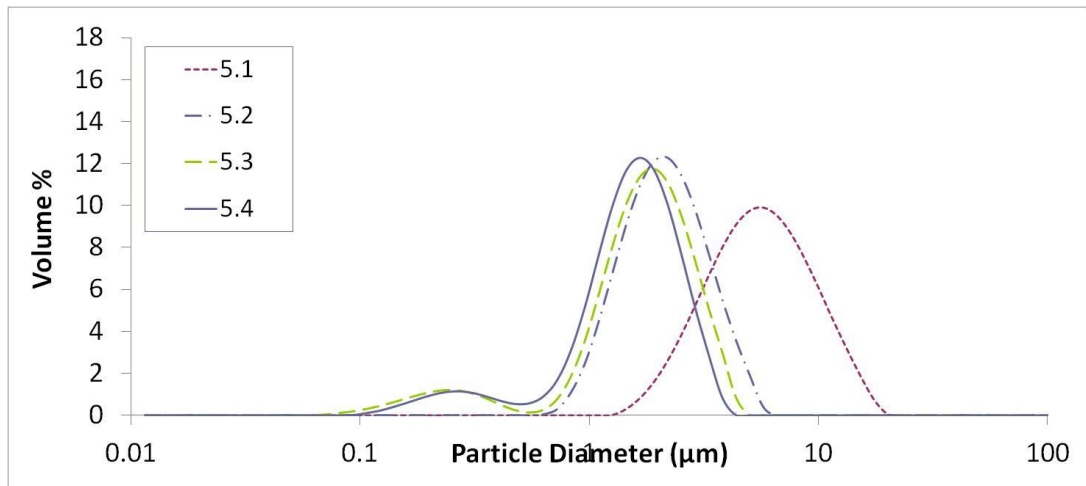


Figure 5-17 Droplet size distribution produced by Malvern Mastersizer 2000 of samples displayed in Table 5-6 following analysis using red light source only.

There is a stark contrast in the difference between the droplet size distribution traces shown in the two figures of the samples, the most noticeable being sample 5.1 is unimodal and that samples 5.3 and 5.4 are bimodal. To observe whether these were artefacts of using only the red laser and to observe whether or not there were any droplets smaller than 100nm the samples were analysed again using the Mastersizer 2000 however this time both red and blue light sources were used.

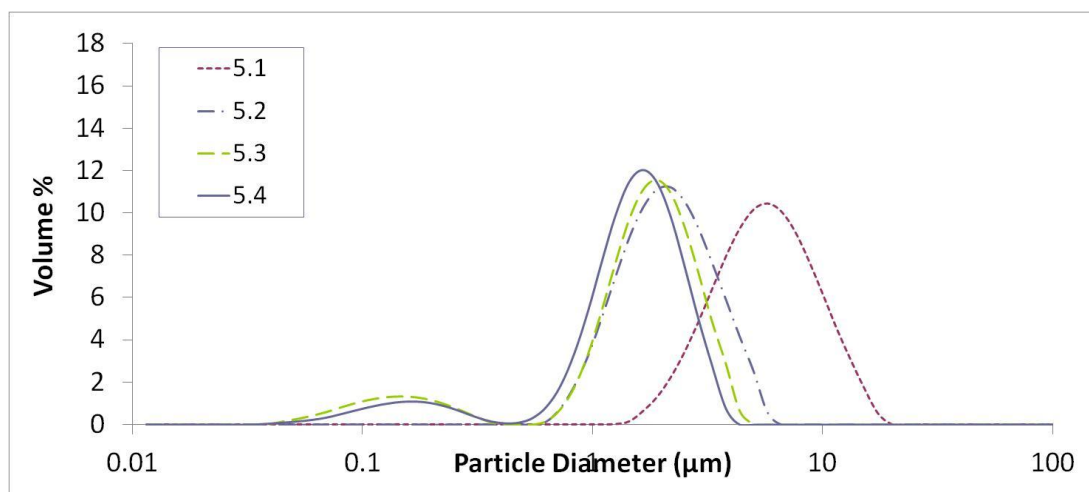


Figure 5-18 Droplet size distribution produced by Malvern Mastersizer 2000 of samples displayed in Table 5-7 following analysis of the samples using the Mastersizer 2000 with both red and blue light sources.

The resulting droplet size distributions were almost identical to those displayed in Figure 5-17 with the exception that the traces for samples 5.3 and 5.4 do not end at around the 100nm mark, but instead finish at 35nm

The difference in droplet size distribution traces between samples 5.3 and 5.4 is so minimal in Figure 5-16, Figure 5-17 and Figure 5-18, and in between the values displayed in Table 5-7, that it can be said at high flow rates, increasing the impeller speed past 5000rpm has little to no impact on the droplet size within the emulsion formulated.

The data in Table 5-8 and Table 5-9 corresponds to Figure 5-19 and Figure 5-21 and it not only supports the proposal that increasing tip speed past a certain point has no impact on the size of the droplets in the product produced but implies that increasing the rotor speed past a certain value can cause the droplets in the final product to increase in size to that of the product produced at a slower tip speed.

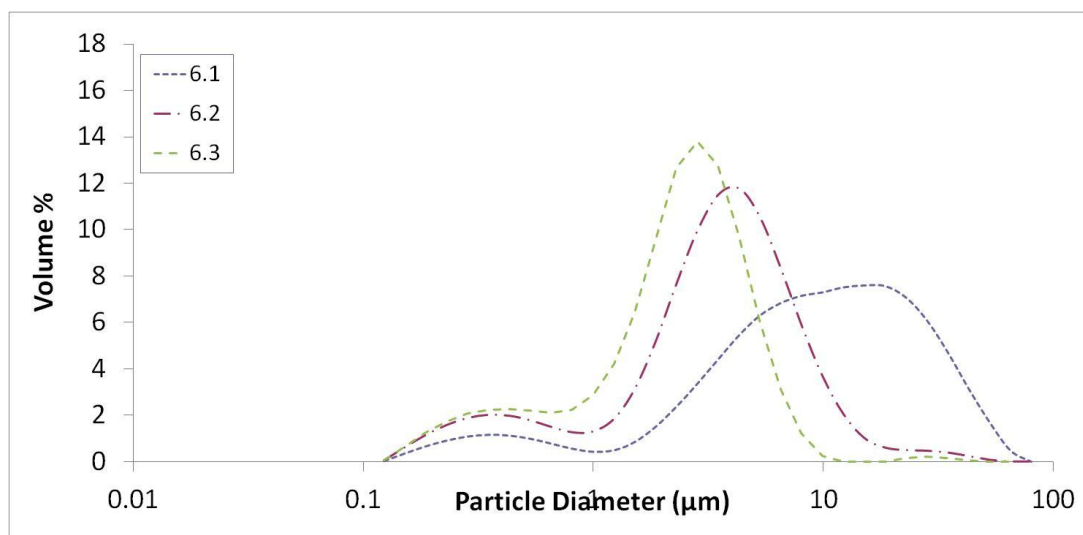


Figure 5-19 Droplet size distribution produced by Malvern Mastersizer X of samples displayed in Table 5-8.

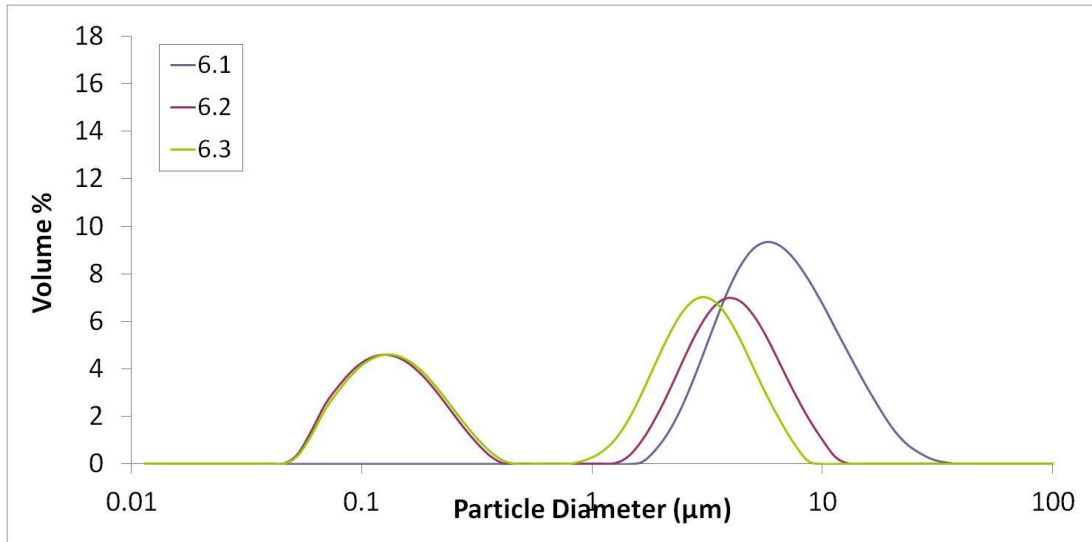


Figure 5-20 Droplet size distribution produced by Malvern Mastersizer 2000 of samples displayed in Table 5-8 following analysis of the samples using the Mastersizer 2000 with a red light source only.

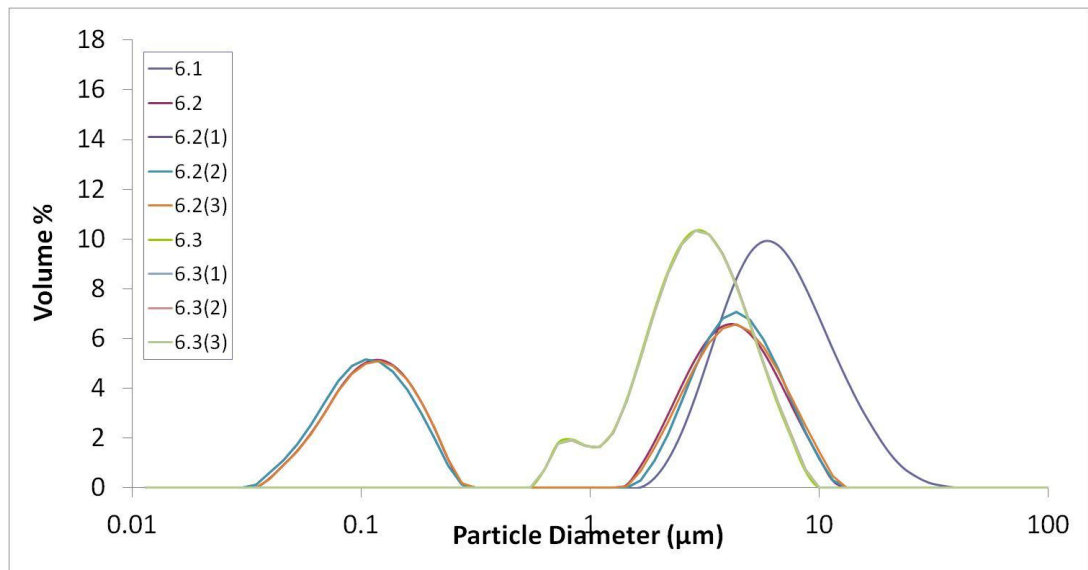


Figure 5-21 Droplet size distribution produced by Malvern Mastersizer 2000 of samples displayed in Table 5-9 following using both red and blue light sources.

Sample 6.2 appears bimodal in Figure 5-19, Figure 5-20 and Figure 5-21 unlike sample 6.1, which as per sample 5.1 discussed earlier, goes from being bimodal when analysed using a Mastersizer X (droplet size distribution displayed in Figure 5-19) to unimodal when analysed using the Mastersizer 2000 (droplet size

distribution displayed in Figure 5-20 and Figure 5-21). Sample 6.3 also appears bimodal in these three graphs however unlike sample 6.2, when analysed using both red and blue light sources the amount of smaller droplets is in fact less than observed when using only a red light source. These measurements were repeated numerous times to ensure that the results were not anomalous as sample 6.3 was processed at a greater impeller speed than sample 6.2 and as a result it was expected to have a smaller droplet size. The repeats all resulted in almost replicas of those displayed and discussed within this chapter, and confirmed that when formulating an emulsion using UMPF the trade-off between total flow rate and impeller speed of the mixer has to be balanced finely, and processing at the maximum capabilities does not necessarily equate to producing an emulsion with the smallest droplet size.

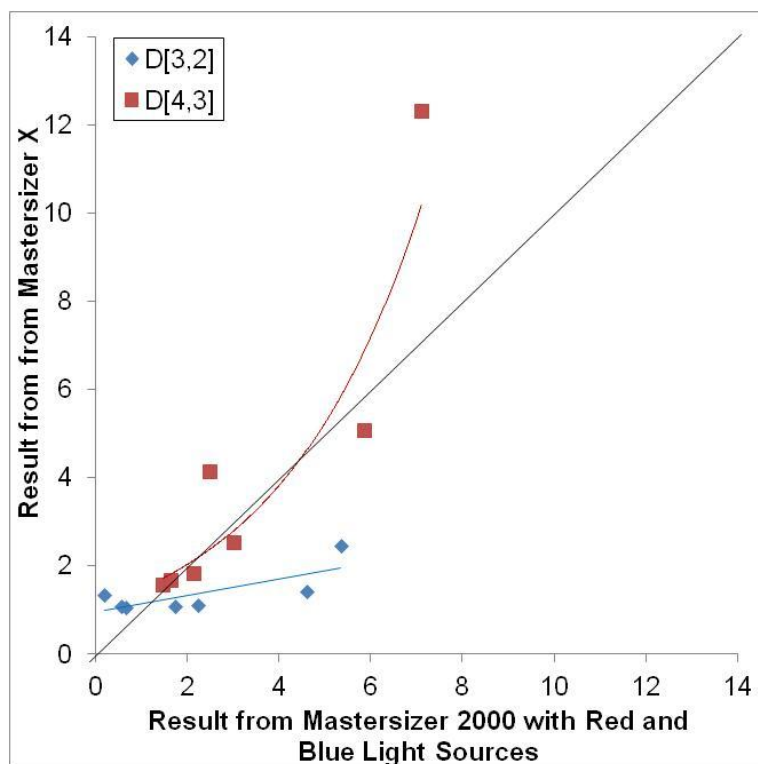


Figure 5-22 Droplet size values as calculated by a Mastersizer X (red light only) versus the same measurements calculated by a Mastersizer 2000 with both blue and red light sources.

Figure 5-22 shows the comparison between the results from Mastersizer X and the results from the Mastersizer 2000 using both red and blue light sources. It can be seen that analysis using the Mastersizer X produced D[4,3] results that correlated well with those by the Mastersizer 2000 however the D[3,2] values were all different; some smaller, some larger. It is believed that this is due to the limitations of both the hardware and the software and that for accurate D[3,2] measurements, the Mastersizer 2000 should be used.

During the trials on the UMPF it was discovered that the formulation, the total flow rate and the impeller speed all have a great impact on the size of the droplets within the emulsion produced. Following numerous trials, involving many possible combinations of total flow rates and impeller speeds, it was concluded that in order to obtain the smallest possible droplet size using the reagents available, within the limitations explored, required the values displayed in Table 5-11. The droplet size distribution for this particular emulsion is displayed as sample 6.2 in Figure 5-19, Figure 5-20 and Figure 5-21. Although there are two very distinct peaks, one of which is $\sim 5\mu\text{m}$ in diameter, the other is $\sim 100\text{nm}$ in diameter and as such the D[3,2] value is closer to this value due to the way in which it is calculated.

The focus of this work was on the smallest possible droplet size, specifically the D[3,2] value, and the parameters listed in produced the emulsion with the smallest D[3,2] value due to the trade off between the total flow rate and the impeller speed.

Table 5-11 Parameters and required values necessary to achieve droplets with the smallest D[3,2] value using the UMPF when analysed using a Malvern Mastersizer 2000 with both red and blue light sources during this work.

Formulation Parameters	Oil Type	Oil Phase Volume (%)	Oil Viscosity	Surfactant Type	Surfactant Phase Volume (%)	Water Phase Volume (%)
Values:	Silicone	57	10cSt	SLES	7	36
Process Parameters	Total Flow Rate (mL/s)	Rotor Speed (rpm)	D[4,3] (µm)	D[3,2] (µm)	Analysed using?	
Values:	54	2,500	2.48	0.20	Mastersizer 2000	

5.5 Conclusion

It can be concluded that the UMPF is capable of producing emulsions made up of droplets with a smaller D[3,2] value than those emulsions produced by the Silverson 150/250 MS mixer. It has also been discovered that the UMPF, at static, is capable of producing emulsions that require the Silverson 150/250 MS mixer to be operating at 5000rpm.

Taking almost identical formulations the UMPF processed in a single pass an emulsion containing the smallest D[3,2] value throughout all the trials performed on both pieces of equipment. This required significantly less time and energy than that produced by the Silverson 150/250 MS 60L reactor, in which the product was re-

processed at a greater impeller speed on each subsequent pass. The formulation that made up this emulsion was, within error, equal to that obtained using the combination of the Formax high-throughput formulation platform and design of experiments [DoE] software.

For particle sizing with a Malvern Mastersizer 2000 emulsion systems containing droplets sub-micron in size, red laser light alone is inappropriate for accurate analysis. To ascertain a true representation of what is present within the product both red and blue laser light should be used as this produces minimal artefacts.

After observing numerous formulation combinations processed using the UMPF, it can be concluded that the combination of the Formax and DoE leads to the quick and efficient determination of the formulation parameters required to produce an emulsion with the smallest possible droplet size on the pilot-plant industrial scale UMPF. This find paves the way for the removal of both the time and reagent volume that would usually be needed if one wanted to map out the formulation space using the industrial scale UMPF and is of great benefit for future work involving this prototype piece of kit.

5.6 Further work

It can be hypothesised, but requires proving, that the formulation parameters used to formulate the emulsion within this chapter using the Silverson 150/250 MS mixer, were in fact the required ones to produce an emulsion with the smallest possible droplet size. This requires mapping out the formulation space using the Silverson 150/250 MS mixer to confirm or prove wrong the hypothesis.

5.7 References

- EL-HAMOUZ, A., Cooke, M., Kowalski, A. and Sharratt, P. 2009. Dispersion of silicone oil in water surfactant solution: Effect of impeller speed, oil viscosity and addition point on drop size distribution. *Chemical Engineering and Processing*. **48** 633-642
- FORGIARINI, A., Esquena, J., González, C. and Solans, C.. 2001. Formation of Nano-emulsions by Low-Energy Emulsification Methods at Constant Temperature. *Langmuir* **17** 2076–2083
- HALL, S., Cooke, M., Pacek, A. W., Kowalski, A. J. and Rothman, D. 2011. Scaling Up Of Silverson Rotor–Stator Mixers. *The Canadian Journal of Chemical Engineering*. **89** 1040 – 1050
- HALL, S., Cooke, M., Pacek, A. W., Kowalski, A. J. and Rothman, D. 2011. Scaling Up Of Silverson Rotor–Stator Mixers. *The Canadian Journal of Chemical Engineering*. **89** 1040 – 1050
- MASON, T. G., Graves, S. M., Wilking, J. N. and Lin, M. Y. 2006a. Extreme emulsification: formation and structure of nanoemulsions. *Condensed Matter Physics*. **9** 193-199
- MASON, T. G., Wilking, J. N., Meleson, K., Chang, C. B. and Graves, S. M.. 2006b. Nanoemulsions: formation, structure, and physical properties. *J. Phys.: Condens. Matter*. **18** 635-666
- MELESON, K., Graves, S. and Mason, T. G. 2004. Formation of Concentrated Nanoemulsions by Extreme Shear. *Soft Materials*. **2** 109-123

- PHADKE, D. S. and Eichorst, J. L. 1991. Evaluation of Particle Size Distribution and Specific Surface Area of Magnesium Stearate. *Drug Dev. Ind. Pharm.* **17** 901-906
- READ, J and Whiteoak, D. 2003. *The Shell Bitumen Handbook*. London: Thomas Telford Publishing. p. 91
- ROBBINS, C. R. 2012. *Chemical and Physical Behavior of Human Hair 5th Edition*. Heidelberg: Springer-Verlag Berlin Heidelberg . p. 340
- SACKETT, L., Pestka, J. and Gisslen, W. 2011. *Professional Garde Manger: A Comprehensive Guide to Cold Food Preparation*. New Jersey: John Wiley & Sons. p. 37
- SOMASUNDARAN, P., Mehta, S. C. and Purohit, P. 2006. Silicone emulsions. *Adv. Colloid Interface Sci.* **128-130** 103-109

Chapter 6 Saponification using an Emulsion feasibility study

6.1 Abstract

The aim of the work within this chapter was to ascertain whether it was possible to emulsify a natural [sunflower seed] oil and use the emulsified reagent in a chemical reaction. The reaction chosen for this work was the formation of soap and involved the emulsification of sunflower oil and then reacting it with sodium hydroxide. This work involved the use of high-throughput robotics to perform multiple reactions at once in order to ascertain the overall reaction time and thus determine the reaction time for emulsions of different droplet size. The results of the work showed that although the high-throughput robotic platform advertised mixing capabilities, adaption of the standard use of the kit had to be performed in order for the multiple-phase reaction to occur within a reasonable time frame.

This work confirmed that not only was it possible to formulate soap using a natural oil emulsion, but that an emulsion with a smaller droplet size had a decreased reaction time compared to that of an emulsion with a larger droplet size.

6.2 Introduction

There are many common consumer products and chemicals found in the Pharmaceutical, Home and Personal Care, Agricultural and Foods sectors that are by-products of chemical reactions and processing of raw materials that have been grown and harvested from plants/animal resources or extracted directly from a crude mineral /fossil source such as oil fields or from mining.

The majority of the raw materials are finite and therefore chemical process industries are under ever increasing pressure to optimise their processes to improve the rates of return and minimise waste from their factories. Focus on the process conditions such as temperature, pH, power input, pressure and concentration gradients, which affect both the rate of reaction and the selectivity of the desired reaction products versus the undesired by-products that can form from partial or secondary reactions, is of key concern.

The majority of reactions undertaken by industry generally consist of two or more phases (e.g. gas, liquid & solid in varying combinations) which may not be completely miscible and therefore need to be intimately mixed during processing for the reaction to take place in a suitable time scale.

The main objective of this project therefore, was to investigate how particular processing or mixing equipment which exhibit varying degrees of distributive and dispersive mixing (refer to section 2.2.1) could be employed to control the rate of reaction of a simple biphasic reactive system and how this reaction could be used as an indication of the relative efficiency of the process. It is hypothesised that increasing the available surface area of a given volume [of reagent], relative to a reactive species, by decreasing the relative droplet size of the reagent within the reactant, through total or partial emulsification, leads to a rise in rate of reaction and thus a decrease in the overall reaction time.

Section 2.7.1 discusses the saponification reaction used in this study, both the historical and modern manufacture of soap, as well as an overview of the process and the properties that additives give the final product. Section 6.3 details a benchmark saponification reaction that was carried out on bench scale mixing equipment to

ascertain a suitable comparison for the further experiments. Sections 6.4 and 6.5 detail the impact that distributive and dispersive mixing [respectively] have on the saponification reaction time. Section 6.6 reports the effect of varying the droplet size of the oil prior to the reaction by emulsification and the use of a high-throughput platform to observe the time taken for the reaction to reach completion.

6.3 Benchmark Saponification Reactions

The saponification reaction used in industry, and described in section 2.7.1, would be used as a reaction system to characterise two types of common place laboratory mixing equipment, which exhibit the different types of mixing, i.e. bulk distributive blending and high shear dispersive mixing, (section refer to section 2.2.1 for further details of distributive and dispersive mixing).

This set of experiments was designed to study the impact a highly distributive overhead stirrer equipped with a pitched blade turbine and a high shear dispersive homogeniser each had on the reaction rates of *saponification* detailed in Figure 2-25 [the two devices are described in Chapter 3]. The intention was to demonstrate empirically that the creation of sufficient interfacial surface between contacting reactants of a biphasic system increases the rate of reaction.

Due to time constraints it was not possible to gain access to industrial saponification reactors to make a benchmark reaction standard for this work. This resulted in the bench scale experiments only being able to be compared with each other, and being used to make qualitative standards on which further comparisons could then be made.

It was necessary to scale down the reactions to make them suitable for the equipment employed and to satisfy the local health and safety protocols, therefore the quantities

of reagents, reaction times, and catalyst quantities were adjusted appropriately. Table 6-2 details the standard reaction conditions that were used.

In order to make a 'hard' soap (to make separation easier) sodium hydroxide [reagent grade, $\geq 98\%$, pellets (anhydrous) Sigma-Aldrich] was chosen as the hydroxide to be used in the saponification reaction, together with a standard food grade sunflower seed oil as the chosen triglyceride [Tesco, UK].

Table 6-1 Parameters of the distributive and dispersive mixers used.

	Distributive Mixing	Dispersive Mixing
Reaction Volume	750mL	200mL
Reaction Vessel	2000mL Pyrex Borosilicate Beaker	250mL Pyrex Schott-Duran borosilicate glass jar with pouring ring
Reaction Vessel Dimensions	190mm height x 128mm diameter	143mm height x 70mm diameter 30mm diameter of neck opening.
Mixing device:	IKA Overhead stirrer equipped with two pitch blade turbines (Refer to Figure 6-3 for experimental set up and blade configuration).	POLYTRON® PT 2100, (Refer to Figure Figure 6-4 for experimental set up and blade configuration).
Diameter of Impeller	74mm	20mm
Rotor speeds	300 – 400rpm	10,000 – 30,000rpm
Tip Speeds	1.16 – 1.55ms ⁻¹	10.47 – 31.42ms ⁻¹

Table 6-2 Benchmark Reaction Conditions

	Distributive Mixing	Dispersive Mixing
Triglyceride	Sunflower seed oil	
Volume of Triglyceride	112.5 – 375mL	30 – 170mL
Hydroxide	Sodium Hydroxide (NaOH)	
Concentrations of Hydroxide	Sodium hydroxide [1M] – [3.2M]	[1M] – [18M]
Temperature	20 – 80°C	
Time samples were taken at to follow reaction progress	7.5 minute intervals until the reaction was deemed complete	30s intervals until the reaction was deemed complete
Pressure	All experiments were performed at standard laboratory pressure.	

6.3.1 Benchmark experimental method

The experimental method for both the distributive mixer experiments and the dispersive mixer experiments was the same with the exception the quantities of reagents used. The molar ratio of hydroxide to triglyceride was kept constant throughout the trials at three to one as this ratio theoretically provides enough hydroxide to react with all the triglyceride as displayed in Figure 6-1 and converts all

the fatty acid chains into carboxylate soaps an example of which is shown in Figure 6-2.

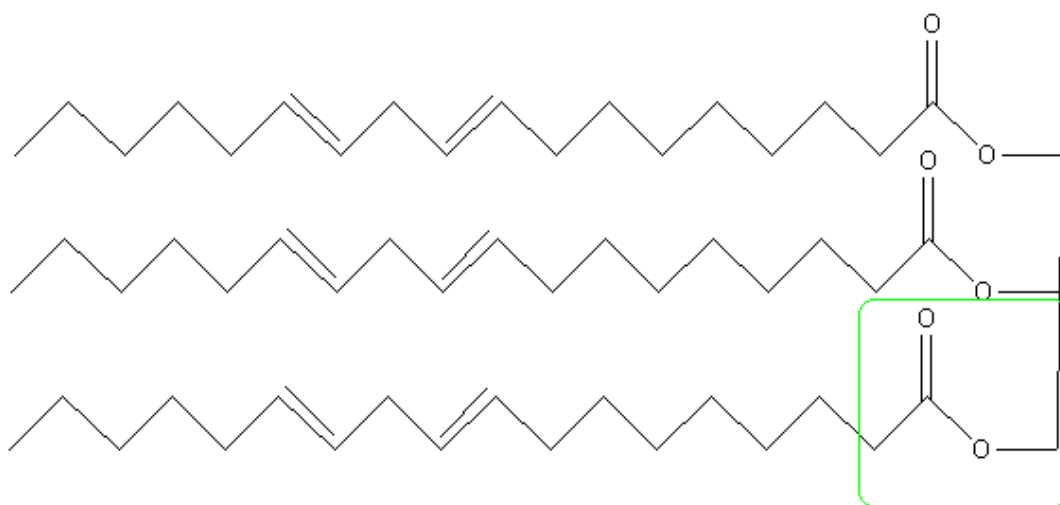


Figure 6-1 Chemical drawing of triglyceride;highlighted is one of the ester groups.

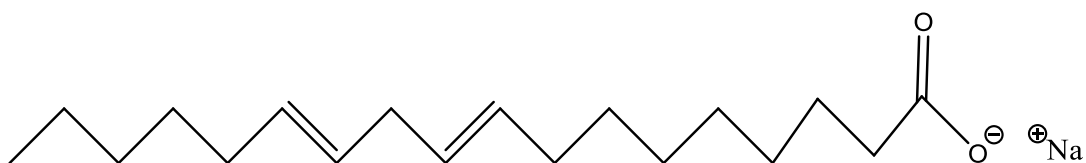


Figure 6-2 Chemical drawing of the predicted structure of the carboxylate salt produced following the saponification of sunflower seed oil.

The reaction temperature, when above that of room temperature, was maintained using a standard heater plate [discussed in section 3.2] with a silicone oil bath. To ensure uniform heat transfer throughout the oil bath and therefore around the reaction vessel, a magnetic stirrer bar was placed in the oil bath and set to rotate at ~500rpm, the speed was chosen such that the oil temperature was uniform (tested regularly throughout experiment using a dip in digital thermometer) and such that the oil was not vortexed which could have led to splashing. The reaction vessels were submerged within the oil bath such that the oil surface covered the majority of the reaction contents. The temperature was continually monitored using a dip in digital

thermometer. Due to the scale of the experiment [and for health and safety reasons] it was not possible sparge the reactions with steam.

The appropriate quantities of sodium hydroxide and distilled water were measured out using a top pan balance and a volumetric measuring cylinder [respectively]. Distilled water was first added to the reaction vessel with the sodium hydroxide added slowly after. A magnetic stirrer bar [discussed in section 3.2] was added to the vessel and used to dissolve the sodium hydroxide.

The temperature of the aqueous sodium hydroxide solution was heated to the predetermined temperature and the heat was distributed uniformly throughout the solution by the magnetic stirrer bar, once the temperature was reached the magnetic stirrer bar was removed using a PTFE magnetic stirrer bar remover. The mixer and the sunflower seed oil was then added to the vessel however as the sunflower oil was not heated prior to addition it cause the temperature of the reaction vessel contents to be lowered. The temperature of the reaction contents was allowed to return to the required value before the mixer was switched on and the speed increased from static to that required for the experiment (refer to Table 6-3 and Table 6-4 for the experimental parameters used in the individual experiments).

6.3.2 End point determination

The end point of the saponification reaction can be determined by any one of three qualitative methods:

1. The addition of phenolphthalein to the reaction vessel. This turns the contents pink initially however if the pH value of the reaction contents is between 8 and 12 it will stay pink, if not the solution will go back to being clear. This is a qualitative end point determination method as the pH of 1M

sodium hydroxide solution is 14 therefore a large quantity of the hydroxide solution has to be used up to reduce the pH to a value of 12 and below.

2. Analysis of the product using infra-red spectroscopy. Infrared spectroscopy gives a yes or no answer as to whether the saponification reaction has completed. This is observed from the clear removal of the distinct ester group (a peak in the region of $1735\text{-}1750\text{cm}^{-1}$) which appears prominently in triglycerides [seen Figure 6-1]. If there are no esters present in the spectra produced then there is no glyceride present which means they have all reacted and the reaction is complete.
3. Terminate any stirring and allowing the reaction to settle out. Theoretically whilst the reaction is incomplete there will be three layers present; surfactant, sunflower seed oil and aqueous sodium hydroxide. The reaction is deemed complete when there are only two layers visible (once the reaction has been left to settle out), one consisting of surfactant and the other of excess hydroxide, water and glycerol [dissolved in the water].

Following hydrolysis and saponification, the ester group highlighted in Figure 6-1 is replaced with a carboxylate group and the long fatty chain becomes a carboxylate salt upon the addition of sodium; a depiction of which is displayed in Figure 6-2. The carboxylate salt contains the same carbon chain as each of the glyceride molecules that make up the triglyceride in Figure 6-2, the main difference being the terminal group at the end of the carbon chain has changed. This is analysed using infrared spectroscopy because the ester group peak which appears between 1735cm^{-1} and 1750cm^{-1} and links the glyceride groups that make up the triglyceride, is broken and replaced with a carboxylate group peak. The replacement of an ester group with an carboxylate group means the removal of the ester peak from the spectra and the

inclusion of a carboxylate peak which appears between 1550-1610 cm^{-1} (Kharagpur, 2012).

6.4 Distributive mixing

The length of the impeller blades was the determining factor in choosing the reaction vessel for this experiment. With an overall diameter of 100mm a standard pyrex two-litre beaker was chosen to be the reaction vessel as it has a diameter of 128mm giving a 14mm clearance from the end of the blade to the vessel wall. This small gap allowed the addition of the oil to the reaction vessel as well as the impeller and also allowed internal temperature readings to be performed without pausing the mixing.

To ensure the mixing device in question was tested appropriately a minimum total of 750mL of reagents were used per experiment as this volume not only covered the blades completely but minimised air entrainment into the reaction vessel thus reducing the impact of another potential variable. Figure 6-3 shows a schematic of the experimental set up and a close up view of the impellor, labelled with key dimensions. The parameters for the experiments are listed in Table 6-3 and satisfy the criteria required to make a decision as to the efficiency of the mixer as a device.

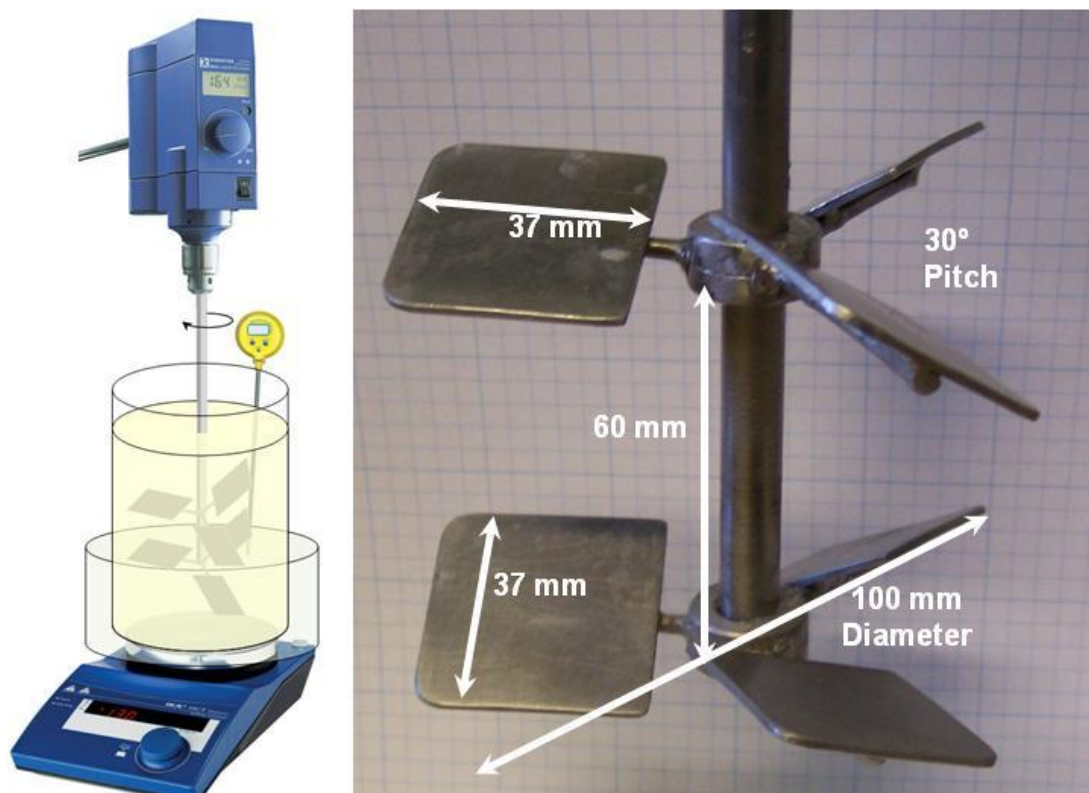


Figure 6-3 Benchmark Saponification reactions were carried out using a 6 pitched blade turbine (PBT) connected to an overhead stirrer. A plate heater and oil bath was used to maintain reaction temperature at 80°C throughout the reaction.

6.4.1 Improvements to the Experimental Method

A rather significant flaw with the experimental method was brought to light during the preliminary trials. The temperature of the beaker contents, due to it having such a large open surface area, took hours to reach 70°C at which point the heating ceased due to extensive heat loss, (10°C below the required temperature for some experiments). To overcome this problem it was deduced that a lid, able to sit on top of the beaker but allow the 6-blade turbine to still operate, would prevent a majority of the heat being lost thus ensuring the reaction vessel would be able to reach temperatures greater than 70°C within a shorter time frame. To enable constant monitoring of the temperature throughout the experimental, a small groove was cut

into the side of the lid large enough to allow the thermometer to remain in its position.

The 6PBT mixer preliminary trials provided answers to some of the questions proposed. The trials provided an answer to the question “Can liquid soap be formed using low phase volume of oil, and with sodium hydroxide not potassium hydroxide?”. Using a low phase volume of oil and following the method stated in the experimental, liquid soap was produced instead of solid soap; when a higher phase volume of oil is used following the method in 6.3.1, solid soap is formed.

6.4.2 Distributive Mixing Trials Results and Discussion

The PBT overhead mixer trials were deemed complete only after two of the three qualitative methods of end point determination listed in section 6.3.2 had been fulfilled. The time taken for each reaction to reach the determined end-point was recorded alongside its parameters in Table 6-3. From the data it can be seen that reactions with low volumes of oil and temperatures of 80°C are the first to reach completion, something one would expect to find.

Table 6-3 Parameters and reaction time for four of the experiments performed using the 6 PBT.

Experiment Label	Volume of oil as % of total volume	Impeller speed (rpm)	Temperature of reaction (°C)	Time taken for reaction to complete
PBT01	15	350	25°C	> 4 hours
PBT02	15	400	25°C	4 hours.
PBT03	16.7	300	80°C	35 Minutes.
PBT04	50	300	80°C	78 Minutes

When the phase volume (the percentage of the total reaction volume) of oil is 15% and the reagents undergo the reaction mechanism described in section 6.4.1, liquid soap is produced. This statement is based on the visual appearance of the final product. When formulating soap it is common to achieve solid, isotropic solution and hexagonal liquid crystalline phases [in the same product] as these all coexist in normal soap bars whereas in super-fatted soaps, part of the hexagonal liquid crystalline phase is converted to lamellar and it is this phase which is responsible for product softness during processing (Kharagpur, 2012). The temperature of the reaction has a direct impact on the phase of the final product and as such it is crucial to maintain the predetermined temperature per experiment

6.5 Dispersive mixing Preliminary Bench-top Trials

The trials involving the PBT discussed in section 6.4 provide some insight into how the reaction proceeded on the bench and allowed sufficient development of the reaction end point determination. It was decided that keeping the vessel diameter to

mixing head ratio as close to constant as possible would provide both a simple means of comparison and, in the case of the homogeniser a better opportunity for bulk mixing of the reactants. The dispersive mixer used for these trials was a high-shear homogeniser shown in Figure 6-4, a POLYTRON® PT 2100 fitted with a 20mm [in diameter] impeller.



Figure 6-4 POLYTRON® PT 2100 fitted with a 15mm rotor, 20mm stator impeller.

The method described in 5.3.1 was used to assess the impact of dispersive mixing on saponification process. As soon as the homogeniser was switched on, the timing of the reaction began. Mixing was stopped approximately (+/- 10 seconds) every 30 seconds to and take a reading of the internal reaction temperature and to assess how far off the reaction was from completion by the addition of a few drops of phenolphthalein. The time required for the solution to turn clear again upon the restarting of the mixer gives an indication of how long the reaction has left to reach completion [section 6.3.2]. Once the end-point has been determined and the reaction

deemed complete, the time was logged. The equipment was then allowed to cool to room temperature before being disassembled, cleaned and set-up again to perform the next experiment.

6.5.1 Dispersive Mixing Trials Results and Discussion

From the results displayed in Table 6-4 it can be seen that the homogeniser trials take a fraction of the time the PBT overhead mixer trials require to reach completion. This is not solely due to the reduction in the total volume of reagents as an equal molar ratio of reagents as performed in the PBT trials (section 6.4) was used.

It is proposed that the reduced reaction time is due to the high-shear homogeniser rapidly reducing the size of the particles of the reagents due to the rotor-stator design which causes an increase in the available reactive surface area, leading to an overall increase in the rate of reaction. The design of the high-shear homogeniser not only causes the reagents to mix; it provides the required energy to break-up both large droplets and even droplets a few microns in size. When it does so, these go on to catalyse the reaction for other broken down droplets leading to an increase in the available active surface area and an increase in the rate of reaction.

Table 6-4 Table listing the parameters and reaction time for each of the experiments performed using the high-shear homogeniser.

Experiment Label	Volume of oil as % of total volume	Impeller speed (rpm)	Temperature of reaction (°C)	Time taken for reaction to complete
HSH01	15	22,000	~25	> 3600s
HSH02	15	11,000	>80	> 1800s
HSH03	15	20,000	>80	1800s
HSH04	15	22,000	>80	900s
HSH05	75	22,000	>80	n/a
HSH06	75	30,000	>80	n/a
HSH07	85	20,000	>80	n/a

It can be determined from the reaction times listed in Table 6-4 that when using the high-shear homogeniser mixer to provide energy for the saponification reaction to occur, both temperature and rpm are the rate determining factors.

For the systems using over 75% phase volume of oil, a solid block of soap was formed in a very short period of time. It is believed that this is a direct result of the high concentration of sodium hydroxide, upon addition, reacting instantly with the oil rather than dispersing throughout the solution. Figure 6-5 displays a photograph of product HSH05 [details in Table 6-4] which was made using 75% phase volume. Alongside the photograph of the product is a labelled illustration of what was observed following termination of the reaction; a gap of air, a layer of solid soap, a layer of oil and another layer of solid soap.



Figure 6-5 Photograph and labelled drawing of product HSH05.

The bottom layer of solid soap is formed along the horizontal axis of the reaction vessel from the base of the impeller shaft of the homogeniser to the sides of the vessel during the first few minutes of the reaction commencing. The layer of soap at the top of the vessel is formed due to this being the location the reagents are forced when processed by the homogeniser as explained in section 3.2.3.

When the reagents are forced out through the holes in the stator of the rotor-stator in a homogeniser they first are forced to the base of the vessel, then to the top. This explains why there is a layer of solid soap formed at the base of the reaction vessel initially and following this the rest of the concentrated hydroxide forms a solid layer of soap at the top of this vessel leaving a layer of oil in the middle as there is no free hydroxide to react with it. It is due to the presence of oil that there is no “Time taken for reaction to reach completion” value for the reactions with a large phase volume in Table 6-4 as these reactions had not reached completion and were unable to do so.

6.6 High-Throughput Saponification

The work performed in sections 6.4 and 6.5 showed that the rate of reaction for saponification is improved with heat, high impeller speed and the use of a dispersive mixer. The dispersive mixer used causes a large decrease in the droplet size of the

reagents as well as mixing them and uniformly distributes them throughout the reaction vessel at speed. This increases the kinetic energy within the system and products are formed within a smaller time frame (Goots et al., 2008).

Having proved that decreasing the size of the droplets of the reagents causes an increase in the rate of reaction, it was decided that observation of the impact emulsifying the reagents had on the rate of reaction should be investigated. Emulsification of the oil prior to the saponification reaction allows the reagents to be reduced in droplet size and become stabilised allowing, if the reaction works, for the size of the droplets and the impact they have on the rate of reaction to be further investigated. It was unknown whether emulsified oil would react, as emulsifying the oil requires the addition of a surfactant. The surfactant used however is, in essence, a carboxylate salt and so it was hypothesised that this would not prevent the reaction from working, but instead it would theoretically catalyse it.

High-throughput experimentation was chosen as the platform on which to perform this investigation as it allowed the running of multiple experiments in parallel.

6.6.1 Experimental

The experiments performed on bench scale provided results that gave insight into what process parameters had the greatest impact on the rate of reaction; they also provided information with regards to the formulation parameters as they showed that when formulating soap, a phase volume of oil of 20% or less causes “liquid” [with a significantly lower viscosity] soap to be the major product upon reaction completion compared to products formulated using a higher phase volume than this. Since the reagents were liquids and no solids were used or formed throughout the reaction the Chemspeed high-throughput robotics platform *ASW2000* was chosen for the work to

be performed on as it allows the user to perform multiple (from 24 through to 80 dependent on the reaction vessel size chosen) experiments at once.

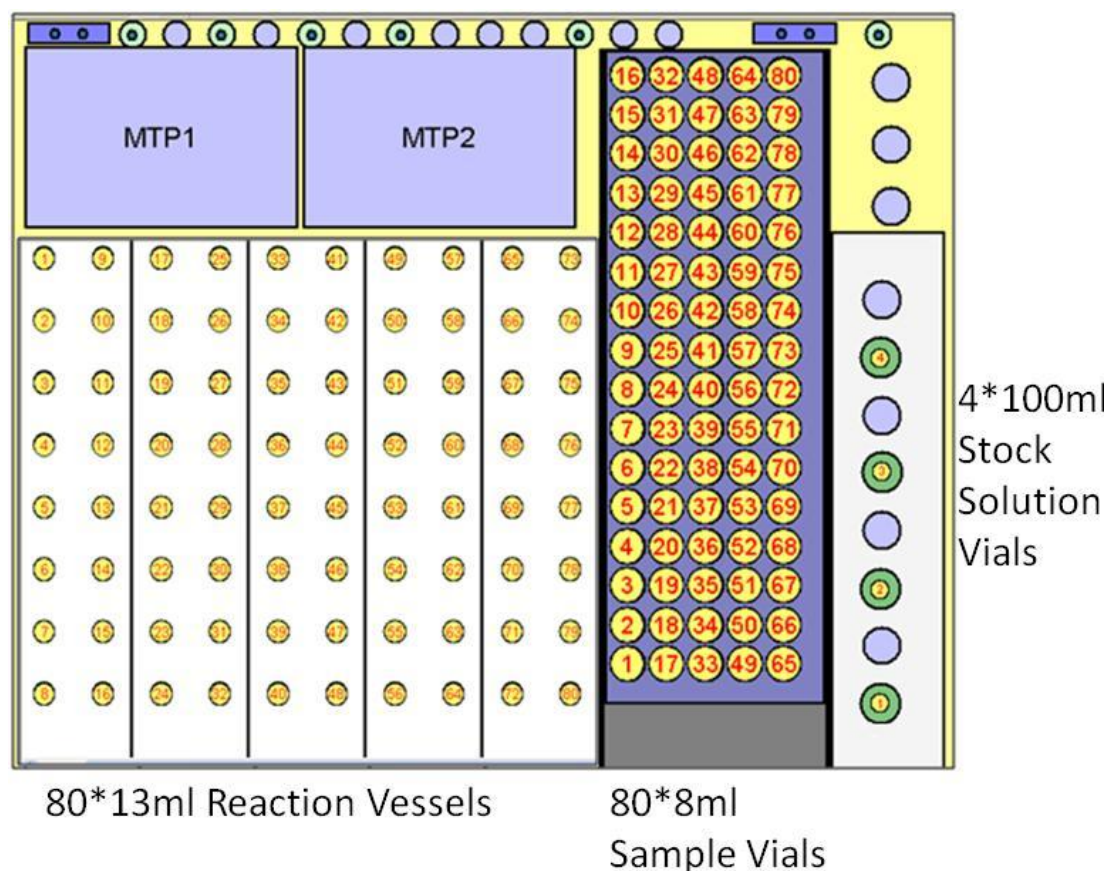


Figure 6-6 Illustration of the layout and set-up of the ASW2000 used.

The ASW2000 is a high-throughput robotic platform designed for use with liquid reagents only. The main control is the robotic arm which contains a single needle attached to two syringe pumps, (one 1mL syringe and one 10mL syringe). The needle and syringe pump can be used to transfer fluid from one vessel to another or add fluid from a reservoir that the syringe pump is attached to should that be desired. Reaction vessels are fitted to the deck and connected to a heater/chiller unit allowing temperature control and the vessels are also connected to a reflux unit. As a result of these factors experiments can be performed under either equal or varying conditions, depending on the choice of the operator. For this work it was decided to keep the

reaction conditions the same [discussed further on], altering only a single parameter, the droplet size of the emulsion, in order to determine the most effective method of formulation, in this case liquid-soap.

To prove that reagent droplet size is a rate determining factor two emulsions of sunflower seed oil were made up and identical experiments performed with one difference between the emulsions; the size of the droplets. To get different sized droplets in an emulsion made up of the same reagents can be done by varying just one of a range of parameters. One emulsion was made up of 79% oil, 20% water and 1% Sodium Lauryl Ether Sulphate [SLES] (a surfactant used in liquid soap formation in industry) and was mixed only by hand; it was rotated 360° around its horizontal axis three times, hand shaken and then added to the reaction vessels where it was then placed under vortex to prevent flocculation and phase separation. The other emulsion was made up of the same formulation however it was mixed using the dispersive high-shear homogeniser operated at 20,000rpm before being added to the reaction vessels (which were under vortex). Both emulsions were sized using a Malvern Mastersizer X [discussed in greater detail in section 2.6] with the presentation code 2NAD. This code contained refractive index (RI) values as close to those being used as possible; 1.4564 for the dispersed oil phase and 1.330 for the continuous phase; 1.4670 is the typical RI value of vegetable oil and 1.330 is the RI of water.

With the ASW2000 being unable to handle solids, the experimental method in section 6.3.1 was modified for use appropriately. The sodium hydroxide was dispersed within the water phase prior to its addition to the reaction vessel. With the viscosity of the emulsion being greater than that of water and standard chemical solvents the needle the ASW2000 was equipped with was unable to transfer the

appropriate amount of reagent successfully. This meant the appropriate amount had to be added to the reaction vessels by hand and then the robot would be able to add the hydroxide solution to the vessel when necessary, in essence reversing the order of addition from that used previously.

The mixing the ASW2000 is capable of is *vortexing*. The reaction vessels are rotated in a circular motion along the x - y axis at speed that forms a vortex in the middle of the reaction vessels (that contain reagents) and thus causes the reagents [usually] to react. The problem with using this platform and the saponification experiment is that the reaction is a two-phase system. The illustration in Figure 5–9 depicts a typical reaction vessel on the platform at static [vessel on the left] and during vortexing [vessel on the right]. When the vessel is static the two phases separate out and the emulsion (yellow phase in Figure 6-7) ends up floating on top of the hydroxide solution (blue phase in Figure 6-7) reducing the interface at which the two phases meet. Even when vortexing is occurring the interfacial surface area is only increased slightly making an experiment involving monitoring the impact on the rate of reaction via reduction in droplet size redundant.

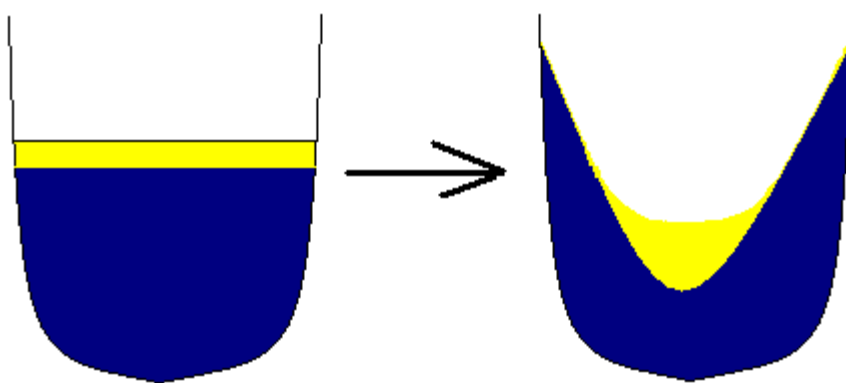


Figure 6-7 Illustration of two-phase system in ASW2000 reaction vessel.

To resolve this matter and increase the interfacial area different techniques were tried such as stopping the vortexing then suddenly starting it again in an effort to force the

phases to mix, however not enough energy was produced and the phases failed to mix. The best technique, and one which was successful, was the extraction of the aqueous phase entirely from the vessel (by having the needle dip into the vessel and once at the base of the vessel remove only the volume of aqueous fluid [volume was calculated based on the volume of water within the reaction vessel]) and then disperse the aqueous phase within the organic phase as depicted in Figure 6-8. This then forced the reagents to react and thus allowed the formation of product within a much shorter time span than if the reagents had just been vortexed and nothing else.

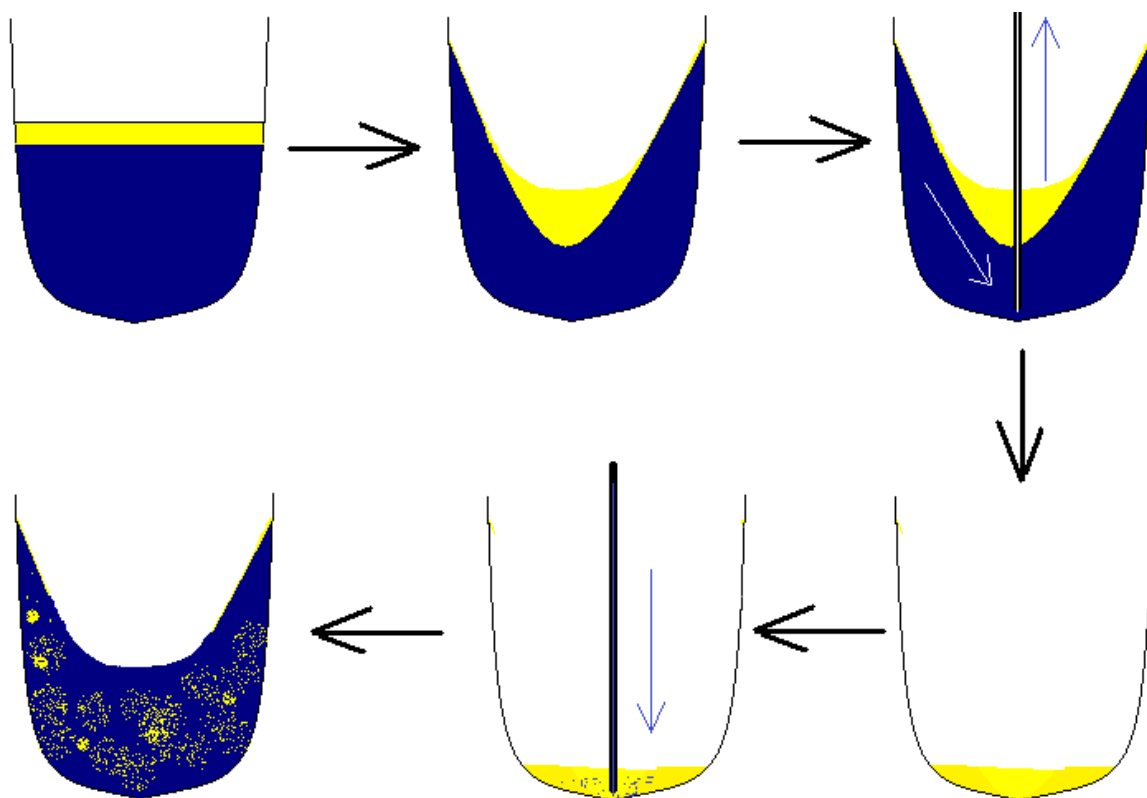
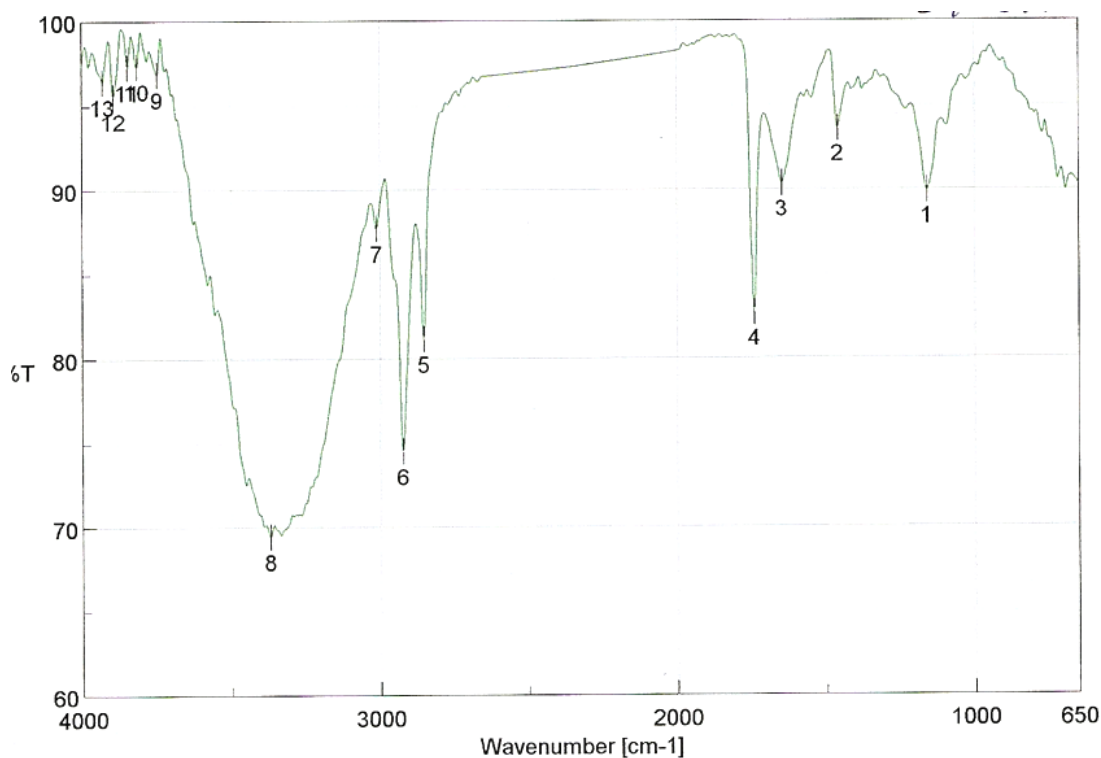


Figure 6-8 Illustration of increasing interfacial area between two phases in ASW2000 reaction vessel.

Each of the high-throughput experiments involving the emulsified oil was repeated to confirm accuracy of results. During the experimental runs, samples were taken at intervals in order to find the time frame during which complete saponification

occurred. The top layer of product sampled from the first few time samples on all experiments showed traces of an ester group present indicating that the triglyceride hadn't been entirely broken down and thus complete saponification hadn't occurred. This was discovered through infrared spectroscopy as the end-point determination methods described in section 6.3.2 were used to determine the end point of the high-throughput trials also. Figure 6-9 presents spectra produced of an incomplete reaction with an ester group present.



Result of Peak Picking			[Comment]			
No.	Position	Intensity	No.	Position	Intensity	Sample Name
1	1159.01	89.8779	2	1459.85	93.572	Comment
3	1646.91	90.3068	4	1741.41	82.6571	User
5	2852.2	81.099	6	2921.63	74.4605	Division
7	3010.34	87.6742	8	3369.03	69.4166	Company
9	3747.01	96.8391	10	3814.51	97.3187	University of Liverpool
11	3845.36	97.2995	12	3893.57	95.5384	
13	3930.22	96.4086				

[Measurement Information]	
Model Name	FT/IR-4100typeA
Serial Number	B085661016
Light Source	Standard
Detector	TGS
Accumulation	16
Resolution	8 cm-1
Zero Filling	On
Apodization	Cosine
Gain	Auto (8)
Aperture	Auto (7.1 mm)
Scanning Speed	Auto (2 mm/sec)
Filter	Auto (30000 Hz)

Figure 6-9 Infrared spectroscopy data of experiment with an ester peak [peak 4] at 1741.41cm^{-1} indicating that the reaction has not yet reached completion.

6.6.2 Results and Discussion

From the results displayed in Table 6-5 it can be seen that the emulsion with the smaller droplet size, mixed using the dispersive mixer, made products faster than the emulsion with the larger droplets that was mixed by hand. This confirms that not

only can the reaction time be reduced by altering the temperature, impeller speed and mixer type, but that emulsifying the oil before the reaction and reducing the droplet size can lead to an increase in the rate of reaction

Table 6-5 Table listing the high-throughput saponification trials parameters and time taken to reach completion.

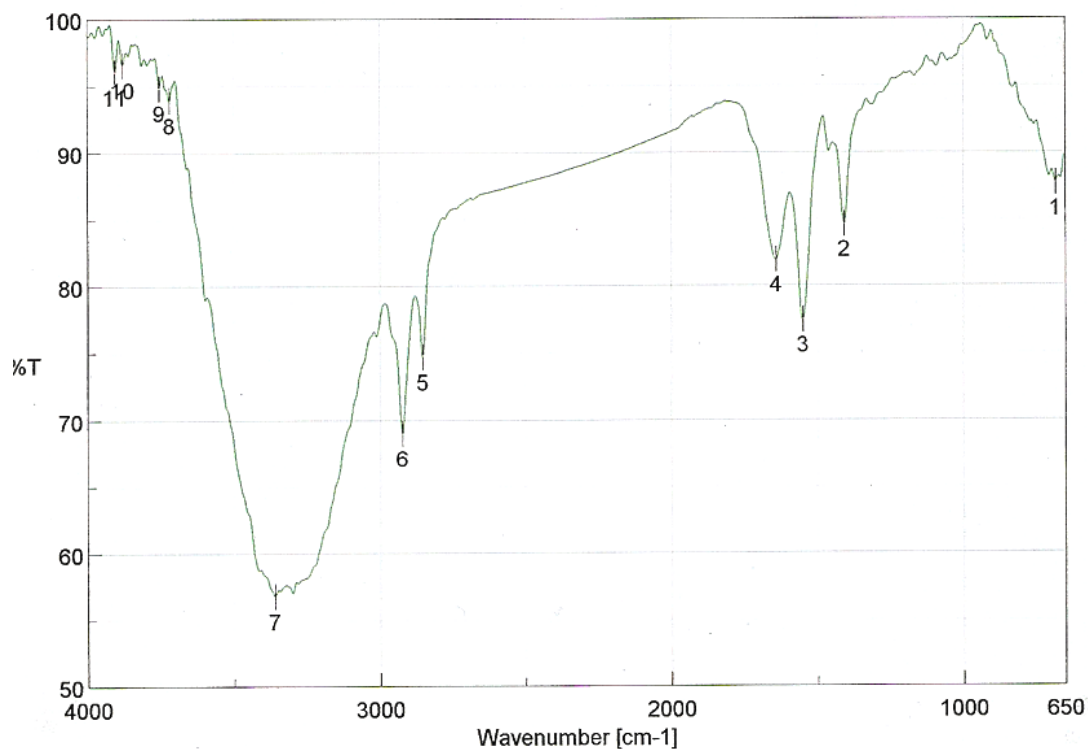
How was pre-emulsion mixed?	At what rpm value?	D[3,2] (μm)	Mean time taken for reaction to complete (s)
Hand shaken	n/a	83.8	7110
Homogenised	15,000	20.8	5430

The infrared spectrum of the products made indicates that all of the products contain an alcohol group which is noted by a strong, broad peak between 3200cm^{-1} and 3600cm^{-1} . This is because not all the glycerol dissolves in the aqueous phase, and some is present in the product phase. Theoretically all the glycerol should dissolve as there is an excess of aqueous solution and glycerol is known to be a very polar compound (due to the 3 alcohol groups present on it). The slight excess of sodium hydroxide in ratio to the volume of oil, in order to ensure that all the oil reacted is believed to prevent the glycerol dissolving in the solution and as a result there is some present in the product phase.

To remove the product from the aqueous phase, a gravitational separating funnel was used. This allowed easy removal of the aqueous phase and kept the product within the separating funnel which allowed easy cleaning of the product. The product was washed thoroughly a minimum of three times with the aqueous phase removed and disposed of appropriately following each clean. This purified to an extent, however

even a trace amount of glycerol present [within the product] leads to a large alcohol peak in the spectra, when analysed using infrared spectroscopy, due to the three alcohol groups that make up the structure.

The presence of glycerol is not important with regards to this experiment as it is a product and thus indicates the reaction is going to completion. With the aim of the reaction being the breakdown of triglyceride into glycerol and soap, the effect of particle size on the overall reaction kinetics can still be calculated, with or without glycerol present.



Result of Peak Picking				[Comment]	
No.	Position	Intensity	No.	Position	Intensity
1	682.677	87.6445	2	1407.78	84.576
3	1550.49	77.369	4	1641.13	81.8866
5	2852.2	74.6387	6	2921.63	68.9595
7	3359.39	56.7647	8	3718.08	93.864
9	3752.8	94.7957	10	3878.15	96.5378
11	3905.15	96.0031			

[Measurement Information]	
Model Name	FT/IR-4100typeA
Serial Number	B085661016
Light Source	Standard
Detector	TGS
Accumulation	16
Resolution	8 cm-1
Zero Filling	On
Apodization	Cosine
Gain	Auto (8)
Aperture	Auto (7.1 mm)
Scanning Speed	Auto (2 mm/sec)
Filter	Auto (30000 Hz)

Figure 6-10 Infrared spectroscopic data of an experiment that has reached completion. There is no peak in the region of $1735 - 1750\text{cm}^{-1}$ but there is a peak at 1550.49cm^{-1} [peak 3] indicating that the reaction has reached completion and the triglyceride has been broken down and formed a carboxylate salt.

6.7 Conclusion

From the results generated during the saponification project it can be concluded that the emulsification of oil prior to the process of saponification decreases the overall reaction time substantially. High-shear homogenising of the reagents required to make the emulsion created one with a reasonably small droplet size and also created a very stable emulsion. This is due to the design of the homogeniser; not only does it reduce the size of the reagents substantially; it also uniformly distributes them throughout the reaction vessel leading to a uniformly dispersed mixture.

6.8 References

- ABBAS, S. H. 2009. *Handbook of Detergents: Applications*. Boca Raton, FL: CRC Press. p. 138
- BEHLER, A., Biermann, M., Hill, K., Raths, H.-C., Saint Victor, M.-E. and Uphues, G. 2001. *Reactions and Synthesis in Surfactant Systems*. Boca Raton, FL: CRC Press. p. 2
- DUNN, K. M. 2010. *Scientific Soapmaking: The Chemistry of the Cold Process*. Farmville, VA: Clavicula Press. p. 311
- GOOTS, J. R., Moore, M. P., Szoc, K. B., Burns, R. J. and Bly, J. H. 2008. *Handbook of Vinyl Formulating*. New Jersey: John Wiley & Sons. p. 60
- HANNAN, H. J. 2007. *Technician's Formulation Handbook for Industrial and Household Cleaning Products*. Waukesha, WI: Kyril LLC. p.119
- KHARAGPUR, IIT. 2012. IR Table document from the Department of Chemistry, Indian Institute of Technology Kharagpur. www.chem.iitkgp.ernet.in/faculty/SDG/Spectroscopy%20III%20IR.pdf. 20th August 2012.
- SILVERSON M. 2012. Images owned by Silverson Machines, Inc. obtained from catalogue.
- ZHANG, H., Hoogenboom, R., Meier, M. A. R. and Schubert. U. S. 2005. Combinatorial and high-throughput approaches in polymer science. *Meas. Sci. Technol.* **16** 203–211

Chapter 7 Batch Sunflower Oil Emulsion

Production

7.1 Abstract

The saponification work in Chapter 6 confirmed that reducing the size of the droplets of a reagent prior to reacting it leads to a decrease in the overall reaction time and thus further work into emulsification using substantially larger volumes was necessary.

The aim in this chapter was to identify mixing equipment and techniques that facilitate the production of sub-micron emulsions at pilot plant scale to improve current emulsion products. The challenge was to discover whether large quantities of an emulsion made up of uniformly distributed sub-micron droplets could be created that would be stable as well as be able to react.

The impact of batch mixing devices and post processing using in-line mixing devices on further reduction in the droplet size of an emulsion is examined for a sunflower seed oil emulsion. The mixers examined in this chapter are the Fluid Division Mixer, a Microfluidizer M-110S and the UMPF (Ultra Mixing and Processing Facility, discussed in section 3.4). The results with a Silverson 150/250 has previously been reported in Chapter 5.

It was discovered that the UMPF is capable of further reducing the size of the droplets of an emulsion with a high phase volume of oil, capable of high flow rates and high production output.

7.2 Introduction

The work with the three mixers examined in this chapter followed a similar procedure to that with the Silverson mixer (Chapter 5). A batch of emulsion was prepared to the desired formulation using the Fluid Division Mixer (FDM). This was then used to examine the impact of further processing using the three mixers of interest. In the case of the FDM the batch was simply processed using additional rotor speeds. In the case of the two in-line mixers (namely the Microfluidizer and the UMPF) the premix prepared by the FDM was used as a feed into the mixers.

The main focus of the work within this chapter was to observe the impact that mixing devices had upon further processing emulsions that had already been made, with specific focus on further reducing the size of the droplets within the emulsions. The UMPF was benchmarked against a Microfluidizer; a small volume, batch processing unit that the manufacturer's brochure claims often reduces droplet size to submicron (Microfluidics, 2005). The Microfluidizer is able to further reduce the size of droplets within an emulsion by forcing the fluid through micro-channels at very high pressures (up to 2000bar) due to the high shear rates in the channels.

All three mixing devices are described in Chapter 3 where dimensions are also provided.

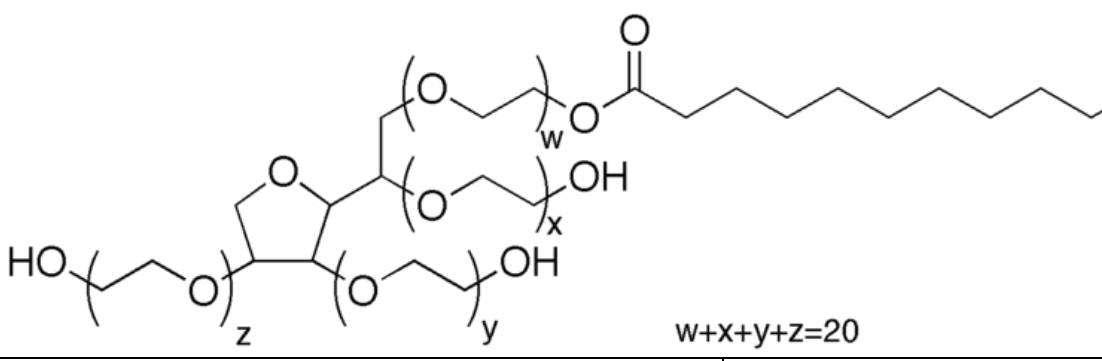
7.3 Experimental

7.3.1 Surfactant

The initial choice of surfactant for the trials was Sodium Dodecyl Sulfate (SDS) as it has been used in numerous academic works previously and we wanted to replicate those using new mixing technology available to us (Meleson, 2004). Unforeseen

problems involving the UMPF however caused trials involving SDS to be stopped. The trials that were stopped involved low viscosity silicone oil (10cSt) at the phase volume and surfactant to oil ratio used in the trials involving the microfluidizer described in this chapter. The trials in this chapter involve sunflower oil and polysorbate 20 instead of silicone oil and SDS and were performed so the impact the mixing device has on the formulation can be observed and whether the mixer is able to decrease the droplet size of the premade sunflower oil emulsions further.

Table 7-1 properties of polysorbate 20.

Surfactant IUPAC Name: Polyoxyethylene (20) sorbitan monolaurate	CAS Number: 9005-64-5
Common Names: Polysorbate 20, TWEEN® 20	Surfactant type: Non-ionic
 <p style="text-align: center;">$w+x+y+z=20$</p>	
CMC: 8.04×10^{-5} M at 21 °C.	HLB: 16.7
Appearance: Clear, yellow to yellow-green viscous liquid.	Relative Density (g/mL): 1.1

7.3.2 Droplet Sizing

Droplet sizing for this work was performed mainly using the Malvern Mastersizer X for analysis with the presentation code 2NAD. This code contained refractive index (RI) values as close to those being used as possible; 1.4564 for the dispersed oil

phase and 1.330 for the continuous phase; 1.4670 is the typical RI value of vegetable oil and 1.330 is the RI of water (O'Brien, 2008).

This work was performed prior to regular access to Mastersizer 2000 and as such that piece of equipment was only used to analyse the samples processed by the microfluidizer. For further information on droplet sizing techniques and information on both Mastersizers see section 2.6.

7.3.3 Fluid Division Mixer (FDM)

The Fluid Division Mixer (FDM) consists of patented rotor-stator mixing technology and is a high shear mixer at high rotor speeds, and an ultra low shear mixer when run at low speed (Maelstrom, 2012).

When the mixer is switched on, fluid enters the mixer and is forced through several small cavities. It is dependent on whether the cavities are rotor or stator as to which way the fluid is rotated as when the rotor spins it is always in an opposite direction to the rotation of the fluid within the stator. The opposing forces cause the fluid within the cavities to collide with one another which imparts hydraulic shear and reduces the droplet size of the fluid whilst minimal shear is impacted on the mixer itself (Maelstrom, 2012).

The model used was a Distromix (Model number; DB50-4-4-15) a batch rotor-stator mixer displayed in Figure 7-1 (Brown, 2010). The work was carried out in a 10 litre mixing vessel that had a clearance of 67.5mm from the mixer head to the vessel wall and a clearance of 175mm from the base of the mixer head to the base of the vessel (for confirmation see Figure 7-1 a). Three litres of fluid has to be added to the mixer vessel for it to come into contact with the base of the mixer head. In order to have an

equal volume of reagents above and below the mixer head requires a total reagent volume of six litres of fluid.

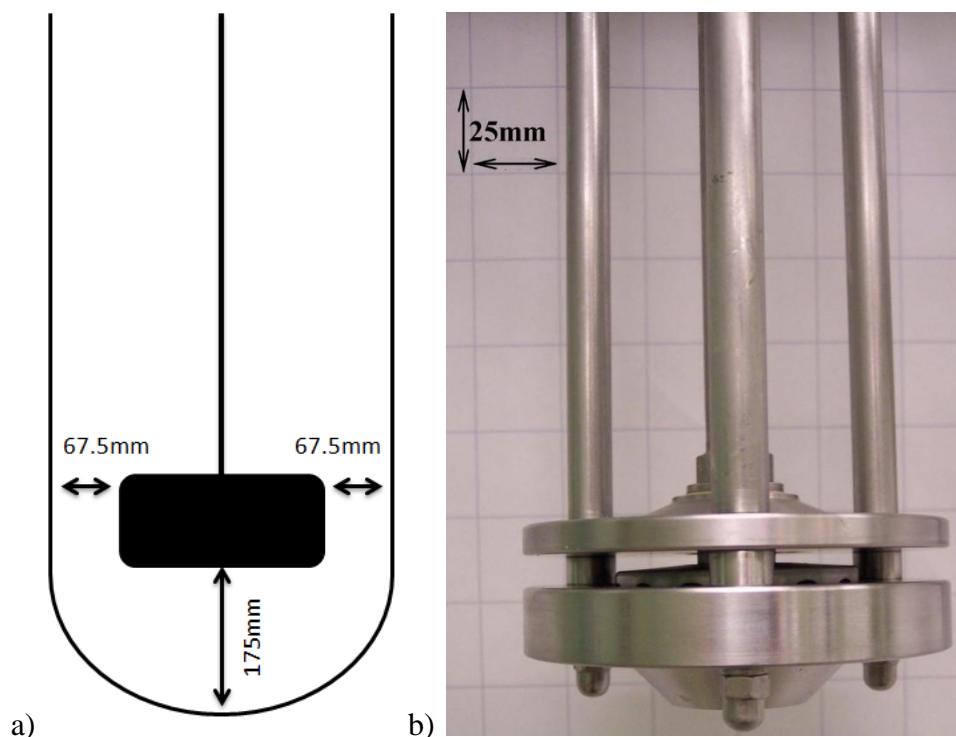


Figure 7-1 a) Schematic drawing showing the clearance of the FDM mixer head from the mixing vessel walls. b) Photograph of the FDM head and shaft.

The total volume of emulsion to be produced was set at six litres of fluid, however the phase volume of the reagents that make up the emulsion, and thus the oil to surfactant ratio, were two variable parameters that it was decided should be investigated.

The order and rate of addition of reagents was kept constant; water was added to the mixing vessel, then surfactant solution. Once the fluid level was covering the gap in the mixer head, the mixer was turned on at a low speed and the rest of the aqueous reagents were slowly added. If bubbles occurred then the impeller was turned off and

the vessel was allowed to deaerate before continuing. Once all the aqueous solution had been added, the oil phase was added slowly. As the oil was slowly added the impeller speed was increased (at a rate of 2000rpm per minute) until it reached maximum speed (6000rpm) at which point the rest of the oil phase was added quickly.

To keep the order of addition the same at high phase volumes of oil required dispersion of the surfactant within water prior to the actual trial. A bulk [6L] stock solution of surfactant was made up using the FDM. This would then be used for the trials, however prior to addition to the mixing vessel, the storage container of the surfactant solution was rotated numerous times to ensure equal distribution of the surfactant throughout the aqueous solution.

All trials using the FDM were conducted at room temperature and as there was no lid on the vessel, the pressure was that of the laboratory [standard]. Kinetic energy generated by the mixer operating at full speed did increase the temperature of the reagents however as this was a by-product of the mixer operating at full speed (which as stated earlier, it was for every trial) then each trial was impacted by this in the same way.

7.3.4 Microfluidizer

The Microfluidizer is discussed in detail in section 3.3.2. The experiments conducted using it involved the processing of pre-made emulsions to observe whether the droplet size could be further reduced. Two emulsions were processed, one of a low phase volume of oil [20%] and one with a high phase volume of oil [60%] (full details are shown in Table 7-5). These emulsions were taken from a bulk batch created using the FDM and the rest of the batch was processed using the UMPF, to

observe and compare the impact it had on the emulsion to that which the Microfluidizer had. As the emulsions were pre-made the order of addition was no longer a variable.

The pressure at which the trials were conducted remained the same throughout [1000bar] as did the flow rate of the fluid from the batch emulsion container into the mixer at a steady $10\text{mL}\cdot\text{s}^{-1}$. The restrictions with using the Microfluidizer are the maximum flow rate is 10ml/s and the “Large Capacity Reservoir” only holds 400mL. This means that for work involving the processing/formulation of batches of emulsion one has to continually top up the reservoir.

7.3.5 Ultra Mixing and Processing Facility (UMPF)

It is hypothesised that on processes further along the development chain than the beginning, when the reagents are emulsified, especially for emulsions with a droplet size $\leq 1\mu\text{m}$, the UMPF will have little to zero impact.

This is proposed because the UMPF is designed to have the greatest impact at the initial stage of emulsion production. As a prototype pilot plant mixer the clearance within the pipe-work of the UMPF is measured in microns and so anything less than a micron in size will theoretically pass through the machine with little to no alteration.

[The UMPF is described in detail in section 3.4.]

As mentioned in the experimental section for the Microfluidizer in this chapter, a pre-made batch of emulsion was produced using the FDM. A small quantity of this was processed using the Microfluidizer, the rest was processed using the UMPF. The UMPF trials were performed at room temperature.

To confirm the hypothesis that the UMPF will produce better emulsions if it is the processing tool in making them and not re-processing them it was decided that a formulation similar to the being made in the FDM be made in the UMPF and compared to that made in the FDM and that processed by the Microfluidizer as well as processing the emulsions made by the FDM.

7.4 Results and Discussion

7.4.1 Impact of the Phase Volume of Oil when using FDM Technology

The initial investigation performed involved observing the impact that altering the phase volume of oil within the emulsion had upon the resulting size of the droplets in the product also allowed the investigation into the impact of the varying oil to surfactant ratios that were used. It is known that increasing the phase volume of oil within an emulsion and/or increasing the percentage of the dispersed phase to a volume greater than that of the continuous phase causes the viscosity of the emulsion to increase (Shakuntala, 2001). Taking this and the turbulent shear principle into account it can be hypothesised that the greater the viscosity [to a limit] of the fluid being mixed, the greater the reduction in droplet size will be when using an FDM and thus the greater the viscosity of the product. This is proposed based on the way in which the turbulent shear principle works, as its focus is on fluid imposing shear on fluid travelling in another direction. From this it is logical to assume that the greater the viscosity of the fluid, the greater the shear imposed and thus the greater the reduction in droplet size of the emulsion produced. This of course only works to a certain point at which the fluid becomes too viscous to process.

Numerous trials involving varying phase volumes of oil were undertaken using the FDM with samples being taken from the same location within the mixing vessel at predetermined intervals. The data shown in Figure 7-2 confirms the hypothesis that increasing the phase volume of oil causes a greater reduction in the size of the droplets in the product formulated. The formulation and process parameters for the data in Figure 7-2 is shown in

Table 7-2 Formulation parameters for data shown in Figure 7-2

Oil Phase %	Surfactant %	Oil : Surfactant Ratio
15	4	3.75
30	4	7.5
60	4	15

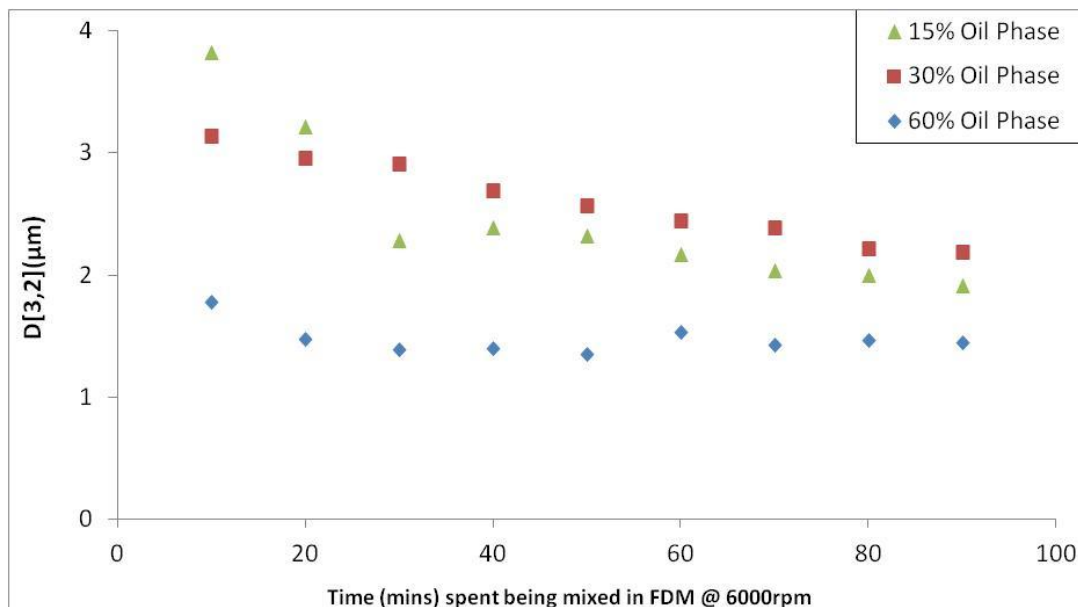


Figure 7-2 Graph showing the effect of varying the phase volume of oil within emulsification using a Fluid Division Mixer at 6000rpm. The level of surfactant in all processes was constant.

The graph shown in Figure 7-2 shows that after only 10 minutes of mixing using FDM technology the droplet size of an emulsion consisting of 60% oil is reduced to 1.75µm whereas for emulsions with a significantly smaller volume percentage of oil [15%] in the formulation even after an hour of mixing the droplets in the emulsion are reduced to only 2µm.

There are a number of different hypotheses that explain why this has occurred. One hypothesis is that the aqueous phase becomes the determining factor for particle size reduction because emulsions with a lower phase volume of oil during these trials have a greater surfactant to oil ratio. A result of this is that it takes a longer time for the FDM to reduce the droplet size of the emulsion as the required amount of energy has to be generated to overcome the stabilising effect of the surfactant.

The data in Figure 7-2 confirms the hypothesis described previously; a lower phase volume of oil leads to a greater volume of aqueous phase, a lower viscosity and thus

less turbulent shear is generated within the mixer head leading to smaller impact on the decrease in droplet size and overall an emulsion with larger droplets is produced. This ties in also with the hypothesis in the previous paragraph that the increased concentration of surfactant leads to stronger bonding and thus greater energy is needed to overcome them, which when the viscosity is less there is less turbulent shear and therefore smaller reduction in droplet size.

An interesting observation from the graph is the impact that the FDM has on emulsion with a 15% phase volume of oil between 20 and 30 minutes of continuous processing. There is a very sudden decrease in droplet size during this time period, the trend line between the data points has a very large gradient compared to the time following this point. Further observation of the first three points shows almost a logarithmic decrease in droplet size until 30 minutes at which point the decrease in droplet size slows and the gradient of the trend line becomes similar to that of the other two series on the graph.

Further to the data displayed in Figure 7-2, it can be seen from the data in Figure 7-3 also that the greater the phase volume of oil (also shown in Table 7-3), the greater the initial reduction in droplet size and the smaller the droplets in the final product. This statement is supported by the fact that the same surfactant to oil ratio was used in both formulations and the emulsion with the 30% phase volume of oil contained larger droplets at every time point it was sampled than the emulsion with the 60% phase volume of oil.

Table 7-3 Formulation parameters for data shown in Figure 7-3

Oil Phase %	Surfactant %	Oil to Surfactant Ratio
30	4	7.5
60	8	7.5

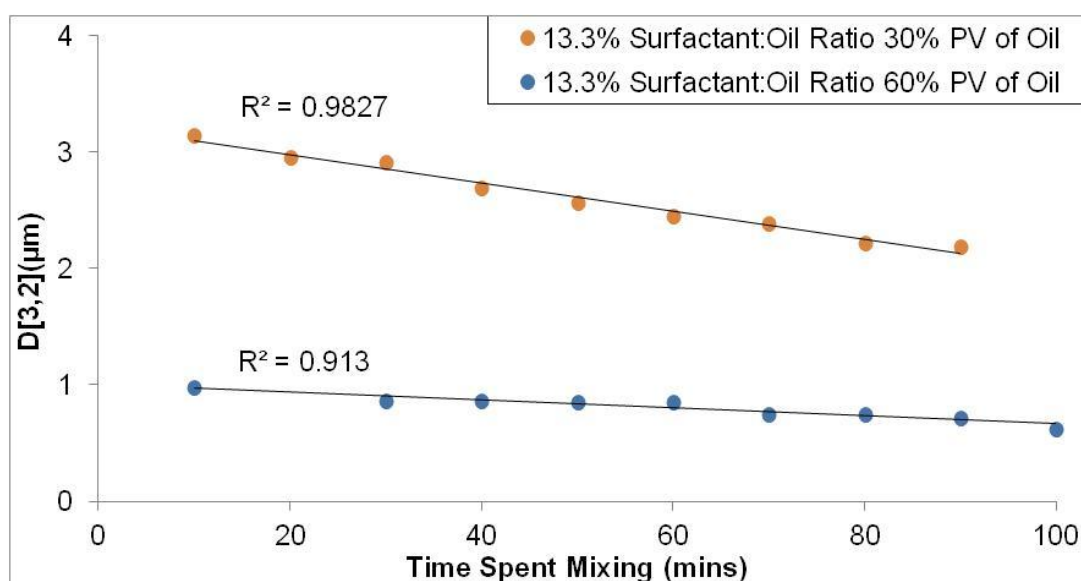


Figure 7-3 Graph showing the effect of phase volume whilst maintaining the surfactant to oil ratio within emulsification, using a Fluid Divison Mixer at 6000RPM.

In order to get a better understanding as to why an emulsion with a phase volume of 15% had a greater decrease in droplet size than an emulsion with a phase volume of 30%, yet an emulsion with a phase volume of 60% had smaller droplets than both of these emulsions required observation of the impact that the surfactant to oil ratio had upon the product and size of the droplets in it. Further trials were performed in which the volume of surfactant was altered but the phase volume of oil was maintained.

The formulation parameters for these trials are shown in Table 7-4 and the resulting droplet sizes presented in Figure 7-4.

Table 7-4 Formulation parameters for data shown in Figure 7-4

Oil Phase %	Surfactant %	Oil to Surfactant Ratio
60	0.25	240
60	1	60
60	4	15
60	4	15
60	8	7.5

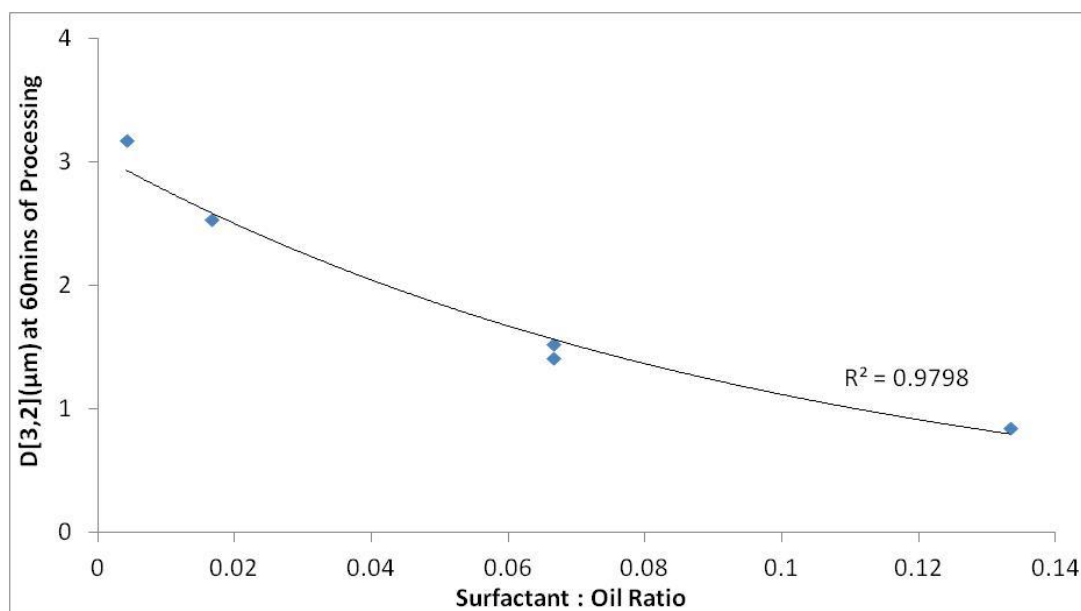


Figure 7-4 Graph showing the effect of varying the surfactant concentration within emulsification after an hour of processing using an FDM at 6000rpm.

The phase volume of oil in all processes was constant (60%).

It can be seen from the data presented within Figure 7-4 that the greater the surfactant to oil ratio, the smaller the droplet size within the emulsion. This is what one would expect to find, as with a greater surfactant to oil ratio it means there is more surfactant in the system so once the oil has been broken down into small droplets it is more likely to be emulsified by the surfactant whilst still small instead of it agglomerating with another droplet and becoming larger.

It is fair to say from analysis of the data collected and presented so far on the FDM that with regards to the formulation parameters, the phase volume of oil during the emulsification procedure is the primary determining factor, then the surfactant phase volume, when it comes to the particle size of the droplets within an emulsion being formulated. The surfactant phase has been proven to reduce the droplet size of the final product as displayed in Figure 7-4, however the data in Figure 7-3 proves that this is secondary to the phase volume of oil as when there is an equal ratio of oil to surfactant the emulsion with the greater phase volume of oil produces an emulsion with smaller droplets.

The work performed using the FDM allowed us to create stable, high oil phase volume emulsions made up of sub-micron droplets. This was determined as repeat measurements of the high oil phase volume [$\geq 50\%$] samples analysed and displayed within this chapter were repeated a month after they were formulated; the samples were shaken gently to ensure uniform distribution of the sample and analysed using the same technique. The results produced data equal in value to that displayed in the graphs and tables within this chapter which is taken from the original analysis post emulsion formulation.

Further work into mixers and subsequent processing of these emulsions was then carried out to ascertain whether the UMPF was capable of further reducing the droplets in size or whether they would prove too stable.

7.4.2 Processing emulsions using the Microfluidizer and Ultra Mixing and Processing Facility (UMPF)

Processing with high pressure equipment was performed to see if a further reduction in the droplet size could be performed. In order to break down small, stabilised droplets a large amount of energy is needed. This energy was, theoretically, to be provided by the mixing equipment operating at high pressure which would enable the breaking of the bonds (both hydrophilic and hydrophobic) of the droplet, and would force a decrease in the size of the droplet and whilst the droplet was small allow for the surfactant to emulsify the small droplet and stabilise it.

The data presented in Table 7-5 shows the size of the droplets in the emulsion following processing with different mixers. The initial emulsification is performed using the FDM and the emulsion is then processed further using the Microfluidizer or the UMPF. The batch made with 60% oil and 4% polysorbate 20 was mixed for under ten minutes to ensure the droplets would be around two microns in size. Once the emulsion had been analysed using the Mastersizer X, a litre of it was placed through the Microfluidizer and the rest was placed in the LIP of the UMPF.

The litre processed by the Microfluidizer was processed, and reprocessed, at 10mL/s and 1000bar. This processing reduced the droplet size greatly and the product was analysed using the Mastersizer 2000 to ensure that the small values were accurate.

Five litres of emulsion were processed using the UMPF at different flow rates and impeller speeds to see which had the greatest impact on the size of the droplets

processed. Interestingly, the process parameters that appeared to have the greatest impact were the flow rate of the fluid through the mixer, but with the impeller static, not rotating at all.

Unfortunately the trials performed on the UMPF were analysed using the Mastersizer X, as this was the only analytical equipment available at the time. From the results in Chapter 4 and Chapter 5 it is now believed that these results may be greater than the droplets within the emulsion actually were as the Mastersizer X has been shown to not produce appropriate values for micron sized emulsions.

It is hypothesised that the size of the droplets processed by the UMPF were actually smaller than the values displayed in Table 7-5. This is based on the droplet size distribution (DSD) produced by the Mastersizer X that is shown in Figure 7-5. The DSD for all the samples analysed are similar to that for sample 6.2 in Figure 5-19. Further analysis using the Mastersizer 2000 showed that sample 6.2 had droplets smaller than the Mastersizer X is able to detect as can be seen by the DSD in Figure 5-21.

It should be noted that the two DSD traces that contain the largest volume percentage of sub-micron sized droplets are those from the emulsions processed at the higher flow rates. Both the emulsions processed at 80mL/s by the UMPF have a DSD trace a clear distance away from that generated by the emulsions processed at 20mL/s and 40mL/s regardless of the impeller speed.

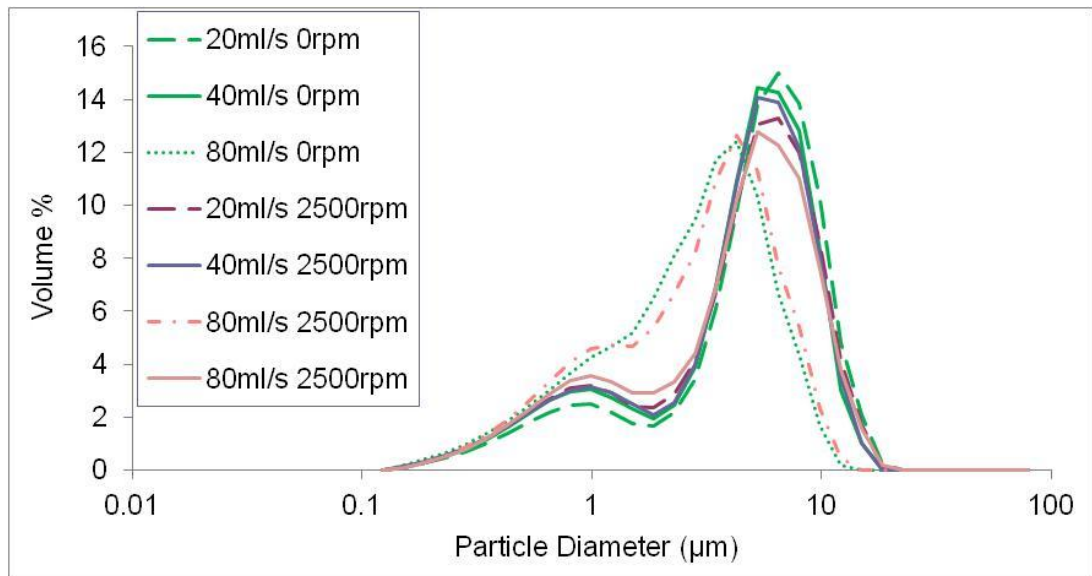


Figure 7-5 Droplet Size Distribution of emulsion after processing using UMPF.

As well as the 60% oil emulsion, a 70% oil emulsion was made using the FDM for further processing using the high pressure mixers. The Microfluidizer was unable to process this emulsion due to its viscosity and so an emulsion with a lower phase volume than 60% was made. The UMPF however had no problem processing the 70% oil emulsion and the increase in the viscosity that prevented the Microfluidizer processing it, suited the UMPF as it the mixer was able to reduce the droplets to a size smaller than obtained when processing the emulsion with 60% phase volume of oil.

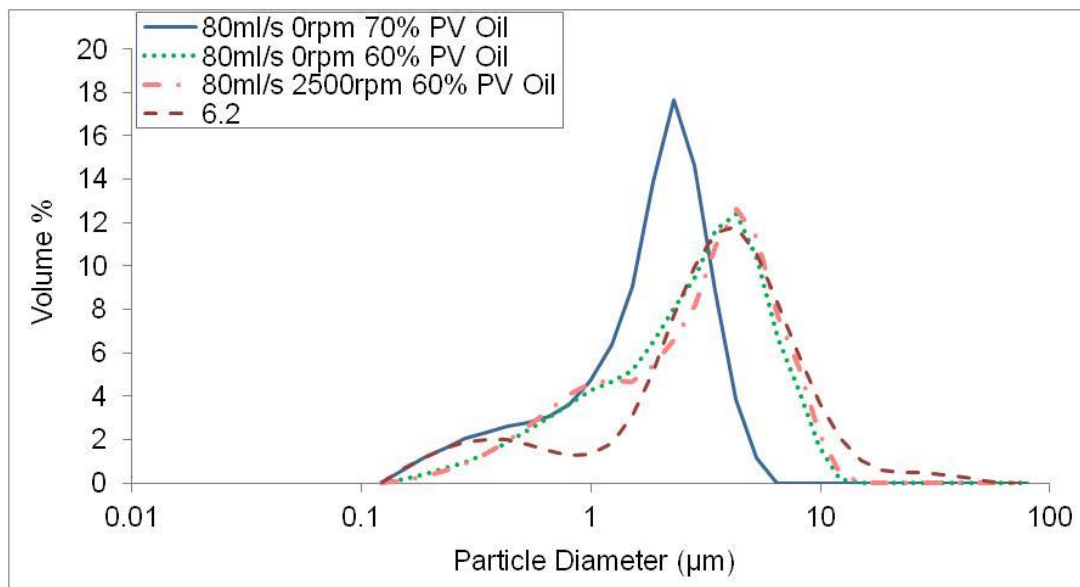


Figure 7-6 DSD of emulsions with a $D[3,2]$ value of $\sim 1.5\mu\text{m}$ according to analysis using a Mastersizer X.

It can be seen from the DSD in Figure 7-6 that the greater the phase volume of oil, the smaller the droplets in the product following processing with the UMPF. The DSD of sample 6.2 has been included to show that the traces are similar implying that the values reported may be greater than the actual $D[3,2]$ of the droplets that make up the emulsions analysed. The data in Table 7-5 confirms that the $D[3,2]$ value (and the $D[4,3]$ value) of the emulsion with a phase volume of oil of 70% contains the smallest droplets following processing with the UMPF compared to emulsions with a phase volume of 60% oil. This is similar to the data discovered during the FDM trials when it was discovered that the phase volume of oil is the primary factor with respect to the $D[3,2]$ value of the emulsion produced.

The Microfluidizer was unable to process the emulsion with a phase volume of oil of 70%, it was discovered that 60% was the greatest phase volume of oil within an emulsion that it could process, and so an emulsion with a phase volume of 21% was produced. This allowed observation of the impact the Microfluidizer has on less

viscous products. It was hypothesised that the lower phase volume of oil would produce an emulsion with a larger droplet size due not only to this being the trend observed with the FDM and the UMPF but because lower viscosity means less force needed to move the emulsion thus when it is moving less kinetic energy is present within the system and as such, theoretically, the droplet size reduction will be less. Interestingly, the opposite happened; the emulsion with the lower phase volume of oil, greater surfactant to oil ratio, was processed by the Microfluidizer and in doing so formulated an emulsion with droplets less than 200nm in size (with respect to D[3,2]).

Table 7-5 Size of droplets within emulsion after one pass through mixer.

Mixing Device	Pressure Used	PV% of Oil	PV% of Poly-sorbate 20	Total Flow Rate (mL/s)	Impeller Speed (rpm)	D[4,3] (nm)	D[3,2] (nm)
FDM	Room	60	4	n/a	6000	5650	2130
Micro-fluidizer	1000bar	21	3.5	10	n/a	333	192
Micro-fluidizer	1000bar	60	4	10	n/a	445	297
UMPF	~20bar	60	4	20	0	5160	2080
UMPF	~20bar	60	4	40	0	4640	1880
UMPF	~20bar	60	4	80	0	2970	1420
UMPF	~20bar	60	4	20	2500	4700	1820
UMPF	~20bar	60	4	40	2500	4580	1810
UMPF	~20bar	60	4	80	2500	3140	1460
UMPF	~20bar	60	4	20	5000	4490	1750
UMPF	~20bar	70	3	80	0	1780	980

According to the data in Table 7-5, the Microfluidizer is more efficient at processing premade emulsions in one pass than the UMPF. If the data shown is to be believed, the impact of the UMPF on premade emulsions is slight however it does process the emulsion at a fraction of the pressure the Microfluidizer operates at. The droplet size is reduced from that of the emulsion made by the FDM (top row of Table 7-5) with or without the impeller turning and is done so using a substantially lower amount of pressure than the Microfluidizer, requiring only 20bar when running at the greatest flow rate used (80mL/s).

It is proposed that should the UMPF be used to process a premade emulsion at pressure equal to the Microfluidizer the droplet size would be equal to, if not lower than that displayed in Table 7-5. This is based on the fact the UMPF has reduced the droplet size of the emulsion made using the FDM by 20% while operating at only 2% of the pressure used by the Microfluidizer.

7.5 Conclusion

The batch production of an emulsion made up of micron sized droplets using the FDM is possible within a short space of time. Through manipulation of the formulation and process parameters it has been proven that it is possible to create batches of an emulsion of a desired droplet size allowing for the production of “tailored” emulsions.

Further processing of an emulsion using high-pressure mixers reduces the size of the droplets that make up the emulsion. As the Microfluidizer is unable to process large quantities of emulsion due to its restricted size and flow rate using the FDM can be used to prepare micron sized emulsion. This allows for the focus of the work to be on the formation of sub-micron emulsions using the Microfluidizer.

On the contrary, for large quantities of uniform, micron sized emulsions the UMPF can be used at low pressure and without the impeller in operation. Relying on the geometry and architecture of the central mixing chamber and the flow rate at which reagents are injected into the central mixing chamber, the UMPF is capable of reducing the size of droplets within an emulsion to a fraction of their original size in a single pass through the mixer.

The UMPF, at a fraction of the pressure usage, is able to be used as a tool to further reduce the size of the droplets of an emulsion with a high phase volume of oil. Capable of significantly greater flow rates and production output than the Microfluidizer, further exploration into the capabilities of the UMPF needs to be explored as these results show that has great potential as a tool for large scale process.

7.6 References

BROWN, P. 2010. E-mail confirmation of FDM make and model by Peter.Brown@maelstrom-apt.com. Maelstrom APT. 25th June 2010

MAELSTROM. 2012. <http://www.maelstrom-apt.com/technologies/fdm/>. 13th May 2012

MELESON, K., Graves, S. and Mason, T. G. 2004. Formation of Concentrated Nanoemulsions by Extreme Shear. *Soft Materials*. **2** 109-123

MICROFLUIDICS, 2005. M-110S Microfluidizer® Materials Processor brochure

SHAKUNTALA, N. and Manay, O. 2001. Food: Facts And Principles Second Edition. New Delhi, New Age International (P) Ltd. p. 148

MICROFLUIDICS. 2005. M-110S Microfluidizer® Materials Processor, © 1998, 2005 by Microfluidics.

Chapter 8 Formulation of Biodiesel

8.1 Abstract

The most commonly used method of making biodiesel involves a simple transesterification reaction that converts plant based oils (soybean, sunflower, etc) into a green fuel via methanolysis in the presence of a sodium hydroxide catalyst. The following investigation was performed to observe whether biodiesel can be formulated using emulsified oil.

The production of submicron emulsions using high-shear mixers substantially increases the surface area of the oil thus allowing biphasic reactions to proceed rapidly, as discovered in Chapter 6. The reasoning behind this approach is not to develop significantly new chemistry, but to apply a combination of known clean chemical transformations to emulsified reagents.

In order to investigate the importance that the droplet-size of oil in a direct emulsion has on the overall rate of reaction for a standard biodiesel reaction, a series of experiments were designed and implemented utilising a combination of traditional and novel emulsion formulation techniques accompanied with analytical and processing methods developed and discussed in previous chapters.

8.2 Introduction

The reasons for looking at increasing the rate of reaction for the production of biodiesel are detailed in section 2.7.2. It is here that the importance and usefulness of biodiesel as a green fuel is explained in detail.

Work performed in Chapter 6 showed that by increasing the available reactive surface area of the oil in a biphasic system the rate of reaction can be increased. As a result it was hypothesised that in reducing the droplet size of the oil, prior to biodiesel formulation, the overall reaction time required to produce the fuel would be decreased making the formulation of the green fuel even greener and cheaper than it currently is. To analyse the droplets within the emulsion, a Malvern Mastersizer was once again used. A full explanation of this equipment is discussed in section 2.6.

Formulating an emulsion is one of the easiest ways of increasing the available reactive surface area of oil. Taking a natural oil, emulsifying it and reducing the droplet size to as small as possible, thus increasing the available surface area of the reagent as greatly as possible, was a logical step in order to improve the rate of reaction of the biodiesel reaction.

8.3 Experimental

8.3.1 Standard Method

The standard method for making biodiesel is listed below:

1. Filtration of the oil; the oil is filtered and any solid impurities removed.
2. The filtered oil is then added to the reaction vessel and heated to temperature (60°C).
3. Methanol is measured out and added to a separate reaction vessel.
4. Sodium hydroxide is measured out into the vessel containing the methanol.
5. The sodium hydroxide is then dissolved in the methanol to form sodium methoxide and heated to the reaction temperature under reflux.

6. When both vessel contents reach the required temperature (60°C), the sodium methoxide is added to the reaction vessel and the reaction timer begins.
7. The contents are mixed for one hour before the reaction is terminated and the contents transferred to a gravimetric separating funnel.
8. The organic and aqueous phases settle out over time, until eventually the biodiesel phase is clear. The aqueous phase is removed at this point and the biodiesel is ready for use.

This method was used for making biodiesel using sunflower oil, 1 wt% sodium hydroxide and a molar ratio of 6:1 of methanol to oil [respectively] and heated using an oil bath to obtain rate of reaction data that could be used as a standard.

8.3.2 Emulsification of Oil

Emulsification of the oil was the first stage in the experiment, as this created the largest increase in the surface area of the oil. A large batch of emulsion was needed to perform multiple experiments and repeats of those experiments, once the optimised method had been deduced. The FDM discussed in section 7.3.3 was used to create a six litre batch of sunflower oil emulsion with a phase volume of oil of 70%. This was because a minimum amount of water was wanted in the emulsion to reduce the impact on the methanol. In addition, the greater the phase volume of oil, the greater the amount of product per given volume of emulsion produced.

An emulsion with an oil phase of 70% was the highest oil phase it was possible to achieve and still be able to process the emulsion; oil phases higher than this created an emulsion too viscous for the FDM. This left an aqueous phase of 30% which was made up of 26% water and 4% non-ionic surfactant polysorbate 20. The emulsion

that was produced was viscous but still flowed and was mixable using the Fluid Division Mixer (FDM).

Following the production of the emulsion, samples were taken from different locations within the batch and analysed to ensure that the size of the droplets was uniform throughout the emulsion. The samples were analysed using a Malvern Mastersizer X and the values produced with respect to the D[3,2] were all $1.66\mu\text{m}$ ($+/- 0.05\mu\text{m}$). The droplet size distribution for each location overlaid almost perfectly (as displayed in Figure 8-1) which showed that the emulsion produced had a uniform distribution of droplets throughout it.

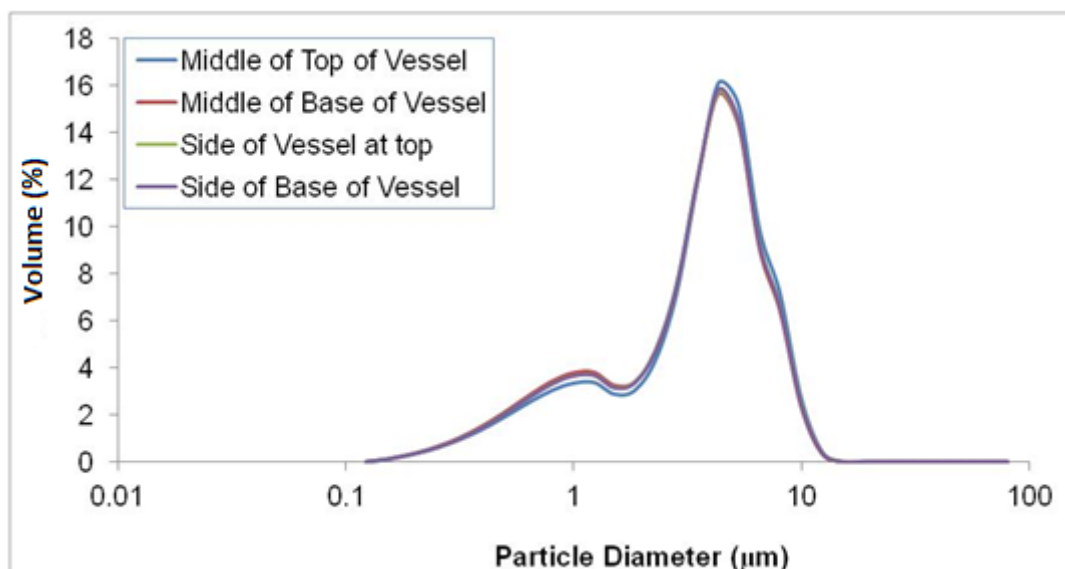


Figure 8-1 DSD of emulsion used to make biodiesel showing uniform distribution throughout the mixing vessel.

8.3.3 Method Development

Biodiesel formulation involves a simple transesterification reaction during which each glyceride chain that makes up the triglyceride chain is converted into a fatty acid methyl ester. Stoichiometrically, at least three times the number of moles of methanol to oil is required for the reaction to reach completion. It has been found

that in order to drive the reaction forward within a reasonable time frame [for sunflower oil] increasing the molar ratio of methanol to oil from 3:1 to 6:1 provides the minimum amount of methanol required to reach completion in the a reasonable time, whilst still producing the greatest product yield (Leung et al., 2009; Rashid et al., 2008). Sodium hydroxide (0.6 wt%) was used to catalyse the reaction as it was found to not only produce minimal unwanted side-products whilst maintaining an efficient rate of reaction, but is also readily available. The value of sodium hydroxide used was 0.4 wt% less than the recommended value. This was due to discovering, during preliminary experiments, that the presence of surfactant and 1 wt% sodium hydroxide causes the formation of soap initially, followed by the formation of some biodiesel. In order to make biodiesel the primary product the values used in this methodology were altered until it was ascertained that 0.6 wt% gave the required catalytic properties whilst making minimal by-product.

The standard experimental method for the formulation of biodiesel is to heat the oil up to temperature before adding sodium methoxide (which too has been heated to the same temperature as the oil) and allowing the reaction to occur at temperature under agitation (Chai et al., 2007; Ting et al., 2008). This method however proved inadequate for direct replacement of oil with an emulsion as it was found [following separation of the phases] that oil droplets were dispersed throughout the biodiesel indicating that the reaction had not gone to completion. Visual assessment of the product indicated that the reaction was incomplete as the organic layer was translucent, not transparent. Confirmation of this was provided following analysis using $^1\text{H-NMR}$, the spectra of which is displayed in Figure 8-2. The spectra shows a peak pattern between 4.1ppm and 4.3ppm that is indicative of triglyceride as well as single peak at 3.65ppm that is indicative of biodiesel.

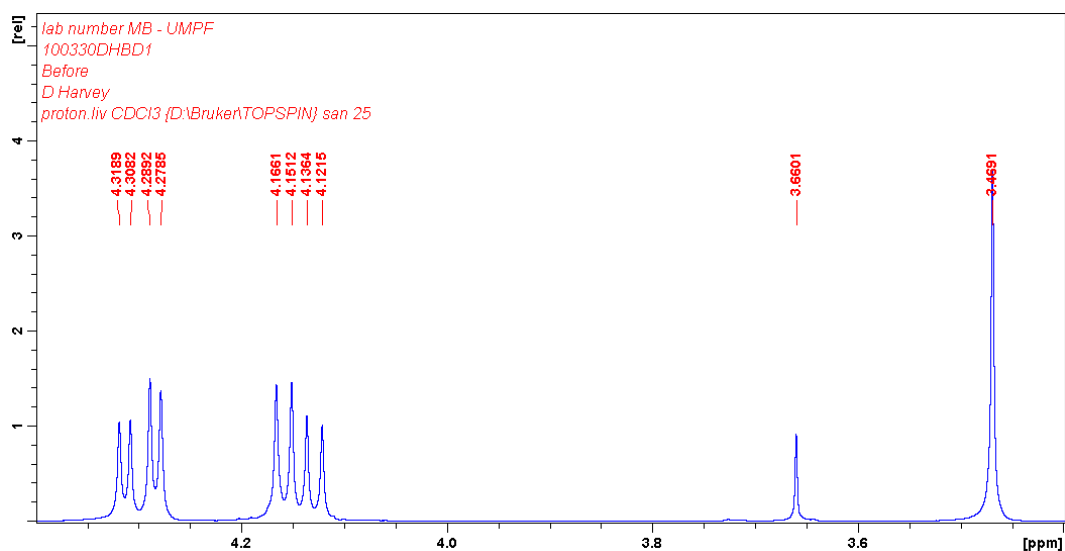


Figure 8-2 ¹H-NMR spectroscopy of an incomplete biodiesel reaction.

To confirm these findings a sample of pure biodiesel made using the standard method in section 8.3.1 was spiked with sunflower oil and analysed using ¹H-NMR. As can be seen by the spectra generated in Figure 8-3, it is similar to that displayed in Figure 8-2 indicating a strong presence of triglyceride and confirming that there was oil that had not reacted present within the sample.

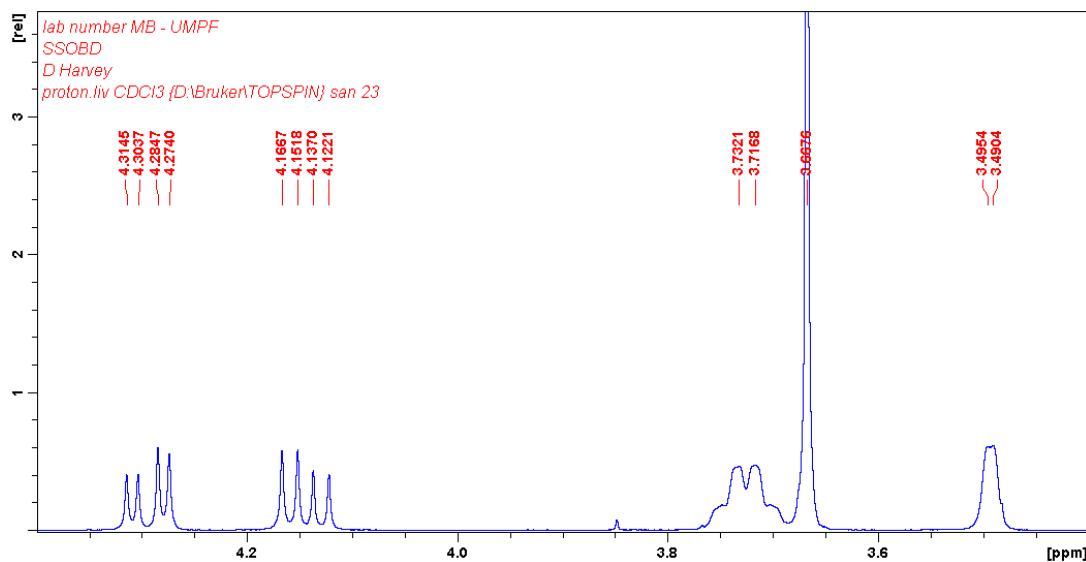


Figure 8-3 ¹H-NMR spectroscopy of biodiesel spiked with sunflower oil.

The experimental procedure was analysed and adapted. It was concluded that the presence of excess water was preventing the methanol reacting with the oil. The

aqueous phase was removed via gravitational separation and the organic phase reacted with sodium methoxide again, as per the standard method in section 8.3.1 with 0.6 wt% sodium hydroxide and a molar ratio of 6:1 methanol to oil. Upon the cessation of agitation, and following the separation of the products into their two distinct layers, visual assessment was that the experiment had worked as the organic phase became transparent. The two-step synthesis was repeated and samples taken at regular intervals to observe how far along the reaction had progressed and the results compared to those time samples taken following the standard method with oil.

The first step of the new two-step synthesis involved using the standard method (section 8.3.1); 0.6 wt% sodium hydroxide was dissolved in methanol (molar ratio of 6:1 methanol to oil was used) to form sodium methoxide, whilst the emulsion was heated to 60°C. Once the emulsion reached temperature, sodium methoxide was added to the emulsion, whilst still undergoing agitation, to the base of the reaction vessel using a long funnel as this ensured the distribution of the reagent throughout the reaction vessel. The vessel was kept at 60°C with agitation provided by a magnetic stirrer bar for exactly 10 minutes before the contents were removed from the reaction vessel and placed in a separating funnel to allow the phases to separate.

Following analysis of both phases, the aqueous phase was removed and stored for future removal and purification through distillation to retrieve the methanol.

The organic phase [of the product of step 1] was heated to 60°C whilst 0.6 wt% sodium hydroxide was dissolved in methanol (molar ratio of 6:1 methanol to oil was used) to form fresh sodium methoxide. Once the organic phase reached temperature the sodium methoxide was added and the reaction continued under agitation, at 60°C and under reflux for a further 25 minutes.

The products were then placed in a separating funnel and allowed to settle out overnight. After ten minutes of settling however, the distinctive colouring of the products could be seen within each phase; biodiesel – a transparent, yellow tinted solution, and glycerine – a more viscous, dark brown liquid.

8.4 Results and Discussion

The data within Table 8-1 confirms that biodiesel has been formed using a two-stage method. The overall percentage of product obtained using the two-stage method was 92.2% with a total reaction time of 35 minutes. The loss of product can be assigned to apparatus, and transfer of product between vessels. As well as the reaction reaching completion within a shorter timeframe and producing a high product yield, it also uses less catalyst than previous methods. The overall time spent (on both steps of the reaction) was thirty five minutes as this allowed observation of when the reaction reached completion. The time that the products were left to separate out is not included in the overall reaction time calculation because no energy was required for the separation to occur (it was a result of gravitational forces).

Table 8-1 Values used in the second step of the adapted method for biodiesel formulation using an emulsion.

Time spent at reaction temperature (mins)	Mass of Organic Phase from Step 1 (g)	Mass of Methanol (g)	Mass of NaOH (g)	Mass of Organic Phase following Separation (g)	Theoretical Mass (g)	Product yield following excess Methanol removal (%)
35	140.89	28.70	1.00	136.59	143.98	92.20
	M_r of Methanol	Moles of Methanol	M_r of Methyl Ester	Moles of Methyl Ester		
	32.04	0.8958	294.47	0.46385		

To confirm the reaction had reached completion, the organic layer of the product was analysed using ¹H-NMR and the spectra of this analysis is displayed in Figure 8-4. Once the transesterification reaction reaches completion, there is trace presence of triglyceride between 4.1 and 4.3ppm, and a significant methyl ester peak in the region of 3.65ppm.

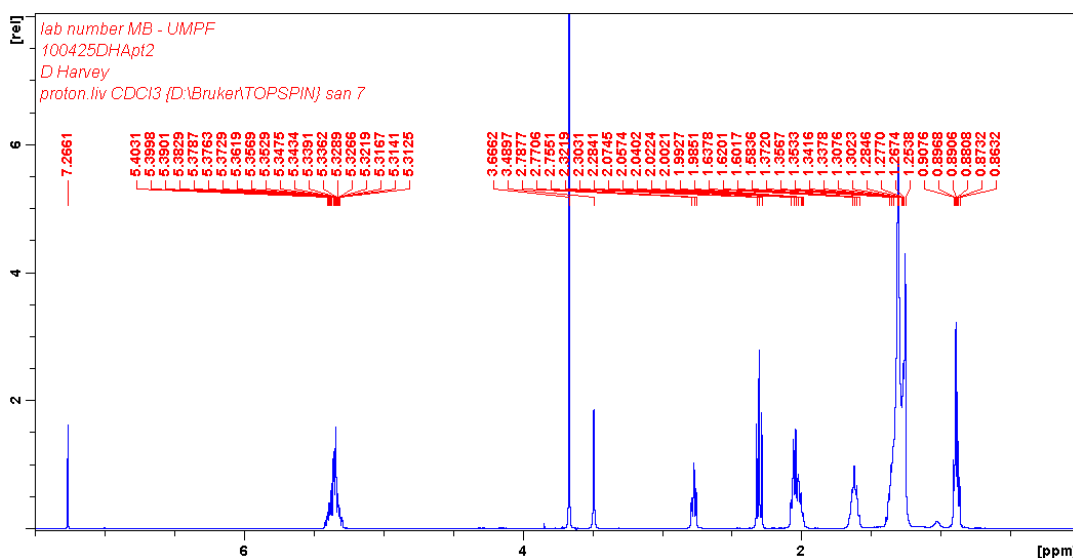


Figure 8-4 $^1\text{H-NMR}$ of the product formed using a sub-micron emulsion and two-step biodiesel formulation synthesis described in this paper.

Quantification of this data was confirmed using the triglyceride conversion calculation reported by López et al., in 2011. Integration of the biodiesel peak and the triglyceride peaks is performed on the spectra, the values are then placed into Equation 8-1 and a value known as the degree of conversion from triglyceride, X_{tag} , is produced.

$$X_{tag} = 100 \left(\frac{(4M - 3G)}{(4M + 9G)} \right)$$

Equation 8-1 Mathematical equation used to calculate the percentage conversion of triglyceride (López et al., 2011).

Where:

M = value of the integrated methyl ester peak

G = value of the remaining tryglyceride peaks.

It can be seen in Equation 8-1 that there are multiples of M and G. The reasoning behind the multiples chosen by López et al., (2011) are; 4M corresponds with four equivalent glyceryl-protons in a triglyceride, 9G corresponds with three methyl-

protons of the three methyl ester moieties transesterificated, and 3G to each of the *hidroxo-protons* in each chain of the triglyceride (López et al., 2011).

The integrated values for *M* and *G* in Equation 8-1 are shown in Table 8-2. When placed into Equation 8-1 and processed the result confirms that the reaction has reached 99% completion, as the initial analysis suggested.

Table 8-2 Values obtained from analysis of Figure 5.

Peak Position (ppm)	Integration	Group
7.27	1.00	CDCl ₃ (_l)
5.35	12.17	Olefin Protons
4.32 to 4.06	0.04	Glycerol (G)
3.66	11.95	Methyl Ester (M)

After confirming that it was possible to produce biodiesel using an emulsion, work was done on monitoring the rate of reaction. Only the second step of the two-step method was monitored, as the first step does not go to completion (as discussed in section 8.3.3). Samples were taken over the course of the reaction and analysed using ¹H-NMR. The peaks were then integrated and the integration values placed into Equation 8-1 to calculate how much triglyceride had been converted.

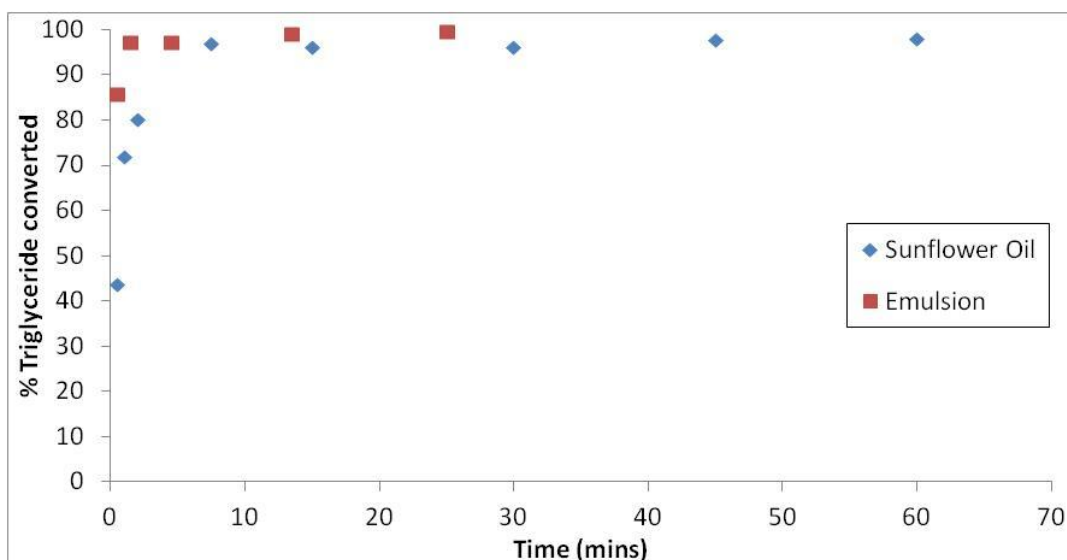


Figure 8-5 Percentage of triglyceride converted with respect to reaction time.

The data presented in Figure 8-5 follows the rate of reaction by monitoring the conversion of triglyceride. It can be seen from the curvature of the graph that triglyceride is more rapidly broken down and converted into biodiesel using emulsified oil. Although it appears that the reaction involving sunflower oil [that has not been emulsified] reaches completion within ten minutes, the reaction takes the full hour as the final couple of percent of triglyceride are not processed until this point. It is the quickness with which the reaction progresses during the initial few minutes that makes sampling and monitoring the rate of reaction tricky. The data in Table 8-3 and Table 8-4 shows the percentage of completion per second, for the first 30 seconds the value is over 1 for sunflower oil and over 2 for pre-emulsified sunflower oil (step 2 of the method). From the data, emulsifying the oil and following the method outlined in section 8.3.3, causes the rate of reaction to double for the first 30 seconds of the reaction.

As the reaction continues, the rate of reaction decreases as the volume of reagents is reduced and turned into products.

Table 8-3 Rate of reaction calculations values for sunflower oil when making biodiesel

Oil or Emulsion?	Time Sampled (s)	% of Reaction Completed	Rate of Reaction (% completion per s)
Sunflower Oil	30	43.81	1.4602
Sunflower Oil	60	72.08	1.2013
Sunflower Oil	120	80.25	0.6688
Sunflower Oil	450	97.18	0.2159
Sunflower Oil	900	96.32	0.1070
Sunflower Oil	1800	96.23	0.0535
Sunflower Oil	2700	97.75	0.0362
Sunflower Oil	3600	98.17	0.0273

Table 8-4 Rate of reaction calculations values for emulsified sunflower oil seconds step when making biodiesel

Oil or Emulsion?	Time Sampled (s)	% of Reaction Completed	Rate of Reaction (% completion per s)
Emulsion	30	85.93	2.8642
Emulsion	90	97.39	1.0822
Emulsion	270	97.27	0.3603
Emulsion	810	99.26	0.1225
Emulsion	1500	99.62	0.0664

It can be seen from the data in Table 8-3 that the reaction does not reach completion until an hour has passed (3600 s). Table 8-4 displays data that shows the oil that was used in the developed method, [section 8.3.3] reaches completion within 25 minutes, a fraction of the time. Taking into account the 10 minutes that the first stage of the reaction requires, the entire time that using the method displayed within this chapter takes is 35 minutes; almost half the time required for untreated oil.

The entire transesterification process involving the breakdown of triglyceride and subsequent conversion to methyl esters occurs in stages involving diglyceride and monoglyceride. The final products however are methyl esters, as this is the case the intermediate products can be ignored, and the reaction thought of as a first order reaction (Jain and Sharma, 2010). Using the equation published by Jain and Sharma

it is possible to calculate the reaction rate constant using the final methyl ester percentage converted and the time taken to reach completion

$$K = \frac{\ln(ME_t) - \ln(ME_0)}{t}$$

Equation 8-2 Integrated equation to calculate the reaction rate constant for the transesterification reaction (Jain and Sharma, 2010).

Where:

K = reaction rate constant

ME_t = Percentage yield of methyl ester at time *t*

ME₀ = Percentage yield of methyl ester at time 0

t = time in minutes

It can be seen in the description for Equation 8-2 that the given unit for time is minutes. This is not the SI unit, however this is the published equation and it is required for a straight comparison. Using Equation 8-2 and the values from the last row of Table 8-3 and Table 8-4, the reaction rate constant for sunflower oil is 0.07645 min⁻¹ and the reaction rate constant for the second stage of the transesterification of the emulsified sunflower oil is 0.1841 min⁻¹. These reaction rate constants are based on the assumption that there is zero methyl ester at the beginning of the reaction. When comparing the sunflower oil reaction rate constant and the second stage of the emulsified sunflower oil reaction rate constant, it can be observed that the latter is more than twice as fast. Taking into account the first stage of the reaction, and thus increasing the time to 35 minutes, produces a reaction rate constant of 0.1315 min⁻¹; still almost double that of the sunflower oil reaction rate constant.

The reaction rate constant for the transesterification reaction published by Jain and Sharma which involved the transesterification of *Jatropha curcas* oil at optimum

conditions took three hours to reach completion and had a reaction rate constant of 0.008 min^{-1} (Jain and Sharma, 2010). By comparison it can be said that the equivalent benchmark with sunflower oil has an order of magnitude faster reaction rate constant, 0.076 min^{-1} , which we were able to more than double to 0.18 min^{-1} and increase the yield. This increase in the rate of reaction is equivalent to increasing the temperature from 40°C to 60°C (Jain and Sharma, 2010).

The production of biodiesel via transesterification of sunflower oil, using either the emulsified two-step method or the standard method, can also be compared to the enzymatic/acid catalyzed hybrid process of biodiesel from soybean oil (Ting et al, 2008). The reaction rate for making biodiesel from soybean oil using an enzymatic/acid catalyzed hybrid process, at optimised parameters, is $0.006382 \text{ min}^{-1}$; a massive twenty times less than using the two-step emulsion method involving sunflower oil as the reagent in this thesis. Enzymatic reactions tend to be slower than chemical reactions, and thus applying the two step process to an enzymatic reaction may yield similar results and improve the commercial attractiveness of enzymatic reactions. In addition, the improved reaction rates of the emulsion route improved the environmental credential of more traditional biodiesel production by being able to perform the reaction at a lower temperature; saving energy and reducing the carbon footprint further.

8.5 Conclusion

It was proven that, with some method development, emulsified oil can be used in the formulation of biodiesel. The overall time taken for the triglyceride to be converted to biodiesel was greater overall as two steps were required; however, the reaction time was significantly less. The total time the reaction was at temperature and under

agitation when using the two-stage method was 35 minutes whereas the standard method requires an hour (section 8.3.1). This proved the initial hypothesis that the rate of reaction within the biphasic system could be increased if the droplet size of the reagent was reduced, and the surface area increased. It is confirmed when observing the benchmark reaction rate constant of the standard sunflower oil to biodiesel reaction (0.076 min^{-1}) and comparing this to the emulsified sunflower oil to biodiesel method presented in this chapter (0.18 min^{-1}), an increase in reaction rate that is more than double.

8.6 Future Work

The option of scaling up the reaction to that of an industrial level is an idea for future work. Using the UMPF to produce large batches of emulsion on which a further investigation into the rate of reaction could be performed.

Interest also lies in the emulsification of waste oil and whether this it is possible to formulate biodiesel by emulsifying waste oil initially.

The two-step method needs to be performed using sunflower oil that has not been emulsified.

8.7 References

- CHAI, F., Cao, F., Zhai, F., Chen, Y., Wang, X. and Su, Z.. 2007. Transesterification of Vegetable Oil to Biodiesel using a Heteropolyacid Solid Catalyst. *Advanced Synthesis and Catalysis*. **349** 1057–1065
- JAIN, S. and Sharma, M. P. 2010. Biodiesel production from *Jatropha curcas* oil. *Renewable and Sustainable Energy Reviews*. **14** 3140–3147
- LEUNG, D. Y. C., Wu, X. and Leung, M. K. H.. 2009. A review on biodiesel production using catalyzed transesterification. *Applied Energy*. **87** 1083–1095
- LÓPEZ, J. M., Cota, T. del N. J. García., Monterrosas, E. E. Galindo., Martínez, R. Nájera., de la Cruz González, V. M., Flores, J. L. Alcántara., Ortega, Y. Reyes. 2011. Kinetic study by ^1H nuclear magnetic resonance spectroscopy for biodiesel production from castor oil. *Chemical Engineering Journal*. **178** 391–397
- RASHID, U., Anwar, F., Moser, B. R. and Ashraf, S. 2008. Production of sunflower oil methyl esters by optimized alkali-catalyzed methanolysis. *Biomass and Bioenergy*. **32** 1202–1205
- TING, W-J., Huang, C-M., Giridhar, N. and Wu, W-T. 2008. An enzymatic/acid-catalyzed hybrid process for biodiesel production from soybean oil. *Journal of the Chinese Institute of Chemical Engineers*. **39** 203–210

Chapter 9 Conclusions and Further Work

The focus of the research within this thesis was on the exploration, validation and use of new and novel mixing equipment to create sub-micron emulsions for use in chemical reactions. Comparison of various mixing equipment was done with a variety of oils including silicone oils. The model reactions of soap and biodiesel were however carried out using the plant oil sunflower seed oil. The new mixer (CDDM) was shown to outperform some traditional mixers, but work is required to optimise the model systems for the mixer, and that is part of a subsequent PhD. The specific interest was given to emulsions of plant oils as a way of improving their available reactive surface area for use in biphasic systems, such as the production of soap and/or biodiesel. Through emulsification of the oil, and manipulation of its droplet size, the reactions were faster with smaller droplets. In the case of biodiesel this requires a new process approach and one that will require further optimisation. Further specific conclusions can be found in the subsequent paragraphs.

1. Presented in Chapter 4 is a method involving the use of the new Formx high-throughput formulation platform and design of experiment (DoE) software that allows for the quick and efficient mapping out of the process and formulation parameters and the impact they have on the size of the droplets within the emulsion produced. The formulation parameters that were discovered included using an oil phase of 60%, a surfactant phase of 8% and a water phase of 32%. The order of addition was found to be adding the oil to the reaction vessel while the impeller was stirring at 200rpm and the scrapers turning at 50rpm, followed by the surfactant then the water. Only after all the reagents were added to re reaction vessel was the impeller speed

and scraper speed increased to the maximum possible speeds (6000rpm and 200rpm respectively). From the results presented in the chapter it can be said that high-throughput formulation is useful in obtaining the formulation parameters required to obtain an emulsion with the smallest possible droplet size in less than three runs with a fully functioning Formax containing twenty-four reaction vessels. As mentioned in the further work section of Chapter 4, the method developed was applied to two other systems, however further work would be needed to ascertain whether this method works with more than just these three emulsion systems. Focus in particular would be on high viscous materials to ascertain the limitations of the Formax.

2. The formulation parameters identified using the Formax were the optimal ones for use on the Ultra Mixing and Processing Facility fitted with Controllable Deformation Dynamic Mixing (CDDM) technology as discussed in Chapter 5. The trials produced an emulsion with a small droplet size, a $D[3,2]$ value of $0.20\mu\text{m}$, which is comparable to the Formax result with the same formulation parameters of $0.46\mu\text{m}$. The method using the Formax enables the identification of the optimal formulation parameters for an emulsion system using small, bench-top quantities (60mL per reaction vessel) that is then transferable to the scale of the UMPF (with CDDM technology) which is able to produce larger quantities (54mL/s) of emulsion made up of even smaller droplets when using the reagents discussed in the chapter.
3. The exploration of the formulation and process space using the UMPF (with CDDM technology) allowed an insight into the capabilities of the mixer. The work presented in Chapter 5 compares the size of the droplets in the

emulsions produced by the UMPF (with CDDM technology), D[3,2] value of 0.20 μm , with those produced by a Silverson 150/250 MS rotor-stator high shear dispersive mixer, D[3,2] value of 2.18 μm after 5 passes. It is reported that the UMPF (with CDDM technology) is capable of producing large quantities of sub-micron emulsions at low pressures and impeller speeds in a single pass, and requires a slower tip speed, compared to the Silverson, which produces micron sized emulsions after numerous passes through the mixer. It is through the unique design of the CDDM technology within the UMPF, which optimises the way deformation is used to cause break-up of the droplets to break them down to sub-micron size (0.20 μm). Further work should be performed using the Formax to map out a different emulsion system (different oil and/or surfactant to those used) and the subsequent scale-up of this to ascertain whether the formulation parameters are transferable from the Formax to the UMPF, or whether that only applies for the emulsion system presented in Chapter 5. In addition more work is required to identify and validate the details of the mechanisms that resulted in the superior performance of the CDDM. This work could, for example, include computational fluid dynamics, flow visualisation and examination of the design details of the internal working surfaces. Trials involving operating the UMPF at maximum “instantaneous” output (approximately one tonne an hour) should be performed also to see if the UMPF is capable of producing sub-micron emulsions at commercially significant volumes.

4. Emulsions made up of droplets a couple of microns in size, following dispersive mixing with a high-shear homogeniser, were shown to have a decreased reaction time when used as a reagent in the saponification reaction

compared to those with a much larger droplet size. The results in Chapter 6 show that reducing the droplet size by 75% leads to a 23% decrease in the overall reaction time. This is because the time taken to reach completion for the emulsion made up of the smaller droplets was less than that for the emulsion made up of larger droplets. Work involving producing an emulsion using the CDDM should be performed as if the CDDM is capable of reducing the droplet size of an emulsion to $0.20\mu\text{m}$, 100 times smaller than the small emulsion used in the experiment in the chapter, the overall reaction time could theoretically be reduced significantly. Such a large reduction leads to a proposal for further work involving performing the reaction within the UMPF itself. Further work involving obtaining the rate of reaction should also be performed, as only the end point was observed for the work recorded within this thesis.

5. Using a Fluid Division Mixer it was possible to create a range of emulsions made up of droplets from 1-4 microns in size. The impact of the UMPF on premade emulsions was explored to observe whether a fine emulsion could be produced and the droplet size further reduced. The data in Chapter 7 shows that the UMPF (with CDDM technology) is able to process premade emulsions and further reduce the size of the droplets by up to 54% (from $2.13\mu\text{m}$ to $0.9\mu\text{m}$). A comparison for this model emulsion was made with the ultra high pressure Microfluidizer which can operate at up to 1,200 bar. By comparison pressures in the CDDM were rather low, at about 30bar, and could not be increased because the flow rate was limited by the pumps used. As a consequence the CDDM was not able to match the size of the droplets in the emulsion processed by the microfluidizer. Two advantages however

were observed for the UMPF; the flow rate was much higher than the Microfluidizer (note the lab unit cannot be scaled up), and more critically the UMPF was able to process emulsions of much greater viscosity. High viscous fluids cannot be pumped effectively by the Microfluidizer implying that for highly viscous emulsions most of the pressure drop will be wasted getting the emulsion into the Microfluidizer rather than be used to break-up the emulsion droplets. Based on these observations in Chapter 7, it is suggested that using equivalent pressures in the Microfluidizer and the UMPF (with CDDM technology), the latter would be able to either create an emulsion of similar droplet size but at much greater quantities, or equivalent flow rate but smaller drop size. Consequently, it is proposed that further work should be performed involving different emulsion systems to confirm this hypothesis.

6. The production of biodiesel, using a micron sized emulsion and an adapted method, takes significantly less reaction time than the current standard method. The data displayed in Chapter 8 shows that emulsifying the oil and following an improved method doubles the reaction rate. takes the overall reaction time down from 60minutes to 35minutes (~40% decrease). The rate of reaction for the first 30seconds of the second step of the reaction is doubled following the method presented. The standard method was adapted to remove the water as methanol is miscible in water. This adaption increased the overall time taken to reach completion, however it reduced the time required for the reagents to be at reaction conditions. Further work should be performed using this method involving different plant oils to determine whether it works with all types. It is also proposed that further

work be undertaken to ascertain whether it is possible to use waste oil as the reagent, emulsify it and subsequently react it to form a useful fuel. It would also be extremely useful for a conceptual engineering design to be developed to address some of the issues with the separation stage. Finally the reaction should be carried out in the UMPF. It is proposed that an experiment be performed involving forming biodiesel in the mixing chamber of the UMPF, and should this work, subsequent experiments involving formation of biodiesel using emulsified waste oil – if this proves feasible. Unfortunately the UMPF facility was still being built and commissioned during this PhD. In particular the extraction system which would be required to allow handling volatile and flammable materials (i.e. methanol in the reaction) was not fully commissioned and thus the proposed trials could not be carried out (as discussed in section 3.4).

In summary the thesis demonstrates that the new CDDM mixer at the heart of the UMPF shows favourable performance when compared to other high shear mixers, producing smaller drop sizes whilst maintaining high flow rates. For two model reactions the thesis demonstrates that smaller particle sizes do produce faster reactions and thus, that in combination with the CDDM significant improvements in reaction rates are envisaged which should improve the economics of such reactions. The key next step would be to carry out such a study and to investigate the basis for the improved performance of the CDDM.

Appendices

9.1 Dimensions of Equipment used

Table 9-1 Dimensions of Fluid Division Mixer

Location	Measurement (mm)
Overall diameter of mixer head	86.0
Diameter of cavities	10.0
Depth from top of mixer head to base of inflow chamber	24.07
Depth of cavities in top row of mixer, from top of mixer to base of cavity	4.96
Depth of cavities in second row of mixer (from top of mixer to base of cavity)	4.49 9.45
Depth of cavities in third row of mixer (from top of mixer to base of cavity)	5.00 14.45
Depth of cavities in fourth row of mixer (from top of mixer to base of cavity)	4.99 19.44
Diameter of inflow	20.05

Table 9-2 Dimensions of Formax Vessels

Location	Measurement (mm)
Vessel Diameter	48.5
Vessel height	113.5
Dissolver disk / Saw tooth clearance	10.0
Dissolver disk / Saw tooth blade diameter	25.0
Rotor-stator blade length	15.0
Clearance between panel of the stator	0.9
Scraper width	14.1
Scraper length including black section which does not come into contact with fluid unless extreme turbulent within vessel	92.5
Scraper length that comes into contact and acts as baffles	75.5
Scraper thickness	2.16

9.2 Wear and Damage to the UMPF

The following is a series of experiments that were designed to test reagents prior to use in the UMPF. This is due to repeated impact of particulates upon a surface will eventually cause damage to the surface due to all bonds having a finite amount of energy they can absorb before they break. When taking into account the pressures that the UMPF is capable of obtaining, that damage is going to be greater and/or occur sooner, due to the scale of the speeds the particulates will be travelling at and the pressures they will be under. In order to minimise the damage that will occur as the result of placing untested reagents through the UMPF a bench-top method was proposed for future particulate testing.

The proposed method in question has been developed based on an adapted Archard's wear rate law equation (Ramalho, 2008);

$$\frac{\delta W}{\delta t} = kPV$$

Equation 9-1 Archard's wear rate law equation (Fillot, 2007).

W = the mass of the metallic/ceramic sample (g)

t = the time the sample is undergoes abrasion (s)

k = wear coefficient

P = pressure applied to metallic sample (N/m²)

V = sliding speed of apparatus (ms⁻¹)

The required components and pieces of equipment to test samples/reagents that researchers wish to use in the UMPF are listed below;

- 10mm diameter circular sample of 17-4PH steel
- 10mm diameter circular sample of ceramic
- 2mL proposed reagent

- Distilled/filtered water
- Ultra-polisher with known sliding speed and pressure
- Analytical balance
- Atomic Force Microscopy (AFM)
- High Resolution Electron Microscopy (HREM)/Scanning Electron Microscopy (SEM)

Method:

1. The steel and ceramic samples are ultra polished down to a fine 500nm finish.
2. The samples are then analysed using AFM, HREM and if possible SEM.
3. The steel and ceramic samples are then weighed using an analytical balance.
4. 2mL of the proposed sample is placed upon the steel/ceramic sample which is in turn placed on an ultra-polisher.
5. The ultra-polisher is then placed under pressure and rotated at high speed for a pre-decided length of time.
6. The above step is repeated for either the steel or ceramic, whichever was not tested.
7. The steel and ceramic are then cleaned using ultrapure water and left to dry.
8. Both steel and ceramic are weighed again using the same analytical balance.
9. The change in mass is then inserted into Equation 9-1.

10. If the value is deemed high then the steel and ceramic samples are analysed again using AFM, HREM and if possible SEM and compared to the images and results taken in step 2 above.

Table9-3 Results Table for the proposed wear rate method.

Reagent Reference	Change in Mass (g)	Time undergoing abrasion (s)	Pressure Applied (Pa)	Sliding speed of Ultrapolisher (ms⁻¹)	Wear Rate Coefficient

Atomic Force Microscopy (AFM) imaging, High Resolution Electron Microscopy (HREM) and Scanning Electron Microscopy (SEM) all provide a visual representation of the damage certain particulates will cause the main components of the UMPF. Once a reagent has been tested its wear rate coefficient and images of the damage it is capable of doing is recorded into a matrix. The matrix in question consists of Mohs Scale hardness particulates within slurry solution and the damage they cause to both the steel and the ceramic materials. This provides a damage estimation for proposed particulates within UMPF and the effects upon its main components.

It is hypothesised that the damage particulates are able to do to the steel/ceramic will increase with increased Mohs scale hardness.

With a wear coefficient value assigned to the damage capable from a known Mohs particulate if a researcher presents a possible reagent for use in the UMPF the sample can be taken, the method applied and the results compared to those known. If the wear rate coefficient and visual image is within certain parameters, and it is deduced

that the particulates within solution posed no immediate danger to the UMPF components, then the sample can be cleared for use within the UMPF.

Another method proposed involves the use of a TE-66 micro-abrasion tester machine. This method allows the calculation of the wear volume and thus a wear-rate-to-time ratio can be calculated.

$$V = \frac{\pi b^4}{64R} \quad \text{Eq. 2.03 [5,6]}$$

V = wear volume (m³)

b = crater diameter (m)

R = radius of the ball (m)

As with the previous proposed matrix this would allow comparison between reagents to be used within UMPF and also allow for a wear volume matrix to be drawn up using values obtained from analysis using Mohs Hardness particulates.

As listed in the operating parameters, temperatures of up to 200°C are obtainable within the feedstock vessels. Temperatures in excess of 300°C however are not recommended and as a result proposed reaction chemistry to occur within the mixer must always be bench tested to make sure that temperatures near this value are not reached. Low temperatures also a problem as the UMPF is unable to operate at temperatures below 15°C so unfortunately any reactions requiring these temperatures or endothermic reactions that reach these temperatures are prohibited from being performed within the UMPF.

9.3 References for 9.1

FILLOT, N., Iordanoff, I. and Berthier, Y. 2007. Wear modeling and the third body concept. *Wear*. **262** 949-957

RAMALHO, A. 2008. A geometrical model to predict the wear evolution of coated surfaces. *Wear*. **264** 775–780

9.4 Data from Chapter 4

Table 9-4 Values of the variables used to produce three of the 22 emulsions and their corresponding D[3,2] values.

Run Name	Oil Viscosity	Oil Phase (%)	[SLES] (%)	Impeller Type	Impeller Speed (rpm)	Scraper Speed (rpm)	D[3,2] (µm)
A	1000cSt	0.6	0.025	Rotor-stator	1000	100	80
B	1000cSt	0.6	0.025	Rotor-stator	6000	100	10.71
C	10cSt	0.6	0.08	Dissolver Disk	6000	100	0.76

Table 9-5 Predicted formulation and process parameters required to obtain the smallest possible droplet size and the value that would be obtained according to MODDE alongside the actual experiments that were subsequently carried out.

The viscosity of the oil and the impeller type in all cases was 10cSt and dissolver disk respectively.

Exp No	Oil Phase (%)	[SLES] (%)	SLES : Oil	Impeller Speed (rpm)	Scraper Speed (rpm)	D[3,2] (µm)
Prediction	0.6	0.08	0.1333	6000	100	0.77
5	0.590	0.082	0.1390	6000	100	0.66
7	0.600	0.080	0.1332	6000	100	0.65
9	0.600	0.080	0.1332	6000	100	0.71
12	0.600	0.079	0.1316	6000	100	0.68

Table 9-6 A summary of the proportionality constants used to obtain predicted D[3,2] values for a dissolver disk impeller.

<u>Term</u>	<u>Value of Proportionality Constant</u>	<u>Term</u>	<u>Value of Proportionality Constant</u>
Constant	-0.274727	Oil Viscosity * Impeller Speed	1.93315e-007
Oil Viscosity	-0.980486	Oil Viscosity * Surfactant Phase Volume	0.951511
Impeller Type	Dissolver Disk	Oil Viscosity * Oil Phase Volume	0.950571
Impeller Speed	0.0218066	Oil Viscosity * Water Phase Volume	0.949986
Surfactant Phase Volume	-1.34399	Impeller Speed * Surfactant Phase Volume	-0.021999
Oil Phase Volume	-0.0996872	Impeller Speed * Oil Phase Volume	-0.0221296
Water Phase Volume	-0.0712075	Impeller Speed * Water Phase Volume	-0.0220239

Table 9-7 A summary of the proportionality constants used to obtain predicted D[3,2] values for a rotor-stator impeller.

<u>Term</u>	<u>Value of Proportionality Constant</u>	<u>Term</u>	<u>Value of Proportionality Constant</u>
Constant	-0.811835	Oil Viscosity * Impeller Speed	1.12538e-007
Oil Viscosity	-2.29055	Oil Viscosity * Surfactant Phase Volume	2.30011
Impeller Type	Rotor-Stator	Oil Viscosity * Oil Phase Volume	229131
Impeller Speed	0.00127221	Oil Viscosity * Water Phase Volume	2.28994
Surfactant Phase Volume	-10.9395	Impeller Speed * Surfactant Phase Volume	-0.000457681
Oil Phase Volume	-0.180203	Impeller Speed * Oil Phase Volume	-0.00147096
Water Phase Volume	0.604889	Impeller Speed * Water Phase Volume	-0.00140513

Table 9-8 A summary of the proportionality constants used to obtain predicted D[4,3] values for a dissolver disk impeller.

<u>Term</u>	<u>Value of Proportionality Constant</u>	<u>Term</u>	<u>Value of Proportionality Constant</u>
Constant	2.01664	Oil Viscosity * Impeller Speed	3.26614e-007
Oil Viscosity	1.06082	Oil Viscosity * Surfactant Phase Volume	-1.05808
Impeller Type	Dissolver Disk	Oil Viscosity * Oil Phase Volume	-1.0614
Impeller Speed	0.0103057	Oil Viscosity * Water Phase Volume	-1.06241
Surfactant Phase Volume	-4.03646	Impeller Speed * Surfactant Phase Volume	-0.0106122
Oil Phase Volume	-0.00155618	Impeller Speed * Oil Phase Volume	-0.0106813
Water Phase Volume	1.32939	Impeller Speed * Water Phase Volume	-0.0107122

Table 9-9 A summary of the proportionality constants used to obtain predicted D[4,3] values for a rotor-stator impeller.

<u>Term</u>	<u>Value of Proportionality Constant</u>	<u>Term</u>	<u>Value of Proportionality Constant</u>
Constant	47.6031	Oil Viscosity * Impeller Speed	4.06359e-006
Oil Viscosity	6.36929	Oil Viscosity * Surfactant Phase Volume	-6.09029
Impeller Type	Rotor-Stator	Oil Viscosity * Oil Phase Volume	-6.37062
Impeller Speed	-0.04157	Oil Viscosity * Water Phase Volume	-6.39552
Surfactant Phase Volume	-45.9366	Impeller Speed * Surfactant Phase Volume	0.0108868
Oil Phase Volume	-16.3148	Impeller Speed * Oil Phase Volume	0.0398261
Water Phase Volume	11.6588	Impeller Speed * Water Phase Volume	0.0346259

Table 9-10 Comparison of products from two almost identical experiments obtained by analysis using Malvern Mastersizer X and Malvern Mastersizer 2000. Viscosity of oil used was 10cSt oil and impeller type was dissolver disk for both experiments.

Oil Phase (%)	[SLES] (%)	SLES : Oil	Impeller Speed (rpm)	Scraper Speed (rpm)	D[3,2] (µm) According to Mastersizer X	D[3,2] (µm) According to Mastersizer 2000
0.606	0.079	11.991	6000	100	0.66	0.501
0.616	0.077	12.508	6000	100	0.71	0.459

Table 9-11 Parameters chosen for the latter 11 experiments. Reactor vessel 7 was undergoing routine maintenance. The reason the final three samples have no particle size measurement is because they formed either oil-in-water gel or oil-in-water-in-oil emulsions and couldn't be sized.

Exp No.	Emulsi- fication Begins	Scra- per rpm	Oil Phase (%)	SLES (%)	[SLES]	Oil : SLES	D[3,2] (µm)	D[4,3] (µm)
1	Water + Surfactant + Oil then Stir	100	0.712	0.0611	20% of H2O	11.6	1.853	2.041
2	Oil then stir + water + SLES	100	0.714	0.0579	20% of H2O	12.3	0.648	3.28
3	Oil + SLES + Water then stir	100	0.714	0.0581	20% of H2O	12.3	0.538	1.394
4	Oil then stir + Surfactant + water	100	0.715	0.0576	20% of H2O	12.4	2.247	3.356
6	Surfactant + Water + Oil then Stir	200	0.714	0.0582	20% of H2O	12.3	0.65	1.825

8	As per above	100	0.715	0.0716	25% of H ₂ O	10.0	1.526	1.662
9	As per above	200	0.715	0.0715	25% of H ₂ O	10.0	1.074	1.767
10	As per above	100	0.896	0.0212	20% of H ₂ O	42.2		
11	As per above	200	0.901	0.0201	20% of H ₂ O	44.8		
12	As per above	200	0.899	0.0253	25% of H ₂ O	35.5		

9.5 Atlas Calorimeter Saponification Trials

Saponification was performed using a new calorimeter being beta tested in the Centre for Materials Discovery within the Department of Chemistry, University of Liverpool. The images shown here are taken from;

CAMPBELL, N., Harvey, D., Clowes, R. and Kowalksi, A. J. 2010. Atlas Potassium Technical Note; “*Calometric Measurement of Saponification Reaction of Sunflower Seed Oil*”

The calorimeter is sold on the premise that it can be used to monitor real time changes occurring within chemical reactions and is displayed in Figure 9-1. The saponification reaction was ideal for testing the apparatus as it involves constant changes of enthalpy, pH and turbidity.



Figure 9-1 Atlas Potassium Calorimetry Reactor equipment setup. **A)** Power controller for power compensation reactor heater, **B)** Jacket-In temperature probe (T_j), **C)** Vacuum triple jacketed 500mL reactor containing 400mL of [1M] $\text{NaOH}_{(\text{aq})}$ with pH, temperature (T_r) and turbidity probes, **D)** Controlled overhead mechanical stirrer, **E)** Reagent feed delivered by controlled Atlas syringe pump, **F)** Feed reservoir of 100mL sunflower oil [8].

In both Figures Figure 9-2 and Figure 9-3 it can be seen that as the reaction progresses, the turbidity increases.

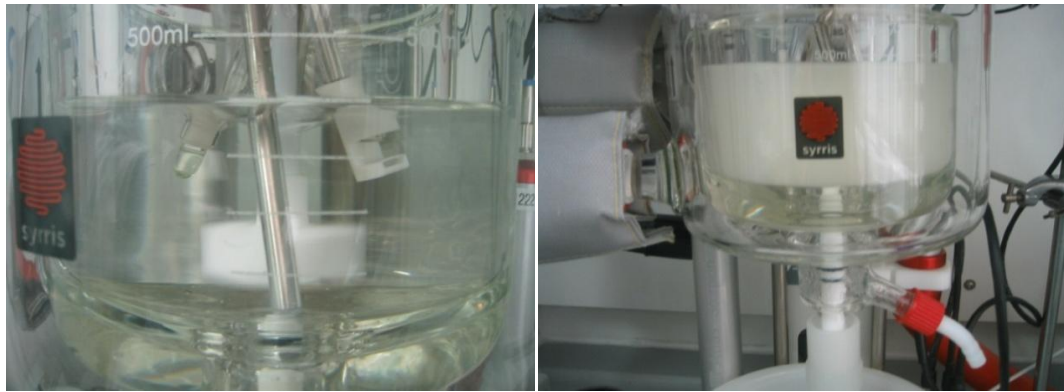


Figure 9-2 Clear sodium hydroxide solution prior to the addition of any oil and thus at reaction time zero (left image); following oil addition the reaction began and a turbid emulsion was formed (right image) and continued to be formed during the reaction.

As soap is formed the turbidity of the reaction vessel contents that is present within increases. Figure 9-2 presents a visual image of how the reaction increases in turbidity from clear hydroxide solution to the final soap product

The oil was added drop-wise to the sodium hydroxide solution at a steady rate via a peristaltic pump and this addition can be seen in Figure 9-3. The turbidity probe it was discovered is very sensitive and as a result the recordings fluctuate throughout the analysis as can be seen from the measurements observable in Figure 9-3. It took approximately ninety minutes from the addition of the probe to the reaction vessel before a steady state was obtained and the readings were deemed suitable enough to accurately represent the turbidity of the hydroxide solution within the reaction vessel.

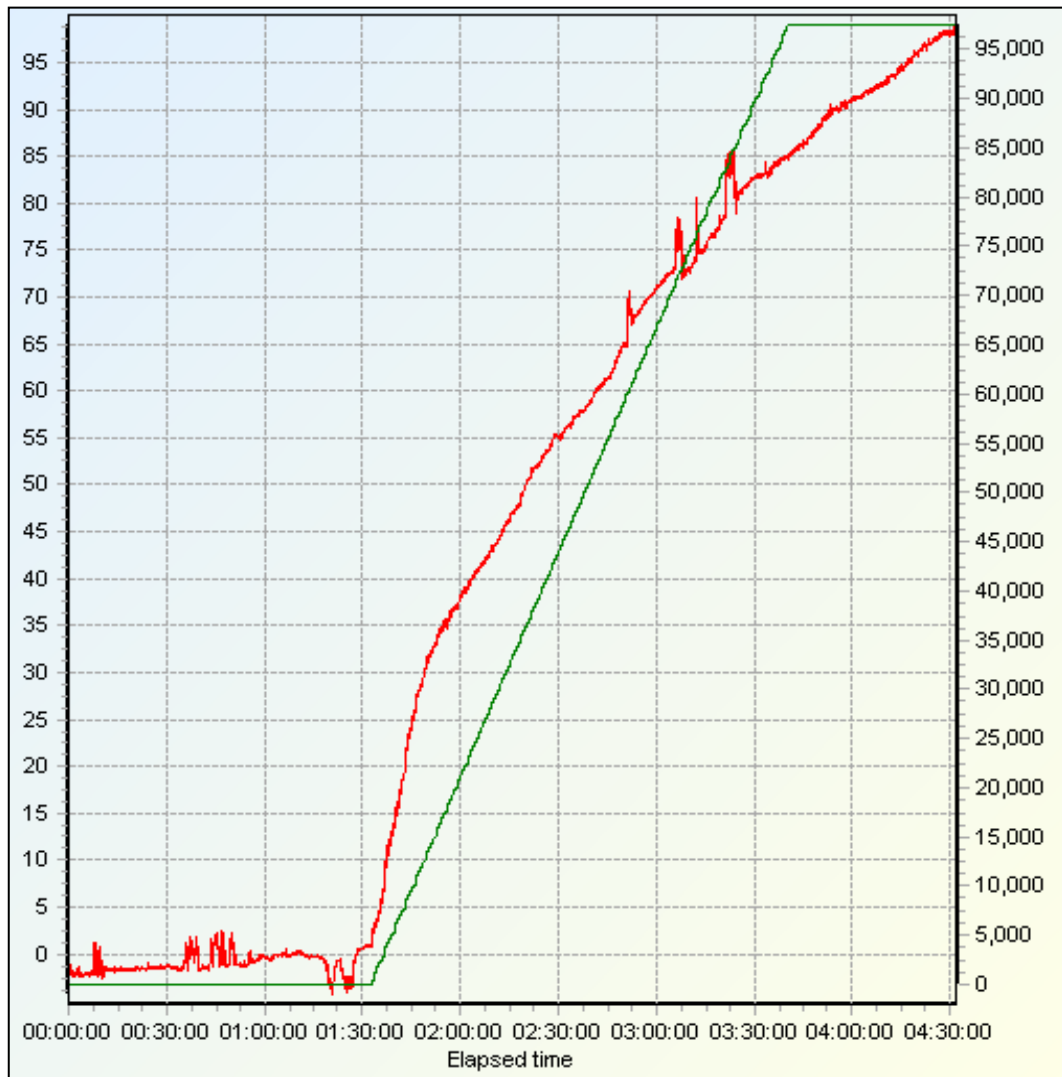


Figure 9-3 Graph calculated using the Atlas software showing real time monitoring of the addition of sunflower oil drop-wise (straight green line) and the corresponding increase in turbidity (wavy, red line) that occurs as soap is formed.

The difference in turbidity is generated as numerical data as the turbidity probe is able to detect the slightest change in translucency from that of the hydroxide solution which was its baseline.

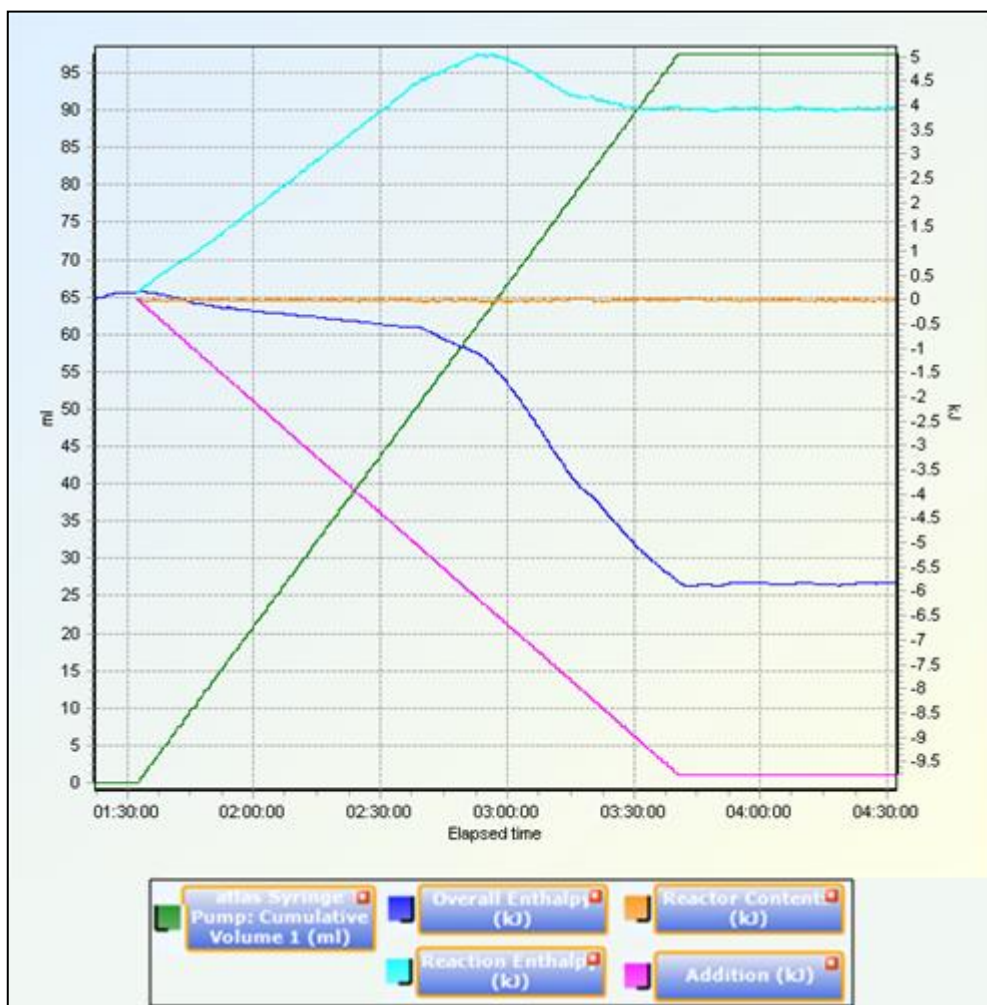


Figure 9-4 Live time monitoring of the reaction occurring using the Atlas Calorimetric software.

As well as turbidity, the reaction enthalpy is calculated by the software and this can also be monitored as the reaction progresses. Figure 9-4 shows an image of what the software displays during the course of the reaction. It can be seen that upon addition of oil to the reaction vessel, the “Reaction Enthalpy” begins to increase steadily due to the reaction being endothermic. After about 90 minutes from the beginning of the reaction, the energy draw required by the reaction ceases and the overall enthalpy of the process falls at a greater rate. This is because there is enough energy in the system provided by the increased heating required to counter the heat draw by the endothermic reaction. After 90 minutes of continually adding heat extra heat to not

only maintain the reaction at the required temperature but to account for the heat draw, a point is reached where there is enough energy for the reaction progress quickly. This appears as exothermic as there is excess energy present in the system.

